TAMPEREEN TEKNILLINEN YLIOPISTO
TAMPERE UNIVERSITY OF TECHNOLOGY

Tuomo Mäki-Marttunen

Modelling Structure and Dynamics of Complex Systems: Applications to Neuronal Networks

Julkaisu 1183 • Publication 1183

Tampere 2013

Tampereen teknillinen yliopisto. Julkaisu 1183
Tampere University of Technology. Publication 1183

Tuomo Mäki-Marttunen

Modelling Structure and Dynamics of Complex Systems: Applications to Neuronal Networks

Thesis for the degree of Doctor of Science in Technology to be presented with due permission for public examination and criticism in Sähkötalo Building, Auditorium S4, at Tampere University of Technology, on the 13th of December 2013, at 13 noon.

Tampereen teknillinen yliopisto - Tampere University of Technology
Tampere 2013

Supervisors	Prof. Keijo Ruohonen Tampere University of Technology Finland
	Adj. Prof. Marja-Leena Linne Tampere University of Technology Finland
Reviewers	Prof. Tatyana Turova Lund University Sweden
	Assoc. Prof. Duane Nykamp University of Minnesota United States of America
Opponent	Reader, Assoc. Prof. Bruce Graham University of Stirling United Kingdom

ISBN 978-952-15-3195-8 (printed)
ISBN 978-952-15-3203-0 (PDF)
ISSN 1459-2045

Abstract

Complex systems theory is a mathematical framework for studying interconnected dynamical objects. Usually these objects themselves are by construction simple, and their temporal behaviour in isolation is easily predictable, but the way they are interconnected into a network allows emergence of complex, non-obvious phenomena. The emergent phenomena and their stability are dependent on both the intrinsic dynamics of the objects, the types of interactions between the objects, and the connectivity patterns between the objects. This work focuses on the third aspect, i.e., the structure of the network, although the other two aspects are inherently present in the study as well. Tools from graph theory are applied to generate and analyze the network structure, and the effect of the structure on the network dynamics is analyzed by various methods. The objects of interest are biological and physical systems, and special attention is given to spiking neuronal networks, i.e., networks of nerve cells that communicate by transmitting and receiving action potentials.

In this thesis, methods for modelling spiking neuronal networks are introduced. Different point neuron models, including the integrate-and-fire model, are presented and applied to study the collective behaviour of the neurons. Special focus is placed on the emergence of network bursts, i.e., short periods of network-wide high-frequency firing. The occurrence of this behaviour is stable in certain regimes of connection strengths. This work shows that the network bursting is found to be more frequent in locally connected networks than in non-local networks, such as randomly connected networks. To gain a deeper insight, the aspects of structure that promote the bursting behaviour are analyzed by graph-theoretic means. The clustering coefficient and the maximal eigenvalue of the connectivity matrix are found the most important measures of structure in this matter, both expressing their relevance under different structural conditions. A range of different network structures are applied to confirm this result. A special class of connectivity is studied in more detail, namely, the connectivity patterns produced by simulations of growing and interconnecting neurons placed on a 2-dimensional array. Two simulators of growth are applied for this purpose.

In addition, a more abstract class of dynamical systems, the Boolean networks, are considered. These systems were originally introduced as a model for genetic regulatory networks, but have thereafter been extensively used for more general studies of complex systems. In this work, measures of information diversity and complexity are applied to several types of systems that obey Boolean dynamics. The random Boolean networks are shown to possess high temporal complexity prior to reaching an attractor. Similarly, high values of complexity are found at a

transition stage of another dynamical system, the lattice gas automaton, which can be formulated using the Boolean network framework as well. The temporal maximization of the complexity near the transitions between different dynamical regimes could therefore be a more general phenomenon in complex networks. The applicability of the information-theoretic framework is also confirmed in a study of bursting neuronal networks, where different types of networks are shown to be separable by the intrinsic information distance distributions they produce.

The connectivities of the networks studied in this thesis are analyzed using graph-theoretic tools. The graph theory provides a mathematical framework for studying the structure of complex systems and how it affects the system dynamics. In the studies of the nervous system, detailed maps on the connections between neurons have been collected, although such data are yet scarce and laborious to obtain experimentally. This work shows which aspects of the structure are relevant for the dynamics of spontaneously bursting neuronal networks. Such information could be useful in directing the experiments to measure only the relevant aspects of the structure instead of assessing the whole connectome. In addition, the framework of generating the network structure by animating the growth of the neurons, as presented in this thesis, could serve in simulations of the nervous system as a reliable alternative to importing the experimentally obtained connectome.

Preface

The work presented in this thesis was carried out in the Department of Signal Processing and Department of Mathematics in Tampere University of Technology during the years 2010 – 2013. I have received funding from TISE doctoral school and KAUTE foundation.

I would like to thank my Ph.D. supervisors, Prof. Keijo Ruohonen and Doc. Marja-Leena Linne, for their professional direction and all the time they have dedicated for guiding me during these four years. Furthermore, I thank Jugoslava Aćimović for all the guidance she has provided to train me in computational neuroscience. I also thank Matti Nykter for including me in his projects and for his professional collaboration, and Juha Kesseli for his insightful help in systems theory. I am also thankful to Riikka Havela, Heidi Teppola, and all the other people in the computational neuroscience research group for their contribution to my work and for the good atmosphere we had in the group. I thank Olli Yli-Harja and Stuart Kauffman for their general advice in science, and all my colleagues at the computational systems biology group for the stimulating discussions and the activities shared together. In addition, I would like to express my gratitude to Alejandro Schinder and Lidia Szczupak for taking me as a visiting scientist in their research groups, and to Lucas Mongiat, Antonia Marín-Burgin, Emilio Kropff, Belén Pardi, and Violeta Medan for their collaboration during these visits, and all the other people in the labs for their friendship. I am also grateful to my former colleagues at the personal positioning research group for the ground-laying education they gave me in numerical science. Moreover, I thank the pre-examiners of this thesis, Prof. Tatyana Turova and Prof. Duane Nykamp, for their comments and suggestions that helped to improve this thesis.

I also want to thank my family, Sointu, Ahti, Reija, and Timo for their good example in life and for the support they have provided me during these years. I am deeply grateful to my dear wife Verónica, you have given me your love and support, you have inspired me, and shared my passion in complex networks and neuroscience. Furthermore, I would like to thank all my friends from Tampere and Kurikka, and from all around the world. Finally, I want to thank God for everything, for a world of joy and sorrow, a world of possibilities to be tracked and mysteries to be uncovered, a world that leaves no experimentalist without awe, no theorist without inspiration, and no modeller without work.

Contents

List of publications

This thesis contains an introductory section and the following publications:

I. **T. Mäki-Marttunen***, R. Havela*, J. Aćimović, H. Teppola, K. Ruohonen, and M.-L. Linne. Modeling growth in neuronal cell cultures: Network properties in different phases of growth studied using two growth simulators. In *Proceedings of the 7th International Workshop on Computational Systems Biology (WCSB 2010)*, pp. 75-78, 2010. (* equal contribution of Mäki-Marttunen and Havela)

II. J. Aćimović, **T. Mäki-Marttunen**, R. Havela, H. Teppola, and M.-L. Linne. Modeling of neuronal growth in vitro: Comparison of simulation tools NETMORPH and CX3D. *EURASIP Journal on Bioinformatics and Systems Biology*, article ID 616382, 2011.

III. **T. Mäki-Marttunen**, J. Aćimović, M. Nykter, J. Kesseli, K. Ruohonen, O. Yli-Harja, and M.-L. Linne. Information diversity in structure and dynamics of simulated neuronal networks. *Frontiers in Computational Neuroscience*, 5:26, 2011.

IV. **T. Mäki-Marttunen**, J. Kesseli, S. Kauffman, O. Yli-Harja, and M. Nykter. Of the complexity of Boolean network state trajectories. In *Proceedings of the 8th International Workshop on Computational Systems Biology (WCSB 2011)*, pp. 137-140, 2011.

V. **T. Mäki-Marttunen**, J. Kesseli, and M. Nykter. Balance between noise and information flow maximizes set complexity of network dynamics. *PLoS ONE*, 8(3): e56523, 2013.

VI. **T. Mäki-Marttunen**, J. Aćimović, K. Ruohonen, and M.-L. Linne. Structure-dynamics relationships in bursting neuronal networks revealed using a prediction framework. *PLoS ONE*, 8(7): e69373, 2013.

The contributions of T. Mäki-Marttunen to the publications are the following. In **Publication I**, T. Mäki-Marttunen together with J. Aćimović and R. Havela designed and concieved the experiments and, together with the rest of the authors, analyzed the results. Together with R. Havela, T. Mäki-Marttunen performed the experiments. The work was divided in such a way that T. Mäki-Marttunen performed the experiments with NETMORPH, while R. Havela performed the CX3D experiments. In **Publication II**, T. Mäki-Marttunen performed the simulations designed by J. Aćimović, and assisted in the analysis of the results. In **Publications III**,

IV, **V** and **VI**, T. Mäki-Marttunen together with the co-authors designed and conceived the experiments and analyzed the results. T. Mäki-Marttunen performed the experiments, and wrote the major part of each of the manuscripts.

List of abbreviations

AMPA	α-amino-3-hydroxy-5-methylisoxazole-4-propionic acid
DIV	day *in vitro*
GABA	γ-aminobutyric acid
HH	Hodgkin-Huxley
LIF	leaky integrate-and-fire
NMDA	N-methyl-D-aspartic acid
NID	normalized information distance
NCD	normalized compression distance
ODE	ordinary differential equation
PDE	partial differential equation
RBN	random Boolean network
SDE	stochastic differential equation
XOR	exclusive or

Mathematical notations

$a, b, c, \ldots$	Scalar variables
$A, B, C, \ldots$	Vectors and matrices
$\mathcal{A}, \mathcal{B}, \mathcal{C}, \ldots$	Sets
$\mathbf{a}, \mathbf{b}, \mathbf{c}, \ldots$	Random variables
$\mathtt{a}, \mathtt{b}, \mathtt{c}, \ldots$	Strings
$\delta_x(\cdot)$	The delta function that is zero everywhere else except at x. Depending on the domain of x, $\delta_x(\cdot)$ is interpreted either as the Kronecker or Dirac delta. If the domain is numerable, $\delta_x(\cdot)$ is the Kronecker delta function, which obeys $\delta_x(x) = 1$. If the domain is innumerable, then $\delta_x(\cdot)$ is the Dirac delta function, the integral of which is defined as $\int_S \delta_x(s)ds = \begin{cases} 0, \text{ if } x \notin S \\ 1, \text{ if } x \in S \end{cases}$
$\mathbf{B}_t$	Brownian motion at time t (or more generally, the Brownian motion process)
$\mathrm{Bin}(n, p)$	Binomial distribution on the set $\{0, \ldots, n\}$ with mean np
$\mathcal{N}(X, \Sigma)$	Normal distribution with mean $X \in \mathbb{R}^n$ and covariance $\Sigma \in \mathbb{R}^{n \times n}$
$\mathbb{I}_m$	Identity matrix of size $m \times m$
$[a, b]$	Closed interval from a to b
(a, b)	Open interval from a to b
$[a, b)$, $(a, b]$	Semi-closed intervals from a to b

Particular physical entities

N	Size of network (number of nodes).
p	(Average) connection probability in the network.
C_m	Membrane capacitance parameter.
V_m	Membrane potential variable.
I	Current variable.
U	Parameter in the model of [Tsodyks et al., 2000] accounting for the maximum amount of readily releasable resources.

Chapter 1

Introduction

The brain is likely to be the most complex organ in a vertebrate body. This complexity rises both from its structure and function as well as the interplay between them. The human brain is comprised of approximately 10^{11} *neurons*, i.e. nerve cells, and 10^{15} *synapses* between them, and in addition, *glial cells* that outnumber the neurons by a factor between 1 and 10 [Azevedo et al., 2009, Allen and Barres, 2009, Sporns, 2011]. The brain functions include (yet are not restricted to) receiving, transferring and processing sensory information, cognitive processes, and conscious and autonomous motor control. Many of these tasks have been found to be concentrated on different brain regions and the capabilities to perform them have been shown to emerge at certain developmental stages. The detailed picture of these processes is, however, poorly understood due to the great number of neurons and other cells as well as the complexity of the cellular and synaptic processes involved.

Both the structural and dynamical aspects of the brain pose a notable challenge for unravelling the mystery of the brain. From the structural aspect, one of the milestones set out for the future is collecting the *connectome*, i.e., a detailed map of the neurons and the synapses in an adult human [Sporns et al., 2005]. Such data have already been collected for *C. Elegans* [White et al., 1986] and certain regions of the mouse brain [Briggman et al., 2011, Bock et al., 2011], but larger networks are yet to be reconstructed. The hitherto described networks have furthered the understanding of the underlying neuronal systems and revealed important deviations between the structure of brain networks and mainstream model networks such as random networks [Watts and Strogatz, 1998, Milo et al., 2002]. From the dynamical aspect, it is yet unclear how the co-function of the neurons forms fundamental cognitive processes such as learning and memory, given either realistic or simplified network structure. Likewise, there are discrepancies over the role of subcellular and subsynaptic level phenomena, as well as the contribution of glial cells to the brain processes [Araque and Navarrete, 2010]. In addition to all this, a major extra challenge is the developmental aspect of the neural network. The connections in the brain as well as the neurons themselves are plastic and subjected to a multitude of regulatory processes [Turrigiano, 2011]. Such processes include pruning of synapses, spike-timing dependent plasticity, and activity-dependent growth of neurons, each of which has been proposed to fundamentally contribute to several brain functions [Shatz, 1990, Chechik et al., 1999, Sjöström et al., 2008].

Neuronal networks have been under a wide range of computational research for the past three decades. Models on both development and activity of neuronal networks have long been available [Izhikevich, 2004, Zubler and Douglas, 2009, Van Ooyen, 2011], and they are increasingly drawing the attention of life scientists due to the advances made in information technology. The systems modelling approach, where the function of the system is studied as an emergent property of the function of the single actors and the interactions between them, has proven a valuable tool [Izhikevich and Edelman, 2008, Hellgren-Kotaleski and Blackwell, 2010, Buzsáki, 2011], although unresolved challenges exist [Gerstein and Kirkland, 2001, Dada and Mendes, 2011]. Theoretical and computational approaches have assisted in revealing many a brain function, and they have correctly predicted certain neuroscientific phenomena, to name a few, the need for a net inhibitory current in order to observe certain Purkinje cell spike patterns [Jaeger et al., 1997], and that synchronization is more easily obtained using inhibition than excitation [Lytton and Sejnowski, 1991]. Far more numerous than such predictions are the *postdictions*, i.e., studies that show or propose a mechanism for an experimentally observed neural phenomenon. Such studies often contribute to the generalization of the experimental findings and can thus provide deep insight into the function of the brain [Abbott, 2008].

The aim of this work is to study the structure and dynamics of neuronal networks by computational means, and uncover certain aspects on how the dynamics is affected by the structure. It is indeed the connections between the actors in a complex network (such as neurons in a neuronal network) that altogether allow the formation of collective activity, and hence, understanding the structure of the network is utterly important. In this thesis, the structure of a neuronal network is studied by simulating the growth of the neurons, and methods for analysing the resulting network structure are introduced. The networks produced by simulators of growth are compared to more abstract network models, such as random and locally connected networks. The networks are also compared from the dynamical point of view. The different types of bio-electrical activity that emerge in neuronal networks with different structure are studied. Especially, the emergence of spontaneous synchronized spiking, namely, the network bursts[1], is studied. In addition, the information diversity of the spiking activity is quantified and the effect of network structure on complexity is screened. For more general analyses on information diversity and complexity in dynamical systems, a simpler model class of *Boolean networks*, which have been used to describe the dynamics of several different types of physical systems, is considered. In these networks, the complex temporal dynamics arise from the interplay of actors whose internal dynamics are reduced to a minimum in a certain sense, namely, to binary functions. The temporal behaviour in these systems is quantified using novel information-theoretic tools. The ultimate goal of the work is to further the understanding of structural aspects in complex networks and their contribution to the type, magnitude, and complexity of the emergent dynamics.

[1]Throughout this work, the term network burst (used interchangeably with the term "burst") is used for a synchronized or nearly synchronized spiking activity (alternative names are *population burst*, *population spike*, *network spike*, *synchronized spike*, *synchronized burst*). This is standard terminology in the literature on neuronal cultures grown on micro-electrode arrays [Kamioka et al., 1996, Marom and Shahaf, 2002]. To make a distinction from bursts of a single cell, which usually occur on a shorter time-scale, the term *intrinsic burst* or *single-cell burst* is used for the latter.

Chapter 2

Theoretical background

In this chapter, the mathematical theory underlying the modelling and analysis of the structure and dynamics of complex networks is introduced. A sound mathematical foundation for the modelling of complex systems is needed in order to guarantee correct temporal behaviour and to improve the predictability and generalizability of the systems. Section 2.1 presents the graph-theoretic tools for assessing network structure, while Section 2.2 introduces the theory of stochastic processes that can be applied to the modelling of non-deterministic dynamical systems — although it is also applicable to deterministic systems as a special case of zero randomness. Section 2.3 provides methods for assessing the amount of information in complex systems.

2.1 Graph theory

Connectivity patterns in networks, such as neuronal, genetic, social, and internet networks, can be best described by graph-theoretic tools. A *graph* is an entity $(\mathcal{G}, \mathcal{E})$, where $\mathcal{G} = \{v_1, \ldots, v_N\}$ is the set of *nodes*, and $\mathcal{E} \subset \{(x, y) | x \in \mathcal{G}, y \in \mathcal{G}\}$ is the set of *egdes* between the nodes, x referring to the source node and y to the target node of the edge. The number N is the number of nodes in the graph, referred to as the *size* of the network. The graph can be either *directed*, meaning that there is a distinction between edges (v_i, v_j) and (v_j, v_i), or *undirected*, where the two edges refer to the same object. Two nodes v_i and v_j are called *neighbours* if there exists an edge (v_i, v_j) or (v_j, v_i) in the set of edges $\mathcal{E}$. The *in-degree* of node v_i, $D_{i,\text{in}}$, is the number of edges projecting to the node v_i, and the *out-degree* $D_{i,\text{out}}$ is the number of edges projected by the node. In *weighted* graphs each edge is affiliated with an additional quantity that represents the *strength* of the connection, while in *unweighted* graphs all the edges are, essentially, equally important.

The focus of this thesis is in directed, unweighted graphs. These graphs can describe, e.g., the connectivity of neuronal networks in a way that the direction of the synapse (which is the sending, *pre-synaptic* neuron and which is the receiving, *post-synaptic* neuron) is respected, but the strength of all existing connections are equal. Such connectivity graphs can be uniquely

described by binary *connectivity matrices* $M \in \{0,1\}^{N\times N}$, where the element M_{ij} denotes the existence (1) or inexistence (0) of edge $(v_i, v_j) \in \mathcal{E}$. The connectivity matrix of a network determines the structure (may also be called the *topology*) of the network, but does not tell anything about the type of interaction, and thus does not alone imply anything about the dynamics of the network.

The number of possible connectivity graphs grows superexponentially (2^{N^2} if self-connections are allowed and $2^{N(N-1)}$ if not) with the size of the network, which brings challenges to the classification of large graphs. Typically, one wants to characterize a specific aspect of the network connectivity, and compare different networks from this aspect. There are several widely applied *graph measures* for such a purpose. Basically, any function $\{0,1\}^{N\times N} \to \mathbb{R}$ would do, but a fair restriction to a graph measure is that it be invariant under the permutation of the nodes and be applicable to any network size N. The graph measures applied in this work are *clustering coefficient*, *geodesic path length*, *node-betweenness*, *length to self*, *average degree*, *degree deviations*, *degree correlation*, *maximum eigenvalue*, and *motif occurrences*, each of which meets the mentioned criteria. In the following these measures are defined.

The *clustering coefficient* measures the degree of community in the network as a quantity of "how likely is it that a neighbour of my neighbour is my neighbour as well". It has originally been introduced for undirected networks as the ratio between the number of triangles, i.e. fully connected triples, and the number of (partially or fully) connected triples [Watts and Strogatz, 1998, Newman, 2003]. However, the definition of the clustering coefficient can be extended for directed networks as follows. First, the local clustering coefficient of a node v_i is defined as

$$C_i = \frac{1}{8\binom{G_i}{2}} \sum_{\substack{j=1\\ j\neq i}}^{N} \sum_{\substack{k=1\\ k\neq i}}^{j-1} (M_{ij}+M_{ji})(M_{ik}+M_{ki})(M_{jk}+M_{kj}), \tag{2.1}$$

where G_i is the number of neighbours of the node v_i. In this definition, each triple of nodes $\{v_i, v_j, v_k\}$ may form 0 to 8 different triangles. The number of triangles is one when there is exactly one unidirected edge between nodes v_i and v_j, between v_i and v_k, and between v_j and v_k. Furthermore, the number of triangles is doubled whenever a unidirected edge is changed to bidirected. Another possibility is to consider the number of traversable triangles:

$$C_i = \frac{1}{2\binom{G_i}{2}} \sum_{\substack{j=1\\ j\neq i}}^{N} \sum_{\substack{k=1\\ i\neq k\neq j}}^{N} M_{ij}M_{jk}M_{ki}. \tag{2.2}$$

Both methods agree in that $C_i = 0$ if there are no connections between the neighbours of v_i, and that $C_i = 1$ if and only if all neighbours of i are bilaterally connected to each other and to i. The former method is used in **Publication VI**, while in **Publication III**, the latter method is employed. The latter method may overestimate the degree of clustering in networks where directed loops of length 3 are promoted. This could be an issue in **Publication VI**, where such graphs are considered among others, and hence the former method is applied. In both cases,

the clustering coefficient of the graph is then calculated as the average of the local clustering coefficients:

$$\bar{C} = \frac{1}{N}\sum_{i=1}^{N} C_i. \tag{2.3}$$

A *geodesic path* from node v_i to node v_j is a minimal set of edges $\{(v_i, v_{K_1})$, (v_{K_1}, v_{K_2}), …, $(v_{K_{l-2}}, v_{K_{l-1}})$, $(v_{K_{l-1}}, v_j)\} \subset \mathcal{E}$ through which one can traverse from v_i to v_j, and the *geodesic path length* of the graph is the harmonic average length of these paths. This can be written in mathematical terms as

$$\bar{L} = \left(\frac{1}{N(N-1)} \sum_{i=1}^{N} \sum_{\substack{j=1 \\ j \neq i}}^{N} L_{ij}^{-1} \right)^{-1}, \tag{2.4}$$

where

$$L_{ij} = \min\{k \in \mathbb{N} | (M^k)_{ij} > 0\} \tag{2.5}$$

is the length of the shortest path from v_i to v_j. If such a path does not exist, the set $\{k \in \mathbb{N}|(M^k)_{ij} > 0\}$ is empty, and the value of L_{ij} is interpreted as ∞. These paths do not contribute to the harmonic mean of the path lengths, unlike they do to the arithmetic mean, which justifies the use of the harmonic mean [Newman, 2003, Boccaletti et al., 2006]. The closely related measure, *length to self*, is an average geodesic path length from a node to itself, calculated as

$$\bar{L}^{\text{self}} = \left(\frac{1}{N} \sum_{i=1}^{N} L_{ii}^{-1} \right)^{-1}. \tag{2.6}$$

The centrality of a node in the graph can be described using the measure of *node-betweenness*. The node-betweenness of a node v_i is an average value of how many geodesic paths the node lies on. It can be calculated as

$$B_i^{\text{node}} = \sum_{\substack{j=1 \\ j \neq i}}^{N} \sum_{\substack{k=1 \\ i \neq k \neq j \\ L_{jk} < \infty}}^{N} \frac{s_{jk}^{(i)}}{s_{jk}}, \tag{2.7}$$

where $s_{jk}^{(i)}$ is the number of such shortest paths from node v_j to node v_k that cross node v_i, and s_{jk} is the total number of shortest paths from v_j to v_k.

A determinant aspect of the graph is the distribution of the number of inputs and outputs of the nodes, that is, the *degree distributions*. The *average degree* of a graph is the sample mean of the in- or out-degrees of the nodes, and can be written as

$$\bar{D} = \frac{1}{N}\sum_{i=1}^{N} D_{i,\text{out}} = \frac{1}{N}\sum_{j=1}^{N} D_{j,\text{in}} = \frac{1}{N}\sum_{i=1}^{N}\sum_{j=1}^{N} M_{ij}. \tag{2.8}$$

Similarly, the *degree deviations* measure the sample standard deviation of in- and out-degree:

$$\sigma_{D_{\text{out}}} = \sqrt{\frac{1}{N-1}\sum_{i=1}^{N}(D_{i,\text{out}} - \bar{D})^2} \tag{2.9}$$

$$\sigma_{D_{\text{in}}} = \sqrt{\frac{1}{N-1}\sum_{i=1}^{N}(D_{i,\text{in}} - \bar{D})^2} \tag{2.10}$$

The *degree correlation*, in turn, measures the correlation coefficient between in- and out-degree, i.e., it assesses how likely it is that a node with many inputs has many outputs as well, and vice versa. This quantity is calculated as

$$\sigma_{D_{\text{in}},D_{\text{out}}} = \frac{\sum_{i=1}^{N}(D_{i,\text{in}} - \bar{D})(D_{i,\text{out}} - \bar{D})}{\sqrt{\sum_{i=1}^{N}(D_{i,\text{in}} - \bar{D})^2}\sqrt{\sum_{i=1}^{N}(D_{i,\text{out}} - \bar{D})^2}} \tag{2.11}$$

The graph properties can also be viewed by using spectral methods. An important quantity is the *maximum eigenvalue*, i.e., the largest eigenvalue of the connectivity matrix. This quantity is real-valued, as the connectivity matrix is non-negative [MacCluer, 2000], and positively correlated to the degree correlation [Restrepo et al., 2007]. Yet another approach is a combinatorial method, where the occurrences of certain connectivity patterns are counted. The *network motifs* are local connectivity patterns of three nodes. There are $2^6 = 64$ such connectivity patterns, when self-connections are excluded, but the number is reduced to 16 when motifs that can be changed to another one by permutation of the nodes are regarded as one motif. Further, in three of these 16 patterns some of the nodes are completely isolated from the others, and thus the number of connectivity patterns for triples of nodes is 13 [Milo et al., 2002]. These motifs are illustrated in Figure 2.1.

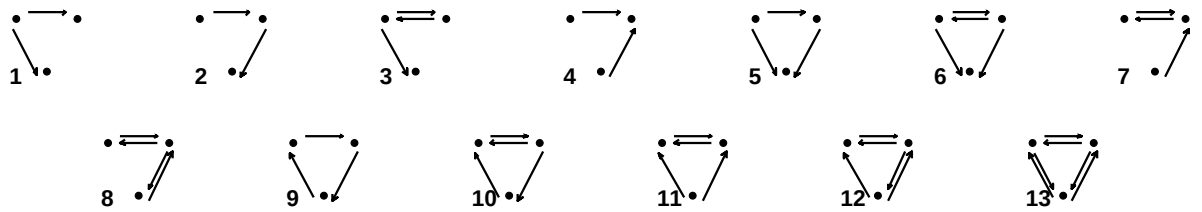

Figure 2.1: The 13 network motifs of three connected nodes. See [Milo et al., 2002] for reference.

2.2 Stochastic processes

The theory of stochastic processes is a useful tool for studying non-deterministic dynamical systems. The collection of random variables $\{\mathbf{X}_t | t \in \mathcal{I}\}$ is a *stochastic process* with *index set* $\mathcal{I}$, if $\mathbf{X}_t : \Omega \to \mathbb{R}^n$ is a random variable for any $t \in \mathcal{I}$, Ω representing the *sample space* of the random variables [Ross, 1996, Øksendal, 2010]. In dynamical systems, the index set $\mathcal{I}$ is considered the set of time points. This set can be either numerable, such as $\mathbb{N}$, which leads to a *discrete-time system*, or innumerable, such as $[0, \infty)$, which implies a *continuous-time system* [Ross, 1996]. The mapping $X_t(\omega) : \mathcal{I} \to \mathbb{R}^n$, where the sample $\omega \in \Omega$ is fixed, is called the *realization* or the *sample path* of the stochastic process.

The manner in which the stochasticity is incorporated in the system dynamics depends on the application. Typically, the state of a dynamic system is considered to evolve according to an "averaged" rule, affected by a constantly present, randomly fluctuating perturbation term [Øksendal, 2010]. Let us take two examples from the biology that are central to this thesis. First, consider a cell whose membrane potential can be measured with an electrode. Further, imagine that the ionic concentrations inside and outside the cell could also be measured and the fraction of open ionic channels could be evaluated in real time. One would find that the membrane potential of the cell is largely dictated by the proportion of open ion-channels that are, in turn, temporally dependent on the membrane potential. However, this dependency would include some amount of noise, which could be an effect of many biophysical intracellular processes (see e.g. [Goldwyn and Shea-Brown, 2011]). As a second example, consider the genes that are expressed in a cell. The product of the gene expression, namely, the proteins and other macromolecules, direct the expression of other genes. Given that a particular set of genes are expressed at a time instant, a named gene will with large probability be expressed in the very near future. However, due to the numerous metabolic aspects of the cell as well as the sparse density of the macromolecules in the cytoplasm, sometimes the considered gene will not be expressed, and by contrast, another gene that should be inhibited by the set of expressed genes could by chance become expressed. The former example (on the membrane potential dynamics) is most convenient to be considered as a continuous-time continuous-state problem, while for the latter example (on the gene expression) many approaches are arguable. This work restricts to discrete-time discrete-state approaches for the latter problem, following the approach of the seminal paper by Kauffman [Kauffman, 1969]. Let us consider the two mathematical frameworks best suited for describing these two types of systems, namely, *stochastic differential equations* and *Markov chains*. Let us start from the latter, simpler system.

A discrete-time discrete-state system $\{\mathbf{X}_t : \Omega \to \mathcal{S} | t \in \mathbb{N}\}$, where $\mathcal{S} = \{a_1, a_2, \ldots\}$ is the (numerable) set of possible states of the system, is a Markov chain if it obeys the *Markov property*. The Markov property can be formulated as [Ross, 1996]

$$\forall i \geq 0, k \geq 0 : P(\mathbf{X}_{i+1} | \mathbf{X}_i = x_i, \ldots, \mathbf{X}_{i-k} = x_{i-k}) = P(\mathbf{X}_{i+1} | \mathbf{X}_i = x_i). \tag{2.12}$$

This means that the future state $\mathbf{X}_{i+1}$ of a system depends on its history only through the previous state $\mathbf{X}_i$. That is, given the previous state $\mathbf{X}_i$, the earlier states of the system, $\mathbf{X}_0, \ldots, \mathbf{X}_{i-1}$,

do not bring any extra information for the estimation of $\mathbf{X}_{i+1}$. The state transitions of a Markov chain are described by the transition matrix [Ross, 1996, Øksendal, 2010]

$$\begin{bmatrix} P_{11} & P_{12} & \cdots \\ P_{21} & P_{22} & \cdots \\ \vdots & \vdots & \ddots \end{bmatrix},$$

where $P_{ij} = P(\mathbf{X}_{i+1} = a_j | \mathbf{X}_i = a_i)$ is the transition probability from state a_i to state a_j. The system is deterministic, if each state of the system inevitably leads to exactly one state, i.e., if $\forall i \exists j \forall k : P_{ik} = \delta_j(k)$, and non-deterministic in any other case. Both types of Markov chains are used in **Publications IV** and **V**.

The stochastic differential equation (SDE) describes the evolution of a continuous-time continuous-state system involving stochastic dynamics. Similarly to ordinary differential equations (ODEs), an SDE is an equation that governs the changes in the state of the system during an infinitesimal time step. It can be written in differential form as [Øksendal, 2010]

$$d\mathbf{X}_t = f(\mathbf{X}_t, t)dt + g(\mathbf{X}_t, t)d\mathbf{B}_t \tag{2.13}$$

and in integral form as

$$\mathbf{X}_t = \mathbf{X}_0 + \int_0^t f(\mathbf{X}_u, u)du + \int_0^t g(\mathbf{X}_u, u)d\mathbf{B}_u. \tag{2.14}$$

The process $\{\mathbf{B}_t | t \in [0, \infty)\}$ is called the (m-dimensional) *Brownian motion*. It can be intuitively derived from a Markov chain that at each time instant either increases or decreases its value by a constant value with equal probabilities, by considering the limit of small state change and small time step [Ross, 1996]. Its main properties are the following[1] [Ross, 1996]:

1. It is at rest at zero, i.e., $\mathbf{B}_0 = 0 \in \mathbb{R}^m$.
2. It has independent increments, i.e., the increment $\int_\tau^{\tau+\Delta t} d\mathbf{B}_u = \mathbf{B}_{\tau+\Delta t} - \mathbf{B}_\tau$ is independent of random variables $\mathbf{B}_t$ for any $t \leq \tau$ and $\Delta t \geq 0$.
3. The increment $\int_\tau^{\tau+\Delta t} d\mathbf{B}_u$ is normally distributed with mean $0 \in \mathbb{R}^m$ and variance $c^2 \Delta t \mathbb{I}_m$ for any $\tau, \Delta t \geq 0$, where c is a normalization constant and $\mathbb{I}_m \in \mathbb{R}^{m \times m}$ is an identity matrix.

The stochastic integral $\int_0^t g(\mathbf{X}_u, u)d\mathbf{B}_u$ is defined as the *Itō integral*, i.e., as the limit random variable of

$$\sum_{i=1}^{k} g(\mathbf{X}_{t_{i-1}}, t_{i-1})(\mathbf{B}_{t_i} - \mathbf{B}_{t_{i-1}}), \tag{2.15}$$

[1] In [Øksendal, 2010], the first and third property are relaxed as follows. The initial distribution may be centered anywhere as long as it is a point-mass distribution, i.e., $P(\mathbf{B}_0 = X) = \delta_{B_0'}(X)$, where $B_0' \in \mathbb{R}^m$ is a fixed vector. This detail is, however, insignificant in the application to the SDEs. As for the third property, any non-negative definite matrix is allowed as the covariance matrix. This can be compensated for in the framework of [Ross, 1996] by choosing the drift function $g : \mathbb{R}^n \times \mathbb{R} \to \mathbb{R}^{n \times m}$ appropriately.

where the number k of subintervals obeying $0 = t_0 < t_1 < \ldots < t_k = t$ is increased to infinity[2]. Another wide-spread interpretation would be the *Stratonovich integral*, which assigns the midpoint value of $g(\mathbf{X}_{(t_i+t_{i-1})/2}, (t_i + t_{i-1})/2)$ for increment $\mathbf{B}_{t_i} - \mathbf{B}_{t_{i-1}}$, instead of the left endpoint value of $g(\mathbf{X}_{t_{i-1}}, t_{i-1})$ as used in the Itō integral. In this thesis, the Itō integral is employed for the sake of its wider support in applied mathematics.

The Equations 2.13 and 2.14 utilize the *bias* term $f : \mathbb{R}^n \times \mathbb{R} \to \mathbb{R}^n$ and the *drift* term $g : \mathbb{R}^n \times \mathbb{R} \to \mathbb{R}^{n\times m}$. These terms may depend on the state of the system, as well as the time, and together they fully determine the time course behaviour of the system. Analytical solutions exist for SDEs with several types of bias and drift functions, but in general the solution has to be obtained numerically. There are two different approaches for this. In the *partial differential equation* (PDE) approach, the Equation 2.13 is first transformed into a partial differential equation, namely, a *Fokker-Planck* equation, where the propagation of the *probability mass distribution* of $\mathbf{X}_t$ is solved through time [Kloeden and Platen, 1992]. In the *sample path approach*, several realizations of the Brownian motion $\{\mathbf{B}_t | t \in [0, \infty)\}$ are generated and the Equation 2.13 is solved for each of these sample paths. Both approaches produce an approximation of the distribution of $\mathbf{X}_t$ for any time instant $t > 0$. The PDE approach is efficient for low-dimensional systems, but the sample path approach is more powerful in large-dimensional systems. The memory consumption of the sample path method is only linear to the dimension n of the variable $\mathbf{X}_t$, while in the PDE approach the memory usage grows exponentially with n. This work considers only the sample path approach in solving the SDEs (or related stochastic equations) — this approach is used in **Publications I**, **II**, **III**, and **VI**.

The simplest numerical sample path method is the *Euler-Maruyama* method which is an extension of the *forward Euler method* for ODEs. The state update formula is as follows [Kloeden and Platen, 1992]:

$$\mathbf{X}_{t+\Delta t}(\omega) = \mathbf{X}_t(\omega) + \Delta t f(\mathbf{X}_t(\omega), t) + g(\mathbf{X}_t, t)(\mathbf{B}_{t+\Delta t}(\omega) - \mathbf{B}_t(\omega)). \tag{2.16}$$

The increment $\mathbf{B}_{t+\Delta t} - \mathbf{B}_t$ obeys the distribution $\mathcal{N}(0, c^2 \Delta t \mathbb{I}_m)$, and hence, $\mathbf{B}_{t+\Delta t}(\omega) - \mathbf{B}_t(\omega)$ can be picked using a Gaussian random number generator. Thus, given the initial state $\mathbf{X}_0$, one can solve the sample path $\{\mathbf{X}_t(\omega) | t \in [0, \infty)\}$ with a chosen resolution. The solution converges to the correct distribution in the limit of infinitely small time step and infinite number of sample paths [Kloeden and Platen, 1992]. There are several extensions for Euler-Maruyama method, e.g., *Milstein method* or *weak second order Taylor method* [Kloeden and Platen, 1992] that outperform the Euler-Maruyama method in their rate of convergence. The effect of these extensions is, however, subject to the form of the bias and drift functions. As an example, the Milstein method is reduced to the Euler-Maruyama method when it is applied to a system with a constant drift term $g(X, t) = g$.

[2] In [Øksendal, 2010], this limit random variable is constructed using a sequence of *elementary* functions, which converge toward $\mathbf{X}_t$. The elementary functions are piece-wise (in time) constant, bounded, and measurable with respect to a specific σ-algebra (see [Øksendal, 2010] for details), and the Itō integral for them is defined as Equation 2.15. The existence of the limit random variable is proven and the convergence (in L^2) shown in [Øksendal, 2010]. For an alternative, more measure-theoretically rigorous construction of Itō integrals, see e.g. [Kallenberg, 2002].

2.3 Information theory

There are two mainstream paradigms for assessing the quantity we call *information*. In the probabilistic paradigm, the information can be quantified for any random variable $\mathbf{X}$ using the measure of *entropy*. This quantity is defined as [Reza, 1961, Li and Vitányi, 2008]

$$H(\mathbf{X}) = -\sum_{x} P(\mathbf{X} = x) \log P(\mathbf{X} = x), \tag{2.17}$$

and it is interpreted as the average amount of uncertainty contained by the random variable $\mathbf{X}$. In the algorithmic paradigm, information can be quantified for *strings*, which can be defined as finite sequences of characters belonging to a certain finite alphabet [Li and Vitányi, 2008]. The amount of information contained by the string is defined as the *length of the shortest program that outputs the string on a universal computer* [Kolmogorov, 1965]. This quantity is called the *Kolmogorov complexity* (also terms *Kolmogorov-Chaitin complexity* and *algorithmic complexity* are frequantly used [Li and Vitányi, 2008, Kolmogorov, 1965]) and denoted by $K(\mathtt{x})$, where $\mathtt{x}$ is a string. Depending on the choice of the universal computer, the values of $K(\mathtt{x})$ may differ from each other by an additive constant [Kolmogorov, 1965].

Both approaches to information have their pros and cons. The main difference is that the probabilistic approach is applicable to random variables, while the algorithmic approach is applicable to realizations of random variables, given that they can be described as strings. The entropy measure is addressable for any random variable whose probability distribution is known. However, in most applications, this is not the case, and instead, the distribution has to be estimated based on sampled data (cf. [Shalizi et al., 2004, Galas et al., 2010]). On the other hand, the Kolmogorov complexity $K(\mathtt{x})$ is in general *uncomputable* [Li and Vitányi, 2008], meaning that $K(\mathtt{x})$ cannot be assigned for an arbitrary string $\mathtt{x}$, regardless the choice of the computer model. The Kolmogorov complexity can, however, be effectively approximated in certain applications by general data compression methods, as discussed in the following.

Normalized compression distance and set complexity

A metric of *normalized information distance* (NID) based on Kolmogorov complexity has been proposed in [Li et al., 2004]. The NID is proposed as a universal[3] distance between two arbitrary strings, and it can be formulated as follows:

$$\mathrm{NID}(\mathtt{x}, \mathtt{y}) = \frac{\max(K(\mathtt{x}|\mathtt{y}*), K(\mathtt{y}|\mathtt{x}*))}{\max(K(\mathtt{x}), K(\mathtt{y}))}. \tag{2.18}$$

In this notation, $\mathtt{x}$ and $\mathtt{y}$ are strings, and $\mathtt{x}*$ and $\mathtt{y}*$ (also strings) are the shortest programs that output strings $\mathtt{x}$ and $\mathtt{y}$, respectively, on a universal computer. Furthermore, the function

[3]That NID is *universal* means that there is no other distance measure among the class of considered normalized distances that gives shorter distances than NID. See [Li et al., 2004] and [Li and Vitányi, 2008] for formal definitions and proofs.

$K(\mathtt{x}|\mathtt{y}*)$ is the length of the shortest program that outputs $\mathtt{x}$ when it is given the string $\mathtt{y}*$ as an auxiliary input. The distance between two strings can be assessed by other means as well, for example, using the *Hamming distance* that is defined as the proportion of differing characters in the two strings. A downside with Hamming distance is, however, that it is, on one hand, applicable to equally long strings only, and on the other hand, fully index-specific. This means that if, for instance, a random binary string is duplicated and the other one is shifted in indices by one character, the Hamming distance between the resulting strings will be close to 0.5, which is the mean Hamming distance of two random, independent binary strings. By contrast, the design of the NID is such that the two strings remain near to each other when the indexing of one of them is shifted by a certain number of characters — in addition, the NID is robust to addition or removal of small substrings. The NID can be estimated by the *normalized compression distance* (NCD), in which the Kolmogorov complexity of a string is replaced by the length of the compressed string. General data compressors, such as `gzip` and `LZMA`, can be used for the computation of this metric. The NCD is defined as

$$\mathrm{NCD}(\mathtt{x},\mathtt{y}) = \frac{C(\mathtt{xy}) - \min(C(\mathtt{x}), C(\mathtt{y}))}{\max(C(\mathtt{x}), C(\mathtt{y}))}, \tag{2.19}$$

where $C(\mathtt{x})$ is the length of the string $\mathtt{x}$ after compression, and $C(\mathtt{xy})$ is the length of the concatenation of strings $\mathtt{x}$ and $\mathtt{y}$ after compression.

Despite the crude approximation (see e.g. the discussion on the subject in [Li et al., 2004]) of the Kolmogorov complexity by general data compressors, there are appealing arguments for the eligibility of the NCD. Firstly, due to the subtraction of two Kolmogorov complexity approximations in Equation 2.19 and division by a third one, the resulting value is approximately invariant to affine transformations of $C(\mathtt{x})$, i.e., transformations of form $\tilde{C}(\mathtt{x}) = aC(\mathtt{x}) + b$. This should outdo a great part of the discrepancies between different data compressors that each add different metadata (such as code dictionaries) in the beginning of the compressed strings, and that each have different average compression rates. Secondly, the NCD has been found effective in showing non-trivial similarities in challenging data. Namely, the method has been successfully applied to reconstruct phylogenetic trees as well as language relation trees, as shown in [Li et al., 2004]. In their work, the phylogenetic tree was obtained by applying the NCD on protein sequences of different species and using hierarchical clustering on the resulting distances, while for the language tree reconstruction the human rights declaration in different languages was used as data [Li et al., 2004]. Likewise, the phylogenetic tree was correctly reconstructed in [Otu and Sayood, 2003] by using distance measures that were slightly different from the NCD but that were as well based on approximating Kolmogorov complexity with general purpose data compressors.

The NID — and its computable approximation, NCD — has been used as a foundation for building a measure of *context-dependent information*, namely, the *set complexity* [Galas et al., 2010]. In this approach, the complexity cannot be addressed for a string, but for a set of strings, and the complexity of the set arises from the amount of non-redundant (yet non-random) information in the strings of the set. The aspect of redundancy versus randomness is quantified through the NCD between the strings: Values of NCD near zero represent too high a redundancy (this is the case for instance when the strings $\mathtt{x}$ and $\mathtt{y}$ are almost identical copies of each other),

while values near one represent too little context (this occurs when, e.g., one of the two strings is random). Obeying these guidelines, the set complexity is defined as

$$\phi(\{\mathtt{x}_1,\ldots,\mathtt{x}_k\}) = \sum_{i=1}^{k} C(\mathtt{x}_i)\frac{1}{k(k-1)} \sum_{\substack{j=1 \\ j\neq i}}^{k} \mathrm{NCD}(\mathtt{x}_i,\mathtt{x}_j)(1-\mathrm{NCD}(\mathtt{x}_i,\mathtt{x}_j)). \tag{2.20}$$

The strength of this measure is its modular architecture: The NCD can be replaced by another measure of information distance [Galas et al., 2010], and similarly, the data compressor used for approximating the Kolmogorov complexity, can be freely chosen. Furthermore, the equalizing function of NCD, i.e. the factor $d(1-d)$, where $d = \mathrm{NCD}(\mathtt{x}_i,\mathtt{x}_j)$, can be changed to any function that is zero at the endpoints $d = 0$ and $d = 1$ and positive on some subinterval $\mathcal{U} \subset (0,1)$. This optionality can, however, also be seen as a weakness of the measure, as different choices can lead to crucially different results. This is discussed in **Publication III**, where, following the ideas of [Nykter et al., 2008], *information diversity* is quantified instead of set complexity. In **Publications IV** and **V**, the set complexity itself is applied.

Chapter 3

Modelling and analysis of complex systems

The function of a complex system can be decomposed to the interplay between ever simpler objects. The vertebrate brain can be seen as the set of finely connected brain regions. The brain regions can, in turn, be decomposed to neurons and glial cells and the connections between them, these cells to the delicate entities of the cellular machinery such as mitochondria and the nucleus stored inside the cell membrane, these to macromolecules, molecules, atoms, and all the way to the elementary particles.

The deeper one goes into the smaller entities, the more identical the actors become. The networks of the brain are composed of a relatively small number of cell types, each of which consists of neurons with alike (although by no means identical [Ascoli et al., 2007]) morphology and functionality. This gives rise to a computational systems approach for studying these networks. If the dynamics of a single neuron can be modelled, and the type and strength of interaction among the neurons is known, then the collective activity in the network can be modelled as well. State-of-the art computer simulations allow the animation of up to millions of neurons in real time, depending on the required level of detail in the processes modelled.

This section deals with the two biological networks that play a central role in this thesis, namely, cortical networks of neurons and gene regulatory networks. First, an overview is given on the models for the structure of complex networks in section 3.1. Abstract models are presented, and for the cortical networks, a more biologically plausible model is introduced. The section 3.2, in turn, introduces the single-node dynamics as well as the emergent network dynamics in these systems.

3.1 Structure of complex systems

The structure of a complex system lays foundation to all collective activity in it. A connectivity graph representing the network structure can be obtained as a realization of a *random graph*

model. The simplest and most widely used random graph model is the Erdős-Rényi network model [Erdős and Rényi, 1960], where the network structure is characterized using a single parameter, namely, the probability p of finding an edge between two arbitrary nodes. The original model concerned undirected graphs, but its extension for directed graphs has been widely used as well. In directed graphs the model results in both in- and out-degree being binomially distributed as $\mathrm{Bin}(N-1, p)$. An alternative means for generating a random graph is to fix the number of inputs, and for each node, choose the inputs (or outputs) by random. This approach is extensively used in e.g. random Boolean networks.

There are several extensions of Erdős-Rényi models, e.g., the *Watts-Strogatz* [Watts and Strogatz, 1998] model of *small-world networks*. The small-world networks are characterized by short geodesic path length and high clustering coefficient — the properties found in many real-world networks, such as biological, social, and technological networks [Boccaletti et al., 2006]. In the original model, the nodes of a Watts-Strogatz network are first placed into a ring and connected to a constant number k of nearest neighbours. Afterwards, a fraction q of connections are randomly rewired. This model has been extensively used to describe the structure in various complex systems. Another popular extension is the *Barabási-Albert* [Barabási and Albert, 1999] model of scale-free networks. In this model, nodes are added to the network one after another and the *preferential attachment* rule directs the resulting network towards a structure that is hierarchical over different scales. Such a network is described by *power-law* distributed degree, meaning that a major part of the distribution obeys the law

$$P(\mathbf{k} = k) = ak^{\gamma} \tag{3.1}$$

for some constant a and exponent γ. The Barabási-Albert model allows tuning the scaling exponent γ of the power-law distribution. Both Watts-Strogatz and Barabási-Albert networks were originally introduced as undirected networks, but their extensions for directed networks have been widely applied as well.

In addition to these two seminal models, there are many other abstract random graph models. In **Publication III**, a model of *partly locally connected networks* (PLCN) is presented and applied. The model is similar to Watts-Strogatz networks in that it creates a continuum of graphs between randomly and locally connected networks. A grave difference is that the rewiring scheme in [Watts and Strogatz, 1998] chooses the new neighbour from a uniform distribution over all possible neighbours, while in the PLCNs, there is no distinct rewiring step but the neighbours are picked from a distance-dependent distribution one after the other. As a consequence, the Watts-Strogatz networks may have a few long-range connections even with a small rewiring probability q, while the length of the furthest reaching connections in the PLCNs are only gradually increased when moving from locally connected networks to random networks. Another difference is that the PLCNs are directed networks with a binomial in-degree distribution, while the original Watts-Strogatz networks are undirected networks with degree distribution sharper than that of Erdős-Rényi networks [Barrat and Weigt, 2000]. In **Publication VI**, directed Watts-Strogatz networks are employed and tuned in such a way that they are allowed to have an arbitrary in-degree distribution. The in-degree distribution can be freely chosen also in the other abstract network models introduced in **Publication VI**, where algorithms for producing

networks with increased numbers of a certain connectivity pattern are presented and applied. One of the network classes promotes the occurrence of feed-forward patterns[1], as the other network classes encourage the formation of directed loops of a certain length. Two specific choices for the in-degree distribution are considered, namely, the binomial distribution that is present in the widely used Erdős-Rényi networks, and the power-law distribution that is a typical feature of the scale-free networks [Barabási and Albert, 1999].

Abstract network models, especially the small-world and scale-free networks, are applicable to many different real-world applications [Boccaletti et al., 2006, Eguiluz et al., 2005]. Nevertheless, there is a rising trend to generate the structure of the network to more and more application-specific detail [Ascoli et al., 2007]. In computational studies of nervous systems, there are two mainstream approaches for this. The first approach is to model the processes underlying the formation of the system, namely, the growth of the neurons and the formation and maturation of the synaptic connections [Van Pelt et al., 2010]. By simulating such models one can achieve a number of network realizations where the connectivity is constrained by biological restrictions. Another approach is to rely on experimentally measured connectivity graphs in the system under study, and import them to the network simulations as such. These data are yet scarce, but there is a trend toward increasing amount of connectivity data and easier, world-wide access to such data [Insel et al., 2003]. This work employs the former approach in **Publications I**, **II**, **III**, and **VI**, either in a central or subsidiary role. In the following, this approach is described in more detail.

Simulating the growth of neuronal networks

The special function of neurons in information transmission is reflected in their tentacular shape [Kandel et al., 2000]. The soma of a neuron extends projections that can be roughly categorized into *dendrites* and *axons*, commonly referred to as *neurites*. The dendrites receive inputs from other neurons, and in case of strong enough excitatory input signals, produce an *action potential* in the neuron. The action potential, also called a *spike*, then proceeds along the axon and activates synapses that may excite other neurons in a similar way or, alternatively, inhibit the activity in them. Hence, much of the prequisites for information processing lies in the pattern of synapses between the neurons [Sporns et al., 2005], also referred to as the *synaptic map* or simply as the *structure* of the neuronal network — although the term "structure" could be thought to include much more information on the anatomical details of the network.

The formation of the neuronal network is an excessively complex phenomenon affected by processes on different scales all the way from molecular to behavioral or cognitive level [Kandel et al., 2000]. Several attempts have, however, been made to model the growth of neurons and the resulting pattern of synapses [Van Ooyen, 2003]. One tool for such a purpose is the NETMORPH [Koene et al., 2009] simulator that combines statistical models of neuronal growth and

[1]The basic form of the feed-forward loop is the Motif 5 in Figure 2.1, but the graph algorithm in **Publication VI** promotes the occurrences of all motifs that include the required pattern. Among the three-node motifs, Motifs 6, 10, 11, 12, and 13 (see Figure 2.1) include at least one instance of the feed-forward loop.

synapse generation based on axo-dendritic distance. Another tool, the CX3D [Zubler and Douglas, 2009] simulator, is a general platform for simulating interactions between biological entities, such as neuron somata and neurites, as well as different chemical species. In addition, CX3D supports the use of external, statistical rules governing the growth of neurons, which makes it a fair parallel for NETMOPRH. In both simulators, the parameters governing the growth as well as the number and initial locations of the neurons can be changed, and the pattern of synaptic connections for each parameter set can be obtained. Although the strengths and locations of the synapses are temporally influenced by various chemical processes, the affinity-based rules for synapse locations can make decent predictions on e.g. the distribution of synapse locations across the neurites [Hill et al., 2012].

In the NETMORPH simulator, the growth of the neurons is first simulated such that all the neurons grow independently of each other, and afterwards, the potential synapses are placed wherever an axon and a dendrite of distinct cells are close enough. The branching and elongation occur solely on the terminal segments of the neurons, and their magnitude depends on time and the morphology of the neuron. The rate of elongation is described as follows [Koene et al., 2009, Van Pelt and Uylings, 2003]:

$$\nu(t) = \nu_0 n(t)^{-f}, \tag{3.2}$$

where $\nu(t)$ represents the average elongation rate of the terminal segments at time t. The parameter ν_0 is the initial rate of elongation, $n(t)$ is the number of terminal segments in the neuron, and the constant parameter f reflects the level of competition for resources between terminal segments. Setting $f = 0$ makes the growth rate independent of the number of terminal segments, while positive values of f make the elongation rate decrease with each branching. The branching is governed as follows [Koene et al., 2009, Van Pelt and Uylings, 2003]:

$$P(\text{Segment } j \text{ branches during } (t_i, t_i + \Delta t]) = n(t_i)^{-c} b_\infty e^{-t_i/\tau}(e^{\Delta t/\tau} - 1)\frac{2^{-s\gamma_j}}{\alpha_i}. \tag{3.3}$$

Here, the constant parameter c determines the level of competition over resources for branching, and parameters b_∞ and τ represent the intensity and time constant of the branching. Different branching probabilities can be given for terminal segments of different *centrifugal order* γ_j through the parameter s. The centrifugal order of a segment is the number of segments lying between it and the soma, or in other words, the number of turning or branching points between the considered segment and the soma. For $s > 0$, the branching is more likely to happen in the terminal segments near the soma (small γ_j), while for $s < 0$ the branching is the more likely the further (larger γ_j) the terminal segment is from the soma. To compensate for this factor, the branching probability is divided by the normalizing variable

$$\alpha_i = \frac{1}{n(t_i)} \sum_{k=1}^{n(t_i)} 2^{-s\gamma_k}. \tag{3.4}$$

Finally, the probability of changing the direction of outgrowth is given as [Koene et al., 2009]

$$P(\text{Segment } j \text{ turns during } (t_i, t_i + \Delta t]) = r_L \Delta L_j(t_i), \tag{3.5}$$

where the parameter r_L describes the frequency of turning points and $\Delta L_j(t_i)$ is the change in the length of the terminal segment j during the time step $(t_i, t_i + \Delta t]$. The magnitude of changes in direction can be controlled as well.

The CX3D, in turn, allows modelling of temporal processes in more detail. The interactions between physical objects, such as neurites and somas, are taken into account [Zubler and Douglas, 2009]. The neuron somas are modelled as balls, while the neurites are modelled as connected springs. The growth of the neurites is modelled through the changes in the spring constant of the springs that represent the terminal segments, and these changes can be given similar statistical dependencies as in NETMORPH, as shown in **Publication II**. Figure 3.1 illustrates the growth of a neuron, extracted from a NETMORPH simulation carried out in a 2D domain.

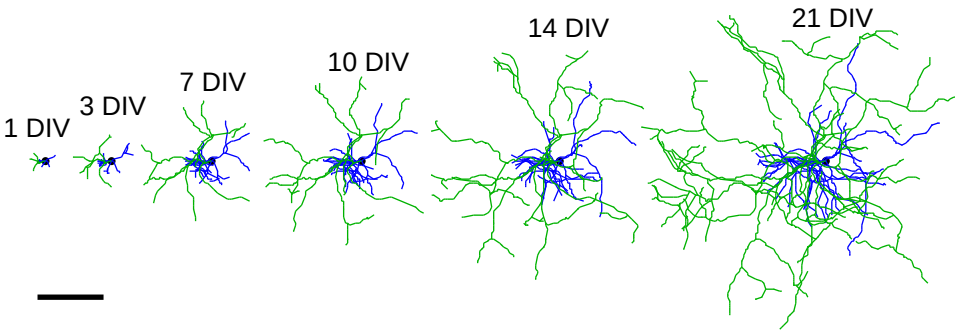

Figure 3.1: Illustration of the morphology of a neuron in a NETMORPH simulation of a cell culture at first, third, seventh, tenth, 14th and 21st day *in vitro* (DIV). Scale bar 200µm. The green branches represent the axonal tree, while the blue branches constitute the dendritic tree.

The NETMORPH simulator combines the models governing the four mentioned events: Elongation, branching and turning of the terminal segments, and the formation of synapses. These four phenomena are themselves simple, as described in Equations 3.2, 3.3, and 3.5, but include a number of interactions. Elongation is dependent on the past branching events, but independent of the turning events. Branching and turning are by construct independent of each other and of the elongation, but can be linked through a parameter defining the minimal segment length that prevents too short terminal segments from turning or branching [Koene et al., 2009]. The synapse formation does not affect any of the mentioned three events, but is influenced by the locations and morphologies of the neurons and thus depends on all of them.

The state of the system can be defined as the collection of the segment starting points, lengths and directions (and notions on which is connected to which), and could therefore be considered as a variable-dimensional stochastic continuous-time continuous-state system. Nevertheless, the system does not include a Brownian noise component, and cannot therefore be described by an SDE. By contrast, certain subsystems of the system, for example the number of terminal segments in a neuron, can be regarded as a *continuous-time discrete-state* system. Advanced simulation methods, such as Gillespie's stochastic simulation algorithm [Gillespie, 1977], could therefore be applied. Employing such methods is, however, out of the scope of this thesis, and

is left for future work.

3.2 Dynamics of complex systems

In this section, the dynamics of the two types of complex systems that are central to this work are considered. For the cortical networks, *point neuron* models[2] with various levels of detail are employed, whereas for the genetic networks the simplistic model of random Boolean networks is used. In both cases, the single-node dynamics are relatively (or extremely) simple, yet the incorporation of an adequate number of nodes leads to complex temporal activity patterns. The neuronal network model is introduced in Section 3.2.1, while the Boolean network model is addressed in Section 3.2.2.

3.2.1 Neuronal networks: Models for neuron and synapse dynamics

The *neuron doctrine* states that a neuron is the basic unit of transferring and processing of information in any neural system [Kandel et al., 2000]. The main mechanism for this processing is the generation and propagation of action potentials, which is an effect of successive opening and closing of the *voltage-gated ion channels*. The main actors are Na^+, Cl^-, Ca^{2+}, and K^+ channels, each of which reacts to the changes in intra- and extracellular ionic concentrations [Kandel et al., 2000]. The proportion of these concentrations determines the difference in potential between the cell and the extracellular medium according to the *Nernst equation*, or its extension, the *Goldman-Huxley-Katz equation* [Junge, 1992]. The dynamics of the membrane potential can be described using the *Hodgkin-Huxley* (HH) model or its variations, which can generally be written as

$$C_m \frac{dV_m}{dt} = \sum_{\text{ionic channel type } i} g_i S_i (V_i^{\text{rev}} - V_m) + I. \tag{3.6}$$

Here, V_m is a temporal variable representing the membrane potential, which is usually measured with respect to the potential of the extracellular medium. The evolution of the membrane potential depends on the ionic conductances g_i, the *reversal potentials* V_i^{rev} of the ions, i.e., the potentials at which no diffusion of the considered ion would occur between the cell and its surroundings, and the *ionic gating variables* S_i. The rate of the evolution is determined by the *membrane capacitance* C_m. The gating variables are dimensionless and usually restricted on interval [0,1], where $S_i(t) = 0$ means that none of the channels of type i are open at time t, and $S_i(t) = 1$ means that all of them are open. The gating variables are temporally dependent on the membrane potential through non-linear differential equations (see e.g. **Publication VI**).

[2]The term "point neuron" refers to a model of a neuron, where the temporal variables, such as the membrane potential, are considered to be constants over the whole spatial domain of the neuron. The opposite of a point neuron is a *compartmental neuron* model, where the neuron consists of distinct interconnected segments that each have their own temporal variables [Dayan and Abbott, 2001]. The neurite segments of compartmental neurons may be modelled as *passive* or *active* segments, depending on whether they only conduct the changes in the membrane potential through diffusion equations or if they also have intrinsic dynamics in their ionic gating variables. In this work, only point neuron models are considered.

The current term I represents all other currents applied to the cell, and could include synaptic currents, currents applied through external electrodes, or just noise.

A down-side of Equation 3.6 is that it is typically time-consuming to solve it numerically due to the fine temporal scale that is required at the time of the spikes. A computationally less expensive neuron model is the *leaky integrate-and-fire* (LIF) model, which is written as

$$C_m \frac{dV_m}{dt} = \begin{cases} g_L(V_L^{\text{rev}} - V_m) + I, & \text{if } t - t_{\text{last spike}} > \tau_{\text{ref}} \\ 0, & \text{otherwise} \end{cases} \qquad (3.7)$$
$$\text{If } V_m > V_{\text{thr}}, \text{ then emit a spike and set } V_m \leftarrow V_{\text{rest}}$$

In this model, the collection of ionic currents is replaced by a single *leak* current that drives the membrane potential toward the leak reversal potential V_L^{rev}. The spikes are discrete events that take place when the membrane potential exceeds the *threshold potential* V_{thr}. Each spike is followed by an instantaneous fall to the *resting potential* V_{rest} and a *refractory period* of length τ_{ref}. During the refractory period the membrane potential stays at the resting potential. Another widely used, fairly recent activity model is the Izhikevich model [Izhikevich, 2003]. This model mixes a spiking threshold potential similar to the one in LIF model, and a recovery variable that represents the opening and closing of the ionic channels [Izhikevich, 2003]. The Izhikevich model is used in **Publication III**, while in **Publication VI** the LIF model and an extension [Golomb et al., 2006] of the HH model are employed. The time course of the membrane potential variable in each of these models is illustrated in Figure 3.2. The dynamics of these three types of models, together with many other neuron models, are reviewed in [Izhikevich, 2004].

Similarly to the modelling of the internal dynamics of a neuron, there are many possible levels of detail for modelling the synaptic currents. What is common for all models of chemical synapses is that the synapse becomes activated at or after some delay from the time of an action potential taking place at the presynaptic neuron. The synapse can have either an *excitatory* or *inhibitory* effect on the post-synaptic neuron, meaning that it either increases or decreases the membrane potential of the post-synaptic neuron. The main excitatory synaptic currents in mature neurons are those mediated by AMPA (α-amino-3-hydroxy-5-methylisoxazole-4-propionic acid) and NMDA (N-methyl-D-aspartic acid) receptors, while the main inhibitory synaptic current is that mediated by GABA (γ-aminobutyric acid) receptors. In reality, both excitatory and inhibitory outward synaptic currents can coexist in a neuron [Gutiérrez, 2005], but experimental evidence indicates that most neurons are specialized into projecting either only excitatory or only inhibitory currents (see e.g. [Connors and Gutnick, 1990]). For this reason, the neurons in the brain can be roughly categorized into excitatory and inhibitory neurons, although dozens of subcategories exist. By contrast, the inward synaptic currents to practically all types of neurons are diverse combinations of different types of currents, although the distal parts of the dendritic tree may be specialized in receiving different types of synaptic currents from those received by the proximal parts (see e.g. [Megías et al., 2001]). This work utilizes synaptic currents to point neurons only, and hence such fine distinctions are neglected.

The synaptic currents to LIF neurons are most often described using either delta functions or exponential decay functions. In this work, the exponentially decaying currents are used due

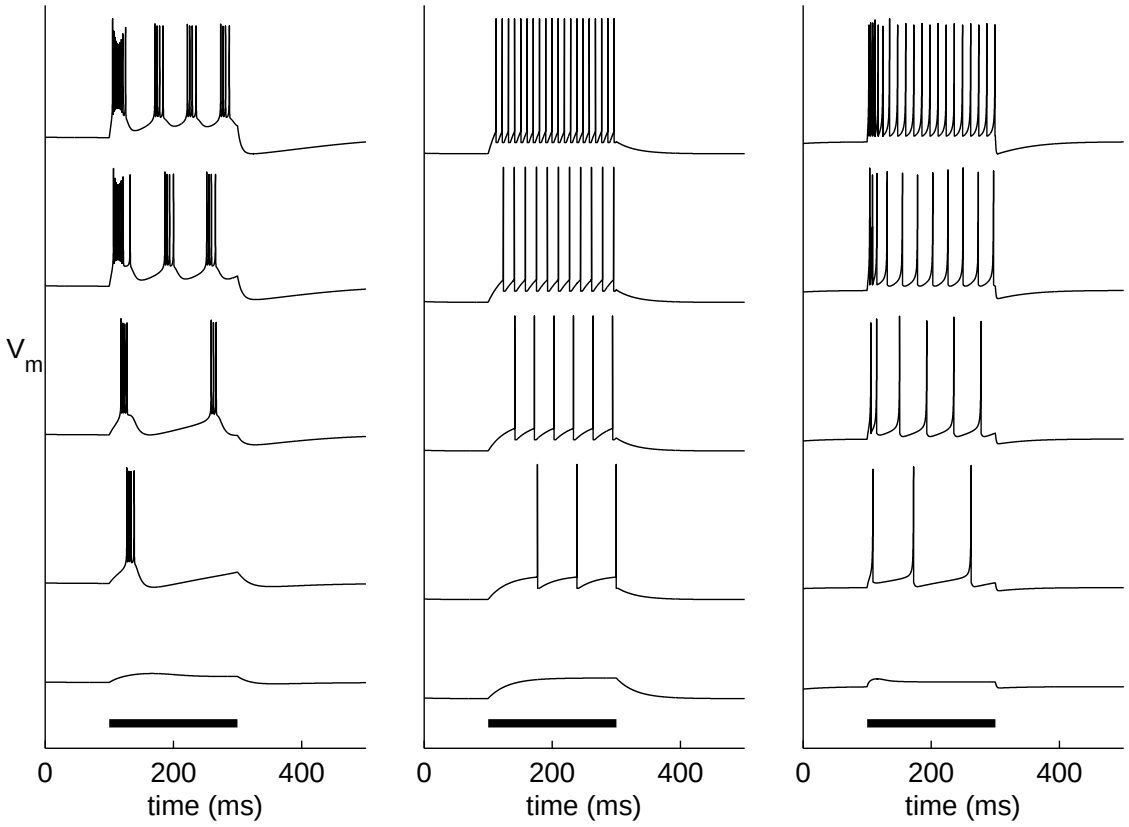

Figure 3.2: Illustration of single-neuron dynamics according to extended HH-model (left), LIF model (middle), and Izhikevich model (right). The x-axis shows the time, and the y-axis shows the membrane potential of the model neuron. Each model neuron is initially at rest. Between $t = 100$ ms and $t = 300$ ms (thick bar), the neuron is given a constant input current, otherwise the neuron does not receive any input. The different curves represent the neuron response to different amplitudes of the input current. With low input, the neuron remains silent (lowest curves), while for higher input currents the neurons fire during the input, yet return to silent mode after the cessation of the input. The model parameters for the extended HH-model and LIF model are identical to the ones used in **Publication VI**, and the Izhikevich model parameters are the default parameters given in [Izhikevich, 2003]. The current amplitudes are (from bottom to top) 0.33, 0.70, 1.00, 3.00, and 4.00 μA/cm^2 in the extended HH-model, 14.75, 15.25, 16.00, 17.50, and 21.00 pA in the LIF model, and 16.00, 16.06, 16.18, 16.41 and 17.30 (dimensionless current units) in the Izhikevich model. The time series were solved using forward Euler method with resolutions Δt=0.0025 ms (extended HH model), Δt=0.5 ms (LIF model), and Δt=0.05 ms (Izhikevich model). The spikes in the LIF model time courses are highlighted by setting the membrane potential to a high value for one time step.

to their better fit to biological data. At the time of the pre-synaptic spike, or after a possible transmission delay, the synaptic current is set to a non-zero value, representing the opening of

the neurotransmitter-gated ionic channels. This is followed by the smooth decay of the current, which represents the gradual closing of the channels. The exponential shape of the synaptic current allows the use of exact integration methods for solving the time course of the membrane potential in an LIF neuron. The reset value of the current following the pre-synaptic spike may be a constant or a dynamical variable. In [Tsodyks et al., 2000], a dynamical scheme is used in order to capture such phenomena as *short-term depression* and *facilitation*. These two are phenomena, where the amplitude of the synaptic current is either decreased or increased, respectively, from the amplitude of a recently occurred spike at the considered synapse. The state of the synapse is described by three to four dynamical variables, x, y, z, and u, where u is constant in synapses that do not express facilitation. The variables x, y, and z represent the fraction of synaptic resources in recovered, active, and inactive state, respectively, and the variable u represents the fraction of resting state resources that are ready to be released. Their dynamics are described as follows:

$$\begin{aligned}
\frac{du}{dt} &= -\frac{u}{\tau_{\text{facil}}} + U(1-u)\delta_{t_{\text{sp}}}(t) \\
\frac{dx}{dt} &= \frac{z}{\tau_{\text{rec}}} - ux\delta_{t_{\text{sp}}}(t) \\
\frac{dy}{dt} &= -\frac{y}{\tau_I} + ux\delta_{t_{\text{sp}}}(t) \qquad (3.8) \\
\frac{dz}{dt} &= \frac{y}{\tau_I} - \frac{z}{\tau_{\text{rec}}}, \qquad (3.9)
\end{aligned}$$

where t_{sp} is the time of the presynaptic spike. With each spike, the value of u is increased by $U(1-u)$, and an amount ux of resources are transferred from resting to active state[3]. This is represented by the positive change in y and negative in x. After the spike, there is a smooth transition from active into inactive resources with time constant τ_{rec}, and another transition from inactive to resting state resources with time constant τ_I. In addition, the amount of readily releasable resources decreases with time constant τ_{facil}. The facilitation can be removed by letting this time constant approach zero. In such a case, the variable u returns to zero in no time after the spike, and hence, the fraction of x transferred to y with the spikes is always Ux. The time constants τ_{rec} and τ_I and the parameter U together control the synaptic depression. The larger the parameter U, the more rapidly the resources are used. The shorter the time constants τ_{rec} and τ_I are, the quicker the resources are replenished.

The synaptic current to neuron j is a weighted sum of the amounts of active state resources (y) in the synapses that input to the neuron:

$$I_{\text{syn},j}(t) = \sum_i w_{ij} y_{ij}(t). \qquad (3.10)$$

The parameter w_{ij} stands for the strength and type (positive for excitatory, negative for inhibitory neuron i) of the synapse between neurons i and j — note the permutated roles of i and

[3]Note that these two state updates that follow a pre-synaptic spike are successive, in the above order, and not synchronous.

j compared to those in [Tsodyks et al., 2000].

In networks of HH type of neurons, no discrete spike events occur, but the dynamics of a synaptic current depend on the membrane potential of the presynaptic neuron. In these models, the synaptic interaction is communicated by gating variables that react to high values of membrane potential in the pre-synaptic neuron. When the pre-synaptic membrane potential exceeds a certain threshold, the gating variable of the synapse is increased. The gating variable, together with the post-synaptic membrane potential, determine the value of the synaptic current in a manner similar to Equation 3.6. For detailed equations, see the supporting information of **Publication VI**.

Analysis of observed network dynamics

Various phenomena can be observed when neurons are interconnected into a network. These include synchronization, population oscillations [Ermentrout and Chow, 2002], and persistent activity [Brunel, 2000b], to name a few. The main neural phenomenon studied in this thesis is the formation of *network bursts*. The network bursts occur as a result of recurrent excitation, when scarce spiking activity is spread over a large population and soon afterwards diminished. Such synchronized activity has been observed in maturing (see e.g. [Chiu and Weliky, 2001]) and behaving (see e.g. [Buzsáki et al., 1983]) animals, but it can also be observed in cultured *in vitro* networks [Robinson et al., 1993, Keefer et al., 2001]. Once initiated, a network burst may cease for several reasons (see e.g. [Compte, 2006] that reviews the relevant mechanisms, although the focus is on longer persistent activity than the time-scale of the aforementioned bursts). In cultured networks, the most likely explanation for the cessation of a burst is the depletion of glutamatergic resources [Maeda et al., 1995], which temporarily weakens the recurrent excitation, bringing the propagation of the burst to an end. This mechanism has been extensively used in computational models of network bursting activity [Tsodyks et al., 2000, Gritsun et al., 2010], **Publications III** and **VI** being no exception. Figure 3.3 shows typical bursting activity produced by the LIF model (Equation 3.7) where the neurons are connected by synapses with short-term dynamics (Equation 3.8).

For illustrations on HH type of model and Izhikevich model network dynamics, see the example figures in **Publications VI** and **III**. Note, however, that there was an error in the implementation of the Izhikevich model in **Publication III**. The article claims to use model parameters $a_{\text{exc}} = 0.02$, $a_{\text{inh}} \in [0.02, 0.1]$, $d_{\text{exc}} \in [6, 8]$, and $d_{\text{inh}} = 2$, both of which affect the updating of the variable r (see Equation 6 in **Publication III**). Due to an error in the simulation code, the update rule rendered the values of r near to zero, and hence, the results shown in **Publication III** closely represent the case $a_{\text{exc}} = a_{\text{inh}} = d_{\text{exc}} = d_{\text{inh}} = 0$, where the variable r is initially at zero. With such model parameters, the variable r remains exactly at zero instead of fluctuating around it. The corrected version of Table A2 of **Publication III** is shown in Table 3.1. Re-running the simulations with these parameters shows that the differences between the bursting frequencies in different network types remain qualitatively the same. The corrected entries of the numbers of bursts that were reported in Table 1 of **Publication III** are shown in Table

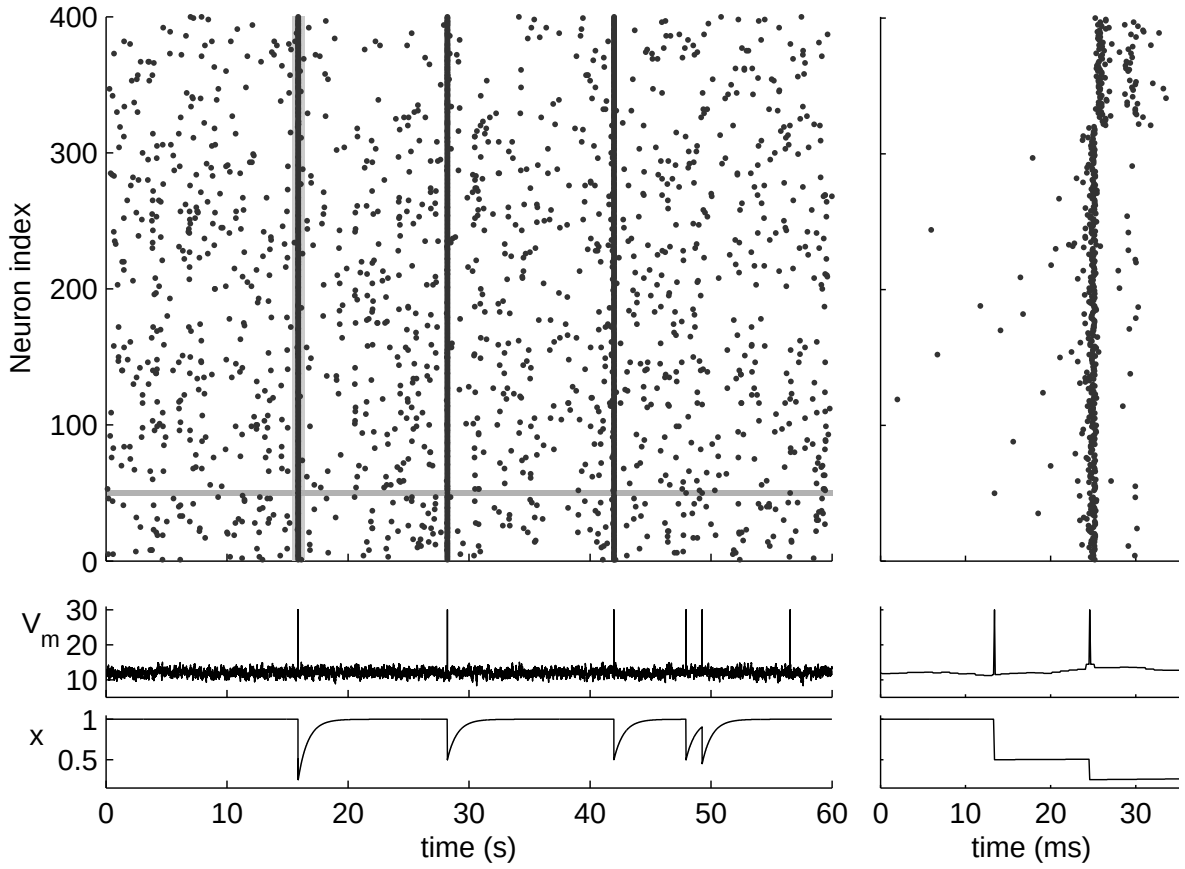

Figure 3.3: Illustration on the network bursts. A network of $N = 400$ LIF neurons (Equation 3.7) is used with short-term dynamical synapses (Equation 3.8). Each neuron is given a white noise component, making them spontaneously active. The model parameters are taken from **Publication VI**, except for the noise level (6.4 mV/ms) and the synaptic weights (η =9.6). The neurons are randomly connected with the connection probability $p = 0.2$. The simulation time is 60s. On the panels on the left, the dynamics during the whole simulation time are illustrated, while the panels on the right focus on a short time period around the burst indicated by the grey vertical bar. The upper panels show the population spike trains. The neurons labelled with indices 1–320 are excitatory, while neurons 321–400 are inhibitory. In the middle and lower panels, the single neuron dynamics of a selected neuron (grey horizontal region in the upper-left panel) are illustrated. The middle panels show the membrane potential (V_m), while the lower panels show the fraction of synaptic resources in the resting state (x) as a function of time. The action potentials are indicated by setting the membrane potential to +30mV for one time step in the middle panels. Following each action potential, there is a discrete fall in the variable x, which is then smoothly replenished in the absence of action potentials.

3.1. The conclusions on the rest of the bursting properties and the information distances that are stated in **Publication III** remain qualitatively unchanged as well (data not shown).

Table 3.1: Corrections for Table A2 and 1 in **Publication III**. The Izhikevich model parameters are shown on the upper table, and the corresponding numbers of bursts are shown below. Note that the values of parameters b in Table A2 are insignificant, as they only affect through the multiplication by a, which is zero.

Table A2 | Izhikevich model parameters.

Model parameters	Excitatory	Inhibitory
a	0	0
b	0	0
c	-65+15$\mathbf{r}_e^2$	-65
d	0	0

Table 1 | Bursting rates of networks of different structure classes.

	W = 0	**W = 1**	**W = ∞**	**NETMORPH**
$p = 0.1$	1.7 ± 1.2	4.8 ± 1.6	10.0 ± 2.0	6.1 ± 1.8
$p = 0.16$	11.7 ± 1.7	13.3 ± 1.3	17.1 ± 2.6	14.7 ± 1.5

Values shown: mean ± SD in bursts/min, calculated from 20 different 1-min recordings per table entry.

The bursts can be effectively detected as follows. First, all the spikes are divided into *candidate bursts* by their spike times in such a way that two successive spikes belong to the same candidate burst if and only if their distance is less or equal to a named constant, *maximum inter-spike interval* [Chiappalone et al., 2006]. In other words, two spikes, whose spike times are t and τ, belong to the same candidate burst if and only if there exists a set of intermittent spikes with spike times $\mathcal{T} = \{t_1, \ldots, t_k\}$ such that $\max(|t - t_1|, |t_1 - t_2|, \ldots, |t_{k-1} - t_k|, |t_k - \tau|) \leq \Delta t$, where Δt is the maximum inter-spike interval. However, many of the candidate bursts might consist of single spikes, and hence, only bursts whose size exceeds a certain threshold are considered as bursts. This can be done by accepting only such candidate bursts that consist of more than a named number of spikes. In addition, one can restrict to consider only such bursts that employ a wide enough population — that is, only such bursts in which a large enough number of individual neurons fired are accepted. In **Publication III** the former condition is used, whereas in **Publication VI** both conditions are applied. The use of both conditions helps to rule out bursts that are spatially too local, i.e., network bursts where only a fraction of the population, although densely spiking, contributes to the burst. Such local bursts could emerge in networks with high in-degree variance, given that the neurons with high in-degree are strongly coupled to each other. This is a possible outcome in certain network classes considered in **Publication VI**, but is hardly an issue in the networks of **Publication III**, and hence the simpler burst detection scheme.

In **Publications III** and **VI**, the numbers and lengths of the bursts are studied in various types of neuronal networks. These measures are descriptive aspects of the dynamics of bursting networks, but other standard measures for characterizing the activity exist as well. Synchronicity of spiking events in the network can be assessed using the *cross-correlation* method [Perkel et al.,

1967]. Given the spike trains of two neurons, one can binarize them into arrays $\{s_i^{(1)}\}_{i\in\{1,\dots,l\}}$ and $\{s_i^{(2)}\}_{i\in\{1,\dots,l\}}$, where l is the length of the arrays. The ith entry of the array corresponds to the number of spiking events of the considered neuron during the interval $[(i-1)\Delta t, i\Delta t)$, where Δt is the bin length. The cross-correlation between the two arrays, when $s^{(2)}$ is shifted by a lag τ, can be calculated as

$$\mathrm{CCG}_{s^{(1)},s^{(2)}}(\tau) = \sum_{i=1}^{l}(s_i^{(1)} - \lambda_1)(s_{i+\tau}^{(2)} - \lambda_2), \tag{3.11}$$

where λ_1 and λ_2 are the average spike counts per bin, i.e., $\lambda_j = \frac{1}{l}\sum_{i=1}^{l} s_i^{(j)}$. Assuming that the values of the arrays $s^{(1)}$ and $s^{(2)}$ are zero outside the considered indices $\{1,\dots,l\}$ and that the average values λ_1 and λ_2 are representative as the mean spiking frequencies over the whole arrays, we can write

$$\sum_{i=1}^{l} s_{i+\tau}^{(2)} \approx (l - |\tau|)\lambda_2.$$

Hence, we have

$$\begin{aligned}\mathrm{CCG}_{s^{(1)},s^{(2)}}(\tau) &\approx \left(\sum_{i=1}^{l} s_i^{(1)} s_{i+\tau}^{(2)}\right) - \lambda_1\cdot(l-|\tau|)\lambda_2 - \lambda_2\cdot l\lambda_1 + l\lambda_1\lambda_2 \\ &= \left(\sum_{i=1}^{l} s_i^{(1)} s_{i+\tau}^{(2)}\right) - (l-|\tau|)\lambda_1\lambda_2. \end{aligned}\tag{3.12}$$

This function, $\mathrm{CCG}_{s^{(1)},s^{(2)}}(\tau)$, is called the *cross-correlogram* between the spike trains. Its integral over a delay period $\tau \in \{-k,\dots,k\}$, where the constant $k \in \mathbb{N}$ is sufficiently small, reflects the coincidence of the spiking events in the two spike trains. The area of the cross-correlogram is normalized by the average spike counts, and hence, is calculated as

$$\begin{aligned}\mathrm{CCGA}(s^{(1)},s^{(2)}) &= \sum_{\tau=-k}^{k} \frac{1}{\lambda_1\lambda_2}\mathrm{CCG}_{s^{(1)},s^{(2)}}(\tau) \\ &= \sum_{\tau=-k}^{k}\left(\left(\frac{1}{\lambda_1\lambda_2}\sum_{i=1}^{l} s_i^{(1)} s_{i+\tau}^{(2)}\right) - (l-|\tau|)\right). \end{aligned}\tag{3.13}$$

Furthermore, the area of the cross-correlogram can be normalized by the auto-correlogram areas in order to cancel the effect of variable auto-correlations. The derived quantity

$$\mathrm{CCC}(s^{(1)},s^{(2)}) = \frac{\mathrm{CCGA}(s^{(1)},s^{(2)})}{\sqrt{\mathrm{CCGA}(s^{(1)},s^{(1)})\mathrm{CCGA}(s^{(2)},s^{(2)})}} \tag{3.14}$$

is called the *cross-correlation coefficient* [Shadlen and Newsome, 1998] between the two spike trains.

The constant k that determines the range of considered time lags is usually chosen according to the time scale of the presumed interaction between the elements. If chosen too small, only very close-by spiking events are registered as concurrent spikes, and chosen too large, any two spikes may be considered concurrent (although, the formula implicitly gives somewhat higher weight to those spikes that are near to the compared spike). A typical value used in spiking neuronal networks is such that value of $k\Delta t$ is several tens of milliseconds. In **Publication III**, where the cross-correlation coefficients between simulated spike trains of neurons in a bursting network are estimated, a value of $k\Delta t = 50$ ms is used.

This section has introduced a number of modelling schemes for the dynamics of both individual neurons and the connections between them, and presented means for analyzing the collective activity. Depending on the size of the system, the neuronal network simulations can be computationally very exhaustive. Recently, specialized tools for the solution of the ODEs governing the neuronal network dynamics have been introduced, including the NEST [Gewaltig and Diesmann, 2007] and NEURON [Carnevale and Hines, 2006] simulators, and many others [Brette et al., 2007]. The former is specialized into simulating networks of integrate-and-fire neurons (although also supports more complex neuron models), while the latter is especially efficient in solving Hodgkin-Huxley type of equations, both in point neuron models as well as compartmental models. Both simulators use efficient integration schemes for the solution of the temporal variables: NEST employs an exact solution whenever possible, while NEURON uses an adaptive time step integration scheme. The use of such schemes restricts the ways to involve stochasticity. Two widely adopted approaches to include the noise in these simulators are randomly timed input events (e.g., Poissonian spike train as an input), or piece-wise constant random currents [Brette et al., 2007]. Both approaches are arguable when the noise is considered to include inputs from neurons outside the modelled system. The latter approach is, however, closer to the SDE approach (although the former approach also converges to SDE equations in the limit of increasing input frequency [Tuckwell, 1988]) and might account for a wider variety of sources of noise, and is hence employed in this thesis in **Publications III** and **VI**. The NEST simulator was used for the simulations of the integrate-and-fire model in **Publication VI**, while the NEURON simulator was used for validation purposes only in the Hodgkin-Huxley type of model in **Publication VI**.

3.2.2 Boolean network model

Boolean networks were first proposed as a model for genetic regulatory networks [Kauffman, 1969], but later, they have become a widely-applied tool for general systems science. A Boolean network consists of N nodes that can have either 0 ("off") or 1 ("on") as their state. The nodes receive inputs from other nodes, and the state of the node at the next time step is determined by the combination of the input nodes' states. The framework of *probabilistic Boolean networks* also allows a noise component that can be incorporated in a multitude of ways (see e.g. the choice for the directions of movement after a collision of two particles in the lattice gas system as described in **Publication IV**). The simplest means for including a noise component in a Boolean network is that the outcome of each node is flipped with probability p_{flip}. Such networks are generally

called *noisy Boolean networks*, although the term could refer to Boolean networks with other types of stochasticity as well, see for instance [Klemm and Bornholdt, 2005].

Mathematically, a noisy Boolean network is a Markov chain, where there are 2^N possible states and a well-defined transition probability between all of them. The construction of such transitivity matrix is, however, unnecessary and impractical due to its large size. Instead, each node is updated independently of others as follows:

$$\mathbf{x}_i(t+1) = f_i(\mathbf{x}_{I_{i,1}}(t), \mathbf{x}_{I_{i,2}}(t), \ldots, \mathbf{x}_{I_{i,k_i}}(t)) \oplus W_i(t) \tag{3.15}$$

The Boolean variable $\mathbf{x}_i(t)$ stands for the state of the node v_i at time $t \in \mathbb{N}$. The index variables I_{ij}, where $0 < j \leq k_i$, are the indices of the input nodes of the node v_i, and k_i is the number of them. The function $f_i : \{0,1\}^{k_i} \to \{0,1\}$ is a Boolean function that maps the combination of the input states into the future state of the node. The variables $W_i(t), t \in \mathbb{N}$ are independent, identically distributed Bernoulli random variables with parameter p_{flip}, and the operator $\oplus$ is the XOR operator. In other words, the state of the node v_i is given the value determined by the function f_i when $W_i(t) = 0$ (which occurs with probability $1 - p_{\text{flip}}$), and the opposite value when $W_i(t) = 1$ (occurring with probability p_{flip}).

The noiseless Boolean networks are a valuable tool in studies of attractor theory. Due to the finite number of states of the network and a deterministic update rule, the system always ends up going around a cycle of states, and the length of this cycle is between 1 and 2^N. These cycles are called *attractors* or *steady-state cycles*. The attractors with cycle length 1, representing a case where the state stays fixed after arriving to it, is called a *point attractor*. The networks can have many different attractors, and depending on the initial state, the network falls on exactly one of them. The states of the network can thus be divided to *basins of attraction*, each of which represents the subset of the state space that leads to a certain attractor. The number of attractors can vary between 1 and 2^N as well. The extreme cases can be easily constructed. The "identity" network, where each node retains its state, has 2^N point attractors, and the "null" network, where each node is always reset to 0, has exactly one attractor, which is also a point attractor. Another extreme among the single-attractor networks could be the one that goes through all 2^N possible states in a cyclic order:

$$(0,0,0,\ldots,0) \mapsto (1,0,0,\ldots,0) \mapsto (0,1,0,\ldots,0) \mapsto$$
$$(1,1,0,\ldots,0) \mapsto \ldots \mapsto (1,1,1,\ldots,1) \mapsto (0,0,0,\ldots,0).$$

In this network, the first node v_1 changes its output every time step, and the other nodes v_j ($j > 1$) change their output if an only if the outputs of all the earlier nodes v_i with $i < j$ are 1. Construction of such a long-attractor network requires a large number of connections, as the number of inputs of the node v_i is $k_i = i$. For comparison, the nodes of the "null" network need not receive any inputs, and the nodes of the "identity" network require but one input, i.e., a connection from the node to itself.

Rich Boolean network dynamics can be obtained merely by picking the connections and the input functions f_i by random. Such networks are called *random Boolean networks* (RBN), and they can show *ordered*, *chaotic*, or *critical* dynamics, depending on the way they are generated. The

ordered dynamics are such that the perturbations applied to the system tend to be suppressed, and by contrast, chaotic dynamics are such that make the perturbations increase by time. These two regimes are separated by the critical regime, where the average perturbation size remains fixed. As an example, a random Boolean network, where each node has $k = 2$ inputs and where the outcomes of the Boolean functions are assigned by random with equal probabilities of 0 and 1 for each combination of the input states, has been shown to possess critical dynamics [Aldana et al., 2003]. The RBNs with and without noise have been used as a model for, e.g., cell type differentiation [Villani et al., 2011]. Typical RBN dynamics are illustrated in Figure 3.4. In this work, RBNs are considered in **Publications IV** and **V**. In the latter, the effect of the noise on the temporal complexity is studied, while the former concentrates on the noiseless case. **Publication IV** also formulates a lattice gas system as a probabilistic Boolean network, and analyzes the complexity of the dynamics therein.

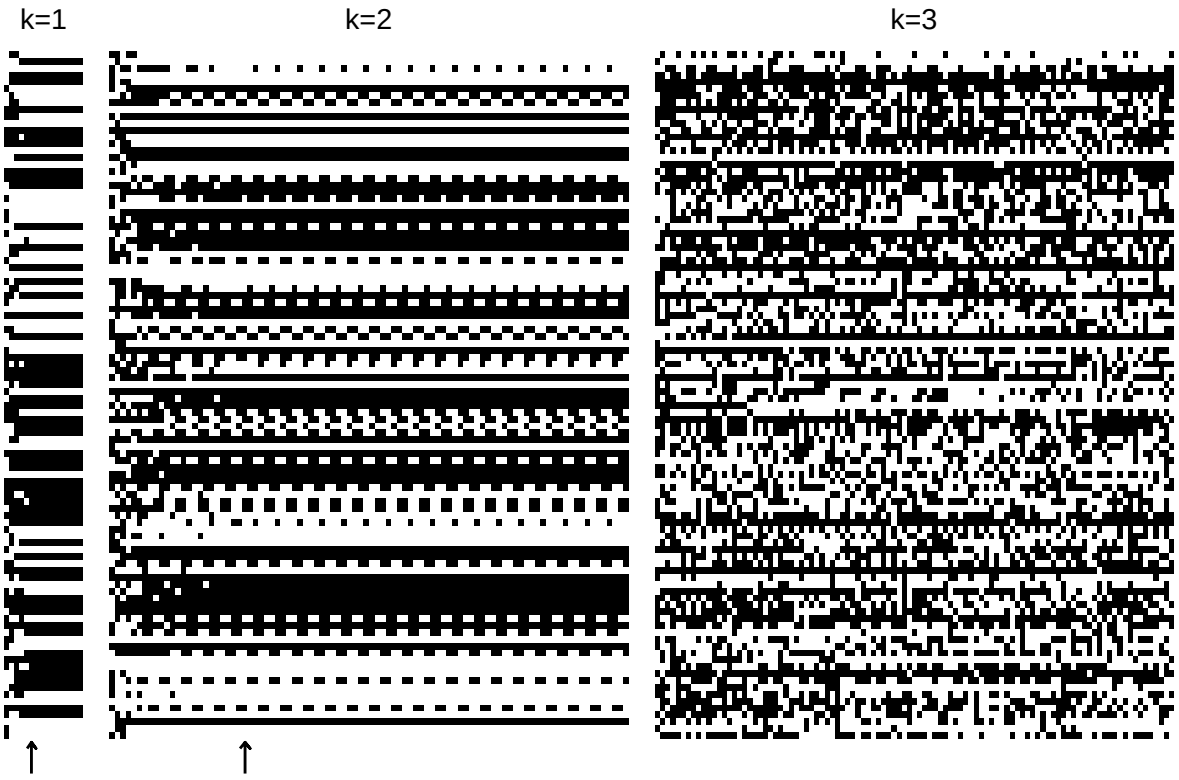

Figure 3.4: Illustration of RBN dynamics. The x-axis represents the time t, and y-axis is the node index. White color stands for the value 0 for corresponding node at the corresponding time instant, while black stands for the value 1. The three different panels represent three different types of RBN, k indicating the number of inputs that each node receives. For $k = 1$, the time instants $t = 1, \ldots, 15$ are shown, and for $k = 2$ and $k = 3$, the time instants $t = 1, \ldots, 100$ are shown. During these intervals, the networks with $k = 1$ and $k = 2$ attain an attractor of length 1 and 4, respectively. By contrast, the network with $k = 3$ does not reach an attractor during the shown period. The arrows indicate the time instants of the first arrival to the attractor state. The RBNs are of size $N = 100$, and the Boolean functions are picked by random with equal probabilities for output being 0 or 1.

Chapter 4

Summary of results

The contributions of this thesis to systems science can be categorized into three groups: 1) the emergent structure of a growing and interconnecting network of neurons, 2) the effect of structure of a bursting neuronal network on its dynamics, 3) the complexity of network dynamics. In the following, the results of the publications included in this thesis are listed under these topics.

Structure of a growing neuronal network

Publication I reveals graph-theoretic aspects of growing neuronal networks. In this work, the growth of a group of neurons is simulated, and candidate synapses are placed wherever axons and dendrites of separate cells come close enough to each other. A fraction of them is considered functional synapses, and the derived map of functional synapses is studied as an unweighted, directed graph. Motif analysis reveals the difference of these networks (both the ones produced by NETMORPH and the one produced by CX3D) from the Erdős-Rényi random networks: They include, e.g., consistently more highly-connected motifs (Motif 13, see Figure 2.1) and less directed loops of length 3 (Motif 9) than the random networks do. The difference between the resulting networks of the two simulators is observed. In **Publication II** this difference is highlighted in a deeper way. In this piece of work, the CX3D is equipped with the same statistical rules of branching, elongation, and synapse formation as NETMORPH. The resulting networks are, however, crucially different in the two simulators. The difference is best seen in the overall number of synapses, and this difference reflects in the distributions of degree, shortest path length, and motifs.

In **Publication III**, the properties of networks produced by NETMORPH are monitored both from structural and dynamical aspects. The NETMORPH networks are compared to an abstract network model similar to the class of Watts-Strogatz networks, where the degree of locality can be controlled by a single parameter. In this network model, one extreme is the Erdős-Rényi random networks, as the other extreme represents networks, where each node takes inputs only from the spatially nearest nodes. The NETMORPH networks are very similar to in-between networks of

this abstract network model, both from the structural and the dynamical point of view. This is confirmed in **Publication VI**, where different activity models are used and different structural aspects are monitored. In this study, the boundary effects are removed in such a way that the neurites that extend outside the square-shaped area where the neurons' somata are located, are considered to appear at the other side of the area. The removal of boundary effects makes the in-degree distribution of the NETMORPH networks nearly binomial. The NETMORPH networks without this removal are shown to have much broader in-degree distribution (**Publications I** and **II**).

Effect of structure on bursting properties

Publication III reveals the differences in the bursting properties between networks with different topologies. Locally connected networks produce more and longer bursts than random networks. This is seen in both sparser and denser connectivities ($p = 0.1$ and $p = 0.16$). This phenomenon serves as a motivation for **Publication VI**, where the aspects of structure that have the greatest effect on bursting are sought for. Various abstract networks together with NETMORPH networks are used for studying the bursting properties. The networks include random networks, Watts-Strogatz networks, networks with high occurrence of feed-forward motifs (Motif 5, see Figure 2.1), and networks with a high number of directed loops of a certain length. The bursting activity is simulated in each network type. In addition, certain graph-theoretic measures of each network type are calculated, and the contribution of these measures to the bursting properties is analyzed. A prediction framework is applied for the data analysis: Different predictors are built, each of which is trained to estimate the bursting properties based on a certain set of graph measures. Statistically, the predictors that utilize clustering coefficient perform the best, when the in-degree distribution is sharp (binomial). By contrast, when the in-degree distribution is broad (power-law), the predictors based on maximum eigenvalue perform the best. Both measures are positively correlated with the number of bursts. Moreover, in networks with binomially distributed in-degree, the clustering coefficient is positively correlated with burst length and negatively correlated with burst size (number of spikes in a burst). Altogether, this explains the observations made in **Publication III** on the difference in bursting frequency and burst length: In locally connected networks, the bursts are numerous and long, whereas in random networks, where the clustering coefficient is much smaller, the bursts are fewer and shorter.

Complexity of dynamical systems

The set complexity and its derivatives are applied to measure the complexity of the dynamics. In **Publication IV**, two systems obeying Boolean logic, namely, RBNs and lattice gas systems, are under study. The temporal complexity is studied by monitoring the set complexity of successive states. In both systems, the set complexity is maximized near a state transition: In RBNs, this transition is the entrance to the attractor, whereas in the lattice gas system it is the stage when the particles (that were initially placed in an orderly fashion) start to mix and spread

throughout the domain. The highest maximal set complexity in RBNs is attained by the critical networks, where each node receives $k = 2$ inputs. Among the RBNs with $k = 3$, the slightly chaotic networks produce the highest maximal set complexity. In **Publication V**, it is shown that the state of maximal complexity can be sustained by introducing a certain amount of noise. The ordered networks ($k \approx 1$) require a relatively large noise component, while for the near-to-critical networks, a small noise component is sufficient to sustain the high set complexity. This result is confirmed with a measure of *statistical complexity* [Shalizi et al., 2004], which is an entropy-based measure on the information content of the dynamics of the system. To be more specific, it measures the information content of a minimal sufficient statistic for predicting the future of the system [Shalizi et al., 2004]. The statistical complexity is, however, subject to restrictions on the structure of the network, whereas in order to evaluate the set complexity the structure of the network need not even be known. The flexibility of the set complexity measure is indicated by the fact that it can be successfully applied to *asynchronous Boolean networks*, as shown in **Publication V**. In these networks, the nodes are updated one at the time, and the one updated is randomly picked every time step. The set complexity is calculated over successive modulo N states, i.e., only every Nth time instant is considered. The results of the set complexity in asynchronous RBNs are surprisingly similar to those in synchronous RBNs.

In **Publication III**, the framework of NCD is applied to simulated data on bursting neuronal activity. Due to its applicability to any data that can be represented by strings, the NCD can be applied on both structure (the connectivity matrix) and time-discretized activity (the population spike train) of the neuronal network. The differences between the network types, shown by phenomenological measures (e.g., number and length of bursts), are also reflected on the distribution of NCD values in the structure and dynamics of the network. Such distinction between the network types is not observed in other, more traditional measures of similarity between spike trains of two neurons, such as Hamming distance or cross-correlation coefficient. The results argue the compatibility of NCD with neuronal data, and pave the way for more delicate means of measuring the complexity in the structure and dynamics of neuronal networks.

Chapter 5

Discussion

This work introduces a wide range of methods for the simulation of neuronal network growth and dynamics. These methods are applied to study the structure-dynamics relationships in neuronal networks. In addition, the complexity of dynamics in several physical systems is measured — for this, the framework of Boolean networks is used. Several conclusions are made both on the characteristics of networks generated with the simulators of neuronal growth, and on the effect of network structure on the network dynamics. This chapter is devoted to discussion of these results.

Abstract models of network connectivity, Erdős-Rényi networks in particular, have dominated the *in silico* studies of the neuronal network function (cf. [Roxin, 2011]). This is partly due to the analytical tractability of such networks [Brunel, 2000a, Van Vreeswijk and Sompolinsky, 1996], and partly due to the fact that many connectivity patterns in the brain are seemingly random (see a discussion on the topic in [Sporns, 2011]). However, in most cases where the neuronal connectivity has been measured in detail, the networks have been found to differ from random networks. For instance, the feedforward loop is overrepresented in the connectome of *C. Elegans* [Milo et al., 2002] when compared to random networks. Recently, the Watts-Strogatz small-world networks [Watts and Strogatz, 1998] have been extensively used due to their resemblance to many real-world networks. Nonetheless, this is only the first step towards understanding the contributions of different structural aspects to network dynamics [Bullmore and Sporns, 2009]. In this work, a special class of network structure, where the connectivity pattern is an outcome of the growth of neurons and affinity-based synapse formation in the network, is considered. Two simulators of neuronal growth, NETMORPH and CX3D are applied. The focus is on creating mid-size ($N \in [10^2, 10^4]$) networks with manageable computational load, disregarding the chemical interactions between the neurons. For the generation of such networks, the NETMORPH simulator is found more suitable than CX3D (**Publications I** and **II**). A recent finding suggests that the use of randomly oriented neurons and affinity-based synapse formation rules be an accurate enough model for describing the connectivity in neocortex [Hill et al., 2012]. Another approach shows that even a simpler model, where the axon is modelled as a straight line that makes contact to nearby neuron somas, can be fit to experimental data on

connection length distributions [Kaiser et al., 2009]. These two examples serve as a motivation for the use of the simulators of growth and the affinity-based models of synapse formation for reproducing reliable connectivities. The result that there are more feed-forward loops in networks produced by the simulators of neuronal growth than in random networks, as shown in **Publication I**, is in line with the results on experimentally observed connectivity graphs [Milo et al., 2002].

Similarly to small-world networks [Watts and Strogatz, 1998], the networks generated by NETMORPH fall between random and locally connected networks with respect to their structural properties (**Publications III** and **VI**). Furthermore, the bursting properties in both NETMORPH networks and Watts-Strogatz in-between networks (or the partly locally connected networks in **Publication III** that are very similar to these) are shown to lie between these two extremes (**Publications III** and **VI**). Similar results have been observed in [Maheswaranathan et al., 2012], where the number of bursts increased rather smoothly when changing from random to locally connected networks — although the authors also reported an opposite trend when the fraction of inhibitory neurons was less than 20%. In other settings the small-world networks between random and local topologies have been shown to possess certain optimal properties, e.g., optimal signal propagation [Lago-Fernández et al., 2000] and maximal dynamical complexity [Shanahan, 2008].

A key aspect where NETMORPH networks deviate from other network classes, such as Watts-Strogatz networks, is the degree distribution. In both models for the networks between random and locally connected networks (**Publications III** and **VI**), the in-degree distribution can be explicitly chosen. This is not the case in NETMORPH networks, where the connectivity patterns are nontrivially dependent on the model parameters. There are, however, ways to affect the degree distribution. The choice of domain and placement of the somata is one crucial aspect. If continuous borders are applied to the domain, the difference in the degrees of "border" neurons versus "central" neurons is abolished, and the degree distribution becomes sharper (**Publication VI**). If, by contrast, the neuron somata are given heterogeneous growth parameter values, the degree distribution could become broader due to difference in neuron morphologies in the network, e.g., due to some neurons extending their axonal or dendritic trees way further than others. In this work, the neurons have rather homogeneous morphologies, although they do have slight randomness in, e.g., the number of basal dendrites (**Publication II**). Fitting the amount and type of heterogeneity in the morphology parameters to produce a given in-degree or out-degree distribution is out of the scope of this work, although such an approach could both shed light on the statistics of network connectivity and offer a valuable tool for goal-directed neuronal network generation. This is left for future studies.

From the viewpoint of the activity properties, such as synchronizability, the degree distributions play an important role. Theoretical and computational studies have highlighted the effect of average degree in regulating the type of activity [Brunel and Hakim, 1999, Jia et al., 2004]. In recent *in silico* studies, the contribution of not only the mean but also the width of the degree distribution has been analyzed. In [Zhao et al., 2011], the effect of second-order connectivity motifs (accounting for the widths and correlation of in-degree and out-degree distributions) on synchronization in neuronal networks was analyzed. In [Roxin, 2011], neuronal activity was

simulated in networks with both in-degree and out-degree distributions predefined. Both [Zhao et al., 2011] and [Roxin, 2011] agree on the shape of in-degree distribution influencing the mode of synchrony in a neuronal network more than the shape of the out-degree distribution does. This is the reason for the choice of a fixed in-degree distribution in **Publications III** and **VI** for networks whose dynamics are compared to each other (in **Publication III** binomial in-degree distribution is chosen, whereas in **Publication VI** both binomial and power-law distribution are considered). However, also the out-degree distribution has been recently [Pernice et al., 2013, Hu et al., 2013] shown to affect the spike train correlation strengths and should thus not be completely ignored.

Despite the fixed in-degree distribution, both **Publication III** and **VI** show that further details of the connectivity graph have a crucial effect on the network dynamics. Both publications agree on the increase of bursting frequency with the increase of local connections. Similar results have been observed in [Litwin-Kumar and Doiron, 2012], where the burstiness of the population, when measured using the Fano factor of the spiking frequency, was shown to increase by the degree of clustering in the connectivity pattern. Opposite results have been reported in [Netoff et al., 2004], where the locally connected networks only produce stably proceeding slow waves, while random and small-world networks produce variable bursting activity. The difference comes from the different regime of synaptic weights: In their paper, the synaptic weights were tuned very high (two action potentials in presynaptic neurons induce an action potential in the target neuron with a probability near to one), which makes the dynamics in the networks with a lot of long-range connections much more variable. Another difference to the models presented in this thesis is that they used a long refractory period (in range of tens of milliseconds) to make sure that the bursts cease and do not reactivate. By contrast, in this work, the bursting activity is re-entrant through excitatory connections until the synaptic resources are depleted. If such a model was used along with the high-weighted synapses of [Netoff et al., 2004], the bursting dynamics in locally connected networks might as well possess variable, non-trivial activity.

In **Publication VI**, the effect of network structure on the bursting is monitored in a wider framework: A number of different types of network structures are considered in order to obtain as general a result as possible. The graph measures introduced in Section 2.1 are evaluated for each network, and a prediction framework is applied to find out which one of them plays the key role with respect to the network dynamics. This should prevent false conclusions on the influence of a certain graph property, when the influence is actually reflected from the effect of another, correlated graph property. Such confusions are a frequent source for misinterpretations in structure-dynamics research [Arenas et al., 2008]. The integrative method of **Publication VI** highlights two graph measures above others, namely, the clustering coefficient and the maximal eigenvalue, the former being effective in networks with a sharp in-degree distribution and the latter in networks with a broad in-degree distribution. The importance of these measures has been stressed in the context of other physical systems. For instance, [Restrepo et al., 2006] showed that there is a critical value of connection weights between Kuramoto [Kuramoto, 1984] oscillators above which the network attains coherency, and that this critical value depends only on the maximum eigenvalue of the connectivity graph and the parameters governing single-node dynamics. For Watts-Strogatz networks of LIF neurons, it has been shown [Masuda and Aihara, 2004] that the clustering coefficient affects the degree of local synchrony more than the path

length does. The results of **Publication VI** confirm the importance of these two measures in bursting neuronal networks. It should be pointed out that much depends on regime of synaptic weights. If the synaptic weights were tuned high, as in the case of [Netoff et al., 2004], the path length might become more determinant than the clustering coefficient (see [McGraw and Menzinger, 2007] for an example in the context of Kuramoto oscillators). However, there is no guarantee that the bursting dynamics be realistic in such high-weighted networks, nor that the dynamics of the neurons remains physically feasible. Considering such a regime is thus left to future studies.

The dynamics of the bursting neuronal networks can be effectively described by statistics on the number and length of the bursts, as well as the size (number of spikes) of a burst and the maximal population firing rate (mFr). The burst length and size are considered in **Publication VI**, while mFr (along with other measures) is monitored in **Publication III**. The effect of the network structure on these measures can be observed in both publications. In **Publication III**, the dynamics of the network is additionally assessed using information-theoretic tools, namely, the NCD distribution between spike trains of neurons. The method shows that different networks can be separated by the distributions of their NCD values, when both structural and dynamical aspects are considered. This is not the case with the Hamming distance, nor with the cross-correlation coefficient.

Similar approaches to classification of spike trains have been applied in, e.g., in [Christen et al., 2006], where a distance measure based on Lempel-Ziv complexity was applied. In their paper, the authors estimated distances between a spike train of interest and a random Poisson spike train. This approach is different from that in **Publication III**, where the spike trains are compared *within* the neuron population. In other words, the approach of **Publication III** requires simultaneous spike train data on different neurons of a population, while the approach of [Christen et al., 2006] compares individual spike trains between a neuron and, in their case, a random spike train. The authors of [Christen et al., 2006] showed that spike trains measured from different brain regions lie on different distances from Poisson spike trains. This is best shown when the classification is aided by another distance measure, which is based on the correlation between the spike trains. Similarly to NCD, their distance metric utilizes the approximation of Kolmogorov complexity and normalization to the range $[0, 1]$. Nevertheless, the authors of [Christen et al., 2006] used the Lempel-Ziv complexity as such to approximate the Kolmogorov complexity, whereas in **Publication III** (as well as in **Publications IV** and **V**) the length of the LZMA-compressed[1] string is used. The LZMA employs the Lempel-Ziv complexity only in the creation of the dictionary for the string that is to be compressed. Another difference is in the way of normalizing the distance measure — arguments for using the normalization as expressed in Equation 2.19 are given in [Li et al., 2004].

The difference between the NCD distributions of spike trains of different network types reflects the difference between the dynamical behaviours of the corresponding network types. The spike trains are, however, discretizations (always in voltage and most often also in time) of the membrane potential, and therefore the NCD values based on them may miss a lot of relevant

[1]The LZMA (Lempel-Ziv Markov chain algorithm) is a lossless compression algorithm used in, e.g., 7-zip compression. See http://www.7-zip.org/ for further information.

information on the system dynamics. By contrast, the NCD can be effectively applied to any discrete-state discrete-time system without the risk of losing information. In **Publications IV** and **V**, the NCD is calculated for the dynamics of different physical systems that can be represented by probabilistic Boolean networks. In these publications, the NCD is calculated between vectorized states at different time instants, unlike in **Publication III**, where the NCD between vectorized spike trains of different neurons is calculated. Hence, although both approaches measure the diversity of the dynamics, the approach of **Publication III** quantifies the diversity *across the population*, and the approach of **Publications IV** and **V** quantifies the diversity *across time*. Quantifying the dynamical diversity across time allows the estimation of complexity of the system at different time instants, which is especially interesting in systems that show changes between states of attraction. Nevertheless, this approach requires data from a large (if not the whole) population at each time instant, whereas the quantification across the population can be applied to the time series of a smaller number of measured nodes, and is hence more easily adaptable to experimental data. Thus, the results obtained by the *across-time* approach are more of theoretical interest, but on the other hand, may tell more about the fine temporal changes than the *across-population* approach. The difference of these two approaches is discussed also in [Gong and Socolar, 2012], where an entropy-based complexity measure was applied to Boolean network dynamics using both approaches.

Publications IV and **V** reveal an interesting tendency of temporal complexity to be maximized near a state transition. In random Boolean networks this transition corresponds to the network attaining an attractor after initial chaotic dynamics, whereas in the lattice gas system, the transition corresponds to the spreading of the gas particles more uniformly over the whole domain. This is a novel (to the best of my knowledge) finding in the field of complex systems, made possible by the recent advances in information theory [Li et al., 2004, Galas et al., 2010]. The phenomenon is also observable using an entropy-based measure of statistical complexity [Shalizi, 2003, Shalizi et al., 2004], as shown in **Publication V**. The modular design of the set complexity and the NCD (the approximator of Kolmogorov complexity can be freely chosen) makes them a practical tool for diverse types of data. The states or time series that the NCD is applied to need not be of the same length, which is a great advance compared to many other approaches, including the Hamming distance and cross-correlation coefficient. In fact, a recent application [Sadot et al., 2013] has shown the feasibility of the NCD measure to very diverse temporal objects. In their framework, the authors applied a model of cell population dynamics that outputs the state of the population at each time point as a text file containing various information on the number and status of the cells. Their results show a fine classification of different genetic conditions through the use of NCD between successive states of the system. Another benefit of the NCD and the set complexity is that they do not require any additional information on the system structure (as the statistical complexity does) nor on the underlying probability distributions (as the entropy-based measures in general do).

This work contributes to many topics in the area of systems science, but the main focus of the thesis is on the dynamics of neuronal networks. Out of the vast number of network-level phenomena related to neuronal networks that can be studied *in silico*, this work concentrates on the network-wide bursts. They are an attractive object due to the fact that they can be observed in relatively simple systems, such as neuronal cultures. Furthermore, the network-wide bursts

can be reproduced computationally by using relatively simple models, such as LIF neurons with short-term synaptic plasticity [Tsodyks et al., 2000]. By using various graph algorithms and graph-theoretic measures, the influence of network structure can be effectively studied. Information-theoretic tools can be used to assess the information diversity of the bursting type of dynamics, although their applications to simpler, discrete systems, such as Boolean networks, may reveal the dynamical aspects of the system in a more extensive manner.

Graph-theoretic approaches to systems science are a central theme in this thesis. In computer simulations, the connectivity patterns can easily be modified, and usually changing one aspect in the structure alters many other structural aspects as well. Recently, advanced graph generation algorithms have been introduced to tackle this problem [Watts and Strogatz, 1998, Barabási and Albert, 1999, Palla et al., 2010]. In this thesis, the existing algorithms are modified to suit the specific needs in the systems discussed here. Special attention is given to the in-degree distribution. A common factor in most of the network structures generated in this study is that the in-degree distribution is fixed, but other aspects are allowed to vary. Future graph generation algorithms should account for the problem of keeping more and more structural aspects pre-defined, and letting other, more detailed aspects, vary. Such schemes would allow finer control over the network structure, and hence, enlighten the often complicated structure-dynamics relationships in ever finer detail.

The future experimental techniques provide ever more detailed data on biological entities and their interactions. The use of computational models for explaining the observed phenomena as complex interplays between the different entities is an arguable approach due to its constantly increasing potential. Given the rapid growth of computer memory capacity and processor performance over the past three decades, the predictive capabilities of the simulations of biological systems could be far beyond the present level after the three decades to come. However, as this thesis along with many other pieces of work shows, it is not only the number of interacting elements, but also the details of the connectivity that play a crucial role in shaping the collective activity. Data on, e.g., the neuronal network connectivity in different animal species are increasing and becoming more accessible for research, and this brings us closer to first understanding and then, by time, reproducing the function of the nervous system. Only through extensive experimental as well as computational research, and their seamless combination, can such ambitious goals be attained.

Bibliography

[Abbott, 2008] Abbott, L. (2008). Theoretical neuroscience rising. *Neuron*, 60(3):489–495.

[Aldana et al., 2003] Aldana, M., Coppersmith, S., and Kadanoff, L. (2003). *Boolean dynamics with random couplings*, pages 23–89. Springer-Verlag.

[Allen and Barres, 2009] Allen, N. and Barres, B. (2009). Neuroscience: Glia -- More than just brain glue. *Nature*, 457(7230):675–677.

[Araque and Navarrete, 2010] Araque, A. and Navarrete, M. (2010). Glial cells in neuronal network function. *Philosophical Transactions of the Royal Society B: Biological Sciences*, 365(1551):2375–2381.

[Arenas et al., 2008] Arenas, A., Díaz-Guilera, A., Kurths, J., Moreno, Y., and Zhou, C. (2008). Synchronization in complex networks. *Physics Reports*, 469(3):93–153.

[Ascoli et al., 2007] Ascoli, G., Donohue, D., and Halavi, M. (2007). Neuromorpho.org: A central resource for neuronal morphologies. *The Journal of Neuroscience*, 27(35):9247–9251.

[Azevedo et al., 2009] Azevedo, F., Carvalho, L., Grinberg, L., Farfel, J., Ferretti, R., Leite, R., Lent, R., and Herculano-Houzel, S. (2009). Equal numbers of neuronal and nonneuronal cells make the human brain an isometrically scaled-up primate brain. *Journal of Comparative Neurology*, 513(5):532–541.

[Barabási and Albert, 1999] Barabási, A. and Albert, R. (1999). Emergence of scaling in random networks. *Science*, 286(5439):509–512.

[Barrat and Weigt, 2000] Barrat, A. and Weigt, M. (2000). On the properties of small-world network models. *The European Physical Journal B–Condensed Matter and Complex Systems*, 13(3):547–560.

[Boccaletti et al., 2006] Boccaletti, S., Latora, V., Moreno, Y., Chavez, M., and Hwang, D. (2006). Complex networks: Structure and dynamics. *Physics Reports*, 424(4):175–308.

[Bock et al., 2011] Bock, D., Lee, W.-C., Kerlin, A., Andermann, M., Hood, G., Wetzel, A., Yurgenson, S., Soucy, E., Kim, H., and Reid, R. (2011). Network anatomy and in vivo physiology of visual cortical neurons. *Nature*, 471(7337):177–182.

[Brette et al., 2007] Brette, R., Rudolph, M., Carnevale, T., Hines, M., Beeman, D., Bower, J., Diesmann, M., Morrison, A., Goodman, P., Harris Jr, F., Zirpe, M., Natschläger, T., Pecevski, D., Ermenttrout, B., Djurfeldt, M., Lansner, A., Rochel, O., Vieville, T., Muller, E., Davison, A., Boustani, S., and Destexhe, A. (2007). Simulation of networks of spiking neurons: A review of tools and strategies. *Journal of Computational Neuroscience*, 23(3):349–398.

[Briggman et al., 2011] Briggman, K., Helmstaedter, M., and Denk, W. (2011). Wiring specificity in the direction-selectivity circuit of the retina. *Nature*, 471(7337):183–188.

[Brunel, 2000a] Brunel, N. (2000a). Dynamics of networks of randomly connected excitatory and inhibitory spiking neurons. *Journal of Physiology – Paris*, 94(5):445–463.

[Brunel, 2000b] Brunel, N. (2000b). Persistent activity and the single-cell frequency-current curve in a cortical network model. *Network: Computation in Neural Systems*, 11(4):261–280.

[Brunel and Hakim, 1999] Brunel, N. and Hakim, V. (1999). Fast global oscillations in networks of integrate-and-fire neurons with low firing rates. *Neural Computation*, 11(7):1621–1671.

[Bullmore and Sporns, 2009] Bullmore, E. and Sporns, O. (2009). Complex brain networks: Graph theoretical analysis of structural and functional systems. *Nature Reviews Neuroscience*, 10(3):186–198.

[Buzsáki, 2011] Buzsáki, G. (2011). *Rhythms of the Brain*. Oxford University Press.

[Buzsáki et al., 1983] Buzsáki, G., Lai-Wo S, L., and Vanderwolf, C. (1983). Cellular bases of hippocampal EEG in the behaving rat. *Brain Research Reviews*, 6(2):139–171.

[Carnevale and Hines, 2006] Carnevale, N. and Hines, M. (2006). *The NEURON Book*. Cambridge University Press.

[Chechik et al., 1999] Chechik, G., Meilijson, I., and Ruppin, E. (1999). Neuronal regulation: A mechanism for synaptic pruning during brain maturation. *Neural Computation*, 11(8):2061–2080.

[Chiappalone et al., 2006] Chiappalone, M., Bove, M., Vato, A., Tedesco, M., and Martinoia, S. (2006). Dissociated cortical networks show spontaneously correlated activity patterns during in vitro development. *Brain research*, 1093(1):41–53.

[Chiu and Weliky, 2001] Chiu, C. and Weliky, M. (2001). Spontaneous activity in developing ferret visual cortex in vivo. *Journal of Neuroscience*, 21(22):8906–8914.

[Christen et al., 2006] Christen, M., Kohn, A., Ott, T., and Stoop, R. (2006). Measuring spike pattern variability with the Lempel-Ziv-distance. *Journal of Neuroscience Methods*, 156:342–350.

[Compte, 2006] Compte, A. (2006). Computational and in vitro studies of persistent activity: Edging towards cellular and synaptic mechanisms of working memory. *Neuroscience*, 139(1):135–151.

[Connors and Gutnick, 1990] Connors, B. and Gutnick, M. (1990). Intrinsic firing patterns of diverse neocortical neurons. *Trends in Neurosciences*, 13(3):99–104.

[Dada and Mendes, 2011] Dada, J. and Mendes, P. (2011). Multi-scale modelling and simulation in systems biology. *Integrative Biology*, 3(2):86–96.

[Dayan and Abbott, 2001] Dayan, P. and Abbott, L. (2001). *Theoretical Neuroscience*. MIT Press.

[Eguiluz et al., 2005] Eguiluz, V., Chialvo, D., Cecchi, G., Baliki, M., and Apkarian, A. (2005). Scale-free brain functional networks. *Physical Review Letters*, 94(1):18102.

[Erdős and Rényi, 1960] Erdős, P. and Rényi, A. (1960). On the evolution of random graphs. *Publications of the Mathematical Institute of the Hungarian Academy of Sciences*, 5:17–61.

[Ermentrout and Chow, 2002] Ermentrout, G. and Chow, C. (2002). Modeling neural oscillations. *Physiology and Behavior*, 77(4):629–634.

[Galas et al., 2010] Galas, D., Nykter, M., Carter, G., Price, N., and Shmulevich, I. (2010). Biological information as set-based complexity. *IEEE Transactions in Information Theory*, 56(2):667–677.

[Gerstein and Kirkland, 2001] Gerstein, G. and Kirkland, K. (2001). Neural assemblies: technical issues, analysis, and modeling. *Neural Networks*, 14(6–7):589 – 598.

[Gewaltig and Diesmann, 2007] Gewaltig, M.-O. and Diesmann, M. (2007). NEST (neural simulation tool). *Scholarpedia*, 2(4):1430.

[Gillespie, 1977] Gillespie, D. (1977). Exact stochastic simulation of coupled chemical reactions. *The Journal of Physical Chemistry*, 81(25):2340–2361.

[Goldwyn and Shea-Brown, 2011] Goldwyn, J. and Shea-Brown, E. (2011). The what and where of adding channel noise to the Hodgkin-Huxley equations. *PLoS Computational Biology*, 7(11):e1002247.

[Golomb et al., 2006] Golomb, D., Shedmi, A., Curtu, R., and Ermentrout, G. (2006). Persistent synchronized bursting activity in cortical tissues with low magnesium concentration: A modeling study. *Journal of Neurophysiology*, 95(2):1049–1067.

[Gong and Socolar, 2012] Gong, X. and Socolar, J. (2012). Quantifying the complexity of random Boolean networks. *Physical Review E*, 85(6):066107.

[Gritsun et al., 2010] Gritsun, T., Le Feber, J., Stegenga, J., and Rutten, W. (2010). Network bursts in cortical cultures are best simulated using pacemaker neurons and adaptive synapses. *Biological Cybernetics*, 102(4):293–310.

[Gutiérrez, 2005] Gutiérrez, R. (2005). The dual glutamatergic – GABAergic phenotype of hippocampal granule cells. *Trends in neurosciences*, 28(6):297–303.

[Hellgren-Kotaleski and Blackwell, 2010] Hellgren-Kotaleski, J. and Blackwell, K. (2010). Modelling the molecular mechanisms of synaptic plasticity using systems biology approaches. *Nature Reviews Neuroscience*, 11(4):239–251.

[Hill et al., 2012] Hill, S., Wang, Y., Riachi, I., Schürmann, F., and Markram, H. (2012). Statistical connectivity provides a sufficient foundation for specific functional connectivity in neocortical neural microcircuits. *Proceedings of the National Academy of Sciences*, 109(42):E2885–E2894.

[Hu et al., 2013] Hu, Y., Trousdale, J., Josić, K., and Shea-Brown, E. (2013). Motif statistics and spike correlations in neuronal networks. *Journal of Statistical Mechanics: Theory and Experiment*, 2013(03):P03012.

[Insel et al., 2003] Insel, T., Volkow, N., Li, T.-K., Battey Jr, J., and Landis, S. (2003). Neuroscience networks: Data-sharing in an information age. *PLoS Biology*, 1(1):e17.

[Izhikevich, 2003] Izhikevich, E. (2003). Simple model of spiking neurons. *IEEE Transactions on Neural Networks*, 14(6):1569–1572.

[Izhikevich, 2004] Izhikevich, E. (2004). Which model to use for cortical spiking neurons? *Neural Networks, IEEE Transactions on*, 15(5):1063–1070.

[Izhikevich and Edelman, 2008] Izhikevich, E. and Edelman, G. (2008). Large-scale model of mammalian thalamocortical systems. *Proceedings of the National Academy of Sciences*, 105(9):3593–3598.

[Jaeger et al., 1997] Jaeger, D., De Schutter, E., and Bower, J. M. (1997). The role of synaptic and voltage-gated currents in the control of purkinje cell spiking: a modeling study. *The Journal of Neuroscience*, 17(1):91–106.

[Jia et al., 2004] Jia, L., Sano, M., Lai, P., and Chan, C. (2004). Connectivities and synchronous firing in cortical neuronal networks. *Physical Review Letters*, 93(8):88101.

[Junge, 1992] Junge, D. (1992). *Nerve and Muscle Excitation*. Sinauer.

[Kaiser et al., 2009] Kaiser, M., Hilgetag, C., and van Ooyen, A. (2009). A simple rule for axon outgrowth and synaptic competition generates realistic connection lengths and filling fractions. *Cerebral Cortex*, 19(12):3001–3010.

[Kallenberg, 2002] Kallenberg, O. (2002). *Foundations of Modern Probability*. Springer.

[Kamioka et al., 1996] Kamioka, H., Maeda, E., Jimbo, Y., Robinson, H., and Kawana, A. (1996). Spontaneous periodic synchronized bursting during formation of mature patterns of connections in cortical cultures. *Neuroscience Letters*, 206(2):109–112.

[Kandel et al., 2000] Kandel, E., Schwartz, J., and Jessell, T. (2000). *Principles of Neural Science*. McGraw-Hill.

[Kauffman, 1969] Kauffman, S. (1969). Metabolic stability and epigenesis in randomly constructed genetic nets. *Journal of Theoretical Biology*, 22(3):437 – 467.

[Keefer et al., 2001] Keefer, E., Gramowski, A., and Gross, G. (2001). NMDA receptor-dependent periodic oscillations in cultured spinal cord networks. *Journal of Neurophysiology*, 86(6):3030–3042.

[Klemm and Bornholdt, 2005] Klemm, K. and Bornholdt, S. (2005). Stable and unstable attractors in Boolean networks. *Physical Review E*, 72:055101.

[Kloeden and Platen, 1992] Kloeden, P. E. and Platen, E. (1992). *Numerical solution of stochastic differential equations*, volume 23. Springer-Verlag.

[Koene et al., 2009] Koene, R., Tijms, B., van Hees, P., Postma, F., de Ridder, A., Ramakers, G., van Pelt, J., and van Ooyen, A. (2009). NETMORPH: A framework for the stochastic generation of large scale neuronal networks with realistic neuron morphologies. *Neuroinformatics*, 7(3):195–210.

[Kolmogorov, 1965] Kolmogorov, A. (1965). Three approaches to the quantitative definition of information. *Problems of Information Transmission*, 1:1–7.

[Kuramoto, 1984] Kuramoto, Y. (1984). *Chemical oscillations, waves, and turbulence*. Springer-Verlag.

[Lago-Fernández et al., 2000] Lago-Fernández, L., Huerta, R., Corbacho, F., and Sigüenza, J. (2000). Fast response and temporal coherent oscillations in small-world networks. *Physical Review Letters*, 84(12):2758–2761.

[Li et al., 2004] Li, M., Chen, X., Li, X., Ma, B., and Vitanyi, P. (2004). The similarity metric. *IEEE Transactions on Information Theory*, 50(12):3250 – 3264.

[Li and Vitányi, 2008] Li, M. and Vitányi, P. (2008). *An introduction to Kolmogorov complexity and its applications*. Springer-Verlag.

[Litwin-Kumar and Doiron, 2012] Litwin-Kumar, A. and Doiron, B. (2012). Slow dynamics and high variability in balanced cortical networks with clustered connections. *Nature Neuroscience*, 15(11):1498–1505.

[Lytton and Sejnowski, 1991] Lytton, W. and Sejnowski, T. (1991). Simulations of cortical pyramidal neurons synchronized by inhibitory interneurons. *Journal of Neurophysiology*, 66(3):1059–1079.

[MacCluer, 2000] MacCluer, C. (2000). The many proofs and applications of Perron's theorem. *SIAM Review*, 42(3):487–498.

[Maeda et al., 1995] Maeda, E., Robinson, H., and Kawana, A. (1995). The mechanisms of generation and propagation of synchronized bursting in developing networks of cortical neurons. *Journal of Neuroscience*, 15(10):6834–6845.

[Maheswaranathan et al., 2012] Maheswaranathan, N., Ferrari, S., VanDongen, A., and Henriquez, C. (2012). Emergent bursting and synchrony in computer simulations of neuronal cultures. *Frontiers in Computational Neuroscience*, 6:15.

[Marom and Shahaf, 2002] Marom, S. and Shahaf, G. (2002). Development, learning and memory in large random networks of cortical neurons: Lessons beyond anatomy. *Quarterly Reviews of Biophysics*, 35(01):63–87.

[Masuda and Aihara, 2004] Masuda, N. and Aihara, K. (2004). Global and local synchrony of coupled neurons in small-world networks. *Biological Cybernetics*, 90(4):302–309.

[McGraw and Menzinger, 2007] McGraw, P. and Menzinger, M. (2007). Analysis of nonlinear synchronization dynamics of oscillator networks by Laplacian spectral methods. *Physical Review E*, 75(2):027104.

[Megías et al., 2001] Megías, M., Emri, Z., Freund, T., and Gulyás, A. (2001). Total number and distribution of inhibitory and excitatory synapses on hippocampal ca1 pyramidal cells. *Neuroscience*, 102(3):527.

[Milo et al., 2002] Milo, R., Shen-Orr, S., Itzkovitz, S., Kashtan, N., Chklovskii, D., and Alon, U. (2002). Network motifs: Simple building blocks of complex networks. *Science*, 298:824–827.

[Netoff et al., 2004] Netoff, T., Clewley, R., Arno, S., Keck, T., and White, J. (2004). Epilepsy in small-world networks. *Journal of Neuroscience*, 24(37):8075–8083.

[Newman, 2003] Newman, M. (2003). The structure and function of complex networks. *SIAM Review*, 45:167–256.

[Nykter et al., 2008] Nykter, M., Price, N., Larjo, A., Aho, T., Kauffman, S., Yli-Harja, O., and Shmulevich, I. (2008). Critical networks exhibit maximal information diversity in structure-dynamics relationships. *Physical Review Letters*, 100(5):58702.

[Øksendal, 2010] Øksendal, B. (2010). *Stochastic differential equations: An introduction with applications*. Springer.

[Otu and Sayood, 2003] Otu, H. and Sayood, K. (2003). A new sequence distance measure for phylogenetic tree construction. *Bioinformatics*, 19(16):2122–2130.

[Palla et al., 2010] Palla, G., Lovász, L., and Vicsek, T. (2010). Multifractal network generator. *Proceedings of the National Academy of Sciences*, 107(17):7640–7645.

[Perkel et al., 1967] Perkel, D., Gerstein, G., and Moore, G. (1967). Neuronal spike trains and stochastic point processes: II. Simultaneous spike trains. *Biophysical Journal*, 7(4):419–440.

[Pernice et al., 2013] Pernice, V., Deger, M., Cardanobile, S., and Rotter, S. (2013). The relevance of network micro-structure for neural dynamics. *Frontiers in Computational Neuroscience*, 7:72.

[Restrepo et al., 2006] Restrepo, J., Ott, E., and Hunt, B. (2006). Emergence of synchronization in complex networks of interacting dynamical systems. *Physica D: Nonlinear Phenomena*, 224(1):114–122.

[Restrepo et al., 2007] Restrepo, J., Ott, E., and Hunt, B. (2007). Approximating the largest eigenvalue of network adjacency matrices. *Physical Review E*, 76:056119.

[Reza, 1961] Reza, F. (1961). *An introduction to information theory*. McGraw-Hill.

[Robinson et al., 1993] Robinson, H., Kawahara, M., Jimbo, Y., Torimitsu, K., Kuroda, Y., and Kawana, A. (1993). Periodic synchronized bursting and intracellular calcium transients elicited by low magnesium in cultured cortical neurons. *Journal of Neurophysiology*, 70(4):1606–1616.

[Ross, 1996] Ross, S. M. (1996). *Stochastic Processes*. John Wiley and Sons.

[Roxin, 2011] Roxin, A. (2011). The role of degree distribution in shaping the dynamics in networks of sparsely connected spiking neurons. *Frontiers in Computational Neuroscience*, 5:8.

[Sadot et al., 2013] Sadot, A., Sarbu, S., Kesseli, J., Amir-Kroll, H., Zhang, W., Nykter, M., and Shmulevich, I. (2013). Information-theoretic analysis of the dynamics of an executable biological model. *PLoS ONE*, 8(3):e59303.

[Shadlen and Newsome, 1998] Shadlen, M. and Newsome, W. (1998). The variable discharge of cortical neurons: Implications for connectivity, computation, and information coding. *Journal of Neuroscience*, 18(10):3870–3896.

[Shalizi, 2003] Shalizi, C. (2003). Optimal nonlinear prediction of random fields on networks. *Discrete Mathematics and Theoretical Computer Science*, AB(DMCS):11–30.

[Shalizi et al., 2004] Shalizi, C., Shalizi, K., and Haslinger, R. (2004). Quantifying self-organization with optimal predictors. *Physical Review Letters*, 93(11):118701.

[Shanahan, 2008] Shanahan, M. (2008). Dynamical complexity in small-world networks of spiking neurons. *Physical Review E*, 78(4):041924.

[Shatz, 1990] Shatz, C. (1990). Impulse activity and the patterning of connections during CNS development. *Neuron*, 5(6):745–756.

[Sjöström et al., 2008] Sjöström, P., Rancz, E., Roth, A., and Häusser, M. (2008). Dendritic excitability and synaptic plasticity. *Physiological Reviews*, 88(2):769–840.

[Sporns, 2011] Sporns, O. (2011). *Networks of the brain*. MIT press.

[Sporns et al., 2005] Sporns, O., Tononi, G., and Kötter, R. (2005). The human connectome: A structural description of the human brain. *PLoS Computational Biology*, 1(4):e42.

[Tsodyks et al., 2000] Tsodyks, M., Uziel, A., and Markram, H. (2000). Synchrony generation in recurrent networks with frequency-dependent synapses. *Journal of Neuroscience*, 20(RC50):1–5.

[Tuckwell, 1988] Tuckwell, H. C. (1988). *Introduction to theoretical neurobiology, Volume 2: Nonlinear and stochastic theories*, volume 8. Cambridge University Press.

[Turrigiano, 2011] Turrigiano, G. (2011). Too many cooks? Intrinsic and synaptic homeostatic mechanisms in cortical circuit refinement. *Annual Review of Neuroscience*, 34:89–103.

[Van Ooyen, 2003] Van Ooyen, A. (2003). *Modeling neural development*. MIT Press.

[Van Ooyen, 2011] Van Ooyen, A. (2011). Using theoretical models to analyse neural development. *Nature Reviews Neuroscience*, 12(6):311–326.

[Van Pelt et al., 2010] Van Pelt, J., Carnell, A., De Ridder, S., Mansvelder, H., and Van Ooyen, A. (2010). An algorithm for finding candidate synaptic sites in computer generated networks of neurons with realistic morphologies. *Frontiers in Computational Neuroscience*, 4:148.

[Van Pelt and Uylings, 2003] Van Pelt, J. and Uylings, H. (2003). Growth functions in dendritic outgrowth. *Brain and Mind*, 4(1):51–65.

[Van Vreeswijk and Sompolinsky, 1996] Van Vreeswijk, C. and Sompolinsky, H. (1996). Chaos in neuronal networks with balanced excitatory and inhibitory activity. *Science*, 274(5293):1724–1726.

[Villani et al., 2011] Villani, M., Barbieri, A., and Serra, R. (2011). A dynamical model of genetic networks for cell differentiation. *PLoS ONE*, 6(3):e17703.

[Watts and Strogatz, 1998] Watts, D. and Strogatz, S. (1998). Collective dynamics of small-world networks. *Nature*, 393:440–442.

[White et al., 1986] White, J., Southgate, E., Thomson, J., and Brenner, S. (1986). The structure of the nervous system of the nematode caenorhabditis elegans. *Philosophical Transactions of the Royal Society of London. B, Biological Sciences*, 314(1165):1–340.

[Zhao et al., 2011] Zhao, L., Bryce Beverlin, I., Netoff, T., and Nykamp, D. (2011). Synchronization from second order network connectivity statistics. *Frontiers in Computational Neuroscience*, 5:28.

[Zubler and Douglas, 2009] Zubler, F. and Douglas, R. (2009). A framework for modeling the growth and development of neurons and networks. *Frontiers in computational neuroscience*, 3:25.

Publications

Publication I

T. Mäki-Marttunen*, R. Havela*, J. Aćimović, H. Teppola, K. Ruohonen, and M.-L. Linne. Modeling growth in neuronal cell cultures: Network properties in different phases of growth studied using two growth simulators. In *Proceedings of the 7th International Workshop on Computational Systems Biology (WCSB 2010)*, pp. 75-78, 2010. (* equal contribution of Mäki-Marttunen and Havela)

MODELING GROWTH IN NEURONAL CELL CULTURES: NETWORK PROPERTIES IN DIFFERENT PHASES OF GROWTH STUDIED USING TWO GROWTH SIMULATORS

T. Mäki-Marttunen[1,2], R. Havela[1]*, J. Aćimović[1], H. Teppola[1], K. Ruohonen[2], and M.-L. Linne[1]*

[1] Department of Signal Processing, Tampere University of Technology,
[2]Department of Mathematics, Tampere University of Technology,
P.O. Box 553, FI-33101 Tampere, Finland

tuomo.maki-marttunen@tut.fi, riikka.havela@tut.fi, jugoslava.acimovic@tut.fi,
heidi.teppola@tut.fi, keijo.ruohonen@tut.fi, marja-leena.linne@tut.fi

ABSTRACT

In this work we study the structural changes in neuronal networks emerging during network maturation. We analyze two computational models proposed in the literature that describe the growth of neurons. The models have planar geometry and the density of cells is chosen to correspond to the 'dense' and 'sparse' cultures reported in the experimental studies. The growth of the model neurons and networks is simulated using two novel publicly available simulators. A graph representation of the networks is obtained from the simulation results and examined at days 7, 14, and 21. The two models are clearly different in nature. The first can model large networks phenomenologically, while the second describes some of the relevant biophysical processes in smaller networks. The difference in modeling approach is evident in the graph properties.

1. INTRODUCTION

Network models of interconnected neurons have been extensively studied in the past to assess the mechanisms of information transmission and processing in different brain regions. Majority of these studies focus on the models of mature cortical circuits. The model neurons are described by dynamics of the cell membrane potential, including various contributing mechanisms at different levels of complexity. The networks have stable topology based on experimental observations. The contacts between neurons, the synapses, are activity-dependent.

The structural properties of the network topology impose limitations to the overall functionality. In this work, we focus on the analysis of realistic topologies without explicitly considering the activity and function of the corresponding networks. Instead, the goal is to examine the structural changes emerging during realistic simulations of growth of neurons and neuronal networks.

Growth models reported in the literature often focus on a single neuron or a single neurite, describing the underlying biophysical processes. For example, the models of initiation, elongation, and retraction of neurites, sensitivity to extracellular chemicals, selection of growth direction, and branching are reviewed in [1]. In addition, the phenomenological models of growth based on the statistical description of these processes and obtained experimentally are studied in [2], [3]. A network level model focusing on axon growth, particularly on selection of growth direction based on extracellular cues, is proposed in [4]. Recently, two simulators of neuronal growth were proposed in [3] and [5]. First of them employs statistical approach from [2]. It allows simulation of large networks with an approximative description of growth. The second simulator includes a detailed description of neurons and extracellular space, but cannot simulate large networks. We analyze the generic model from [5], but the implementation of new models is also supported.

The relevant aspects of growth greatly depend on the considered experimental conditions. We focus on *neuronal cell cultures* which allow monitoring of growth for several months, and inspection of the structural changes at least during the first weeks. Staining and microscopy techniques provide the tools for monitoring the structural changes. Various parameters like initial cell density and environmental chemicals can be easily controlled.

We study the two models proposed in [3] and [5]. In order to model neuronal cultures, the planar geometry is imposed as well as the several biophysical parameters defining the neuron behavior. The presented results correspond to the days 7, 14, and 21 *in vitro*. A directed graph capturing the network connectivity pattern is extracted, and various structural measures are computed according to [6], [7]. The network activity is not explicitly considered in any of the models, so the obtained synapses correspond to the 'potential synapses', i.e. the places where a contact between two neurons *can* be established in the presence of activity. According to [8], only a fraction of these 'potential synapses' become functional synapses, which is taken into account when examining the connectivity.

*** The first two authors equally contributed to this paper.**

2. MATERIALS AND METHODS

We analyze the two recently published simulators of neuronal growth and their generic models corresponding to neuronal cell cultures described in [3], [5]. The model implemented in NETMORPH focuses on statistical description of elongation, branching, and selection of growth direction [2]. The interaction between neurons, and the role of extracellular substances are not considered. The second simulator, CX3D, allows free selection of the model with many biophysical details included [5]. We adopt the generic model for neuronal cell cultures. It includes interaction between neurons through extracellular space. Cells diffuse guidance cues into the extracellular space and the branching and direction selection of their neighbors depends on the concentration of these cues.

2.1. NETMORPH simulator for modeling network growth phenomenologically

The NETMORPH is a neuronal growth simulator for generating large-scale networks with realistic morphologies [3]. The simulator allows neurons to grow axons and dendrites but not to divide or to evoke movement. Synapses are formed when axons and dendrites come close enough to each other. The growth of the neurites includes elongation, branching, and the choice of growth direction.

The elongation of a terminal segment of a neurite is described in [3], [2] as

$$\nu(t) = \nu_0 n(t)^{-F}.$$

Here, $\nu(t)$ represents the average elongation rate of a terminal segment at time t, ν_0 is a constant, $n(t)$ is the number of terminal segments in the neuron, and F is a constant parameter determining the level of competition for resources between terminal segments. The branching process is defined in [3], [2] by the probability of a terminal segment j branching at time step $(t_i, t_i + \Delta t)$ into two new terminal segments as follows

$$p_{i,j} = n_i^{-E} B_\infty e^{-t_i/\tau}(e^{\Delta t/\tau} - 1)2^{-S\gamma_j}/C_{n_i}.$$

Here, n_i is the number of terminal segments in the whole cell at time t_i, E is a constant determining the magnitude of competition, and B_∞ and τ are constant parameters governing the intensity and slowness of the branching. The variable γ_j is the centrifugal order of the terminal segment j, i.e. the number of segments between the soma and the terminal segment, S is a constant that determines the effect of the centrifugal order on the branching rate, and $C_{n_i} = \frac{1}{n_i}\sum_{k=1}^{n_i} 2^{-S\gamma_k}$ is a normalization constant.

Neurites can change growth direction, and the probability of the change at time $t + \Delta t$ depends on the increase in length of the terminal segment during the time interval $(t, t + \Delta t)$. The new direction depends on the previous growth directions for the considered neurite segment.

The above-mentioned models are used with the following parameters. Axon growth: $F = 0.16$, $\nu_0 = 45\ \mu$m/day, $B_\infty = 17.38$, $E = 0.39$, $S = 0$, $\tau = 14$ days, dendrite growth: $F = 0.39$, $\nu_0 = 12\ \mu$m/day, $B_\infty = 4.75$, $E = 0.39$, $S = 0$, $\tau = 3.7$ days. In the synapse formation a filling fraction of $1/4$ is used, i.e. only one quarter of potential synapses are accepted as functional synapses. For other parameters the default values of the NETMORPH simulator are assigned. Simulation time step is set to 2.4 hours.

2.2. CX3D simulator for modeling network growth biophysically

The CX3D is a simulation package suitable for modeling biophysical processes related to growth of neurons. Both intracellular and extracellular processes can be taken into account. The user can specify which processes should be included and at what level of complexity. We study the model of neuronal cell cultures proposed for this simulator in [5].

A fixed number of neurons is randomly distributed in the planar space that corresponds to the cell culture. No cell division or death can occur. All cells secrete a substance which acts as a guidance cue attracting the neurites of other cells. This is the only chemical implemented in the model. A number of initial neurite segments are placed on each cell. Neurite elongation occurs with a fixed rate that is adopted from NETMORPH, i.e. $\nu = 12\ \mu$m/day for dendrites and $\nu = 45\ \mu$m/day for axons. Neurite branching, the splitting of the neurite tip into the two new segments, occurs with a certain probability if the concentration of the guidance cue is large enough. During elongation dendrites gradually become thinner, losing 0.1% of their diameter in each time step, and branching stops when a certain threshold in the diameter is reached. Extracellular gradients of the guidance cue determine the direction of growth of neurites. When the concentration of guidance cue is small the neurites will grow straight. Mechanical tensions between soma and neurites, present during elongation, retraction and branching, are included in the model as described in [5]. The filling fraction and the simulation time step are equal to ones used in NETMORPH.

2.3. Characterization of network properties

The simulated networks are converted into unweighted directed graphs and analyzed using the following graph properties: degree distribution, geodesic path length, clustering coefficient, and motifs. Neurons represent graph nodes and the functional synapses form the edges. The edges are considered unweighted. Multiple synapses between two neurons form only one edge.

The set of nodes is denoted as $V = \{v_i\}_{i=1\ldots N}$ and the edges between them as $E = \{e_{ij}\}_{i,j=1\ldots N}$. The in-degree of a node is the number of edges arriving at the node, and the out-degree is the number of edges leaving the node. The geodesic path from node v_i to v_j is the shortest path between v_i to v_j, and the corresponding geodesic path length is the number of edges in this path or paths (there might be more than one shortest path for a pair of cells). The geodesic path length of the network is calculated by averaging over the geodesic path lengths of all connected nodes.

The local clustering coefficient of node v_i is defined as follows. Take all *neighbors* of v_i, i.e. such nodes v_j that $e_{ij}, e_{ji} \in E$, and calculate the ratio between the number of existing connections and the maximal number of possible connections. The global clustering coefficient is the average over local clustering coefficients of those nodes that have more than one neighbor. Clustering can also be assessed by analyzing *motifs* [7], [6]. All possible connections between triplets of nodes represent one of the 13 motifs (see Figure 2). The proportions of triples representing the motifs to the total number of triples tells us about the way the network is clustered.

3. RESULTS AND CONCLUSIONS

We simulated small networks of 100 neurons using both simulators, and the bigger networks of 10000 neurons using NETMORPH only. The cell density was selected according to the experimental studies reported in the literature [9]; we studied sparse (590 neurons$/mm^2$) and dense (1600 neurons$/mm^2$) networks at days 7, 14, and 21 *in vitro* (DIV). The simulations started from random initial conditions (cell positions, number of neurites per cell), and the presented results are the average over many repetitions. The summary of the results obtained for measures described in Section 2.3 is given in Figures 1 and 2, and in Table 1. The in- and out-degree distributions are shown in Figure 1, and the frequency of motifs in Figure 2. The remaining measures are given in Table 1. For comparison, the same measures are evaluated for random networks chosen to have the same mean of the degree distribution as the simulation results.

Difference between the two models is already visible in the degree distributions in Figure 1. The NETMORPH model significantly deviates from the random network (shaded area in figures). The CX3D model differs less and the difference is bigger for the out-degree distribution and for the networks with higher overall connectivity (cultures in latter development stage). The observed difference in results is expectable considering the intrinsic properties of the models. In NETMORPH the neurites grow in random directions, without interaction between the cells. Connections are formed when dendrite-axon pairs become close enough, which depends on several model parameters and on the initial conditions. In the CX3D model cell interaction is implemented through guidance cues secreted from the cells. The neurites are more likely to grow toward higher concentrations of guidance cues. This way, the neurons have tendency to strongly connect to the neighbors with less variability than in NETMORPH. Due to the small network size this clustering effect is not emphasized since all the neurons are close enough to form connections. The majority of results in motifs analysis significantly differ from the random values (U-test, confidence level 0.05). The rare similar values are marked with 'o' in Figure 2. In the NETMORPH model the increase in number of motifs with 'loops' between pairs of cells, most of all the number of motifs 12, happens between days 14 and 21. In addition to the two small scale models, in Table 1 are shown results for a larger model (10000 neurons) simulated in NETMORPH. There is a visible increase in the shortest path length, as a result of the overall network size. The clustering coefficient remains similar to the one in smaller networks.

In summary, the two neuronal growth models from the literature were compared to each other and to the random networks. The obtained results are significantly different, and different from random networks. More detailed analysis focused on particular aspects of neuronal growth will be carried out in the future.

4. ACKNOWLEDGMENTS

The authors would like to acknowledge the following funding: TISE graduate school, Academy of Finland project grants no. 106030, no. 124615, and no. 132877, and Academy of Finland project no. 320071 (Center of Excellence in Signal Processing).

5. REFERENCES

[1] B. Graham and A. van Ooyen, "Mathematical modeling and numerical simulation of the morphological development of neurons," *BMC Neuroscience*, vol. 7, no. Suppl 1, pp. S9, 2006.

[2] J. van Pelt and H. Uylings, *Natural Variability in the Geometry of the Dendritic Branching Patterns*, Taylor & Francis, Boca Raton, Florida, USA, 2005.

[3] R. Koene, B. Tijms, P. van Hees, F. Postma, A. de Ridder, G. Ramakers, J. van Pelt, and A. van Ooyen, "Netmorph: A framework for the stochastic generation of large scale neuronal networks with realistic neuron morphologies," *Neuroinform*, vol. 7, pp. 195–210, 2009.

[4] R. Segev and E. Ben-Jacob, "Generic modeling of chemotactic based self-wiring of neural networks," *Neural Networks*, vol. 13, pp. 185–199, 2000.

[5] F. Zubler and R. Douglas, "A framework for modeling the growth and development of neurons and networks," *Frontiers in Computational Neuroscience*, vol. 3, no. 25, 2009.

[6] R. Milo, S. Shen-Orr, S. Itzkovitz, N. Kashtan, D. Chklovskii, and U. Alon, "Network motifs: Simple building blocks of complex networks," *Science*, vol. 298, pp. 824–827, October 2002.

[7] S. Boccaletti, V. Latora, Y. Moreno, M. Chavez, and D.-U. Hwang, "Complex networks: Structure and dynamics," *Physics Reports*, vol. 424, pp. 175–308, 2006.

[8] A. Stepanyants and D. Chklovskii, "Neurogeometry and potential synaptic connectivity," *TRENDS Neurosci*, vol. 28, no. 7, pp. 387–394, July 2006.

[9] D. A. Wagenaar, J. Pine, and S. Potter, "An extremely rich repertoire of bursting patterns during the development of cortical cultures," *BMC Neuroscience*, vol. 7, no. 1, pp. 11, 2006.

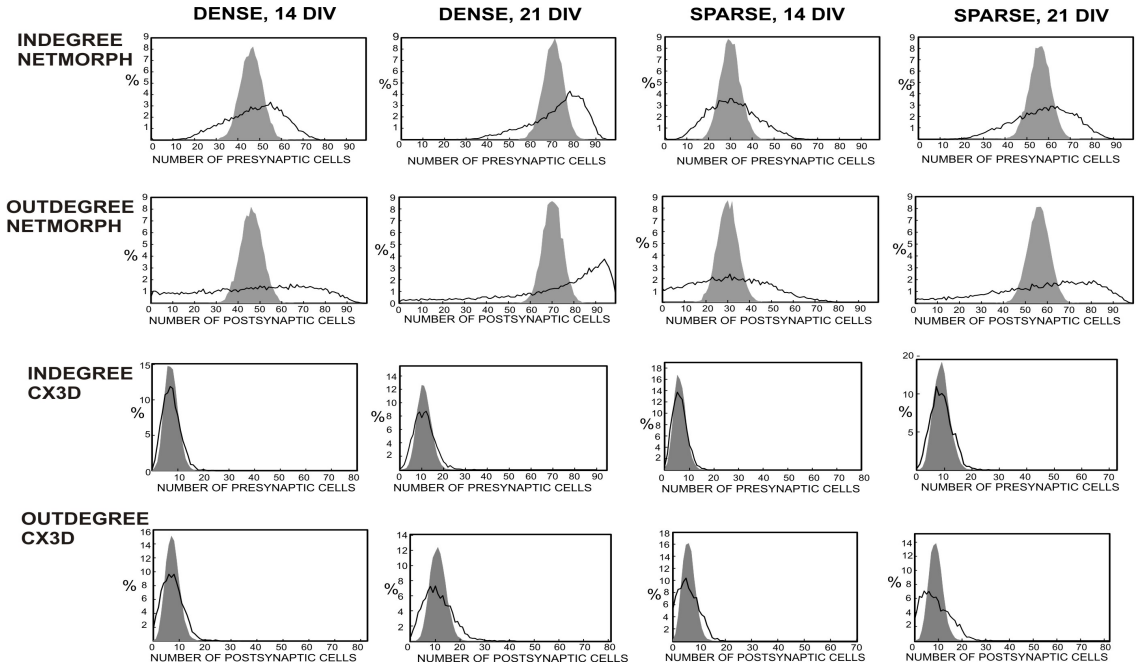

Figure 1. **In-degree and out-degree distribution.** Upper rows - degree distributions obtained using NETMORPH; bottom rows - CX3D results. Left columns - dense cultures, 14 and 21 DIV. Right columns - sparse cultures, 14 an 21 DIV. The x axis - the number of presynaptic (for in-degree) and postsynaptic (for out-degree) neurons. The y axis - degree probability (in %).

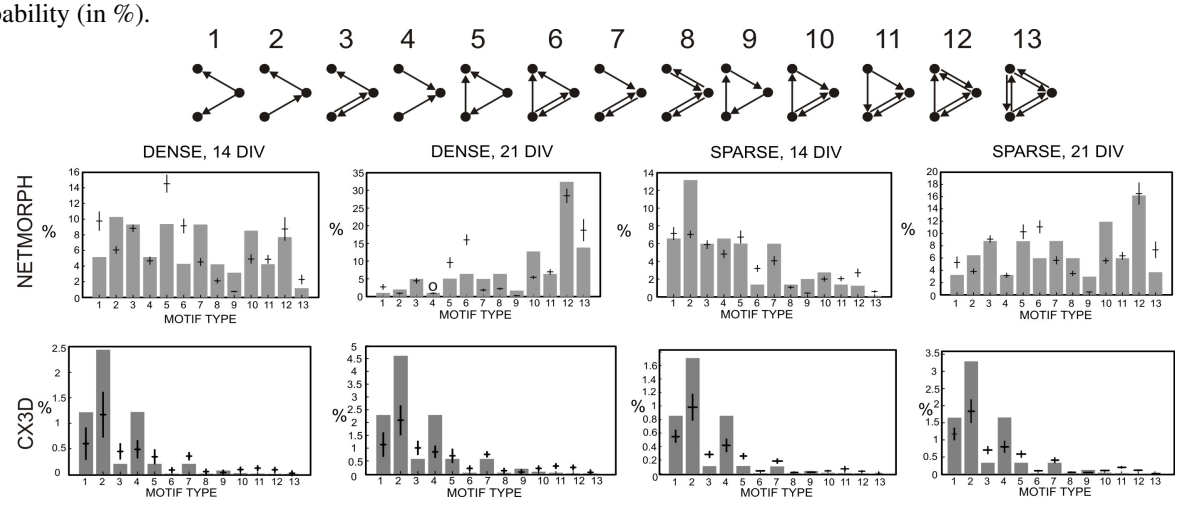

Figure 2. **Distribution of motifs** - sparse and dense networks, 14 and 21 DIV, two simulators. Gray - random networks, the results from simulated models are marked with '+', vertical arm representing the ST deviation. 'o' - not significantly different from random networks (U-test, confidence level 0.05).

		SPARSE		DENSE	
		Geodesic	Clustering	Geodesic	Clustering
CX3D SMALL	7DIV	5.1 ± 1	–	5.5 ± 1	0.3 ± 0.1
	14DIV	3.3 ± 0.3	0.5 ± 0.08	3.2 ± 0.2	0.5 ± 0.04
	21DIV	2.7 ± 0.1	0.5 ± 0.06	2.6 ± 0.1	0.6 ± 0.03
NETMORPH SMALL	7DIV	3.1 ± 1.2	0.3 ± 0.3	2.3 ± 0.8	0.3 ± 0.2
	14DIV	1.8 ± 0.6	0.6 ± 0.1	1.5 ± 0.5	0.7 ± 0.08
	21DIV	1.4 ± 0.5	0.7 ± 0.06	1.3 ± 0.5	0.8 ± 0.04
NETMORPH LARGE	7DIV	12.8 ± 5.2	0.3 ± 0.3		
	14DIV	6.7 ± 3.2	0.5 ± 0.09		
	21DIV	4.5 ± 2.3	0.6 ± 0.06		

Table 1. Computed measures (mean $\pm$ standard deviation). Each row corresponds one of two simulators, one time point, and small (100 cells) or large (10000 cells) networks. All results are significantly different from the random network.

Publication II

J. Aćimović, T. Mäki-Marttunen, R. Havela, H. Teppola, and M.-L. Linne. Modeling of neuronal growth in vitro: Comparison of simulation tools NETMORPH and CX3D. *EURASIP Journal on Bioinformatics and Systems Biology*, article ID 616382, 2011.

Hindawi Publishing Corporation
EURASIP Journal on Bioinformatics and Systems Biology
Volume 2011, Article ID 616382, 13 pages
doi:10.1155/2011/616382

Research Article

Modeling of Neuronal Growth *In Vitro*: Comparison of Simulation Tools NETMORPH and CX3D

J. Aćimović,[1] T. Mäki-Marttunen,[1,2] R. Havela,[1] H. Teppola,[1] and M.-L. Linne[1]

[1] *Department of Signal Processing, Tampere University of Technology, P.O. Box 553, 33101 Tampere, Finland*
[2] *Department of Mathematics, Tampere University of Technology, P.O. Box 553, 33101 Tampere, Finland*

Correspondence should be addressed to J. Aćimović, jugoslava.acimovic@tut.fi

Received 8 November 2010; Accepted 13 January 2011

Academic Editor: Carsten Wiuf

We simulate the growth of neuronal networks using the two recently published tools, NETMORPH and CX3D. The goals of the work are (1) to examine and compare the simulation tools, (2) to construct a model of growth of neocortical cultures, and (3) to characterize the changes in network connectivity during growth, using standard graph theoretic methods. Parameters for the neocortical culture are chosen after consulting both the experimental and the computational work presented in the literature. The first (three) weeks in culture are known to be a time of development of extensive dendritic and axonal arbors and establishment of synaptic connections between the neurons. We simulate the growth of networks from day 1 to day 21. It is shown that for the properly selected parameters, the simulators can reproduce the experimentally obtained connectivity. The selected graph theoretic methods can capture the structural changes during growth.

1. Introduction

Development of computational tools has been one of the central topics in the computational neuroscience community. Several simulators of bioelectrical activity are publicly available and considered well-established tools. Both the cellular mechanisms behind this activity and the communication between cells, through the exchange of activity, can be modeled and analyzed using these tools [1]. In addition to the bioelectrical activity, the morphological structure of neurons and neuronal networks can be reconstructed by methods based on the experimentally verified morphological constraints [2]. Recently, two simulators were proposed, aiming to reproduce the morphological and structural changes of neuronal networks during growth [3, 4]. These two tools reproduce the morphological characteristics of neurons in each step of growth and not only in its final phase. Both provide a set of components that can be combined in a user-defined model, including functions defining axonal and dendritic growth, morphology of different types of neurons, or environmental constraints. They can reproduce growth in planar and three-dimensional space. Currently, they simulate solely the morphological aspects of neuronal circuits, but they will likely be extended, in the near future, to include the development of bioelectrical activity.

Various aspects of growth in neuronal systems can be analyzed using models [5]. Some models concentrate on details of biophysical processes related to one phenomenon, while others describe several processes with less details [6, 7]. Examples of analyzed phenomena are initialization of dendritic and axonal arbors [5], dynamics of intracellular chemicals involved in axonal and dendritic outgrowth [6], and selection of axon growth direction following guidance cues in the environment [8, 9]. The framework for phenomenological modeling of growth is proposed in [3, 10, 11]. Here, the statistics of morphological changes, including branching and elongation, are computed without a reference to the intracellular or extracellular processes leading to those changes. Finally, the models of growth of neuronal populations and formation of networks are proposed in [9, 12]. In [9], the influence of guidance cues on axonal growth and the developed network properties are studied. In [12], a study of activity-dependent growth of neuronal networks is presented. Recently, an activity-dependent model of growth was utilized to examine the self-tuning to criticality [13].

In this work, we assess the applicability of NETMORPH and CX3D simulators, proposed in [3, 4], to study the growth in neocortical cultures. The neocortical cultures represent an experimental model of moderate size neocortical circuits, consisting of 10,000–100,000 neurons. The immature neurons are extracted from the neocortex of rat embryos and plated on a dish. Such neurons, regularly supplied with nutrients, develop their full morphology and functionality. The proportion of different neuronal subtypes observed in cultures is similar as in the neocortex [14]. The neurons retain similar morphological and functional properties as those found in the neocortex [14–17]. Still, the cultures contain only a moderate number of cells which live in a suboptimal environment. Their organization is substantially different from the one observed in the neocortical tissue, since neurons form planar networks different from the layered three-dimensional columns in the neocortex.

Several aspects make cultures a valuable tool for the study of cortical circuits. In cultures, the study of relation between morphology and functionality is feasible, since both can be studied simultaneously using the established experimental techniques. The morphological changes can be followed using a combination of cell staining and microscopy [15–17]. At the same time, their functionality can be assessed using either the patch-clamp recordings from single neurons [18] or by recording the activity from several locations in the network using the microelectrode arrays (MEA) [14, 19]. The morphological and functional properties of neurons can be manipulated by changing the content of the extracellular space. Properly maintained cultures can survive for several months [14, 19], and all of the described methods can be applied at different times during the culture life which provides an experimental framework for study of growth. The simulated model of neocortical cultures is constructed using the information available in the literature. We opted for a model based on the statistical description of morphological changes during growth, proposed in [10, 11], without trying to model intracellular or extracellular biophysical processes. These models are the intrinsic part of NETMORPH simulator and the implementation of fundamentally different growth rules would require changing the core of the simulator. The CX3D allows more flexibility in model description, and the adopted growth rules are implemented following [3, 10, 11]. The considered model allows the precise reconstruction of single neuron morphology and the constraints it imposes on the connectivity between neurons. Still, the model employs relatively simple rules and does not depend on many parameters. Therefore, it is suitable for the analysis of structural changes in neuronal networks during growth. The implemented model does not consider the role of activity that spontaneously emerges in neuronal cultures, but it mimics the synapse formation. Potential synapses are formed whenever the presynaptic and the postsynaptic sites are close enough. A certain percentage of these synapses can be considered "functional". According to [20], the percentage of potential synapses that can be considered functional is 25% *in vivo*. This percentage might be significantly different in cultures, due to the absence of columnar organization, smaller number of neurons that form synapses, and smaller density of dendrites and axons. The experimental studies estimate that in a culture a neuron directly connects to 10–30 of other neurons through functional synapses [14, 18].

Section 2 presents the methodology used in this work. A description of simulators is given in Section 2.1. The implemented model is described in detail in Section 2.2. Section 2.3 describes the graph theoretical measures of connectivity of network structure. Section 3 describes the obtained results and conclusions. In Section 3.1, we discuss the properties of the two simulators from the user point of view. In Section 3.2, the number of synapses per cell and per dish is evaluated, while varying model parameters and the obtained statistics are compared to the experimental evidences from the literature. Section 3.3 shows the basic statistics evaluated on network graph, extracted from the simulation results at different development days. Finally, Section 4 gives the discussion of the obtained results and their implications in study of morphological changes during growth of neocortical cultures *in vitro*.

2. Material and Methods

In this section, the adopted model of neuronal growth in neocortical cultures is presented in detail, together with the implementation details in the two simulators. In addition, the measures used to assess the simulation outcomes to evaluate the two simulators are listed.

2.1. Simulators of Growth. Recently, two simulators that can reproduce growth and development of neuronal systems were published in [3, 4]. Although both aim at simulating growth and development of neurons and neuronal networks, the methodology, implementation, and set of problems where they can be employed differ significantly. From the user point of view, the difficulty of model implementation, control of the parameters of the implemented model, and efficiency of simulations are also very different when using the two tools.

The NETMORPH simulator (http://netmorph.org/) has been developed at the Department of Experimental Neurophysiology at VU University Amsterdam. It is based on the extensive work on mathematical models that describe the morphology of dendritic and axonal arbors and the changes in the morphology during growth [7, 10, 11]. The software was written in C++ and provides a set of ready-made model components. The user can select the components and define the model parameters in a textual file called from the command line or directly from the command line. The software provides separate simulators for 2D and for 3D models which use the same set of model components.

The CX3D (http://www.ini.uzh.ch/~amw/seco/cx3d/) has been developed at the Institute of Neuroinformatics of the University of Zurich and ETH Zurich. The simulator includes a wide range of phenomena related to growth and development. Although we examine it in the context of growth in cultures, it can be employed to test many other processes including cell migration, formation of cortical columns, cell mitosis and apoptosis, and axon guidance through extracellular cues. The simulator is implemented in

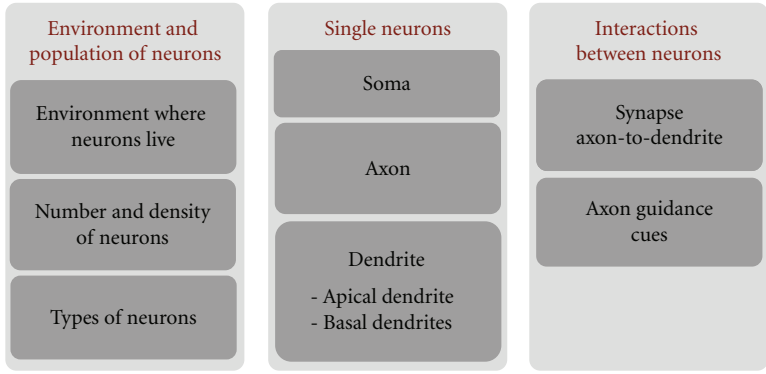

Figure 1: Schematic representation of a model of neocortical culture. Each block in the figure represents a set of related model components and model parameters that were selected from the literature.

Java and the users are expected to write their own classes defining the model components and combining them into the models of neuronal systems. The simulator essentially represents three-dimensional systems, but it can be adapted for the simulation of cultures.

We used the versions of the simulators that were available on the listed web sites in January 2010. The software was tested on Linux and Unix servers and on the personal computers (4 GB RAM, 3 GHz processor) working under Windows or under MacOS. Both simulators can be straightforwardly installed and run under Linux and MacOS. The CX3D can easily be installed and used under Windows, while NETMORPH needs the Cygwin environment on Windows. Simulation time did not depend significantly on the choice of operating system when working on computers of comparable performances.

2.2. Model of Neocortical Culture. In the presented study, we focus on growth in neocortical cultures. The models describing this phenomenon can be schematically represented as in Figure 1. The leftmost block defines the context, the characteristics of the environment where neurons live, and the characteristics of modeled neuronal population. The central block describes the model on single neuron level, for each implemented type of neuron. The rightmost block defines the interactions between neurons. Details of the model are illustrated on Figure 2(a), including the explanation of neuron anatomy and the meaning of the model parameters.

The environment block describes the shape and size of the space occupied by the neurons. In our model, this is a circular two dimensional dish in NETMORPH implementation, and a very flat cylinder, with the height equal to a cell diameter, in CX3D implementation. The CX3D models cannot be two dimensional due to properties of the simulator, but can be made nearly two dimensional by constraining the range of z coordinates to very small values. The dish radius is computed based on the number and density of neurons. In addition, the environment might define the properties of the medium that neurons live in, and the presence of particular chemicals that may influence growth. We do not model such extracellular chemicals explicitly, but the assumptions regarding the medium reflect on the choice of model parameters. It is assumed that neurons grow in an environment similar to the standard culturing medium, for example, as in [19]. The parameters are chosen to correspond to these conditions as well as possible.

The number and density of neurons are chosen as a tradeoff between the limitations of the simulators and the experimental evidence from the literature. The implemented networks consist of 100 neurons, which is the maximum number that can be simulated using both tools on standard personal computers. The selected density is 100 cells/mm^2. The densities reported in the experimental literature vary from 300 cells/mm^2 to 1380 cells/mm^2 depending on preparation and the addressed question [18, 19, 21, 22]. The density in our model is lower than in the experimental studies to compensate for the intensive axonal and dendritic growth and the lack of apoptosis. The axons and dendrites grow simultaneously in the model, while in the experiments the beginning of axonal growth precedes the dendritic one [15]. The total number of neurons is fixed in the model, as a result of NETMORPH constraints, but in the experiments, the number of neurons starts to decrease after the second week *in vitro* [21]. The radius of the "dish" is computed to preserve the chosen density for 100 neurons. This gives the radius of 564.2 μm. The "dish" determines the space where neuron somata are located, but the dendrites and axons are allowed to extend beyond its boundaries, in order to avoid boundary effect that would be severe for such a small radius. Effectively, we simulate a small portion of 0.1–1% of a neuronal culture.

We model the two most frequent *types of neurons* observed in cultures, the excitatory pyramidal neurons, and the inhibitory multipolar nonpyramidal neurons that correspond to the large GABAergic neurons reported in [17, 22]. The model culture consists of 80 pyramidal and 20 nonpyramidal neurons, following the usual proportion of excitatory and inhibitory neurons found in *in vivo* and *in vitro* [14]. An example of a pyramidal neuron, simulated using the CX3D, is shown on Figure 2(a). In addition, neuron soma (S), axon (AX), a basal dendrite (BD), and the apical dendrite (AD) are indicated on the figure.

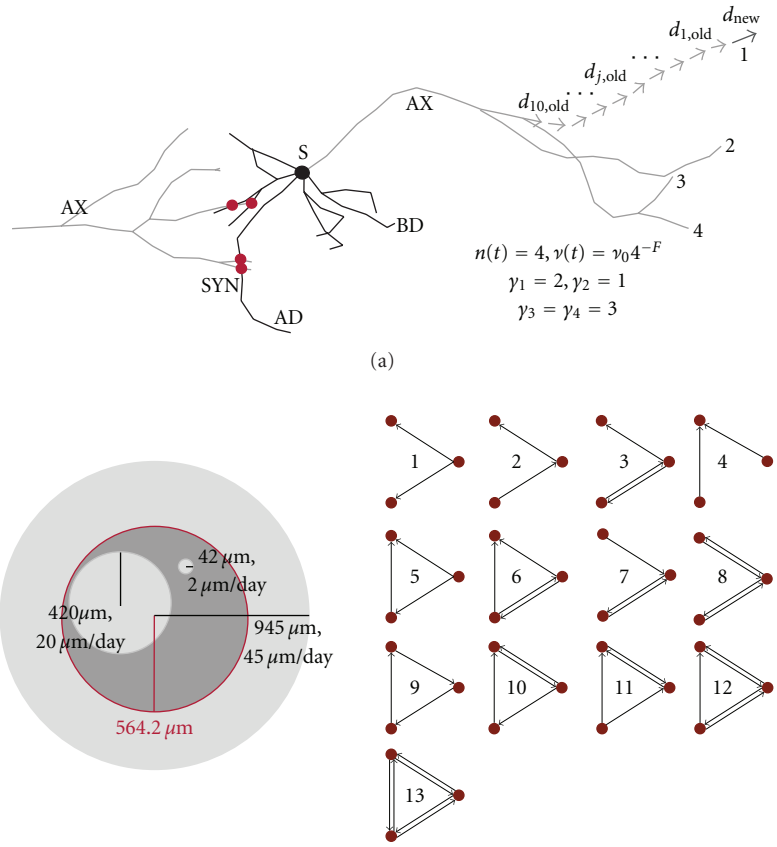

FIGURE 2: (a) shows one pyramidal neuron (simulation in CX3D) and its soma (S), axon (AX), basal dendrite (BD), and apical dendrite (AD). In order to show synapse formation, axon of a proximal neuron is also shown. The synapses (SYN) are marked with red circles on the figure. The right side of the panel shows computation of the elongation rate ($n(t)$), centrifugal order for four terminal tips (γ_k, where $k = 1 \ldots 4$), and the new growth direction (d_{new}) from the direction of ten preceding segments. (b) illustrates the influence of elongation rate on the synapse formation. For smaller elongation rates, for example, 2 μm/day, the maximal space covered by dendrites (or axons) at the end of a simulation is small and neurons cannot reach each other easily. For the larger values, for example, 20 μm/day, every neuron can cover a substantial part of the dish and other neurons. For the large values, for example, 45 μm/day, the dendrites extend beyond the dish space and are able to reach every one of 100 neurons. (c) illustrates all possible connectivity patterns between three neurons. These patterns are called *motifs*, and their frequency in a network represents the structural properties of that network.

The description of soma includes the soma size, its shape, and the number of dendrites extending from the soma. The diameter of the soma is fixed to 10 μm for all the neurons following the experimental results from [21]. The somas are spheres or circles in the model, and their natural shape is mimicked using a particular placement of neurites on the soma. In pyramidal neurons, the apical dendrite is positioned opposite to the axon and the basal dendrites grow on the axon half of the soma. In the nonpyramidal neurons dendrites are placed randomly on the entire soma. The total number of dendrites in all neurons is between 4 and 6. In the case of pyramidal neurons, one of them is the apical dendrite, and the remaining 3–5 are the basal dendrites.

The models for axons and dendrites are based on the statistical description of morphological changes during growth proposed in [7, 10, 11]. All the axons and dendrites use the same description with different parameter values. The parameter values are mainly obtained from NETMORPH tutorial paper [3]. The axon parameters are originally estimated from neurons growing in cultures and are available in [3]. The parameters for basal dendrites are taken from the three examples of reconstructed neurons *in vivo* available on NETMORPH web site. These parameters are consistent for the three examples, and we assumed that they grow similarly *in vitro*, since they are relatively short and placed around the soma and do not depend much on the guidance cues that exist *in vivo* but not *in vitro*. The parameters for apical dendrites are not available in the literature, and they evidently have different properties than those observed *in vivo* [15]. We assumed that they grow similarly to basal dendrites and used the same model, except that we adopted two times bigger initial elongation rate, following the microscopy images from [15]. The dendrites of nonpyramidal neurons are selected from the example of reconstructed basket cells, also available in [3] and on the web site. The motivation for this choice is found in [17], where large GABAergic neurons

Table 1: The list of the relevant model parameters. Model parameters are listed in the third column. The references used to obtain these parameters are given in the last column. Reference [3] points to the parameters that can be found directly in NETMORPH tutorial paper, while [3]* points to the reconstructed neurons from the same paper, which parameters can be found on the simulator web site. The notation "simulators" points to the value selected as a result of simulator constraints. The parameters for apical and basal dendrites differ only for ν_0 and they are shown together in the table (the ν_0 for the apical dendrites is given between the brackets). The initial elongation rates ν_0, marked with +, are varied in the simulations.

	Parameter	Value	Unit	Selection criteria
	Number of neurons	100		Simulators
	Proportion pyr.	80	%	[14]
	Proportion nonpyr.	20	%	[14]
	Density of neurons	100	cells/mm^2	Simulators, [14, 18, 19, 22]
	Soma diameter	10	μm	[21]
Axon	ν_0^+	45	μm/day	[3]
	F	0.16		[3]
	B_{inf}	17.38		[3]
	τ	14	days	[3]
	E	0.39		[3]
	S	0		[3]
Basal (apical) dendrite	ν_0^+	9.635 (19.27)	μm/day	[3]* ([3]*, [15])
	F	0		[3]*
	B_{inf}	2.52		[3]*
	τ	3.006	days	[3]*
	E	0.73		[3]*
	S	0.5		[3]*
Nonpyr. dendrite	ν_0^+	9.635	μm/day	[3]*, [17]
	F	0		[3]*, [17]
	B_{inf}	2.6475		[3]*, [17]
	τ	4.706	days	[3]*, [17]
	E	0.594		[3]*, [17]
	S	−0.259		[3]*, [17]
Synapses NETMORPH	Distance pyr.-pyr.	1	μm	[3]
	Distance pyr.-nonpyr.	0.1	μm	[3]
	Distance nonpyr.-pyr.	1	μm	[3]
	Distance nonpyr.-nonpyr.	0.1	μm	[3]
Synapse CX3D	Spine length	3	μm	[4], [23]
	Bouton length	2	μm	[4]

are studied *in vitro*. The study suggested that these neurons may be similar to the basket cells found *in vivo*. All the relevant model parameters are listed in Table 1.

The model for every axon or dendrite consists of three components: elongation of the terminal segments, branching of the terminal segments, and the model defining the shape of terminal segments and, consequently, the shape of segments between successive branching points. These components are also illustrated on Figure 2(a). The CX3D is a general purpose simulator, and various models of growth can be implemented and tested. On the contrary, NETMORPH focuses on a particular set of models that reproduce the statistics of axonal and dendritic morphology but do not tackle the biophysical mechanisms leading to this statistics. Therefore, the model is mainly constrained by NETMORPH, which, also, makes it more adapted to this simulator.

The elongation of terminal segments depends on the initial elongation rate ν_0 and on the current number of terminal segments in the same arbor $n(t)$ and is given by (1), described in details in [3]. The dependency on the number of terminal segments is regulated by the parameters F. The terminal segments in the same arbor elongate with the same speed at a given time. Although they can vary for small random values, this choice made CX3D implementation simpler. To illustrate, the elongation rate is computed for an axon with 4 terminal segments and shown on Figure 2

$$\nu(t) = \nu_0 n(t)^{-F}. \quad (1)$$

The branching of terminal segments is defined by the probability of branching, the initial length assigned to the two new segments, and the initial angle between them. The probability of branching, p_k, for the terminal segment with index k is given by (2), described in details in [3]. It depends on the expected number of branchings in the arbor, B_{inf}, on the total number of terminal segments at the considered time instant $n(t)$, and on the centrifugal order of the considered terminal segment k, γ_k. This last parameter is equal to the number of branching points between the considered terminal tip and the root of the arbor it belongs to. Figure 2 illustrates computation of circular order for the 4 terminal segments of the axon. The remaining model parameters are the time constant τ, dependency on the number of terminal tips E, and dependency on the centrifugal order S. The normalizing coefficient is denoted as C_k. The parameter Δt indicates the time step used to simulate the model

$$p_k(t) = \frac{B_{\text{inf}}}{C_k} e^{-t/\tau}\left(e^{\Delta t/\tau} - 1\right) n(t)^{-E} 2^{-S\gamma_k},$$
$$C_k = \frac{1}{n(t)} \sum_{j=1}^{n(t)} 2^{-S\gamma_j}. \tag{2}$$

The initial length of new segments depends on the simulator. In NETMORPH, they are selected randomly by dividing the last elongated part of the terminal segment. In CX3D, they are controlled by the segment "default length" set to 10 μm. The choice of the initial length affects the overall simulation result less in CX3D than in NETMORPH. The first one implements the tensions in a segment during elongation and retraction, as well as the mechanical interaction between different segments and different neurons. This intrinsic model dynamics modulates the length of the developed axons and dendrites. The initial angle between each new pair of segments is $\pi/3$ in both simulators, since it is fixed to that value in CX3D.

The shape of the axons and dendrites is determined by the model component that defines growth direction in each time step. In NETMORPH, the shape is entirely defined by the sequence of movements directions of the terminal segment. It is computed as the weighted sum of the directions of previous segments, taking into account the segments up to the last branching point. The new direction is defined as $\mathbf{d}_{\text{new}} = \sum_j (M_j/D_j^{1.2})\mathbf{d}_{j,\text{old}} + \boldsymbol{\alpha}$. Here, M_j is the length of the considered segment j, D_j is the distance between its center and the tip of the terminal segment (computed along the segments), $\mathbf{d}$ are direction vectors, and $\boldsymbol{\alpha}$ is a random perturbation. Computation of the new direction vector $\mathbf{d}_{\text{new}}$ from the set of previous direction vectors $\{\mathbf{d}_{j,\text{old}}\}_{j=1..10}$ is shown on Figure 2 for one terminal segment of the axon. The probability that direction changes is equal to $2 \cdot \Delta L(t)$, where $\Delta L(t)$ is the elongation during the last time step. In CX3D, the shape is determined dynamically. The movement direction in each time step is initially computed as the random perturbation of the direction from the previous time step as $\mathbf{d}_{\text{new}} = 5 \cdot \mathbf{d}_{\text{old}} + \boldsymbol{\alpha}$. Still, the final movement direction depends on the internal and external forces that affect the segment. The internal mechanical tensions in the segment determine how much it can be elongated or retracted. The segments tend to avoid obstacles which lead to changes in direction and bending of the segments. We also implemented NETMORPH growth direction model in CX3D, but the obtained result did not seem to represent the growth better than the original choice.

The model for synapse formation is based on the proximity criteria between pairs of axons and dendrites. Still the implementation of the model significantly differs in the two simulators. The NETMORPH requires a user-defined maximal distance between the presynaptic and the postsynaptic sites. For each axon-dendrite pair being on a distance smaller than the maximal, a synapse can be created with the likelihood inversely proportional to the distance. The maximal distances can be defined for different types on neurons and are listed in the Table 1. In CX3D, the actual growth of axonal boutons and dendritic spines is simulated. The length of the formed boutons and spines corresponds to the experimentally observed values. If a spine and a bouton touch each other, they form a synapse with certain probability than can be specified by the user. The model for synapse formation is the same for all neuron types, a choice imposed by the simulator. Figure 2 illustrates formation of four synapses (red circles) on the contacts between the dendrites of the depicted neuron, and the axon of another proximal neuron (not shown on the figure).

The axon guidance cues are the chemical species in the extracellular space that influence the axon growth directions when sensed by its tip. Both simulators allow some possibility to model the guidance cues, but only CX3D allows the simulation of chemical diffusion in the space. We opted to leave this mechanism out of the presented study and consider its influence only in the future work.

Parameters Varied in Simulations. In order to test the network formation in model cultures, we varied a parameter that significantly influences the growth and synapse formation. The probability of synapse formation is determined by the capability of neurons to reach each other, which is controlled by the elongation rate of axonal and dendritic trees. Figure 2 illustrates the maximal portion of the space covered by basal dendrites of a single neuron for different elongation rates. Four different elongation rates can be varied in the model: for axons, for apical and basal dendrites of pyramidal neurons, and for the dendrites of nonpyramidal neurons. In the simulations, the initial elongation rate ν_0 is varied for basal dendrites. The same parameter for axons, apical dendrites, and dendrites in nonpyramidal neurons is chosen as the value for basal dendrites multiplied by 4.5, 2, and 1, respectively. The examined values for the elongation rate of basal dendrites are 1, 2, 4, 6, and 8 μm/day in NETMORPH and 2, 6, 10, 14, and 22 μm/day in CX3D. Axons and dendrites in CX3D are elongating slower due to their internal dynamics, and somewhat bigger values for ν_0 were needed to obtain the comparable results to NETMORPH.

2.3. Statistical Measures of Graph Properties. The neuronal networks developed until days 4, 7, 10, 14, and 21 are extracted and converted into unweighted directed graphs.

Every neuron represents a node in the graph, and every synapse between two neurons introduces an edge between the two corresponding nodes. Multiple synapses between the same pair of neurons are not considered. Denote the set of nodes as $V = \{v_i\}_{i=1\ldots N}$ and the set of edges as $E = \{e_{ij}\}_{i,j=1\ldots N}$. For the obtained graphs, properties such as in- and out-degree distribution, shortest path length, and the frequency of motifs are computed.

The in-degree of a node is computed as the number of edges arriving at the node, that is, the number of postsynaptic contacts of the corresponding neuron. The out-degree of a node is the number of edges leaving the node, that is, the number of presynaptic contacts of the corresponding neuron.

For every pair of nodes, v_i and v_j, the number of edges in every path connecting these nodes is computed. The smallest number of edges determines the shortest path. The distribution of shortest paths for all the pairs of nodes in the network measures the global connectivity in that network. It indicates how well the nodes are connected and how fast information can be transmitted within the network.

The count of motifs [24, 25] is a measure of local connectivity. It indicates how well the neighbors connect, how pronounced the clustering in a network is, and how often the nodes form loops. All triplets of nodes in the network are examined in order to count different connectivity patterns. Such patterns between triplets of nodes are called motifs, and there are, in total, 13 different motifs (shown in Figure 2 and in [24, 25]). The frequency of different motifs is considered to be an indication of distinct structural properties [25].

3. Results

This section summarizes the results and conclusions obtained by simulating the described model of growth using the two tools, NETMORPH and CX3D. A network of 100 neurons was constructed using the parameter set described in Table 1 and Section 2.2. Some of the parameters were varied, namely, the initial elongation rate (v_0) for axons and all types of dendrites. The proportion between the elongation rates of axons, basal, apical, and nonpyramidal dendrites is fixed and only the overall intensity of growth influencing all of them is varied. Five different parameter sets were tested for each of the simulators. The simulations reproduce the growth of neurons from the first day after plating them on a dish until the end of the third week (day 21) on the dish. The simulation step size was fixed to 0.1 h, a value sufficiently small to ensure stable simulations with both tools.

3.1. Computational Efficiency. The efficiency of the tested simulators was considerably different. In NETMORPH, the execution of one batch simulation consisting of 120 repetitions for five sets of parameters required between 2 hours and 7 days depending on the choice of model parameters. In CX3D, the same simulation required between 4 and 40 hours for a single repetition and a single set of parameters. Therefore, collecting 120 repetitions for five parameter sets would require several weeks. From the simulation efficiency point of view, NETMORPH was evidently superior to CX3D. It should be pointed out that we selected the model adjusted to NETMORPH, so the differences in performance are not surprising. In CX3D, the limiting factor that influences the efficiency is the internal dynamics associated to every model element, that is, soma and neurite segment. It is created to mimic the natural interactions between model elements, but it requires memory space and computational time. The purpose of CX3D simulator is to provide a basis for modeling and analysis of virtually unlimited set of problems. The aim of the developers was to propose a sufficiently efficient general purpose tool, which might be suboptimal when focusing on one single class of models like in this study.

3.2. Dependence of Synapse Density on Model Parameters. The first set of simulations, summarized in Figure 3, was used to test the simulator and model properties. We focused on how well the simulators and models reproduce the synapse formation. The results obtained from the two simulators were compared with the corresponding experimental results found in the literature [21].

The number of postsynaptic and presynaptic sites, that is, the number of inputs and outputs, was computed for every neuron in every simulation repetition (120 repetitions in NETMORPH, 50 in CX3D). For each set of parameters, the mean and standard deviation were computed from the values obtained for 100 neurons and all the repetitions. Figures 3(a) and 3(b) show the results obtained for NETMORPH, and the bottom panel the results for CX3D. The curves on the panels connect the mean values obtained for days 4, 7, 10, 14, 16, and 21. The standard deviations are indicated with the one-side bars attached to the curves. The five curves, from blue to red, correspond to the five different values for the initial elongation rates. The chosen initial elongation rates for the basal dendrites of pyramidal neurons are indicated in the figure (see legend). For NETMORPH these values are $v_0 = 1$, 2, 4, 6, and 8 μm/day, and for CX3D, they are $v_0 = 2$, 6, 10, 14, and 22 μm/day. For the axons, apical dendrites, and dendrites of nonpyramidal neurons, the initial elongation rates are set to $4.5v_0$, $2v_0$, v_0, respectively. Figure 3(b) is a magnification of the region of interest from Figure 3(a), that is, for days 7–14 which represents the most accurately simulated phase of growth using the described model. Before day 7, the synapse formation is affected by timing of axonal and dendritic growth. It has been shown that axonal growth precedes the dendritic one [15]. This aspect of growth cannot be included in our simulation, due to the NETMORPH constraints. After day 14, the overall synapse density decreases due to the pronounced apoptosis in cultures [21]. This is, also, excluded from our model that has a fixed number of neurons.

Figures 3(a) and 3(b), obtained for NETMORPH, indicate an exponential increase in number of synapses per neuron over time. As expected, these numbers also increase when increasing the initial elongation rate. On average, increasing the elongation rate by 1 to 2 μm/day increases the number of synapses 2-3 times for the same day of growth. All of the obtained values are significantly higher than the experimental results shown in [21]. The reported experimental values, computed as the total number of synapses divided by the total number of neurons, are around

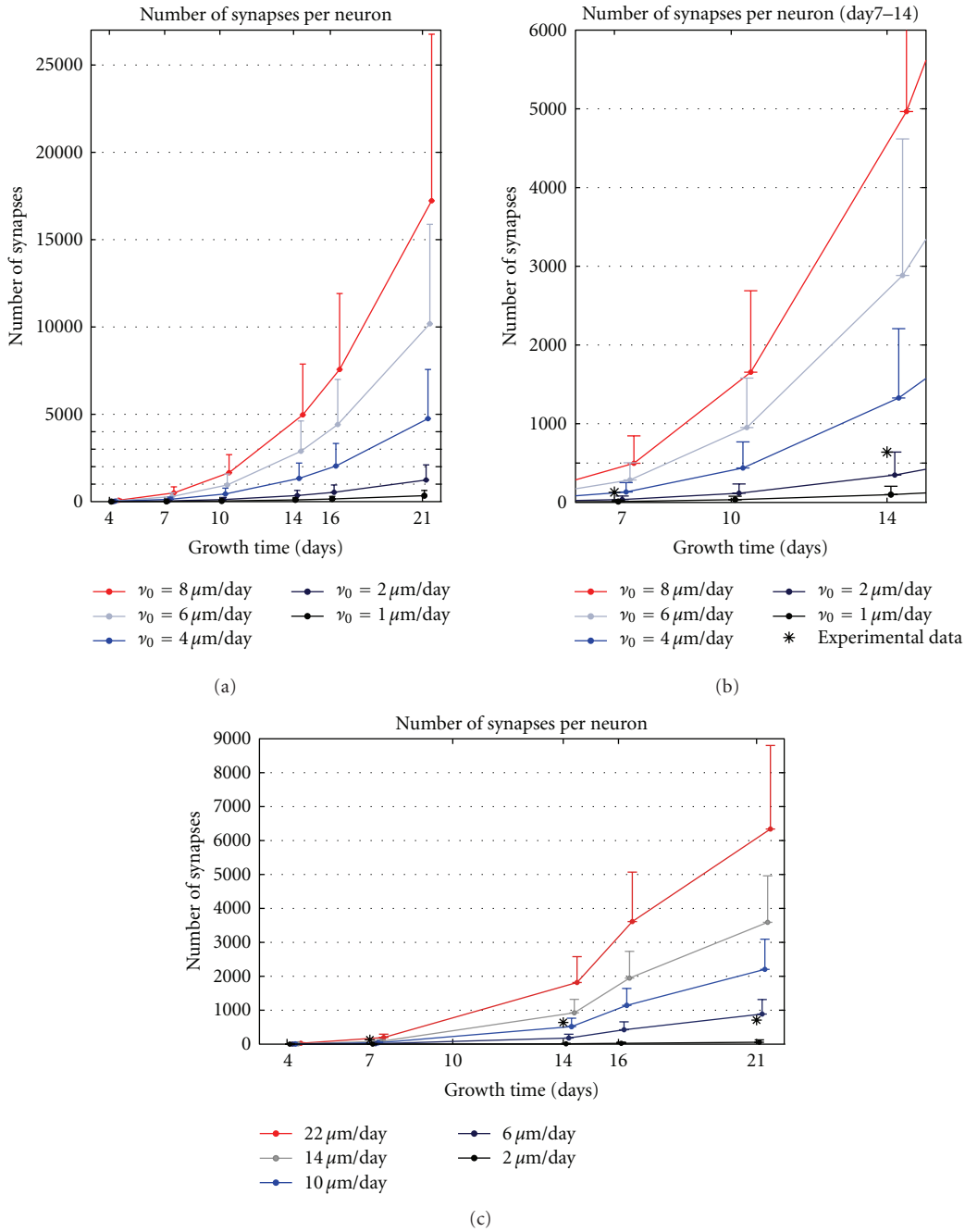

FIGURE 3: Synapse density. The upper row gives results for NETMORPH and the bottom row for CX3D. The curves mark the mean values, and the bars show the standard deviations. (a) shows the mean number of synapses per neuron when the elongation rate for basal dendrites takes values 1, 2, 4, 6, and 8 μm/day. (b) shows the magnified region of interest from (a), that is, the interval between 7 and 14 developmental days. The "$*$" mark the experimental values for the corresponding days, taken from [21]. (c) shows the synapse density obtained using CX3D, and the elongation rates for basal dendrites equal to 2, 6, 10, 14, and 22 μm/day. The experimental data ($*$) correspond well to the values obtained for $\nu_0 = 2\,\mu$m/day.

64 synapses per neuron at day 7, 319 at day 14, 355 at day 21, and 1130 at day 28 [21]. In Figure 3(b), the double values of these experimental data for days 7 and 14 are marked with "$*$". The values are doubled, since we consider every synapse twice, once for the presynaptic and once for the postsynaptic neuron. The density computed in [21] "assigns" every synapse to one neuron although it belongs to the two neurons. These values fall between the simulation results obtained for $\nu_0 = 2\,\mu$m/day and $\nu_0 = 4\,\mu$m/day. Regarding the increase in the number of synapses between days 7 and 14, it most likely resembles the curve for $\nu_0 = 2\,\mu$m/day. The high number of synapses may be explained by the tendency

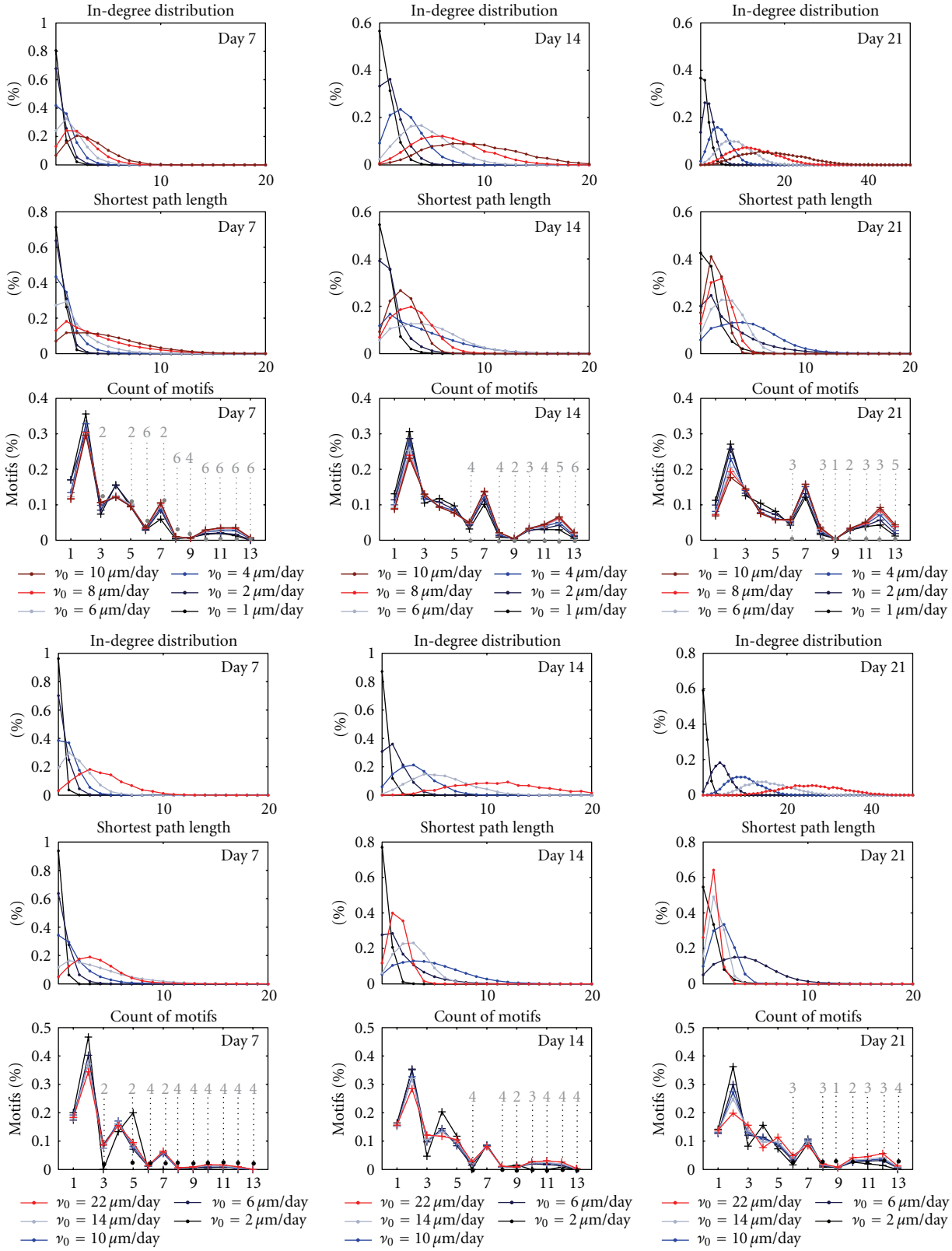

FIGURE 4: Structural changes of the growing networks: in-degree distribution, shortest path length, and the count of motifs. Three upper rows: NETMORPH results, three lower rows: CX3D results. Different curves correspond to different initial elongation rates ν_0, and the employed values are given in the legends (1, 2, 3, 6, 8, and 10 μm/day for NETMORPH, 2, 6, 10, 14, and 22 μm/day for CX3D). Grey interrupted lines indicate motifs that are significantly more frequent than in random networks (t-test, 0.01 significance level). The corresponding numbers show for which parameters this holds; for example, 2 means "holds only for the two smallest values." For CX3D, $\nu_0 = 2\,\mu$m/day was excluded since it gives too sparse random networks.

of the NETMORPH simulator to produce many synapses between the same pair of neurons.

Figure 3(c), obtained for CX3D, shows much better agreement with the experimental results. The increase in synapse number is not so dramatic as in NETMORPH, and the maximal values stay in the range of a couple of thousands. The differences obtained for different elongation rates are not so big as in NETMORPH. Finally, the simulation results obtained for $\nu_0 = 10\,\mu$m/day show very good agreement with the experimental values for days 7 and 14.

3.3. Statistics of the Network Graphs. The extracted networks obtained in different phases of growth are analyzed using graph theoretic measures. The results for both simulators are illustrated in Figure 4. The three upper rows show the statistics of in-degree distribution, shortest path length, and motifs count computed from the networks simulated in NETMORPH. The three bottom rows give these same measures evaluated for the networks simulated in CX3D. Each panel corresponds to one of days 7, 14, or 21. Different curves in the same panel show the results obtained for different values of the initial elongation rate ν_0, and the values of ν_0 used for the basal dendrites are indicated in the legends. The statistics for all NETMORPH results is computed for 100 neurons in each network, and for 120 repetitions of each condition. The number of repetitions for CX3D simulations was 50.

The in-degree distribution in all the panels shifts toward higher values during growth and is higher for bigger values of growth rate. These results can be compared to the experimentally estimated connectivity in cultures, shown to be in the interval of 10–30% [14, 18]. This indicates that the values $\nu_0 = 1$ and $2\,\mu$m/day give too small, while the $\nu_0 = 8$ and $10\,\mu$m/day result in too high connectivity. Taking into account the conclusions from Figure 3, the values $\nu_0 = 4$ and $6\,\mu$m/day may give the results closest to the desired ones. A similar observation holds for the networks simulated in CX3D. Here, the overall growth of the neurites is slower due to properties of the simulator, so we used somewhat higher values for the elongation rates. The smallest tested value also gives too sparse networks, while the highest overestimated the connectivity. In CX3D, the values 10 and $14\,\mu$m/day give the connectivity closest to the expected. Similar results were observed for the out-degree distribution.

The shortest path length distribution depends on the selected initial elongation rates. The slowly growing networks ($\nu_0 = 1, 2, 4\,\mu$m/day for NETMORPH, $\nu_0 = 2, 6\,\mu$m/day for CX3D) form a small number of connections until day 7. Most of the neurons are not connected or connected to a few neighbors. The shortest path is computed from this small set of short local connections, which results in a narrow distribution peaked around 0. As the network grows, new connections are established and distant pairs of neurons start to connect indirectly through other neurons. This shifts the shortest path length toward higher values. Neurons in the faster growing networks ($\nu_0 = 8, 10\,\mu$m/day for NETMORPH, $\nu_0 = 14, 22\,\mu$m/day for CX3D) already form direct and indirect connections at day 7. In the following days, new connections are added which continuously decreases the shortest path, since more neurons become directly connected.

The motifs count is shown as the percentage of total number of connected triplets of neurons (see Figure 4). The obtained counts are similar for all the parameter values, particularly in the NETMORPH examples. The peaks are visible for the motifs 2, 4, and 7. In the equivalent random networks, the motifs with two edges only (1, 2, and 4) or three edges (3, 5, 7, and 9) are the most frequent. Still, not all of them are equally represented in the simulated networks. In order to compare the simulation results with the corresponding random networks, that is, the networks with the same probability of connection, the statistical tests are done (t-test, with 0.01 significance level). The results are also shown in Figure 4, where dashed gray lines indicate the motifs that are significantly more frequent in the networks simulated using NETMORPH or CX3D than in the random networks. The number above each line shows for how many parameter values this holds, assuming that these are the smallest values from the set. In other words, number 4 indicates that a certain motif appears significantly more often in the networks simulated for the four smallest values among all the tested values, and it is either significantly smaller or not significantly different for the bigger elongation rate values. In CX3D figures, the smallest elongation rate was not considered, since it often gave very sparse random networks where motifs comparison was not possible. Expectedly, the motifs with four or more edges appear much more often in the networks simulated using NETMORPH or CX3D.

4. Discussion

4.1. Comparison of the Simulators. The presented results reveal several important differences between the two simulators, and indicate when each of them should be employed.

Our general conclusion is that NETMORPH, which implements computationally inexpensive models, could be more useful in theoretical studies and particularly for analysis of large networks. The NETMORPH models do not depend on many parameters, and the influence of each parameter can be carefully monitored. The main problem in the current version of the simulator is the excessive formation of synapses, which leads to unrealistically high number of synapses per neuron, and consequently, to very large output files. Such files are difficult to manipulate and analyze, which is particularly limiting when working with large networks. Recently, the authors of the simulator proposed an advanced algorithm for synapse formation [26] that might help to overcome this problem.

The principal advantage of CX3D is its flexibility. The authors aimed at constructing a multipurpose simulator of neuronal growth that can be used to model development of different neuronal systems, and include various relevant mechanisms. This simulator is valuable when modeling a small number of neurons equipped with intracellular and extracellular chemical species. It might be useful for constructing multilevel models that incorporate cellular and network levels, and in the future the level of genetic networks. On the other hand, when implementing systems

of 100 or more neurons with axons and dendrites that branch extensively, this simulator led to slow and memory consuming simulations. The complex dynamics of model elements, which is an intrinsic part of this simulator, requires time-consuming computations in every time step. In addition, it limits the maximal simulation time step that can be safely employed. Although the implemented model mainly behaved according to expectations, from time to time unwanted outcomes emerged as a result of the boundaries imposed by the nearly two-dimensional geometry of the environment. It was possible to observe axons or dendrites growing in a tight zigzag pattern in the situation when those segments found themselves "imprisoned" between the boundaries of the two-dimensional space and the surrounding objects. Finally, the complexity of the simulator imposed many "hidden" variables that were difficult to control, and whose influence on the simulation results was not obvious.

4.2. The Employed Model. We analyzed a phenomenological model established in the literature and adapted it to model the growth in neocortical cultures [3, 7, 10]. The model neither describes the role of the activity as in [12, 13], nor the biophysical processes governing growth as in [9], but it can reproduce the growth of axons and dendrites and can be used to study the network formation. In addition, it is relatively simple and depends on a small number of parameters.

The complete list of model parameters is given in Table 1. The parameters that define population of neurons, like number and density of neurons, or percentage of pyramidal and nonpyramidal neurons, are either well established knowledge in the literature or imposed by the simulator constraints. The density can be chosen more freely, but, when focusing on synapse formation, varying the density is equivalent to varying the elongation rate, since both parameters determine how fast pairs of proximal neurons can reach each other. The synapse formation is determined by the maximal distance between pairs of neurons that can form a contact. In NETMORPH, it is set to very small values, and increasing them leads to even bigger production of synapses. In CX3D, these parameters are set according to the well known estimation of dendritic spines and axonal boutons length. Increasing the parameters would lead to unrealistic synapse formation model. Finally, the set of parameters that defines branching and elongation of dendrites and axons is the most interesting to test. In total, the model has six parameters for each of the four types of arbors, axons, basal and apical dendrites of pyramidal neurons, and basal dendrites of nonpyramidal neurons. Five of six parameters define the branching probability, which determines the overall shape of the arbor and also influence elongation. The elongation rate influences solely the size of the arbors and how far a neuron can "reach." Different neuron types have distinct morphology, and the branching rate parameters should be selected to provide the correct morphology. The elongation rates should also be chosen to reflect the size of axons and dendrites relative to each other. In this work, we opted to examine solely the influence of the elongation rate, the parameter that most directly affects neuron size and, consequently, the probability of forming synapses. This is also motivated by the choice of neuron models in [12, 13], where neurons are represented as circular fields without detailed morphology. The global connectivity measures, like in-degree distribution or shortest path length, are likely dominantly influenced by the elongation rate. This dependency is visible on the presented results. The local connectivity measures, like motifs frequency, might significantly depend on the local shape of axonal and dendritic arbors. The influence of branching rate parameters on the arbor shape and the frequency of motifs will be the subject of future studies.

Several adopted choices in the model can be reconsidered. For example, all of the neurons have the same model for axon, which might not be correct. The branching of the apical dendrite is not very precisely set although the elongation reflects the ratio between the growth of basal and apical dendrites of the same neuron [15]. The environment in which neurons live might affect the growth. Finally, the model for axon guidance is not considered here although it is known that it influences the growth of axons and their capacity to reach other neurons. Some of the listed criticisms can be corrected by fitting the model from the experimental data instead of using the parameters available in the literature. Such data can be collected using conventional methods, like the combination of staining and microscopy. Still, the available methodology requires time-consuming experiments in order to provide sufficiently rich data set for parameter fitting.

4.3. Structural Changes During Growth, Graph Theoretic Study. Three measures were evaluated in order to analyze structural changes in networks during growth, in-degree distribution, shortest path length, and motifs count. Expectedly, since no criteria for stopping the growth were implemented, the number of synapses and the connections between neurons increased continuously. For the selected model parameters, the realistic values of in-degree and out-degree distributions, that correspond to experimental results, were obtained for days 7 to 14. The shortest path between a pair of neurons is initially small, with only a few connections established. As the network grows and new connections are added, the shortest path increases due to the new established pathways. When the number of direct connections between neurons increases enough, the average shortest path starts to decrease again. The motifs count reveals certain motifs that are more frequent in simulated than in the corresponding random networks for all the developmental days and majority of tested model parameters. These motifs have bi-directional connections. This might indicate that randomly placed neurons on the dish tend to find a proximal neuron and strongly connect to it by forming a loop.

The standard graph theoretic measures have been used in the literature to characterize mature cortical networks. Both small-scale networks of neurons and large-scale networks of cortical regions have been analyzed [27]. The statistics obtained *in vitro* cannot be straightforwardly related to the *in vivo* studies, since neurons develop outside of three-dimensional cortical columns and without the guidance cues present *in vivo*. In our study, the global

measures of connectivity, like in-degree distribution and shortest path length, show expected results and can be used to indicate when the network becomes connected and which elongation rates give realistic results during the first two weeks of growth. The motifs count does not give straightforward result, but mainly indicates frequent bidirectional connections in the simulated growth models compared to the random networks. In this study, we analyzed the connectivity of unweighted graphs, assuming that neurons that are likely to connect form multiple synapses and sufficiently strong connections. Also, synapse pruning is not taken into account, a mechanism that would remove connections formed through small number of synapses. The study on weighted graphs, where each weight corresponds to the number of synapses between a pair of neurons, will give more accurate results. This work will be pursued in the future.

To conclude, in this study we constructed a phenomenological model of neuronal growth in cultures and tested it on the two recently published simulators of growth. The graphs extracted from the obtained networks were analyzed and the observations were compared to experimental results. Both simulators can reproduce the considered experimental values, but their overall behavior might be improved by implementing additional mechanisms. The analysis of the network structure revealed the expected structural changes during growth and formation of local motifs.

Acknowledgments

The authors would like to acknowledge the following funding: TISE graduate school, Academy of Finland Project Grants nos. 106030, 124615, and 132877, and Academy of Finland Project no. 213462 (Center of Excellence in Signal Processing).

References

[1] R. Brette, M. Rudolph, T. Carnevale et al., "Simulation of networks of spiking neurons: a review of tools and strategies," *Journal of Computational Neuroscience*, vol. 23, no. 3, pp. 349–398, 2007.

[2] G. A. Ascoli, J. L. Krichmar, R. Scorcioni, S. J. Nasuto, S. L. Senft, and G. L. Krichmar, "Computer generation and quantitative morphometric analysis of virtual neurons," *Anatomy and Embryology*, vol. 204, no. 4, pp. 283–301, 2001.

[3] R. A. Koene, B. Tijms, P. Van Hees et al., "NETMORPH: a framework for the stochastic generation of large scale neuronal networks with realistic neuron morphologies," *Neuroinformatics*, vol. 7, no. 3, pp. 195–210, 2009.

[4] F. Zubler and R. Douglas, "A framework for modeling the growth and development of neurons and networks," *Frontiers in Computational Neuroscience*, vol. 3, no. 25, 2009.

[5] B. P. Graham and A. van Ooyen, "Mathematical modelling and numerical simulation of the morphological development of neurons," *BMC Neuroscience*, vol. 7, supplement 1, p. S9, 2006.

[6] G. Kiddie, D. McLean, A. Van Ooyen, and B. Graham, "Biologically plausible models of neurite outgrowth," *Progress in Brain Research*, vol. 147, pp. 67–80, 2004.

[7] J. van Pelt, B. P. Graham, and H. B. M. Uylings, *Formation of Dendritic Branching Patterns*, MIT Press, Cambridge, Mass, USA, 2003.

[8] J. K. Krottje and A. V. Ooyen, "A mathematical framework for modeling axon guidance," *Bulletin of Mathematical Biology*, vol. 69, no. 1, pp. 3–31, 2007.

[9] R. Segev and E. Ben-Jacob, "Generic modeling of chemotactic based self-wiring of neural networks," *Neural Networks*, vol. 13, no. 2, pp. 185–199, 2000.

[10] J. van Pelt and H. B. M. Uylings, *Natural Variability in the Geometry of the Dendritic Branching Patterns*, Taylor & Francis, Boca Raton, Fla, USA, 2005.

[11] J. Van Pelt, A. Van Ooyen, and H. B. M. Uylings, "The need for integrating neuronal morphology databases and computational environments in exploring neuronal structure and function," *Anatomy and Embryology*, vol. 204, no. 4, pp. 255–265, 2001.

[12] A. van Ooyen, J. van Pelt, M. A. Coroner, and S. B. Kater, *Activity-Dependent Neurite Outgrowth: Implications for Network Development and Neuronal Morphology*, MIT Press, Cambridge, Mass, USA, 2003.

[13] C. Tetzlaff, S. Okujeni, U. Egert, F. Wörgötter, and M. Butz, "Self-organized criticality in developing neuronal networks," *PLoS Computational Biology*, vol. 6, no. 12, 2010.

[14] S. Marom and G. Shahaf, "Development, learning and memory in large random networks of cortical neurons: lessons beyond anatomy," *Quarterly Reviews of Biophysics*, vol. 35, no. 1, pp. 63–87, 2002.

[15] A. Kriegstein and M. A. Dichter, "Neuron generation in dissociated cell cultures from fetal rat cerebral cortex," *Brain Research*, vol. 295, no. 1, pp. 184–189, 1984.

[16] A. D. De Lima, M. O. P. Merten, and T. Voigt, "Neuritic differentiation and synaptogenesis in serum-free neuronal cultures of the rat cerebral cortex," *Journal of Comparative Neurology*, vol. 382, no. 2, pp. 230–246, 1997.

[17] A. D. De Lima and T. Voigt, "Identification of two distinct populations of γ-aminobutyric acidergic neurons in cultures of the rat cerebral cortex," *The Journal of Comparative Neurology*, vol. 388, no. 4, pp. 526–540, 1997.

[18] K. Nakanishi and F. Kukita, "Functional synapses in synchronized bursting of neocortical neurons in culture," *Brain Research*, vol. 795, no. 1-2, pp. 137–146, 1998.

[19] D. A. Wagenaar, J. Pine, and S. M. Potter, "An extremely rich repertoire of bursting patterns during the development of cortical cultures," *BMC Neuroscience*, vol. 7, article 11, 2006.

[20] A. Stepanyants and D. B. Chklovskii, "Neurogeometry and potential synaptic connectivity," *Trends in Neurosciences*, vol. 28, no. 7, pp. 387–394, 2005.

[21] M. Ichikawa, K. Muramoto, K. Kobayashi, M. Kawahara, and Y. Kuroda, "Formation and maturation of synapses in primary cultures of rat cerebral cortical cells: an electron microscopic study," *Neuroscience Research*, vol. 16, no. 2, pp. 95–103, 1993.

[22] A. D. De Lima and T. Voigt, "Astroglia inhibit the proliferation of neocortical cells and prevent the generation of small GABAergic neurons in vitro," *European Journal of Neuroscience*, vol. 11, no. 11, pp. 3845–3856, 1999.

[23] H. Hering and M. Sheng, "Dendritic spines: structure, dynamics and regulation," *Nature Reviews Neuroscience*, vol. 2, no. 12, pp. 880–888, 2001.

[24] S. Boccaletti, V. Latora, Y. Moreno, M. Chavez, and D. U. Hwang, "Complex networks: structure and dynamics," *Physics Reports*, vol. 424, no. 4-5, pp. 175–308, 2006.

[25] R. Milo, S. Shen-Orr, S. Itzkovitz, N. Kashtan, D. Chklovskii, and U. Alon, "Network motifs: simple building blocks of complex networks," *Science*, vol. 298, no. 5594, pp. 824–827, 2002.

[26] J. van Pelt, A. Carnell, S. de Ridder, H. D. Mansvelder, and A. van Ooyen, "An algorithm for finding candidate synaptic sites in computer generated networks of neurons with realistic morphologies," *Frontiers in Computational Neuroscience*, vol. 4, article 148, 2010.

[27] O. Sporns, *Networks of the Brain*, MIT Press, Cambridge, Mass, USA, 2011.

Publication III

T. Mäki-Marttunen, J. Aćimović, M. Nykter, J. Kesseli, K. Ruohonen, O. Yli-Harja, and M.-L. Linne. Information diversity in structure and dynamics of simulated neuronal networks. *Frontiers in Computational Neuroscience*, 5:26, 2011.

frontiers in
COMPUTATIONAL NEUROSCIENCE

ORIGINAL RESEARCH ARTICLE
published: 01 June 2011
doi: 10.3389/fncom.2011.00026

Information diversity in structure and dynamics of simulated neuronal networks

Tuomo Mäki-Marttunen[1,2]*, Jugoslava Aćimović[1], Matti Nykter[1], Juha Kesseli[1], Keijo Ruohonen[2], Olli Yli-Harja[1] and Marja-Leena Linne[1]

[1] *Department of Signal Processing, Tampere University of Technology, Tampere, Finland*
[2] *Department of Mathematics, Tampere University of Technology, Tampere, Finland*

Edited by:
Arvind Kumar, Albert-Ludwig University, Germany

Reviewed by:
Birgit Kriener, Norwegian University of Life Sciences, Norway
Kanaka Rajan, Princeton University, USA

***Correspondence:**
Tuomo Mäki-Marttunen, Department of Signal Processing, Tampere University of Technology, P.O. Box 553, FI-33101 Tampere, Finland.
e-mail: tuomo.maki-marttunen@tut.fi

Neuronal networks exhibit a wide diversity of structures, which contributes to the diversity of the dynamics therein. The presented work applies an information theoretic framework to simultaneously analyze structure and dynamics in neuronal networks. Information diversity within the structure and dynamics of a neuronal network is studied using the normalized compression distance. To describe the structure, a scheme for generating distance-dependent networks with identical in-degree distribution but variable strength of dependence on distance is presented. The resulting network structure classes possess differing path length and clustering coefficient distributions. In parallel, comparable realistic neuronal networks are generated with NETMORPH simulator and similar analysis is done on them. To describe the dynamics, network spike trains are simulated using different network structures and their bursting behaviors are analyzed. For the simulation of the network activity the Izhikevich model of spiking neurons is used together with the Tsodyks model of dynamical synapses. We show that the structure of the simulated neuronal networks affects the spontaneous bursting activity when measured with bursting frequency and a set of intraburst measures: the more locally connected produce more and longer bursts than the more random networks. The information diversity of the structure of a network is greatest in the most locally connected, smallest in random networks, and somewhere in between in the networks between order and disorder. As for the dynamics, the most locally connected and some of the in-between networks produce the most complex intraburst spike trains. The same result also holds for sparser of the two considered network densities in the case of full spike trains.

Keywords: information diversity, neuronal network, structure-dynamics relationship, complexity

1 INTRODUCTION

Neuronal networks exhibit diverse structural organization, which has been demonstrated in studies of both neuronal microcircuits and large-scale connectivity (Frégnac et al., 2007; Voges et al., 2010; Sporns, 2011). Network structure, the connectivity pattern between elements contained in the network, constrains the interaction between these elements, and consequently, the overall dynamics of the system. The relationship between network structure and dynamics has been extensively considered in theoretical studies (Albert and Barabási, 2002; Newman, 2003; Boccaletti et al., 2006; Galas et al., 2010). In networks of neurons, the pattern of interneuronal connectivity is only one of the components that affect the overall network dynamics, together with the non-linear activity of individual neurons and synapses. Therefore, the constraints that structure imposes on dynamics in such systems are difficult to infer, and reliable methods to quantify this relationship are needed. Several previous studies employed cross-correlation in this context (Kriener et al., 2008; Ostojic et al., 2009), while the study reported in Soriano et al. (2008) proposed a method to infer structure from recorded activity by estimating the moment in network development when all of the neurons become fully connected into a giant component.

The structure and activity can be examined in a simplified but easily tractable neuronal system, namely in dissociated cultures of cortical neurons. Neurons placed in a culture have the capability to develop and self-organize into functional networks that exhibit spontaneous bursting behavior (Kriegstein and Dichter, 1983; Marom and Shahaf, 2002; Wagenaar et al., 2006). The structure of such networks can be manipulated by changing the physical characteristics of the environment where neurons live (Wheeler and Brewer, 2010), while the activity is recorded using multielectrode array chips. Networks of spiking neurons have been systematically analyzed in the literature (for example, see Brunel, 2000; Tuckwell, 2006; Kumar et al., 2008; Ostojic et al., 2009). In addition, models aiming to study neocortical cultures are presented in (Latham et al., 2000; Benayon et al., 2010), among others.

In this work, we follow the modeling approach of a recent study (Gritsun et al., 2010) in simulating the activity of a neuronal system. The model is composed of Izhikevich model neurons (Izhikevich, 2003) and the synapse model with short term dynamics (Tsodyks et al., 2000). We employ an information theoretic framework presented in Galas et al. (2010) in order to estimate the information diversity in both the structure and dynamics of simulated neuronal networks. This framework utilizes the normalized compression distance (NCD),

which employs the approximation of Kolmogorov complexity (KC) to evaluate the difference in information content between a pair of data sequences. Both network dynamics in the form of spike trains and network structure described as a directed unweighted graph can be represented as binary sequences and analyzed using the NCD. KC is maximized for random sequences that cannot be compressed and small for the regular sequences with lot of repetitions. Contrary to KC, a complexity measure taking into account the context-dependence of data gives small values for the random and regular strings and is maximized for the strings that reflect both regularity and randomness, i.e., that correspond to the systems between order and disorder (Galas et al., 2010; Sporns, 2011). The notion of KC has been employed before to analyze experimentally recorded spike trains, i.e., the recordings of network dynamics, and to extract relevant features as in Amigó et al. (2004) and Christen et al. (2006). Another examples of application of information theoretic methods in the analysis of spike train data can be found in Paninski (2003).

The NCD has been used for analysis of Boolean networks in Nykter et al. (2008), where it demonstrated the capability to discriminate between different network dynamics, i.e., between critical, subcritical and supercritical networks. This study employs NCD in a more challenging context. As already mentioned, in neuronal networks the influence of structure on dynamics is not straightforwardly evident since both network elements (neurons) and connections between them (synapses) possess their own non-linear dynamics that contribute to the overall network dynamics in a non-trivial manner. The obtained results show that random and regular networks are separable by their NCD distributions, while the networks between order and disorder cover the continuum of values between the two extremes. The applied information theoretic framework is novel in the field of neuroscience, and introduces a measure of information diversity capable of assessing both structure and dynamics of neuronal networks.

2 MATERIALS AND METHODS

2.1 NETWORK STRUCTURE

Different types of network structures are considered in this study. In locally connected networks (LCN) with regular structure every node is preferentially connected to its spatially closest neighbors. Only for high enough connectivity a node connects to more distant neighbors. In random Erdős–Rényi (RN) networks every pair of nodes is connected with equal probability regardless of their location. Finally, networks with partially local and partially random connectivity (PLCN) possess order and disorder in their structure. In Algorithm 1, we describe a unified scheme for generating these three types of networks.

Algorithm 1 | Scheme for generating distance-dependent networks.

for node index $i \in \{1,\ldots,N\}$ **do**
  Take number of in-neighbors $n_i \sim Bin(N-1, p)$.
  for in-neighbor index $j \in \{1,\ldots,n_i\}$ **do**
    1. Give weights w_k to all nodes $k \neq i$ that are not yet connected to i s.t. $w_k = D_{ik}^{-W}$, where D_{ik} is the spatial distance between nodes i and k.
    2. Normalize by $P(k) = \frac{w_k}{\sum_k w_k}$, where $P(k)$ represents the probability to draw node k.
    3. Randomly pick k from the probability mass distribution P and create a connection from k to i.
  end for
end for

The scheme uses three parameters: probability of connection between a pair of nodes $p \in [0,1]$, factor that defines dependence on distance $W \geq 0$, and the spatial node-to-node distance matrix $D \in \mathbb{R}^{N\times N}$. The matrix D is presumed positive and symmetric. For $W = 0$ the scheme results in a RN, as for $W = \infty$ we obtain a LCN. These latter networks are considered the limit cases of an arbitrarily big factor W: when choosing the in-neighbor one always picks the spatially closest one that has not yet been chosen as an in-neighbor. Randomness in the picking of the in-neighbors is applied only when there are two or more possible in-neighbors with the exact minimal distance from the considered node. In these cases, the in-neighbor is chosen by random.

It is notable that regardless of the choice of the distance-dependence factor W the scheme results in a network with in-degree distributed binomially as $Bin(N-1, p)$. Equal in-degree distribution makes the considered networks comparable: each network has the same average number of neurons with a high number of synaptic inputs as well as those with a low number. This property does not arise in most studied models of networks with varying distance-dependence, as Watts–Strogatz networks (Watts and Strogatz, 1998) or Erdős–Rényi based models where the probability of connection is altered by the spatial distance between the nodes (see e.g., Itzhack and Louzoun, 2010).

2.1.1 NETMORPH: a neuronal morphology simulator

In addition to networks described above, we study biologically realistic neuronal networks. NETMORPH is a simulator that combines various models concerning neuronal growth (Koene et al., 2009). The simulator allows monitoring the evolution of the network from isolated cells with mere stubs of neurites into a dense neuronal network, moreover, observing the network structure determined by the synapses at given time instants *in vitro*. It simulates a given number of neurons that grow independently of each other, and forms synapses whenever an axon of a neuron and a dendrite of another neuron come near enough to each other. The neurite segments are static in the sense that when they are once put onto their places they are not allowed to move for the rest of the simulation.

The growth of the axons and dendrites is described by three processes: elongation, turning, and branching, all of which are only applied to the terminal segments of the dendritic and axonal trees. The elongation of a terminal segment obeys the equation

$$\nu_i = \nu_0 n_i^{-F}, \tag{1}$$

where ν_i is the elongation rate at time instant t_i, ν_0 is the initial elongation rate, n_i is the number of terminal segments in the arbor that the considered terminal segment belongs to, and F is a parameter that describes the dependence of the elongation rate on the size of the arbor.

The terminal segments continue to grow until a turning or branching occurs. The probability that a terminal segment j changes direction during time interval $(t_i, t_i + \Delta t)$ obeys equation

$$P_{i,j} = r_L \Delta L_j(t_i), \tag{2}$$

where $\Delta L_j(t_i)$ is the total increase in the length of the terminal segment during the considered time interval and r_L is a parameter that describes the frequency of turnings. The new direction of growth is

obtained by adding perturbation to a weighted mean of previous growing directions. The most recent growing directions are given more weight than the earliest ones.

The probability that a terminal segment branches is given by

$$p_{i,j} = n_i^{-E} B_\infty e^{-t_i/\tau}\left(e^{\Delta t/\tau} - 1\right) 2^{-S\gamma_j} / C_{n_i}, \quad (3)$$

where n_i is the number of terminal segments in the whole neuron at time t_i and E is a parameter describing the dependence of branching probability on the number of terminal segments. Parameters B_∞ and τ describe the overall branching probability and the dependence of branching probability on time, respectively – the bigger the constant τ, the longer the branching events will continue to occur. The variable γ_j is the *order* of the terminal segment j, i.e., how many segments there are between the terminal segment and the cell soma, and S is the parameter describing the effect of the order. Finally, the probability is normalized using the variable $C_{n_i} = \frac{1}{n_i}\sum_{k=1}^{n_i} 2^{-S\gamma_k}$.

Whenever an axon and a dendrite of two separate neurons grow near enough to each other, there is a possibility of a synapse formation. The data consisting of information on the synapse formations, and hence describing the network connectivity, is output by the simulator. Technical information on the simulator and the model parameters that are used in this study are listed in Appendix 6.1.

2.1.2 Structural properties of a network

In this study we consider the network structure as a directed unweighted graph. These graphs can be represented by connectivity matrices $M \in \{0, 1\}^{N\times N}$, where $M_{ij} = 1$ when there is an edge from node i to node j. The most crucial single measure characterizing the graphs is probably the degree of the graph, i.e., the average number of in- or out-connections of the nodes. When studying large networks, not only the average number but also the distributions of the number of in- and out-connections, i.e., in- and out-degree, are of interest.

Further considered measures of network structures are the shortest path length and the clustering coefficient (Newman, 2003). We choose these two standard measures in order to show differences in the average distance between the nodes and the overall degree of clustering in the network. The shortest path length l_{ij} (referred to as path length from now on) from node i to node j is the minimum number of edges that have to be traversed to get from i to j. The mean path length of the network is calculated as $L = \frac{1}{N^2}\sum_{i,j=1}^{N} l_{ij}$, where such path lengths l_{ij} where no path between the nodes exists are considered 0. The clustering coefficient c_i of node i is defined as follows. Consider $\mathcal{N}_i$ as the set of neighbors of node i, i.e., the nodes that share an edge with node i in at least one direction. The clustering coefficient of node i is the proportion of traversable triangular paths that start and end at node i to the maximal number of such paths. This maximal number corresponds to the case where the subnetwork $\mathcal{N}_i \cup \{i\}$ be fully connected. The clustering coefficient can thus be written as

$$c_i = \frac{\left|\left\{(j,k) \in \mathcal{N}_i^2 \,|\, M_{i,j} \wedge M_{j,k} \wedge M_{k,i}\right\}\right|}{|\mathcal{N}_i|\left(|\mathcal{N}_i| - 1\right)}. \quad (4)$$

As the connections to self (autapses) are prohibited, one can use the diagonal values of the third power of connectivity matrix M to rewrite Eq. 4 as

$$c_i = \frac{\left(M^3\right)_{ii}}{|\mathcal{N}_i|\left(|\mathcal{N}_i| - 1\right)}. \quad (5)$$

This definition of clustering coefficient is an extension of Eq. 5 in Newman (2003) to directed graphs. The clustering coefficient of the network is calculated as the average of those c_i for which $|\mathcal{N}_i| > 1$.

Examples of connectivity patterns of different network structure classes, including a network produced by NETMORPH, are illustrated in **Figure 1**. The figure shows connectivity of a

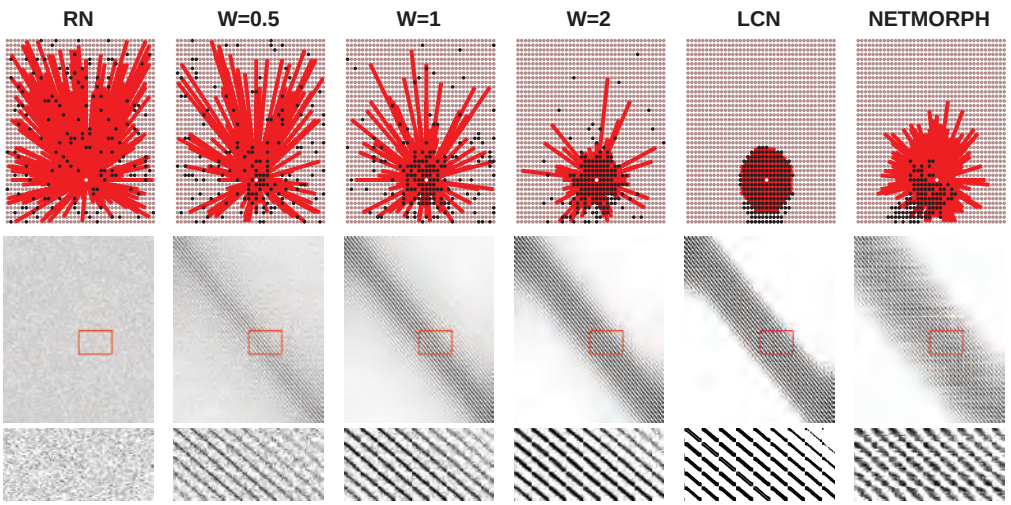

FIGURE 1 | Upper: Examples of the connectivity patterns. White: target cell, red: cells having output to the target cell, black: cells receiving input from the target cell; Middle: Connectivity matrix. Y-axis: From-neuron index, X-axis: To-neuron index; Lower: Selected part of the connectivity matrix magnified.

single cell (upper row), the connectivity matrix in total with black dots representing the ones (middle row) and a zoomed in segment of the connectivity matrix (bottom row). The structure classes shown are a RN, three examples of PLCN obtained for different values of distance-dependence factor W, a LCN and a NETMORPH network. Connection probability $p = 0.1$ is used in all network types. Note the variability in the spread of neighbors within different networks: for RNs they are spread totally random, as for LCNs they are distributed around the considered neuron. Due to the boundary conditions the spread of the out-neighbors in LCN is not circular, as the nodes near the border have on average more distant in-neighbors than the ones located at the center. In NETMORPH networks the spread of the out-neighbors is largely dictated by the direction of the axonal growth.

2.2 NETWORK DYNAMICS

2.2.1 Model

To study the network activity we follow the modeling approach presented in Gritsun et al. (2010). We implement the Izhikevich model (Izhikevich, 2003) of spiking neurons defined by the following membrane potential and recovery variable dynamics

$$\begin{aligned}\frac{dv}{dt} &= 0.04v^2 + 5v + 140 - r + I \\ \frac{dr}{dt} &= a(bv - r)\end{aligned} \tag{6}$$

and the resetting scheme

$$\text{if } v \geq 30, \text{ then } \begin{cases} v \leftarrow c \\ r \leftarrow r + d \end{cases}. \tag{7}$$

Parameters a, b, c, and d are model parameters and

$$I = I_{syn} + I_G \tag{8}$$

is an input term consisting of both synaptic input from other modeled neurons and a Gaussian noise term. The synaptic input to neuron j is described by Tsodyks' dynamical synapse model (Tsodyks et al., 2000) as

$$I_{j,syn}(t) = \sum_i A_{ij} y_{ij}(t). \tag{9}$$

The parameter A_{ij} accounts for the strength and sign (positive for excitatory, negative for inhibitory) of the synapse whose presynaptic cell is i and postsynaptic cell j – note the permutated roles of i and j compared to those in Tsodyks et al. (2000). The variable y_{ij} represents the fraction of synaptic resources in the active state and obeys the following dynamics:

$$\begin{aligned}\frac{dx}{dt} &= \frac{z}{\tau_{rec}} - ux\delta\left(t - t_{sp}\right) \\ \frac{dy}{dt} &= -\frac{y}{\tau_I} + ux\delta\left(t - t_{sp}\right) \\ \frac{dz}{dt} &= \frac{y}{\tau_I} - \frac{z}{\tau_{rec}}.\end{aligned} \tag{10}$$

Variables x and z are the fractions of synaptic resources in the recovered and inactive states, respectively, and τ_{rec} and τ_I are synaptic model parameters. The time instant t_{sp} stands for a spike time of the presynaptic cell; the spike causes a fraction u of the recovered resources to become active. For excitatory synapses the fraction u is a constant U, as for inhibitory synapses the dynamics of the fraction u is described as

$$\frac{du}{dt} = -\frac{u}{\tau_{facil}} + U(1-u)\delta\left(t - t_{sp}\right). \tag{11}$$

To solve the differential equations we apply Euler method on Eqs 6 and 7 and exact integration (see e.g., Rotter and Diesmann, 1999) on Eqs 10 and 11. The simulation setup for the activity model described above is discussed further in Section 3.1. Values of the model parameters and the initial conditions of the model are given in Appendix 6.2. **Figure 2** illustrates a typical population spike train of different network classes with connection probability 0.1, and a magnified view of one of their bursts.

2.2.2 Synchronicity analysis

Given a population spike train, we follow the network burst detection procedure as presented in Chiappalone et al. (2006), but using a minimum spike count minSpikes = 400 and maximal interspike interval ISI = 10 ms. Once the starting and ending time of the burst are identified, the spike train data of the burst are smoothed using a Gaussian window with deviation 2.5 ms to obtain a continuous curve as shown in **Figure 3**. The shape of the burst can be assessed with three statistics that are based on this curve: the maximum firing rate (mFr), half-width of the rising slope (Rs) and half-width of the falling slope (Fs) (Gritsun et al., 2010).

In addition to the network burst analysis, we estimate the cross-correlations between spike trains of two neurons belonging to the same network. We follow the method presented in Shadlen and Newsome (1998), where the cross-correlation coefficient (CC) between spike trains of neurons j and k is defined as $CC_{jk} = \frac{A_{jk}}{\sqrt{A_{jj}A_{kk}}}$. Here, the variable A_{jk} represents the area below the cross-correlogram and is computed as

$$A_{jk} = \sum_{\tau=-100}^{100} \left(\left(\frac{1}{\lambda_j \lambda_k} \sum_{i=0}^{T-1} x_j(i) x_k(i+\tau) \right) - \Theta(\tau) \right). \tag{12}$$

The variable $x_j(i)$ is 1 for presence and 0 for absence of a spike in the ith time bin of spike train of neuron j, λ_j is the mean value of $x_j(i)$ averaged over i, and T is the number of time bins in total. The running variable τ is the time lag between the two compared signals, and the weighting function Θ is chosen triangular as $\Theta(\tau) = T - |\tau|$.

2.3 INFORMATION DIVERSITY AS A MEASURE OF DATA COMPLEXITY

Complexity of different types of data and systems has been studied in numerous scientific disciplines, but no standard measure for it has been agreed upon. The most widely used measures are probably Shannon information (entropy) and the theoretical KC. Shannon information measures the information of a distribution. Thus, it is based on the underlying distribution of the observed random variable realizations. Unlike Shannon information, KC is not based on statistical properties, but on the information content of the object itself (Li and Vitanyi, 1997). Hence, KC can be defined without

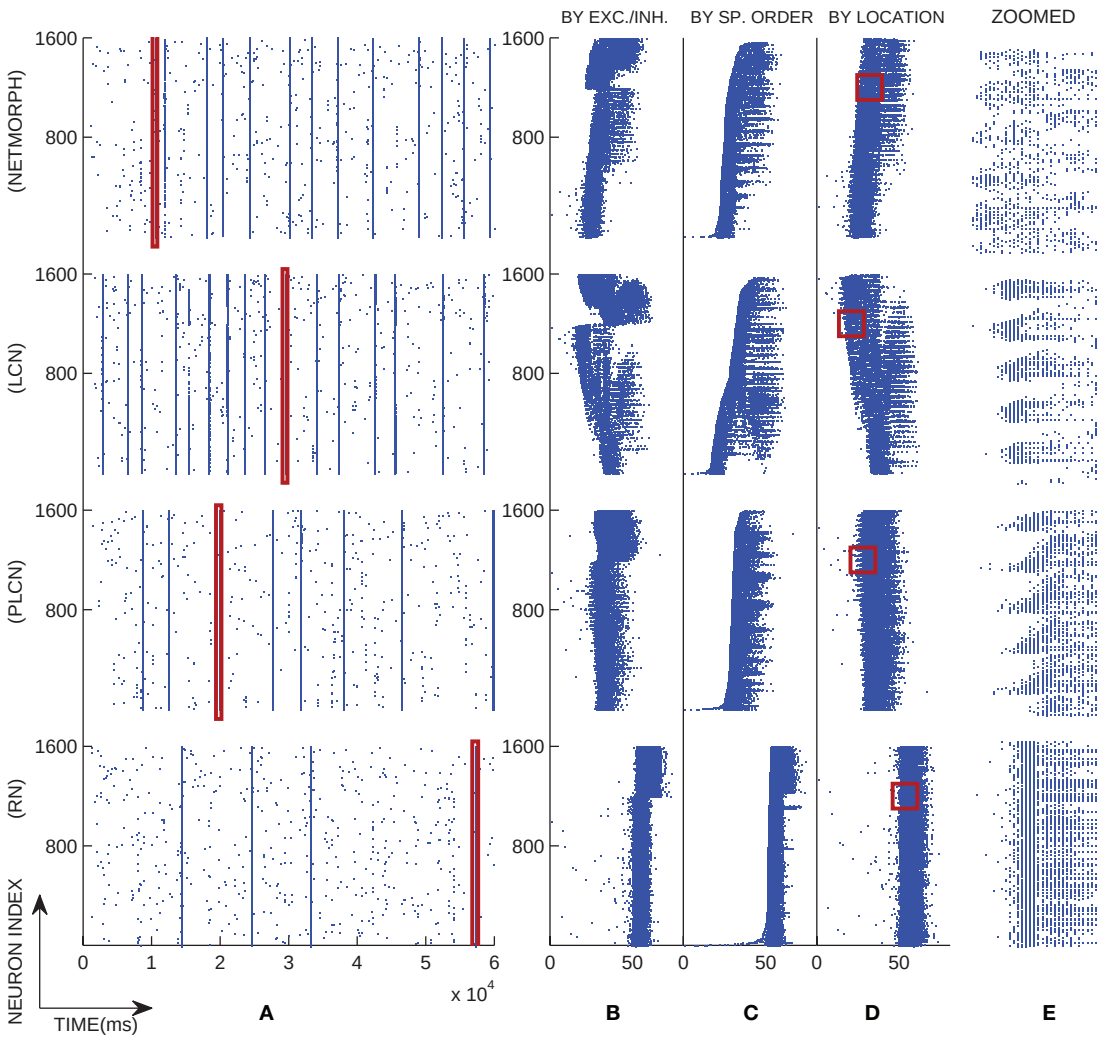

FIGURE 2 | An example of population spike trains of four different networks with a selected burst magnified. The distance-dependence factor $W = 1$ is used in the PLCN network. **(A)**: The full population spike train, **(B–D)**: The spiking pattern of the selected burst illustrated by different orderings of the neurons, and **(E)**: The selected region in **(D)** magnified. In **(B)** the neurons are primarily ordered by their type and secondarily by their location in the grid such that the lower spike trains represent the excitatory neurons and the upper spike trains the inhibitory neurons. In **(C)** the neurons are ordered by the time of their first spike in the selected burst, i.e., the lower the spike train is, the earlier its first spike occurred. In **(D)** the neurons are ordered purely by their location in the grid.

considering the origin of an object. This makes it more attractive for the proposed studies as we can consider the information in individual network structures and their dynamics. The KC $C(x)$ of a finite object x is defined as the length of the shortest binary program that with no input outputs x on a universal computer. Thereby, it is the minimum amount of information that is needed in order to generate x. Unfortunately, in practice this quantity is not computable (Li and Vitanyi, 1997). While the computation of KC is not possible an upper bound can be estimated using lossless compression. We utilize this approach to obtain approximations for KC.

In this work we study the complexity of an object by the means of diversity of the information it carries. The object of our research is the structure of a neuronal network and the dynamics it produces. There are numerous existing measures for the complexity of a network (Neel and Orrison, 2006), and a few measures exist also for the complexity of the output of a neuronal network (Rapp et al., 1994), but no measure of complexity that could be used for both structure and dynamics has – to the best of our knowledge – been studied. To study the complexity of the structure we consider the connectivity matrix that represents the network, as for the complexity of the network activity we study the spike trains representing spontaneous activity in the neuronal network. We apply the same measure for assessing complexity in both structure and dynamics.

2.3.1 Inferring complexity from NCD distribution

We use the NCD presented in Li et al. (2004) as a measure of information distance between two arbitrary strings. The NCD is a computable approximation of an information distance based on KC. The NCD between strings x and y is defined by

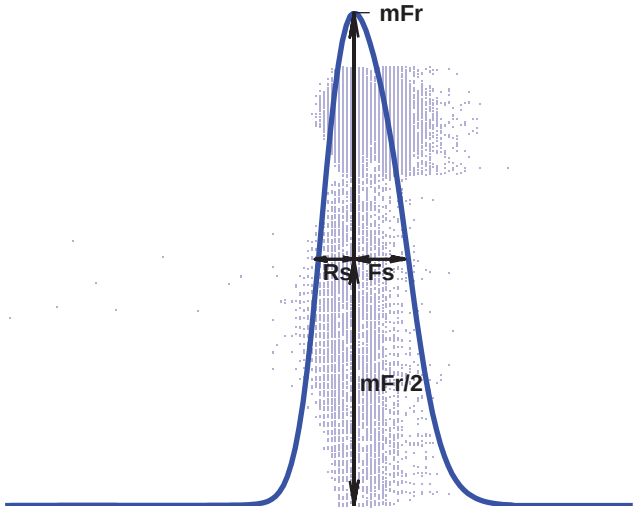

FIGURE 3 | Illustration of the meaning of variables mFr, Rs, and Fs. (as defined in Gritsun et al., 2010).

$$\mathrm{NCD}(x,y)=\frac{C(xy)-\min\big(C(x),C(y)\big)}{\max\big(C(x),C(y)\big)}, \tag{13}$$

where $C(x)$ and $C(y)$ are the lengths of the strings x and y when compressed – accounting for approximations of KCs of the respective strings – and $C(xy)$ is that of the concatenation of strings x and y. In our study we use standard lossless compression algorithms for data compression[1].

The NCD has recently been used in addressing the question whether a set of data is similarly complex as another (Emmert-Streib and Scalas, 2010), based on a statistical approach. In another study (Galas et al., 2010), the complexity of a set of strings is estimated using a notion of context-dependence, also assessable by the means of the NCD. We follow the latter framework and aim at estimating the complexity of an independent set of data – in our study, this set of data is either a set of connectivity patterns or a set of spike trains. In Galas et al. (2010) the *set complexity* measure is introduced; it can be formulated as

$$\Psi(S)=\sum_{i=1}^{N}C(x_i)\sum_{j\neq i}\frac{1}{N(N-1)}f\big(d_{ij}\big)g\big(d_{ij}\big). \tag{14}$$

To calculate the set complexity Ψ one has to approximate the KCs of all strings x_i in the set $S=\{x_1,\ldots,x_N\}$ and the NCDs $d_{ij}=\mathrm{NCD}(x_i,x_j)$ between the strings. The functions f and g of NCD values are continuous on interval [0,1] such that f reaches zero at 1 and g reaches zero at 0.

In this study we, for reasons to follow, diverge from this definition. We define the complexity of a set of data as the *magnitude of variation* of NCD between its elements: the wider the spread of NCD values, the more versatile the set is considered. That is, a complex set is thought to include both pairs of elements that are close to each other from an information distance point of view, pairs of elements that are far from each other, and pairs whose distance is somewhere in between.

[1]http://7-zip.org/

Although the variation of NCD by no means captures all the properties that are required of a complexity measure and fulfilled by the set complexity Ψ, it lacks the difficulty arising in determining the functions f and g in Eq. 14. Let us consider this in more detail from the point of view that we do not know how the functions f and g should be like – which is a fact, apart from the knowledge on them having roots in 0 and 1. Suppose we have two finite sets of strings, $S_1=\{s_1^{(1)},\ldots,s_n^{(1)}\}$ and $S_2=\{s_1^{(2)},\ldots,s_m^{(2)}\}$. Denote the NCDs between the strings of set S_1 by $d_{ij}^{(1)}\in\mathbb{Q}$, where $i,j\in\{1,\ldots,n\}$, and accordingly, let $d_{ij}^{(2)}$ be the NCDs between the strings of set S_2. If any of the NCDs $d_{ij}^{(1)}$ $(i\neq j)$ is unique in the sense that it is unequal to all NCDs $d_{kl}^{(2)}$ $(k\neq l)$, then we find an ε-neighborhood $B_\varepsilon(d_{ij}^{(1)})$ that contains an NCD value of S_1 but none of those of S_2. Thereby, we can choose the functions f and g such that the value of $f\times g$ is arbitrarily large at $d_{ij}^{(1)}$ and arbitrarily small outside $B_\varepsilon(d_{ij}^{(1)})$, leading to $\Psi(S_1)>\Psi(S_2)$. We can generalize this to a case of any finite number of sets $S_1,\ldots,S_N$: if for set S_I, $I\in\{1,\ldots,N\}$ there is an NCD value $d_{ij}^{(I)}$ $(i\neq j)$ that is unequal to all other NCD values $d_{kl}^{(J)}$ $(J\neq I,\ k\neq l)$, then the functions f and g can be configured such that $\forall J\neq I{:}\Psi(S_I)>\Psi(S_J)$. Hence, the lack of knowledge on functions f and g imposes severe restrictions on the eligibility of the set complexity Ψ as such.

What is incommon for the proposals for f and g presented in Galas et al. (2010) is that the product function $f\times g$ forms only one peak in the domain [0,1]. The crucial question is: where should this peak be located – ultimately, this is the same as asking: where is the boundary between "random" and "ordered" sets of data? Adopting the wideness of NCD distribution as a measure of data complexity is a way to bypass this problem. The wider the spread of NCD values, the more likely it is that some of the NCD values produce large values for $f\times g$. Yet, difficulties arise when deciding a rigorous meaning for the "wideness" or "magnitude of variation" of the NCD distribution. In the present work, the calculated NCD distributions are seemingly unimodal; thereby we use the *standard deviation* of the NCD distribution as the measure of complexity of the set.

2.3.2 Data representation for complexity analysis

Two different data analysis approaches to studying the complexity are possible (Emmert-Streib and Scalas, 2010): one can assess (1) the complexity of the process that produces a data realization, or (2) the complexity of the data realization itself. In this study we will apply the approach (2) in both estimating the complexity of structure and the complexity of dynamics. To study the complexity in the context-dependent manner described in Section 2.3.1 we divide the data into a set of data, and represent it as a set of strings. For the structure, the rows of the connectivity matrix are read to strings, i.e., each string s shows the out-connection pattern of the corresponding neuron with s_i = "0" if there is no output to neuron i and s_i = "1" if there is one. The NCDs are approximated between these strings. In order to compute the NCD of the dynamics every spike train is converted into a binary sequence. Each discrete time step is assigned with one if a spike is present in that time slot, and with zero otherwise. For example, a string "0000000000100101000" would correspond to a case where a neuron is at first silent, then spikes at time intervals around $10\Delta t$, $13\Delta t$ and $15\Delta t$, where Δt is a sampling interval.

For the compression of strings we use the general purpose data compression algorithm 7zip[2]. The compressor parameters and the motivation for this particular compression method are given in Appendix 6.3.

3 RESULTS

3.1 SIMULATION SETUP

In the present paper we study both structural and dynamical properties of networks of $N = 1600$ neurons. Regarding the choice of the structure of neuronal networks we base our approach on the growth properties of those networks produced by the NETMORPH simulator. To choose a trade-off between biological reality and ease of comparison to other types of networks we set the initial cell positions in a two-dimensional regular 40×40 grid. The present work does not consider continuous boundaries, i.e., the physical distance between the neurons is the standard Euclidean distance. The distance between adjacent neurons is set ≈25 μm, which is chosen such that the density of neurons corresponds to one of the culture densities examined in Wagenaar et al. (2006) (1600 cells/mm^2). **Figure 4** shows the average connection probability in a NETMORPH network as a function of time, where the average is taken over 16 simulation realizations. The standard deviation of the connection probability is found very small between different realizations (<0.002), hence only mean values are plotted here.

The main emphasis throughout this article will be on connection probabilities $p = 0.02$, 0.05, 0.1, 0.16 that, according to **Figure 4**, correspond to days 8, 11, 15, and 19 *in vitro*. The selected range of days *in vitro* is commonly considered in experimental studies of neuronal cultures. The connection probabilities 0.1 and 0.16 of 15th and 19th DIV, respectively, are in accordance with experimental studies that consider the connectivity of a mature network to be 10–30% (Marom and Shahaf, 2002).

Other considered networks are generated by Algorithm 1 using the abovementioned connection probabilities. The distance-dependence factors for these networks are chosen as $W = 0$, 0.5, 1, 2, 4, 10, ∞.

The spiking activity in the abovementioned networks is studied by simulating the time series of the $N = 1600$ individual neurons according to Section 2.2. The connectivity matrix of the modeled network defines which synaptic variables y_{ij} need to be modeled: the synaptic weights A_{ij} are non-zero only for non-zero connectivity matrix entries M_{ij}, hence for such (i,j) that $M_{ij} = 0$ the synaptic variables y_{ij} can be ignored in terms of Eq. 9. In this article we disallow multiple synapses from a neuron to another. Throughout the paper the fraction of the inhibitory neurons is fixed to 25%, which are picked by random, and the sampling interval is fixed to 0.5 ms.

3.2 NETWORK STRUCTURE CLASSES DIFFER IN THEIR GRAPH THEORETIC PROPERTIES

We first study the structural properties of the network classes presented above by the means of measures introduced in Section 2.1.2. The in-degree distributions of the networks generated by Algorithm 1 are always binomial, as the out-degree distributions vary. Empirically calculated out-degree distributions, path length distributions, and local clustering coefficient distributions are shown in **Figure 5**, together with the respective NETMORPH distributions.

One can observe an increase in the mean path length as well as mean clustering coefficient with the increase of distance-dependence factor W, i.e., when moving from RN toward LCN. The out-degree distributions of NETMORPH networks are wider than those of any other type of network, but regarding the width and mean of the path length and clustering coefficient distributions the NETMORPH networks are always somewhere between RN and LCN.

3.3 NETWORKS WITH DIFFERENT STRUCTURE SHOW VARIATION IN BURSTING BEHAVIOR

For the activity part we simulate 61 s of spike train recordings using the models described in Section 2.2 and the model parameters described in Appendix 6.2. In all of our simulations a network burst occurs in the very beginning due to the transition into a steady state, which is why we ignore the first second of simulation. We simulate a set of spike trains for structure classes $W = 0$, 1, ∞ and NETMORPH using connection probabilities $p = 0.02, 0.05, 0.1, 0.16$. The average connection weight and other model parameters stay constant, only the connectivity matrix varies between different structure classes and different connection probabilities. In the case of $p = 0.02$ none of the networks shows bursting behavior, for $p = 0.05$ a burst emerges in about one out of three 1-min simulations, as for $p = 0.1$ and $p = 0.16$ there are bursts in every 1-min recording. **Table 1** shows the acquired mean bursting frequencies – they are comparable to the ones obtained in Gritsun et al. (2010). We concentrate on the two bigger connection probabilities.

[2]http://7-zip.org/

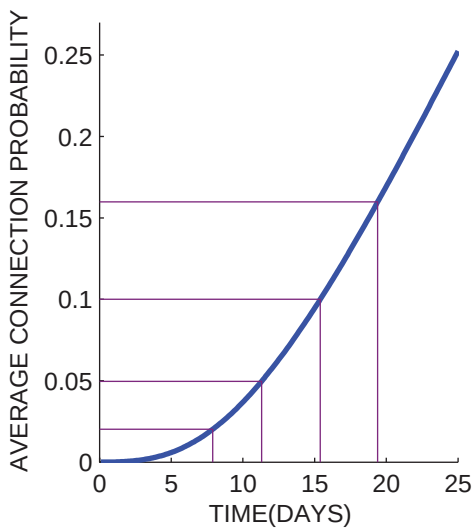

FIGURE 4 | Connection probability as a function of time in the structure of networks generated by the NETMORPH simulator.

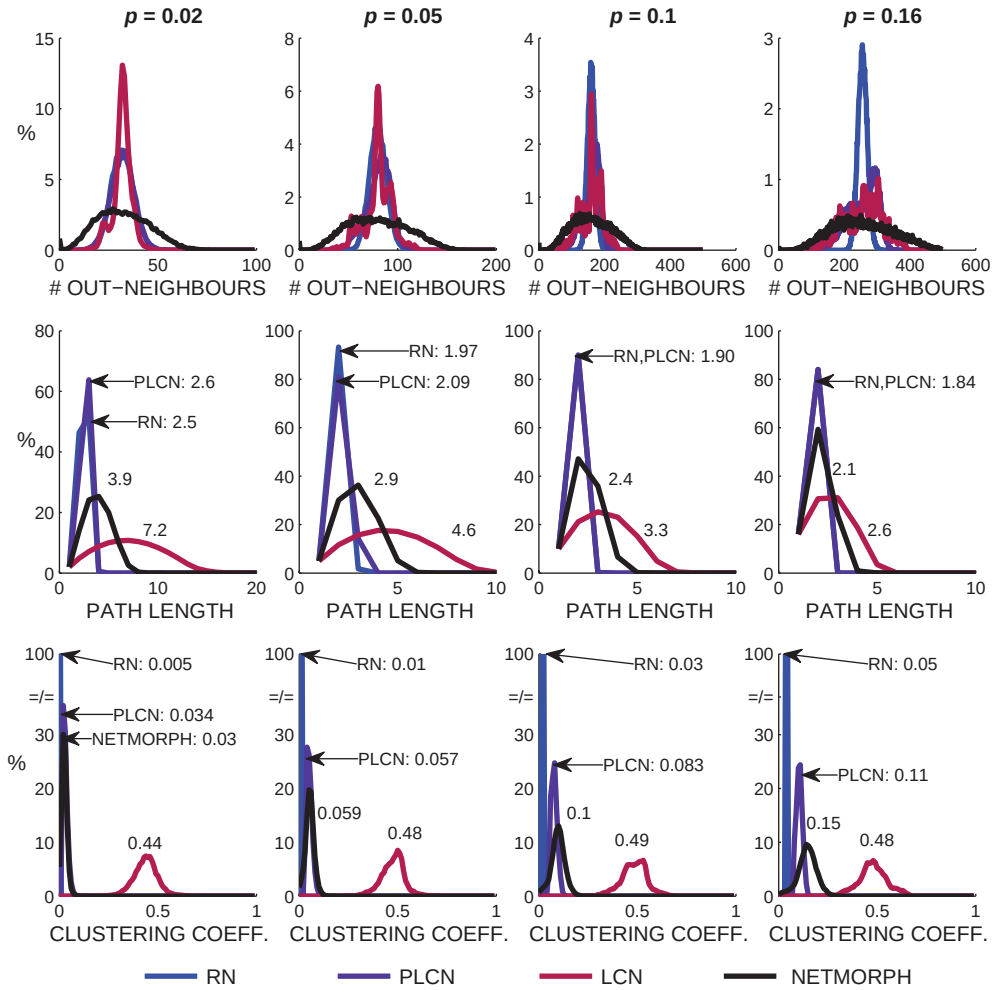

FIGURE 5 | Out-degree, path length and clustering coefficient distributions plotted for different network classes and different connection probabilities. The power coefficient $W = 1$ is used for PLCN networks. The mean path lengths and mean clustering coefficients are shown in association with the respective curves.

Table 1 | Bursting rates of networks of different structure classes.

	$W = 0$	$W = 1$	$W = \infty$	NETMORPH
$p = 0.1$	4.1 ± 1.3	7.5 ± 2.0	13.3 ± 0.9	10.7 ± 2.2
$p = 0.16$	16.4 ± 1.2	17.6 ± 1.2	19.8 ± 2.0	19.0 ± 1.6

Values shown: mean ± SD in bursts/min, calculated from 16 different 1-min recordings per table entry.

The difference between the intraburst patterns of the different networks can already be observed in the magnified burst images in **Figure 2**, particularly in 2C where the effect of the location of the neuron in the grid is neglected. We show the difference by studying the following burst statistics: spike count per burst (SC), and the three burst shape statistics defined above (mFr, Rs, and Fs). **Figure 6** shows the distribution of these statistics in activity simulations of different network structure classes. The means as well as the medians of the three latter measures for both the NETMORPH and $W = 1$ networks constantly fall between the two extremes, LCN and RN. The same does not hold for SC.

We test the difference of the medians statistically between different structure classes using *U*-test. The null hypothesis is that the medians of two considered distributions in a panel of **Figure 6** are equal. The distributions of each measure (SC, mFr, Rs, Fs) and each network density are tested pairwise between the different network types. The test shows similarity of medians of Rs distributions between NETMORPH network and PLCN with connection probability 0.1 (p-value = 0.59), but not in the case of connection probability 0.16 (p-value = 1.7×10^{-13}). The same holds for medians of Fs distributions of these networks, respective p-values being 0.20 and 0.0027. In all the rest of the cases the null hypothesis of medians of any measure being the same between any two distributions of different structure classes can be rejected, as none of the p-values exceeds 0.002. The variances of the distributions are not tested, but one can observe that LCNs clearly produce the widest SC, Rs, and Fs distributions.

3.4 COMPLEXITY RESULTS IN STRUCTURE AND DYNAMICS

We start by studying simultaneously the KC of the rows of a connectivity matrix and the KC of the spike trains of the corresponding neurons. We generate a network for each structure class ($W = 0, 0.5,$

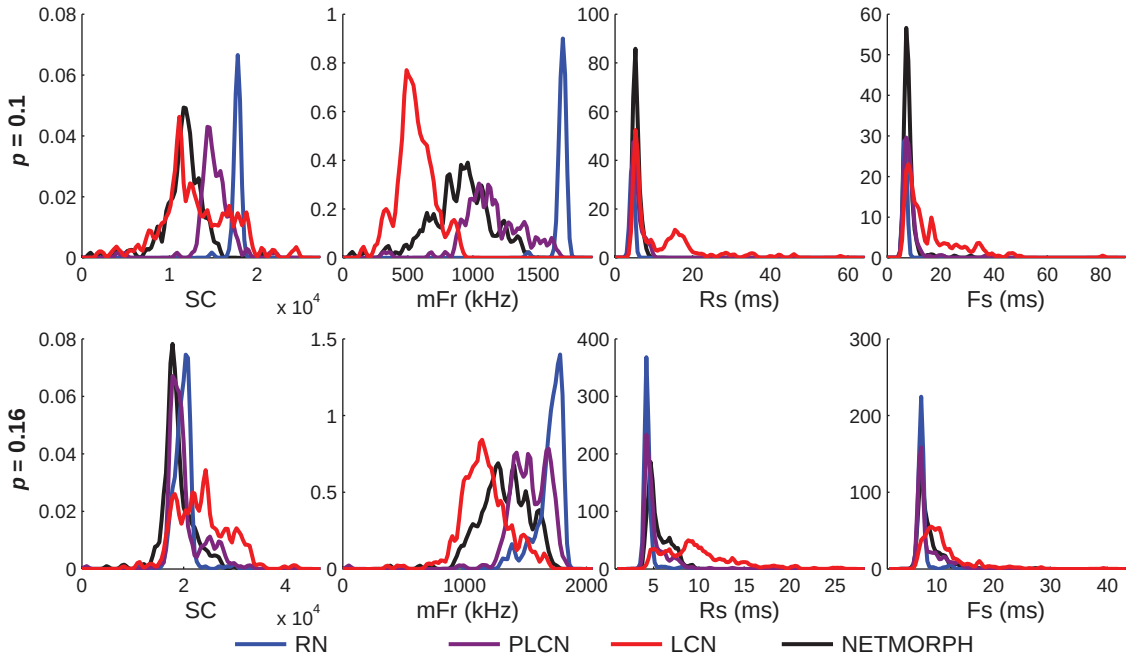

FIGURE 6 | Distributions of spike count/burst (SC, far left), maximum firing rate in a burst (mFr, middle-left), rising slope length (Rs, middle-right), and falling slope length (Fs, far right) for spike trains obtained by using different structure classes and different connection probabilities (upper: 0.1; lower: 0.16). The distance-dependence factor $W = 1$ is used for PLCN. Histograms are smoothed using a Gaussian window with standard deviation = range of values/100.

$1, 2, 4, 10, \infty$; NETMORPH) and a population spike train recording for each of these networks. A set of 80 neurons is randomly picked from the $N = 1600$ neurons retaining the proportion of excitatory and inhibitory neurons. This data set is considered representative of the whole set of neurons. **Figure 7** shows approximations of KCs for both structure and dynamics of different structure classes and different connection probabilities. The value of C(struc) shows the length of a compressed row of the connectivity matrix as C(dyn) is the length of the compressed spike train data of the corresponding neuron.

Figure 7 shows that the mean of the compression lengths of full spike train data descends when moving from local to random networks, as the mean compression length of columns of connectivity matrix ascends. The rising of the C(struc) is in accord with the fact that random strings maximize the KC of a string, whereas the descending of the mean values of C(dyn) can be explained by the decrease in the number of bursts. A slightly similar trend is visible when studying the KC of intraburst spike trains, but more than that, the range of values of C(dyn) seems to decrease when moving from local to random networks.

However, as pointed out earlier, the KC alone does not tell much about diversity of the data set, only the information content of each element of the set alone. We wish to address the question of to what extent the information in one element is repeated or near-to-repeated in the other elements. We first analyze the structure and dynamics data using alternative measures, namely, Hamming distance (HD) and cross-correlation coefficient (CC). HD counts the proportion of differing bits in two binary sequences: it equals zero for identical sequences and one for sequences that are inverse of each other. The same elements as those in **Figures 7A,C** are analyzed using HD, i.e., the rows of connectivity matrix and spike trains of the corresponding neurons. The same number of 80 sample neurons is picked randomly, and HD is computed between the $\binom{80}{2} = 3160$ pairs of neurons. In addition, the dynamics is analyzed using CC between pairs of spike trains. The CC measures similarity between two spike trains and is capable of capturing time shifts between the signals. Hence the CC serves as an extension of the HD, or of the inverse of HD (as cross-correlation measures similarity and HD measures divergence). **Figure 8** shows the distribution of HD computed for both structure and dynamics (**Figures 8A,C**) and that of CC computed for dynamics versus HD computed for structure (**Figures 8B,D**).

In **Figures 8A,C** one can observe the widening of the HD distribution in both structure and dynamics when moving from random to local networks. The same applies for the CC distribution (**Figures 8B,D**). The HD(struc) distributions of the most locally connected networks are wider than that of RN, because for each neuron there exist some neurons with a lot of common out-neighbors (the spatially nearby neurons, small HD value) and some neurons with zero or near to zero common out-neighbors (the spatially distant neurons, large HD value). For some of the considered networks a bimodal distribution of HD(dyn) can be observed. In such cases, the peak closer to zero corresponds to the comparison of neurons of the same type (excitatory–excitatory or inhibitory–inhibitory), while the peak further from zero corresponds to comparison of neurons of different type (excitatory–inhibitory). This bimodality is due to the difference in intraburst patterns between excitatory and inhibitory neurons: **Figure 2B** shows that on average the inhibitory population starts and ends bursting later than the excitatory one. This effect is most visible

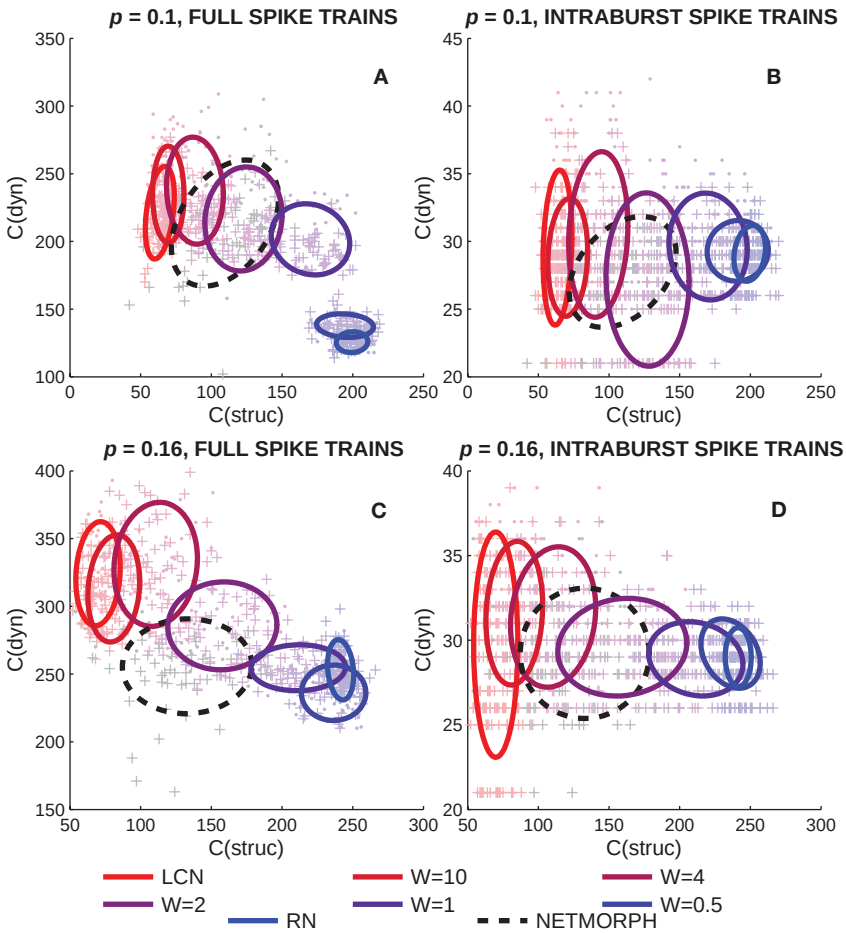

FIGURE 7 | Kolmogorov complexity approximation of a spike train of a neuron (dyn) versus the KC approximation of the respective row of connectivity matrix (struc). (A,C): The full spike train of a neuron read into the string to be compressed. **(B,D)**: Intraburst segments of the spike train read into separate strings (i.e., several "C(dyn)"-values possible for each "C(struc)"-value). In **(A,B)** the connection probability of the networks is 0.1, in **(B,D)** 0.16. The markers "+" represent excitatory neurons, as "·" are inhibitory. The ellipses drawn represent 67% of the probability mass of a Gaussian distribution with the same mean and covariance matrix as the plotted data.

in RNs, as can be observed both in **Figures 2 and 8A**. As for the CCs, the distributions are unimodal. This indicates that the differences between the spiking patterns of inhibitory and excitatory neurons are observable on small time scale (HD uses the bins of width 0.5 ms), but not on large time scale (cross-correlations are integrated over an interval of ±50 ms). This is further supported by the fact that when the time window for CC calculations is narrowed, the CCs between neurons of same type become distinguishable from those between neurons of different type (data not shown).

Both HD and cross-correlation, however, assess the similarity between the data by observing only local differences. The HD determines the average difference between the data by comparing the data at exact same locations, as the cross-correlation allows some variation on the time scale. Both measures fail to capture similarities in the data if the similar patterns in the two considered data sequences lie too far from each other. This is also the case if the sequences include more subtle similarities than time shifts, e.g., if one sequence is a miscellaneous combination of the other's subsequences. Thereby, we proceed to the information diversity framework presented in Section 2.3.1. We take the same elements as in **Figure 7** – rows of connectivity matrix and full spike train data of neurons or intraburst segments only – and calculate the NCDs between these elements. These NCD distributions are plotted in **Figure 9**.

One can observe a gradual increase in the mean values of NCD(struc) with the increase of randomness to the structure of the network in **Figure 9**. This is rather expected: the more randomness applied to the structure of the network, the further away the connectivity data of different neurons are from each other. As for the NCD(dyn) values between full spike train data of neurons, one can observe a gradual decrease in the mean value with the increase of randomness, and a slightly similar evolution is visible in the burst-wise calculations as well. Both this and the decrease in the deviation of the NCD(dyn) values are in accordance with the properties of intraburst spike patterns illustrated in **Figure 2**: the spike train data seem more diverse and wider-spread in the local networks than in the random ones. Furthermore, as the bursting frequency is higher in LCNs than in RNs (**Table 1**), the analyzed LCN spike trains (1 min recordings) show more variability than

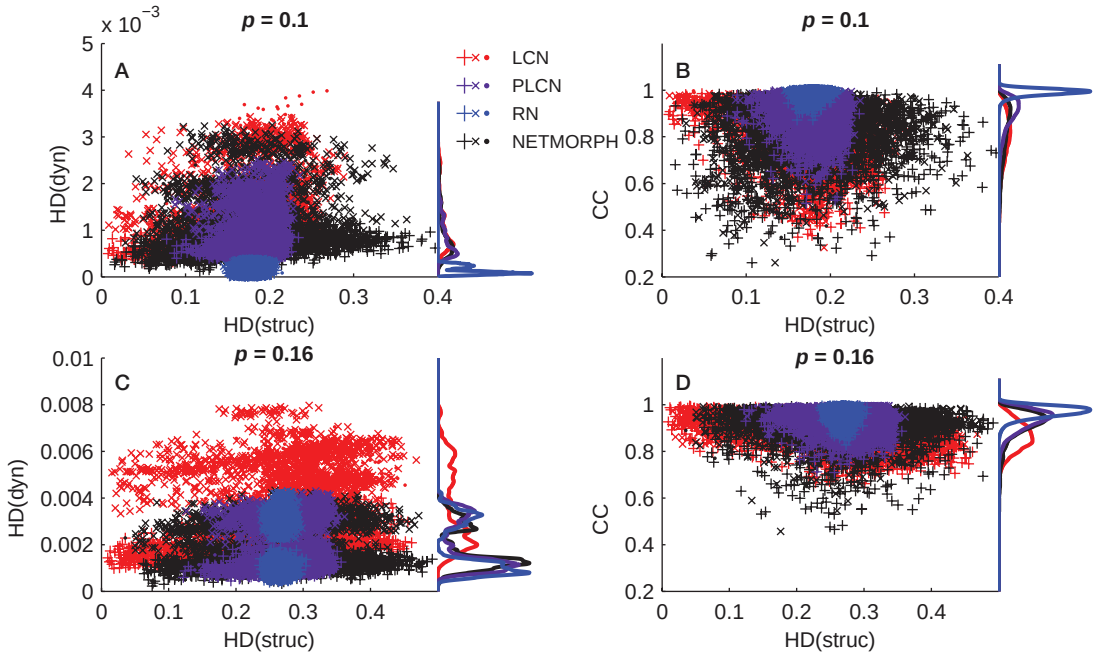

FIGURE 8 | (A,C): Hamming distances between spike trains (dyn) versus the HD between the corresponding rows of connectivity matrix (struc). **(B,D)**: Cross-correlation coefficient between spike trains (CC) versus the HD between the corresponding rows of connectivity matrix. In all panels the markers "+" represent comparisons of two excitatory neurons, "x" are comparisons between excitatory and inhibitory neurons, and "·" are comparisons between two inhibitory neurons. The distance-dependence factor $W = 1$ is used for the PLCN.

those of RN. Consequently, the mean NCD(dyn) is visibly higher in LCN. When analyzing the dynamics of the intraburst interval, data variability is less pronounced and the difference between the means of NCD(dyn) distributions is smaller.

We repeat the experiment of **Figure 9** 10 times, and for each entry we calculate the standard deviations of NCD distributions (i.e., the complexities in our definition) of both structure and dynamics. **Table 2** shows the mean complexities and their standard deviations, and the network classes in which the complexity is significantly different from that of a RN. The table shows that the structural complexity decreases with the increase of randomness to the structure. The complexity of full spike trains shows a less consistent trend. For sparser networks ($p = 0.1$), the more locally connected networks produce more complex full spike trains than RNs, as for denser networks ($p = 0.16$), only one of the PLCNs has statistically different complexity from that of RNs. We consider the latter statistical difference an outlier as a clear trend is absent. For the intraburst complexities the results suggest that the LCNs together with NETMORPH and some of the most locally connected PLCNs produce more complex dynamics than RNs.

The information diversity results of **Table 2** do not clearly indicate which network produces the most complex dynamics. The *p*-values for the test whether the information diversity of the most complex full spike trains is different from that of the second most complex are 0.13 and 0.38 for sparse and dense networks, respectively. For the intraburst complexities the respective *p*-values are 0.80 and 0.62. The results for the complexity of structure are qualitatively the same when considering the *columns* of connectivity matrix, i.e., the in-connection patterns, instead of rows (data not shown). Furthermore, the decrease in the complexity of the structure by the increase in randomness is also present in the case where the neurons in the connectivity matrix are randomly permutated. This shows that the trend in the structural complexity in **Table 2** is not an artifact of the order in which the neuron connectivities are read into strings.

3.5 CONCLUSION

The structure of RNs are described by low path length and low clustering coefficient, and further by high KC and low information diversity. The RN dynamics is described by short and relatively rare bursts, and hence low KC of the spike train data. As the opposite, the structure of LCNs show longer path length and greater clustering coefficient, and the KC approximations of the structural data are small while the information diversity is large. The bursts in the LCN spike trains are longer and more frequent than in RN spike trains. The KC approximations of the LCN spike train data are large on average. Based on the variation in NCD, the intraburst complexity is higher in LCN output than in that of RN, and for the sparser of the two network densities the same holds for complexities of full spike trains.

The in-between networks, PLCNs, fall between the two extremes (RN and LCN) by their structural properties as well as their bursting behavior. The same holds for the biologically realistic NETMORPH networks. The information diversity of the structure of these networks is between that of RN and LCN. Similarly to LCNs, the intraburst dynamics of NETMORPH networks as well as the most locally connected PLCNs are more complex in terms of NCD variation than that of RNs.

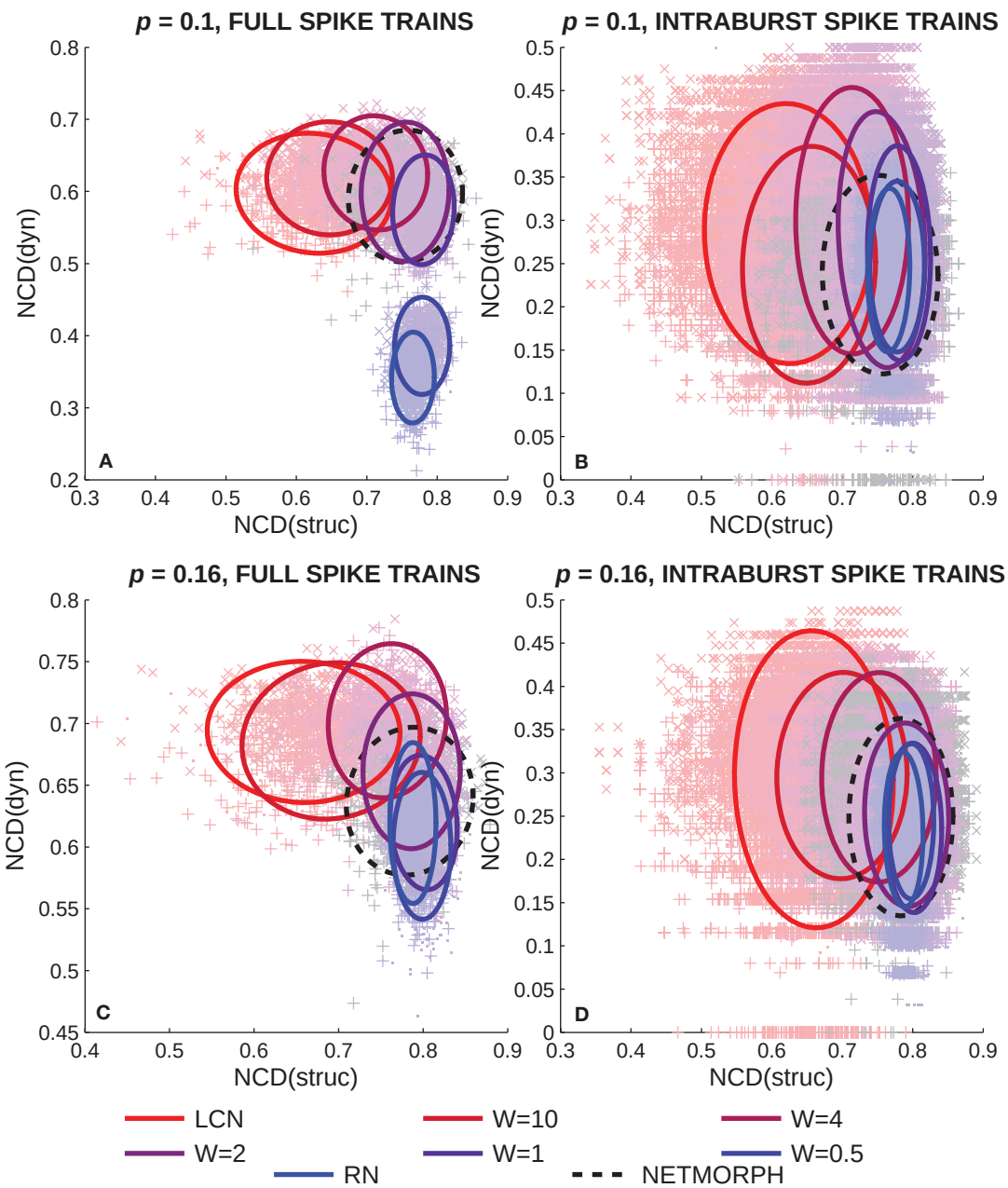

FIGURE 9 | Normalized compression distances between spike trains of neurons (dyn) versus the NCD between respective rows of connectivity matrix (struc). The four figures arranged in a similar manner as in **Figure 7**, i.e., in **(A,C)** full spike trains are considered, and in **(B,D)** intraburst spike trains are considered. The ellipses drawn represent 90% of the probability mass of a Gaussian distribution with same mean and covariance matrix as the plotted data.

4 DISCUSSION

In this work we present and apply an information diversity measure for assessing complexity in both structure and dynamics. According to this measure the neuronal networks with random structure produce less diverse spontaneous activity than networks where the connectivity of neurons is more dependent on distance. The presented study focuses on only one neuronal activity model, i.e., Izhikevich type neurons with dynamical model of synapses (Tsodyks model), and the networks of fixed size ($N = 1600$). The further studies testing alternative models and examining the influence of network size are needed to confirm these findings. Still, the presented results demonstrate capability of the employed measure to discriminate between different network types.

The basis for the present study is the question: if one changes the structure of the neuronal network but keeps the average degree (or even the whole in-degree distribution) constant, how does

Table 2 | Complexities calculated as standard deviations of NCD distributions for both elements of structure and dynamics.

	STRUCT	DYN (full)	DYN (bursts)	STRUCT	DYN (full)	DYN (bursts)
LCN	0.054 ± 0.003*	0.040 ± 0.003*	0.071 ± 0.012*	0.051 ± 0.003*	0.027 ± 0.003	0.057 ± 0.006*
W = 10	0.045 ± 0.002*	0.041 ± 0.004*	0.067 ± 0.008*	0.045 ± 0.003*	0.030 ± 0.003	0.053 ± 0.003*
W = 4	0.036 ± 0.002*	0.042 ± 0.003*	0.075 ± 0.006*	0.036 ± 0.004*	0.027 ± 0.002	0.057 ± 0.007*
W = 2	0.029 ± 0.001*	0.045 ± 0.004*	0.074 ± 0.015*	0.027 ± 0.002*	0.027 ± 0.003	0.048 ± 0.004*
W = 1	0.022 ± 0.001*	0.034 ± 0.004*	0.055 ± 0.007*	0.019 ± 0.001*	0.025 ± 0.002*	0.047 ± 0.006
W = 0.5	0.017 ± 0.001*	0.028 ± 0.002	0.048 ± 0.020	0.014 ± 0.001*	0.029 ± 0.002	0.042 ± 0.003
RN	0.014 ± 0.001	0.028 ± 0.002	0.042 ± 0.002	0.013 ± 0.001	0.029 ± 0.003	0.044 ± 0.005
NETM	0.040 ± 0.004*	0.039 ± 0.006*	0.053 ± 0.008*	0.033 ± 0.002*	0.027 ± 0.003	0.052 ± 0.005*

The three leftmost columns are calculated from simulations with connection probability p = 0.1, three rightmost with p = 0.16. Each entry represents the mean ± standard deviation of the wideness of the NCD distribution, calculated over 10 repetitions for each entry. The entries where the median of values is significantly different (U-test, p-value 0.05) from the corresponding RN entry are marked with asterisk (*).

the spontaneous activity change? In the activity simulations, all model parameters remain constant, only the connectivity matrix is changed between the simulations of different network types; hence the variation in bursting properties emerges from the structure of the network only. The selected algorithm for generation of network structure possesses the capability to tune distance-dependence on a continuous scale. As a result, we have not only fully locally connected networks, where a neuron always first connects to its nearest spatial neighbors before the distant ones ($W = \infty$, i.e., LCN), and fully random networks ($W = 0$, i.e., RN), but everything in between ($0 < W < \infty$, PLCN). The RNs correspond to directed Erdo˝s–Rényi networks that are widely used in similar studies in the field. These networks are characterized by a binomial degree distribution; hence the choice of binomial in-degree distribution for all network types. The only network class to violate this binomiality are the NETMORPH networks, which are considered in order to increase the biological plausibility of the study. The results showing that the NETMORPH networks are placed somewhere between the LCNs and RNs by most of their structural and dynamical properties also support the use of Algorithm 1 for the network generation. If this was not the case, one would have to try to find another way to produce networks with as extreme properties as those in NETMORPH networks. The range of networks between LCN and RN could also be produced with an application of Watts–Strogatz' algorithm (Watts and Strogatz, 1998). The crucial difference is that in our in-between networks (PLCNs) the "long-range connections" are the shorter the bigger the parameter W is, while in Watts–Strogatz' model the long-range connections are (roughly) on average equally long in all in-between networks. By a long-range connection we mean any connection to neuron A from neuron B when A is not yet connected to all neurons that are spatially nearer than B.

The complexity framework presented in this paper is adopted from Nykter et al. (2008), where critical Boolean networks are found to have the most complex dynamics out of a set of various Boolean networks. The method for estimating the complexity in the present work is different in the way that we apply the NCD measure between elements of a set that represents the object whose complexity is to be estimated (connectivity matrix, population spike train), not between different output realizations as in Nykter et al. (2008). This allows the estimation of the complexity of the object itself, not of the set of objects generated with the same process. The complexity of the object is assessed by the diversity of the information it carries. Although technically applicable to any set of strings, this is not supposed to be a universal measure of complexity. However, its use lacks the difficulties that arise when applying an alternative set complexity measure defined in Galas et al. (2010), as discussed in Section 2.3.1. The said non-universality of our measure stems from the limited range of deviation values that a NCD distribution can have, and on the other hand, the plain standard deviation might not be a good measure of wideness if the underlying distributions were multimodal. In this work all studied NCD distributions are unimodal. Furthermore, we only apply this complexity measure on data of comparable lengths and comparable characteristics, hence the resulting complexities are also comparable to each other. This may not be true in the opposite case, for example, spike trains of length 1 s and 1 h cannot be compared in an unbiased way.

In this study we show how the NCD values of both structure and dynamics of a neuronal network are distributed across the $[0,1] \times [0,1]$-plane in the model networks (**Figure 9**), and calculate the mean information diversities of both structure and dynamics (**Table 2**). The **Figures 9A,C** themselves give a good overview of the interplay between structural and dynamical information diversity. They show that the NCD distributions, computed for the considered types of networks, follow a visible trajectory. This trajectory is not evident when observing the widths of the NCD distributions only, nor when computing simpler distance measures (e.g., HD). The trajectory follows an "L"-shape, which is slightly violated by the NETMORPH NCD distribution (see **Figure 9C**). Whether there exists a network of the same degree that would span the whole "L"-shaped domain or a "superdiverse" network whose NCD values would cover also the unoccupied corner of the "L"-rectangle remains an open question. We have shown that such networks do not exist among the model classes studied here, and in the light of the results shown we also doubt the existence of such networks altogether, given the constraints of binomial in-degree distribution and the selected connection probability.

The different networks are separable also by the KC approximations of their structure and dynamics (**Figure 7**). However, we consider the KC analysis alone insufficient because it lacks the notion of context-dependence: the KC of a spike train would be maximized when the on-set of neurons (i.e., spikes) are as frequent as off-set of neurons (i.e., silent time steps) and randomly distributed

in time. The effect of number of spikes on KC is already seen in **Figures 7A,C**: the KCs of spike trains of dense networks, where the number of spikes is greater, are on average greater than those of sparse networks. This is contrary to the case of context-dependent complexities, as shown in **Table 2**, where the information diversities of full spike trains of dense networks are on average smaller than those of sparse networks. This leads to a profound question: how much spiking and bursting can there be before the activity is too random in order to contain any usable information? We believe that in order to address this question one has to apply a context-dependent measure of complexity instead of KC.

The complexity result in **Table 2** concerning the information diversity of structure seems to contradict with the general notion according to which the most regular structure should be less complex than the structure that possesses both regularity and randomness (Sporns, 2011). It should be noted, however, that also the most regular networks studied in this work (LCNs) occupy a degree of randomness, since their in-degree distribution is binomial and since farthest neighbors of a neuron are picked by random out of all equally distant ones. There is a multitude of possibilities for the most ordered structure, other than the one chosen in this work. For example, in Sporns (2011) a fully connected network is suggested to be a highly ordered neuronal system. Applying the information diversity measure to such structure in the framework of **Table 2** gives a structural complexity of ≈0.0268, which is less than that of the majority of the studied PLCNs. Hence, we regard the proposed measure eligible to assess the complexity of the structure.

In addition to analysis of well defined models, the presented measure can be used for analysis of experimental data. The method is straightforwardly applicable to neuronal activity recorded in the form of spike trains. Conversion of spike trains into binary sequences is described in the method section of this paper, as well as in the previous studies (Christen et al., 2006; Benayon et al., 2010). It can be observed that variability in NCD distribution corresponds to the variability in spiking patterns within population bursts. Similar measures of entropy and KC have been applied before, but the capability of the NCD to capture context between different data makes it suitable for assessing data complexity. The presented measure can be used to analyze different phases in neuronal network growth, where the structure is simulated by publicly available growth simulators (Koene et al., 2009; Acimovic et al., 2011). Analysis of network structure, using the procedure described in this paper, can be employed for this study. Analysis of the structure and dynamics of the presented models can be used in relation to the *in vitro* studies with modulated network structure. The results of model analysis can help to predict and understand the recorded activity obtained for certain network structures imposed by the experimenter (Wheeler and Brewer, 2010). Finally, the NCD variation as a measure of structural complexity, can be applied to analyze the large-scale functional connectivity of brain networks, similarly to the examples pointed in Sporns (2011).

The framework proposed in this study provides a measure of data complexity that is applicable to both structure and dynamics of neuronal networks. According to this measure, the neuronal networks with random structure show consistently less diverse intraburst dynamics than the more locally connected ones. The future work will incorporate a larger spectrum of different network structures in order to discover the extreme cases that more clearly maximize or minimize the complexity of dynamics.

5 ACKNOWLEDGMENTS

The authors would like to acknowledge the following funding: TISE graduate school, Academy of Finland project grants no. 106030, no. 124615, and no. 132877, and Academy of Finland project no. 129657 (Center of Excellence in Signal Processing). Constructive comments provided by the reviewers were very useful in preparing the paper. The authors are grateful to the reviewers for pointing out the shortcomings in the first versions of the manuscripts and helping to improve it.

REFERENCES

Aćimović, J., Mäki-Marttunen, T., Havela, R., Teppola, H., and Linne, M.-L. (2011). Modeling of neuronal growth in vitro: comparison of simulation tools NETMORPH and CX3D. *EURASIP J. Bioinform. Syst. Biol.* 2011, Article ID 616382.

Albert, R., and Barabási, A.-L. (2002). Statistical mechanics of complex networks. *Rev. Mod. Phys.* 74, 47–97.

Amigó, J. M., Szczepański, J., Wajnryb, E., and Sanchez-Vivez, M. V. (2004). Estimating the entropy rate of spike trains via Lempel-Ziv complexity. *Neural Comput.* 16, 717–736.

Benayon, M., Cowan, J. D., van Drongelen, W., and Wallace, E. (2010). Avalanches in a stochastic model of spiking neurons. *PLoS Comput. Biol.* 6, e1000846. doi: 10.1371/journal.pcbi.1000846

Boccaletti, S., Latora, V., Moreno, Y., Chavez, M., and Hwang, D.-U. (2006). Complex networks: structure and dynamics. *Phys. Rep.* 424, 175–308.

Brunel, N. (2000). Dynamics of sparsely connected networks of excitatory and inhibitory spiking neurons. *J. Comput. Neurosci.* 8, 183–208.

Chiappalone, M., Bove, M., Vato, A., Tedesco, M., and Martinoia, S. (2006). Dissociated cortical networks show spontaneously correlated activity patterns during in vitro development. *Brain Res.* 1093, 41–53.

Christen, M., Kohn, A., Ott, T., and Stoop, R. (2006). Measuring spike pattern variability with the Lempel-Ziv-distance. *J. Neurosci. Methods* 156, 342–350.

Emmert-Streib, F., and Scalas, E. (2010). Statistic complexity: combining Kolmogorov complexity with an ensemble approach. *PLoS ONE* 5, e12256. doi: 10.1371/journal.pone.0012256

Frégnac, Y., Rudolph, M., Davison, A. P., and Destexhe A. (2007). "Complexity in neuronal networks," in *Biological Networks*, ed. François Képès (Singapore: World Scientific), 291–338.

Galas, D. J., Nykter, M., Carter, G. W., Price, N. D., and Shmulevich, I. (2010). Biological information as set-based complexity. *IEEE Trans. Inf. Theory* 56, 667–677.

Gewaltig, M.-O., and Diesmann, M. (2007). Nest (neural simulation tool). *Scholarpedia* 2, 1430–1434.

Gritsun, T. A., Le Feber, J., Stegenga, J., and Rutten, W. L. C. (2010). Network bursts in cortical cultures are best simulated using pacemaker neurons and adaptive synapses. *Biol. Cybern.* 102, 293–310.

Itzhack, R., and Louzoun, Y. (2010). Random distance dependent attachment as a model for neural network generation in the *Caenorhabditis elegans*. *Bioinformatics* 26, 647–652.

Izhikevich, E. M. (2003). Simple model of spiking neurons. *IEEE Trans. Neural Netw.* 14, 1569–1572.

Koene, R. A., Tijms, B., van Hees, P., Postma, F., de Ridder, A., Ramakers, G. J. A., van Pelt, J., and van Ooyen, A. (2009). NETMORPH: a framework for the stochastic generation of large scale neuronal networks with realistic neuron morphologies. *Neuroinformatics* 7, 195–210.

Kriegstein, A. R., and Dichter, M. A. (1983). Morphological classification of rat cortical neurons in cell culture. *J. Neurosci.* 3, 1634–1647.

Kriener, B., Tetzlaff, T., Aertsen, A., Diesmann, M., and Rotter, S. (2008). Correlations and population dynamics in cortical networks. *Neural Comput.* 20, 2185–2226.

Kumar, A., Rotter, S., and Aertsen, A. (2008). Conditions for propagating synchronous spiking and asynchronous firing rates in a cortical network model. *J. Neurosci.* 28, 5268–5280.

Latham, P. E., Richmond, B. J., Nelson, P. G., and Nirenberg, S. (2000). Intrinsic dynamics in neuronal networks. I. Theory. *J. Neurophysiol.* 83, 808–827.

Li, M., Chen, X., Li, X., Ma, B., and Vitányi, P. M. B. (2004). The similarity metric. *IEEE Trans. Inf. Theory* 50, 3250–3264.

Li, M., and Vitanyi, P. (1997). *An Introduction to Kolmogorov Complexity and Its Applications*, 2nd Edn. New York: Springer-Verlag.

Marom, S., and Shahaf, G. (2002). Development, learning and memory in large random networks of cortical neurons: lessons beyond anatomy. *Q. Rev. Biophys.* 35, 63–87.

Neel, D. L., and Orrison, M. E. (2006). The linear complexity of a graph. *Electron. J. Comb.* 13, 1–19.

Newman, M. E. J. (2003). The structure and function of complex networks. *SIAM Rev.* 45, 167–256.

Nykter, M., Price, N. D., Larjo, A., Aho, T., Kauffman, S. A., Yli-Harja, O., and Shmulevich, I. (2008). Critical networks exhibit maximal information diversity in structure-dynamics relationships. *Phys. Rev. Lett.* 100, 058702.

Ostojic, S., Brunel, N., and Hakim, V. (2009). How connectivity, background activity, and synaptic properties shape the cross-correlations between spike trains. *J. Neurosci.* 29, 10234–10253.

Paninski, L. (2003). Estimation of entropy and mutual information. *Neural Comput.* 15, 1191–1253.

Rapp, P. E., Zimmerman, I. D., Vining, E. P., Cohen, N., Albano, A. M., and Jimenez-Montano, M. A. (1994). The algorithmic complexity of neural spike trains increases during focal seizures. *J. Neurosci.* 14, 4731–4739.

Rotter, S., and Diesmann, M. (1999). Exact digital simulation of time-invariant linear systems with applications to neuronal modeling. *Biol. Cybern.* 81, 381–402.

Shadlen, M. N., and Newsome, W. T. (1998). The variable discharge of cortical neurons: implications for connectivity, computation, and information coding. *J. Neurosci.* 18, 3870–3896.

Soriano, J., Rodrígez Martinez, M., Tlusty, T., and Moses, E. (2008). Development of input connections in neural cultures. *Proc. Natl. Acad. Sci. U.S.A.* 105, 13758–13763.

Sporns, O. (2011). *Networks of the Brain*. Cambridge, MA: The MIT Press.

Tsodyks, M., Uziel, A., and Markram, H. (2000). Synchrony generation in recurrent networks with frequency-dependent synapses. *J. Neurosci.* 20, 1–5.

Tuckwell, H. C. (2006). Cortical network modeling: analytical methods for firing rates and some properties of networks of LIF neurons. *J. Physiol. Paris* 100, 88–99.

Voges, N., Guijarro, C., Aertsen, A., and Rotter, S. (2010). Models of cortical networks with long-range patchy projections. *J. Comput. Neurosci.* 28, 137–154.

Wagenaar, D. A., Pine, J., and Potter, S. M. (2006). An extremely rich repertoire of bursting patterns during the development of cortical cultures. *BMC Neurosci.* 7, 11–29. doi: 10.1186/1471-2202-7-11

Watts, D. J., and Strogatz, S. H. (1998). Collective dynamics of small-world networks. *Nature* 393, 440–442.

Wheeler, B. C., and Brewer, G. J. (2010). Designing neural networks in culture. *Proc. IEEE* 98, 398–406.

Conflict of Interest Statement: The authors declare that the research was conducted in the absence of any commercial or financial relationships that could be construed as a potential conflict of interest.

Received: 15 October 2010; accepted: 17 May 2011; published online: 01 June 2011. Citation: Mäki-Marttunen T, Aćimović J, Nykter M, Kesseli J, Ruohonen K, Yli-Harja O and Linne M-L (2011) Information diversity in structure and dynamics of simulated neuronal networks. Front. Comput. Neurosci. ***5****:26. doi: 10.3389/fncom.2011.00026*

6 APPENDIX

6.1 MODEL PARAMETERS FOR NETMORPH

The parameters used for generating realistic networks by NETMORPH are listed in **Table A1** in Appendix. We use the implementation netmorph2D, which allows the simulation of strictly two-dimensional networks. The version 20090224.1225 of the simulator is used. The parameters are obtained from Koene et al. (2009), where the axonal parameters were optimized to fit growth statistic obtained from real data. We are unaware of any similar parameter optimization study done for dendritic growth, hence we use the dendritic parameters listed in the context of Figure 12D in Koene et al. (2009).

We take into account that not all synapses become functional by applying a 25% fraction of effective synapses, i.e., on average every fourth of the candidate synapses proposed by the simulator is actually accepted as a synapse. In addition, we apply the cell placement in a fixed 40-by-40 grid where distance between adjacent neuron somas is 24.99 μm. To do this we had to recompile the simulator with our own extension that overrides the cell soma data created by the simulator (code not shown). For parameters not mentioned above we use the default values.

6.2 ACTIVITY MODEL PARAMETERS

The activity simulations are run on MATLAB. The parameters for Izhikevich model (Eqs 6 and 7) are obtained from Izhikevich (2003). They are listed in **Table A2** in Appendix.

The parameters are randomized such that the random numbers $\mathbf{r}_e$ and $\mathbf{r}_i$ are drawn *neuron*-wise from a uniform distribution $U(0,1)$. The noise term I_G (Eq. 8) is a piecewise constant (constant for 1 ms time windows) zero-mean Gaussian variable with standard deviation $8.8\frac{1}{\text{ms}}$. This value is chosen to make the silent periods have a spiking frequency not too scarce and not too dense (see the inter-burst periods in **Figure 2** for the result). The simulation time step is chosen 0.5 ms.

The synapse parameters (Eq. 10) are taken from Tsodyks et al. (2000), and they are listed in **Table A3** in Appendix.

For each synapse the values of variables τ_{rec} and τ_{facil} are first drawn from a Gaussian distribution with the shown mean and standard deviation of half of the mean. Values lower than 5 ms are replaced by the minimum value 5 ms. The procedure is similar with the resource fraction parameter U (Eq. 11), but for U both minimum and maximum value are applied. The minimum and maximum values are chosen following a test case in the NEST (Gewaltig and Diesmann, 2007) simulator, although the simulator itself is not used due to difficulties in simultaneous implementation of Tsodyks' synapse model and Izhikevich's neuron model.

For each neuron i the initial values for the membrane potential variable v_i is drawn from uniform distribution $U([c_i,30])$, where c_i is the reset potential parameter of the neuron. The initial recovery variable of the neuron is set $b_i v_i$, where b_i is the sensitivity parameter of the neuron. The synaptic resources are initially in the recovered state, i.e., $x_{ij} = 1$, $y_{ij} = 0$, $z_{ij} = 0$. The initial effective fraction variables u are set $u_{ij} = U_{ij}$, where U_{ij} is the resource fraction constant of the synapse ij.

6.3 COMPRESSION METHOD

6.3.1 A test study of compressors

The quality of the complexity estimation presented in Section 2.3 heavily depends on the precision of KC approximation. In this section we motivate our choice of compression method by examining different compressors in a simple test case. Recent studies incorporating NCD with data compressors have used mostly gzip and bzip2 (Li et al., 2004; Emmert-Streib and Scalas, 2010); in addition to these two we study 7zip[3]. All compressors are run with the default parameters, in addition 7zip is run in a heavy mode that requires more memory and computation time. The challenge in the compression of strings used in this study is the recognition of similar data patterns that may lie very far from each other and differ from each other in a more or less subtle way.

[3]http://7-zip.org/

Table A2 | Izhikevich model parameters.

Model parameters	Excitatory	Inhibitory
a	0.02	$0.02 + 0.08\mathbf{r}_i$
b	0.2	$0.25 - 0.05\mathbf{r}_i$
c	$-65 + 15\mathbf{r}_e^2$	–65
d	$8 - 6\mathbf{r}_e$	2

Table A3 | Tsodyks model parameters.

	Excitatory	Inhibitory
DYNAMICAL BEHAVIOR PARAMETERS		
τ_{rec} (average)	800 ms	100 ms
τ_{facil} (average)	0	1000 ms
τ_I	3 ms	3 ms
RESOURCE FRACTION PARAMETERS		
U (average)	0.5	0.04
U_{min}	0.1	0.001
U_{max}	0.9	0.07

Table A1 | The parameter values used in NETMORPH.

Model selection parameters:		Growth and branching model parameters:	Axon	Dendrite
arbor_elongation_model	van_Pelt	growth_nu0	0.00052083	0.00013889 (μm/s)
branching_model	van_Pelt	growth_F	0.16	0.39
TSBM	van_Pelt	B_inf	17.38	4.75
synapse_formation.PDF	uniform	E	0.39	0.5
direction_model	segment_history_tension	S	0	0
History_power	2	tau	1209600	319680 (s)

We test the performance of the above compressors in a simple problem, where the data to be compressed consists of a duplicated random string. **Figure A1** in Appendix shows compression rate of these strings, i.e., plots of $C(xx)/L(x)$, where x is a random string with equal probabilities of occurrences of "0" and "1", $L(x)$ is the length of the uncompressed string x and $C(xx)$ is the length of the compressed duplicated string.

The mainly descending trend of the compression rates is due to a supposedly constant size coding overhead, whose proportion of the compressed code diminishes as the length of the string is increased. One can observe a shift in the compression rate when exceeding the block size in both gzip, bzip2 and 7zip at some length of data, but not in 7zip-heavy. The latter compressor also most successfully approaches the mean limit compression efficiency of 1/8, the value which is dictated by 8 bits in an ASCII character relative to the one bit required for the representation of "0"s and "1"s, taking into account that the compressed string consists of two identical strings. The value 1/4 would be expected as the maximal mean compression efficiency of compressors with block size smaller than $L(x)$, as one would have $C(xx) \approx 2C(x)$ – this value is best approached by the compressor 7zip.

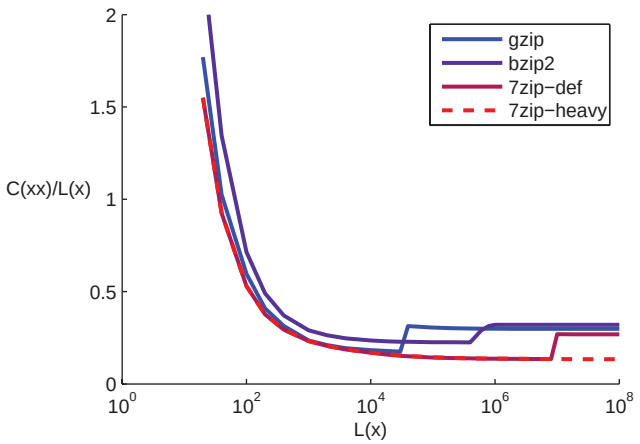

FIGURE A1 | Compression efficiencies when compressing a duplicated random string.

The reason we chose duplicated random strings as a test for compressors is that the strings are slightly similar from the compressibility point of view when calculating, e.g., NCD between two rows of a connectivity matrix. For example, in the case of a LCN two halves of the string will not be fully identical but most often merely shifted and some of the bits replaced by their opposite. Also in the case of calculating NCD between spike trains of two neurons, most of the spikes will probably be clustered around the same time indices (the time index of a burst) surrounded by hundreds or thousands of "0"s (silent periods). Surely our test case does not capture all the phenomena related to this kind of compression challenges where most of the data in the two halves of the string are equal but not all, but this at least shows that even small challenges – compressing strictly duplicated data – are managed far less efficiently by some compressors than the others. Basing on this test, we choose to use the 7zip-heavy compressor to compute all the results presented in this work.

6.3.2 Compression software

For compression of data strings we use the LZMA SDK 4.65 provided by the 7-zip website[4]. To improve the default compression rate we set the number of fast bytes to 273 (default 128), the dictionary size to 1 Gb (default 8 Mb) and the number of match finding cycles to 750 (default 10), while keeping the rest of the parameters (number of literal context and position bits) default.

[4]http://7-zip.org/

Publication IV

T. Mäki-Marttunen, J. Kesseli, S. Kauffman, O. Yli-Harja, and M. Nykter. Of the complexity of Boolean network state trajectories. In *Proceedings of the 8th International Workshop on Computational Systems Biology (WCSB 2011)*, pp. 137-140, 2011.

OF THE COMPLEXITY OF BOOLEAN NETWORK STATE TRAJECTORIES

T. Mäki-Marttunen[1,2], J. Kesseli[1], S. Kauffman[3], O. Yli-Harja[1] and M. Nykter[1]

[1]Department of Signal Processing, Tampere University of Technology,
[2]Department of Mathematics, Tampere University of Technology,
P.O. Box 553, FI-33101 Tampere, Finland
[3]Complex Systems Center, University of Vermont, Burlington, VT 05405
tuomo.maki-marttunen@tut.fi, kesseli@cs.tut.fi, Stuart.Kauffman@uvm.edu,
yliharja@cs.tut.fi, matti.nykter@tut.fi

ABSTRACT

We study the complexity of network dynamics in a couple of very different model classes: The traditional random Boolean networks (RBN) and Frisch-Hasslacher-Pomeau lattice gas automata (FHP). For this we formulate the FHP dynamics as a probabilistic Boolean network (PBN). We use the set complexity of successive network states to assess the complexity of the dynamics. We find that the complexity is maximised near a transition state in both types of dynamical systems.

1. INTRODUCTION

Boolean networks are one of the simplest existing dynamical systems, yet they can produce an extremely wide range of different observable types of behavior. This makes them a suitable target for complexity research: a broad diversity of dynamics that is reducible to simple building blocks. Boolean network models have been used to establish and study several fundamental properties of dynamical systems. These include, among others, characterization of attractor structure, information processing properties, dynamical regimes, and ability to store information [1]. Remarkably, many of these properties are present in multiple other classes of dynamical systems, and some of these properties have been found in real systems, such as living cells.

While Boolean networks are a highly useful model class, there are multiple limitations. Some of these become apparent when one wants to understand the complexity of processes that pertain to physical quantities such as work or energy. Additionally, standard random Boolean model does not capture spatial positioning of the nodes. To extend the analysis beyond random Boolean networks, we utilize a model class that captures spatial positioning and pertains to the quantities such as work and energy: a lattice gas model. We use both of these model classes to show that our observations about the dynamical behavior holds also for both of these systems. Finally, we will establish a connection between lattice gas model and probabilistic Boolean networks. This connection allows comparison and generalization of results between these systems.

In this work we will study complex behavior of dynamical systems during the transition towards a steady state. Specifically, we address the complexity of the trajectories during this transition. Using an information theoretical measure, set complexity, we show that the maximally complex dynamical behavior is observed during the transition period. Additionally, we show that this property is shared between Boolean networks and lattice gas model.

2. METHODS

2.1. Random Boolean networks

A Boolean network is defined as a collection of nodes $\{V_1, \ldots, V_N\}$ where at each time step t each node is assigned a Boolean value $x_i(t)$, i.e.

$$\forall t \in \mathbb{N}\, \forall i \in \{1, \ldots, N\} : x_i(t) \in \{0, 1\}.$$

Each node receives input from 0 to N nodes and the state of the node at time instant $t+1$ is a Boolean function of the states of its neighbors at time instant t:

$$x_i(t+1) = f_i(x_{I_{i1}}(t), \ldots, x_{I_{in_i}}(t)),$$

where I_{ij} ($j \in \{1, \ldots, n_i\}$) are the indices of the input nodes of node i, $n_i \in \{0, \ldots, N\}$ denoting the number of them.

By Random Boolean Networks (RBN) we mean such Boolean networks where the inputting nodes as well as the Boolean functions are picked by random. We denote the probability of the output of a Boolean function in the network being 1 by p. For simplicity, we keep the number of inputting nodes a network-wide constant: $\forall i : n_i = K$. The parameters p and K together determine the dynamics of the network through a sensitivity parameter $s = 2Kp \cdot (1-p)$. Networks with $s = 1$ are critical networks, as networks with $s > 1$ are chaotic and $s < 1$ stable [2].

RBNs should not be confused with probabilistic Boolean networks (PBN) that are such Boolean networks where each node may have a number of functions. The choice of which function to use to update the state of the node depends on a random process. In the present paper we will use PBNs but skip the formal definitions of the underlying probability spaces.

2.2. Lattice gas

Movement of gaseous particles in a 2-dimensional box can be studied using a Frisch-Hasslacher-Pomeau (FHP) lattice gas model [3]. This is a model where the spatial domain is divided into a hexagonal grid, and each hexagonal box in the grid can contain up to six particles. The particles always move into one of the six directions and can only move with velocity of one hexagon/time step. Given that two or more particles are in the same hexagon, they must have different momenta, that is, different directions of momentum.

The momentum of a particle can only change with 1) a collision with the wall and 2) a collision with another particle. A collision with a wall occurs whenever a particle enters a hexagon occupied by a wall, and a collision between particles takes place if a) exactly two particles with opposite momenta come to the same hexagon or b) exactly three particles with momenta that add up to 0 come to the same hexagon. In collisions 1 and 2b the momenta of the particles is changed in a deterministic way whereas in 2a the momenta of the particles are chosen by random between the two possibilities (see Figure 1).

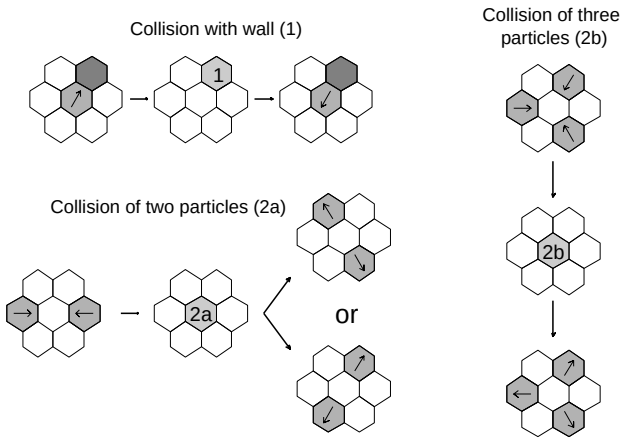

Figure 1. The collisions in FHP model.

The lattice gas automaton described above can be presented as a PBN. Each hexagon in the spatial grid contains six nodes, each of which can contain a particle moving into one of the six directions, i.e. the state of the node is '1' when there is a particle in the hexagon moving into the specified direction and '0' when there is not. The state of the node at time instant $t+1$ is determined by the state of its surrounding nodes at time instant t. The update rule is deterministic in all cases but collision 2a — in that case the outcomes of the four nodes of the possible scattering directions are random but correlate and anti-correlate with each other. The Boolean functions of a node V_{i_0} whose parent hexagon does not contain a wall are listed in Figure 2. If in contrast the parent hexagon contains a wall, then the only input node is in the opposite direction of the node (i.e. V_{i_4} would be input for V_{i_0} in Figure 2), and the Boolean function is identity.

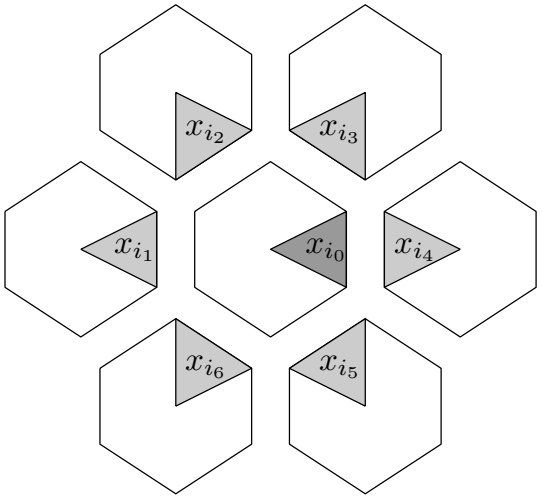

f :

000000: 0	010000: 0	100000: 1	110000: 1
000001: 0	010001: 0	100001: 1	110001: 1
000010: 0	010010: 0/1	100010: 1	110010: 1
000011: 0	010011: 0	100011: 1	110011: 1
000100: 0	010100: 0	100100: 0	110100: 1
000101: 0	010101: 1	100101: 1	110101: 1
000110: 0	010110: 0	100110: 1	110110: 1
000111: 0	010111: 0	100111: 1	110111: 1
001000: 0	011000: 0	101000: 1	111000: 1
001001: 0/1	011001: 0	101001: 1	111001: 1
001010: 0	011010: 0	101010: 0	111010: 1
001011: 0	011011: 0	101011: 1	111011: 1
001100: 0	011100: 0	101100: 1	111100: 1
001101: 0	011101: 0	101101: 1	111101: 1
001110: 0	011110: 0	101110: 1	111110: 1
001111: 0	011111: 0	101111: 1	111111: 1

Figure 2. The input nodes of a node moving right in the Boolean network representation of the FHP model. Here, the state of the node x_{i_0} is determined as $x_{i_0}(t+1) = f(x_{i_1}(t), x_{i_2}(t), x_{i_3}(t), x_{i_4}(t), x_{i_5}(t), x_{i_6}(t))$. The values of function f are listed on the right for each input. In the type 2a collisions both values '0' and '1' are possible: in these cases the scattering direction of the collision is picked by random and the outcome of the node i_0, together with the other nodes in the hexagon, depends on this scattering direction.

2.3. Set complexity

Complexity of Boolean network dynamics can be studied by the means of the context-dependent information it carries. The dynamics of a Boolean network is represented by a set of its successive states that are read into strings. To the obtained set of strings one can apply a recently proposed all-purpose measure, *set complexity* [4], defined as:

$$S(\{x_1, ..., x_N\}) = \sum_j C(x_j) \frac{1}{N(N-1)} \sum_{j \neq k} d_{jk}(1 - d_{jk}),$$

where $C(x_j)$ is the Kolmogorov complexity — or its approximation — of string x_j. The variable d_{jk} stands for the *normalized compression distance* (NCD) of strings x_j

and x_k, defined as

$$d_{jk} = \mathrm{NCD}(x_j, x_k) = \frac{C(x_j x_k) - \min(C(x_j), C(x_k))}{\max(C(x_j), C(x_k))},$$

where $x_j x_k$ is the concatenation of strings x_j and x_k. In the present study we use the length of the LZMA encoded string as an approximation for the Kolmogorov complexity of the string.

3. RESULTS

3.1. Information content of dynamics of RBN

We consider RBNs of size $N = 1000$ with variable number of neighbors ($K = 1, 2, 3$). The state of the network is read into a string of length N, and the complexity of the dynamics is approximated by the set complexity of successive states. Figure 3 shows the set complexity of the states using a sliding window of four successive states. At the transition to a short-cycle steady state the set complexity is maximised, as seen for networks with sensitivities $s = 0.5$ and $s = 1$. In the case of $K = 3, s = 1.5$ the dynamics of the network is too chaotic for the set complexity of four states to find any pattern in — in our simulations a network of this type never returned to one of its previous states during the $T = 224$ time steps, indicating a lengthy path to a steady state, a long steady state cycle, or both. For comparison, the median steady state cycle lengths are 1 for all networks with $s = 0.5$, 16 for networks with $K = 2, s = 1$, and 10 for networks with $K = 3, s = 1$.

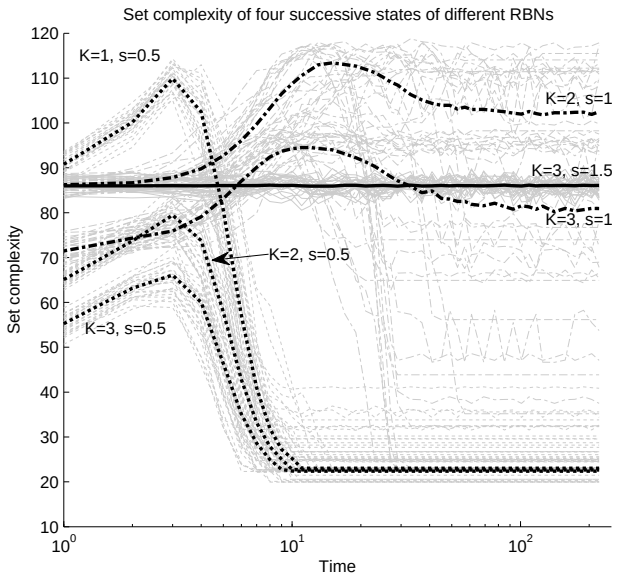

Figure 3. Set complexity of RBN dynamics. Different numbers of neighbors (K) and different sensitivities s are used. The thin curves represent samples of set complexity trajectories, as the thick curves are medians of 1000 trajectories.

Next we study the maximum values of this kind of set complexity trajectories in more detail. We consider RBNs with the same fixed numbers of neighbors ($K = 1, 2, 3$)

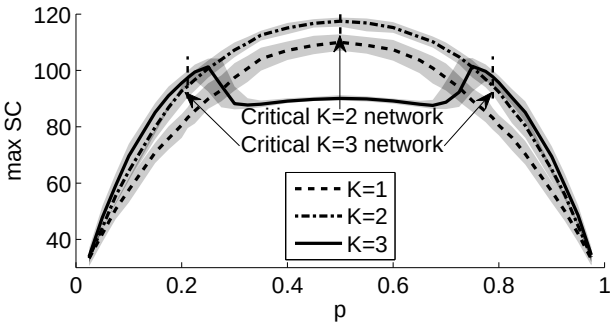

Figure 4. Set complexity maximum values of different RBNs. The curves represent medians with the area between 10% and 90% quantiles shaded. Number of samples is 130. The values of p that induce a critical BN are marked, $p = 0.5$ for $K = 2$ and $p = \frac{1}{2} \pm \frac{\sqrt{3}}{6}$ for $K = 3$ networks.

but with variable p; hence, with variable sensitivity s. Figure 4 shows the distribution (the quantiles) of the maximum set complexity value as a function of p. For networks with $K = 2$ the critical network produces the dynamics that has the greatest maximum set complexity, as for $K = 3$ that holds for slightly chaotical ($s \approx 1.1$) networks. Notice the symmetricity: the dynamical characteristics of networks with $p = q$ and $p = 1 - q$ are identical with only the role of 0's and 1's interchanged.

3.2. Information content of dynamics of the lattice gas

The lattice gases considered are set up in a $M \times M$ grid of hexagonal boxes, surrounded by impenetrable walls. In the beginning all particles are situated in three overlapping rectangle-shaped regions on the left side of the box. The first rectangle lies in the upper-left corner of the box and consists of particles that are moving lower-right, the second one occupies the whole height of the box and consists of particles moving right, and the third one lies in the lower-left corner and moves upper-right. The rectangle sizes are chosen such that it takes an exact number of time steps (16 in our simulations) before the first particles hit a wall on the opposite side of the box. The rectangles are densely packed: in each slot of the rectangle a particle exists with probability $p = 0.95$. This particular setup was chosen as a reference to a classical example in thermodynamics in which particles spread from a densely packed cluster to the whole spatial domain to obtain a maximal entropy.

In the beginning of the simulation there is a short period of time during which the particles do not collide but move in the most ordered fashion, each of the six $M \times M$ planes only being shifted in their direction of movement. In contrast, toward the end of the simulation the particles move chaotically, colliding frequently with each other as well as with the surrounding walls. Between these phases lies a period of transition from the orderly motion into the chaotical one. Figure 5 shows that the set complexity of

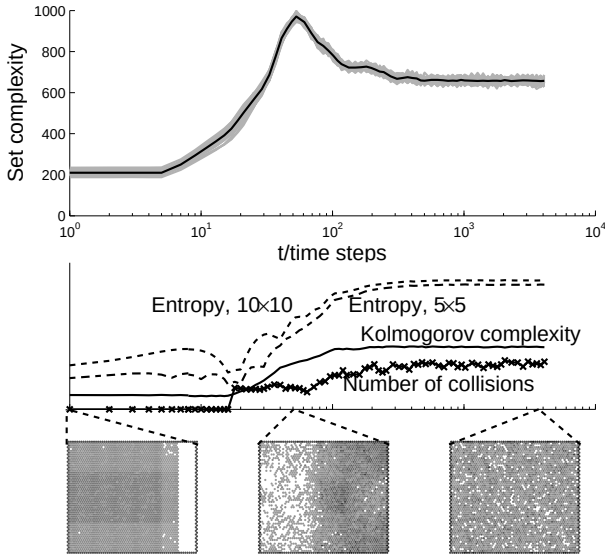

Figure 5. Simulation of a spreading lattice gas. Upper axes: The set complexity of twelve successive states of the lattice gas versus time. A number of realizations (N=100) plotted in gray, median plotted in black. Lower axes: Both entropy (dashed), Kolmogorov complexity estimate (solid) and number of collisions (solid + x) plotted versus time. The entropy is calculated using the traditional thermodynamical definition. The state space is divided into 5-by-5 (10-by-10) boxes, and the number of particles in all of these microboxes is calculated. The entropy is proportional to the logarithm of the number of all possible configurations with the said number of particles in the microboxes. For simplicity, only the interior of the spatial domain is considered when calculating the entropy, i.e. the number of particles colliding with the walls do not contribute to the entropy. Bottom figures: Lattice gas states visualized at the beginning of the simulation ($t = 0$), during the transition period ($t = 56$) and in the end ($t = 4096$).

12 successive states of the lattice gas is maximised during this transition period. In contrast, the Kolmogorov complexity of the state as well as the traditional entropy shows a mere rising trend in its trajectory. For the compression the state of the lattice gas is read into a string first column by column, last plane by plane — i.e. the distance of two nodes in the same hexagon is always a multiple of M^2 in the string.

4. CONCLUSION AND DISCUSSION

In this article, we have considered set complexity as a measure of dynamical complexity of state transitions using two models, RBNs and FHP lattice gases as case studies. Using these models, we have found that there is a point of maximal complexity in time, occurring before the system settles down to its long-term behavior. Although the generality of the phenomenon is yet to be assessed in full, it can be suggested that such maximal complexity can be found in a range of other models of dynamical systems as well.

A random Boolean network can be thought of as performing a type of a classification task, taking the initial state of the system and finding out, by computing its characteristic state transitions, to which attractor basin the input vector belongs. Such a parallel calculation can perform a huge variety of functions, and what we see in the set complexity measure can be taken to quantify this observed complexity. In accordance with this idea, critical or near-to-critical networks show the highest peaks of set complexity due to the complex dynamics emerging at the phase transition from ordered to chaotic networks. For the FHP lattice gas model, the state of the particles changes through a transient towards a steady state equilibrium. In this case, the characteristics of the steady state are not dependent on the structured initial state we have selected and statistically speaking, the end result is always the same. However, the complexity of the trajectory still reaches its maximum before equilibrium, showing the generality of our set complexity approach.

Previously, set complexity has been quantified on the attractor cycle, with critical networks showing the highest complexity in that case as well [4]. Our results agree with these previous observations, but move the focus to the transitional states before the attractors are reached. In the case of biological systems, it can be argued that such states are more significant in determining the response of the system to external inputs and variations in the state due to noise. In future work, such response should be studied explicitly, using suitable Boolean network models. The effects of different network characteristics on the complexity of calculation in the transients can then be studied together with traditional measures of criticality, to see how the network response is shaped.

5. ACKNOWLEDGMENTS

The authors would like to acknowledge the following funding: TISE graduate school, Academy of Finland projects 132877 and 213462 (Center of Excellence).

6. REFERENCES

[1] M. Aldana, S. Coppersmith, and L.P. Kadanoff, "Boolean dynamics with random couplings," *Perspectives and Problems in Nonlinear Science*, vol. 93, no. 4, pp. 23–90, 2003.

[2] P. Rämö, S. Kauffman, J. Kesseli, and O. Yli-Harja, "Measures for information propagation in Boolean networks," *Physica D: Nonlinear Phenomena*, vol. 227, no. 1, pp. 100–104, 2007.

[3] U. Frisch, B. Hasslacher, and Y. Pomeau, "Lattice-gas automata for the Navier-Stokes equation," *Physical Review Letters*, vol. 56, no. 14, pp. 1505–1508, 1986.

[4] D.J. Galas, M. Nykter, G.W. Carter, N.D. Price, and I. Shmulevich, "Biological information as set-based complexity," *IEEE Transactions on Information Theory*, vol. 56, no. 2, pp. 667–677, 2010.

Publication V

T. Mäki-Marttunen, J. Kesseli, and M. Nykter. Balance between noise and information flow maximizes set complexity of network dynamics. *PLoS ONE*, 8(3): e56523, 2013.

OPEN ACCESS Freely available online

PLOS ONE

Balance between Noise and Information Flow Maximizes Set Complexity of Network Dynamics

Tuomo Mäki-Marttunen[1,2]*, Juha Kesseli[1], Matti Nykter[1]

1 Department of Signal Processing, Tampere University of Technology, Tampere, Finland, **2** Department of Mathematics, Tampere University of Technology, Tampere, Finland

Abstract

Boolean networks have been used as a discrete model for several biological systems, including metabolic and genetic regulatory networks. Due to their simplicity they offer a firm foundation for generic studies of physical systems. In this work we show, using a measure of context-dependent information, set complexity, that prior to reaching an attractor, random Boolean networks pass through a transient state characterized by high complexity. We justify this finding with a use of another measure of complexity, namely, the statistical complexity. We show that the networks can be tuned to the regime of maximal complexity by adding a suitable amount of noise to the deterministic Boolean dynamics. In fact, we show that for networks with Poisson degree distributions, all networks ranging from subcritical to slightly supercritical can be tuned with noise to reach maximal set complexity in their dynamics. For networks with a fixed number of inputs this is true for near-to-critical networks. This increase in complexity is obtained at the expense of disruption in information flow. For a large ensemble of networks showing maximal complexity, there exists a balance between noise and contracting dynamics in the state space. In networks that are close to critical the intrinsic noise required for the tuning is smaller and thus also has the smallest effect in terms of the information processing in the system. Our results suggest that the maximization of complexity near to the state transition might be a more general phenomenon in physical systems, and that noise present in a system may in fact be useful in retaining the system in a state with high information content.

Citation: Mäki-Marttunen T, Kesseli J, Nykter M (2013) Balance between Noise and Information Flow Maximizes Set Complexity of Network Dynamics. PLoS ONE 8(3): e56523. doi:10.1371/journal.pone.0056523

Editor: Derek Abbott, University of Adelaide, Australia

Received October 4, 2012; **Accepted** January 10, 2013; **Published** March 13, 2013

Funding: This work was funded by TISE doctoral school and Academy of Finland projects 132877, 251937. The funders had no role in study design, data collection and analysis, decision to publish, or preparation of the manuscript.

Competing Interests: The authors have declared that no competing interests exist.

* E-mail: tuomo.maki-marttunen@tut.fi

Introduction

Dynamical systems theory is being developed to understand temporal behavior of complex systems. Groundlaying studies of dynamical systems range from modeling of, e.g., genetic [1], neuronal [2], and ecological [3] networks to structural analyses of complex networks [4–6]. Results obtained for the function of a dynamical network of a particular type are always subject to the temporal behavior of the underlying dynamical units, which vary substantially between objects of interest [7]. To this end, Boolean network models have been used as a generic tool to study a wide range of fundamental properties of dynamical systems. These include features of attractor structure [8], information propagation and processing [9–11], dynamical regimes [12], structure-function relationship [13], and the ability to store information [14,15]. Although many of these aspects can be studied with a range of other models (e.g., [16]) the strength of Boolean networks is that they are based on simple building blocks that can give rise to varied dynamics [17]. Random networks can be generated in such a way that changing one or two parameters in how the networks are generated makes the resulting network dynamics ordered, critical, or chaotic [8]. Aspects of Boolean network dynamics have been suggested as a model of biological network dynamics, such as cell types determined in part by genetic regulatory networks [18], and they have later proved efficient in, e.g., correctly reproducing observed gene expression patterns [19].

A recent development in the field of information theory is the normalized information distance [20], which can be applied to any two objects stored on a computer (e.g., genome sequences, networks, or state representations). This distance uniquely specifies the informational difference between two objects and is defined in terms of the Kolmogorov complexity. The Kolmogorov complexity [21], K(x), of an object x is defined to be the length of a shortest program to output x on a universal computer (i.e., on an all-purpose machine). Intuitively, K(x) represents the minimal amount of information required to generate x by any effective process and can be thought of as the ultimately compressed form of x. Although the normalized information distance, like the Kolmogorov complexity itself, is not computable, it can nonetheless be effectively approximated by using real-world data compressors.

Recently, a context-dependent measure of information, *set complexity*, has been applied to quantify various aspects of network topology and dynamics [22,23]. This measure assesses the complexity of a set of strings in such a way that the approximate Kolmogorov complexities of the strings are balanced by a function of the pairwise normalized information distances within the set. The motivation for this context-dependent measure of information is that it should be able to quantify the total amount of non-redundant information, rather than the overall complexity of the data. This means that while a standard measure of information, such as Kolmogorov complexity, is maximized for random data,

the set complexity quantifies the trade-off between randomness and identically repeated symbols.

The complexity of Boolean networks has hitherto been analyzed using many approaches. These include, e.g., the computational complexity of a Boolean network circuit [24,25], the entropy of the basins of attractors [9], and the statistical complexity of the steady state of a network or the complexity of single nodes averaged over time [26]. However, the temporal complexity of the Boolean network dynamics is still poorly understood. How does the complexity of Boolean network dynamics vary in time? To what extent does the complexity change when settling to an attractor? If there are processes that allow transitions between attractors, how do they affect the complexity? Is it by any means feasible to assess the temporal complexity of Boolean networks? In our earlier study [27] we shed light on some of the questions by applying the set complexity measure to successive states of Boolean networks. We found that the complexity of the dynamics was temporally maximized near a transition to an attractor. This raised many more questions, most important ones being whether this phenomenon is real and whether the stage of maximal complexity could be prolonged by introducing noise to the network. In the present work we justify our findings using another complexity measure, namely, the statistical complexity, which was originally presented in [28] and refined in a series of papers by Shalizi [29,30]. We also show that the high complexity can indeed be retained just by tuning the system with a suitable amount of noise. Noisy Boolean networks have been extensively studied with an aspect to robustness and stability of the attractor states [31–33]. In this work we employ the white noise model used in e.g. [31]. The noise imposes a challenge for the information processing and storage, and hence, we also consider the noise-induced disruption in information flow in different networks with variable levels of noise. We show that the networks near the critical regime can most easily be added a noise component that elevates the steady-state complexity value without making the dynamics too random.

Results

Complexity of noiseless Boolean network dynamics is temporally maximized prior to an attractor

To attain the quantification of temporal complexity, we start by reprising the study on dynamical complexity in [27], now in the context of noiseless Poisson networks. Fig. 1 shows the complexity of Poisson network dynamics as a function of time. Poisson networks with different expected number of neighbors $\langle K\rangle$ obtain statistically different dynamical complexities. As seen in [27] with fixed-K networks, Fig. 1 shows that the critical ($\langle K\rangle=2$) networks possess a *transient state* where the set complexity of the dynamics is maximized, and which is followed by a descent to an attractor level value. The transient state is also observed in the slightly subcritical ($\langle K\rangle=1.5$) network, but not in the slightly supercritical ($\langle K\rangle=2.5$) network. The dynamical complexity in highly subcritical ($\langle K\rangle=1$) networks is quickly reduced to a steady low value that represents attaining a short cycle attractor, whereas the supercritical ($\langle K\rangle=2.5$, 3) networks seldom reach an attractor by the end of the simulation. Due to long transition period the dynamics of slightly supercritical ($\langle K\rangle=2.5$) networks seem to exhibit higher steady-state complexity than critical networks (Fig. 1). This is consistent with the finite size network results reported by [11].

For reference, let us consider the extreme values for set complexity empirically. The distribution of LZMA-estimated values of $C(x)$, where x is a random binary string of length $N=1000$, is well approximated by a Gaussian distribution with mean 224.14 and standard deviation 2.96 (data not shown) — the maximum value we came across among all data of the present work was 238. Thereby, Eq. 2 can be used to infer the maximal set complexity value for networks of this size as $S_{\max}=59.5\approx 60$, as the theoretical minimum is $S_{\min}=0$. Fig. 1 shows that the range of all possible set complexity values is fairly well covered by the complexity values of RBN dynamics.

A moderate amount of noise elevates the complexity of the network dynamics

To model the dynamical behavior under noisy conditions, we study the effect of nonzero flip probability p. Fig. 2 shows complexity trajectories of noisy networks with zero, moderate, and high levels of noise. One can observe that for a moderate level of noise the set complexity value does not fall to a low value that is typical to a regime of noiseless ordered dynamics.

To explain this observation, we can analyze Eq. 2 to gain an insight into how the differences in the set complexity values arise. One can find three different causes for high values of set complexity. Firstly, the average Kolmogorov complexity $\frac{1}{N}\sum_k C(x_k)$ of the strings may be high, implying higher values for set complexity. Secondly, the average value of the function of NCDs ($\frac{1}{N(N-1)}\sum_k\sum_{j\neq k} d_{jk}(1-d_{jk})$) may be high, likewise increasing the set complexity. Greatest set complexities are attained when the values of NCD (d_{jk}) are as close as possible to 0.5, which maximizes the inline function $d(1-d)$. Third cause would be a combinatory effect of these two such that, although the mean values of both mentioned quantities were relatively small, there may be a few strings x_k with high Kolmogorov complexity $C(x_k)$ that lie on average on a distance of 0.5 from most of the other strings and hence raise the set complexity value. In Poisson networks the Kolmogorov complexities $C(x_k)$ show little variation across both time and network realizations as each string is, ultimately, a random binary string with equal probabilities of 0 and 1. Therefore, the high values of set complexity must be due to the values of NCD being close to 0.5. Fig. 3 shows the evolution of the NCD distributions through time and explains the differences observed between the set complexity curves of critical networks in Fig. 2.

The temporal rise and descent of the complexity in Boolean networks is not a property of the set complexity measure only. In fact, we can observe similar behavior using a measure of *statistical complexity* [30]. In this approach, the complexity is estimated as the logarithm of the number of causal states of the system. The causal states are unions of such past configurations that produce equal or almost equal distribution of the future configurations. These distributions have to be estimated from the data. The method is not as such applicable to our network types, as even the fixed-K networks have variation in the out-degree of the nodes. However, the fixed-K networks can be modified with minimal changes to produce fixed out-degree as well, and this allows the use of statistical complexity measure, yet only in the case where past and future are considered no more than one step away from the present. Fig. 4 shows the statistical complexity time series for such "fixed-K_{in}-K_{out}" networks.

Let us next quantify the difference between the networks with varying level of noise that can be observed in Fig. 2. We estimate the average set complexity of the "steady state" of the network, which we consider, in networks of this size, all but the first 100 time steps of the simulation. Fig. 5 shows the median of steady-state set complexities in Poisson networks and fixed-K networks with $K=3$. The set complexities are lowest in the regime of the

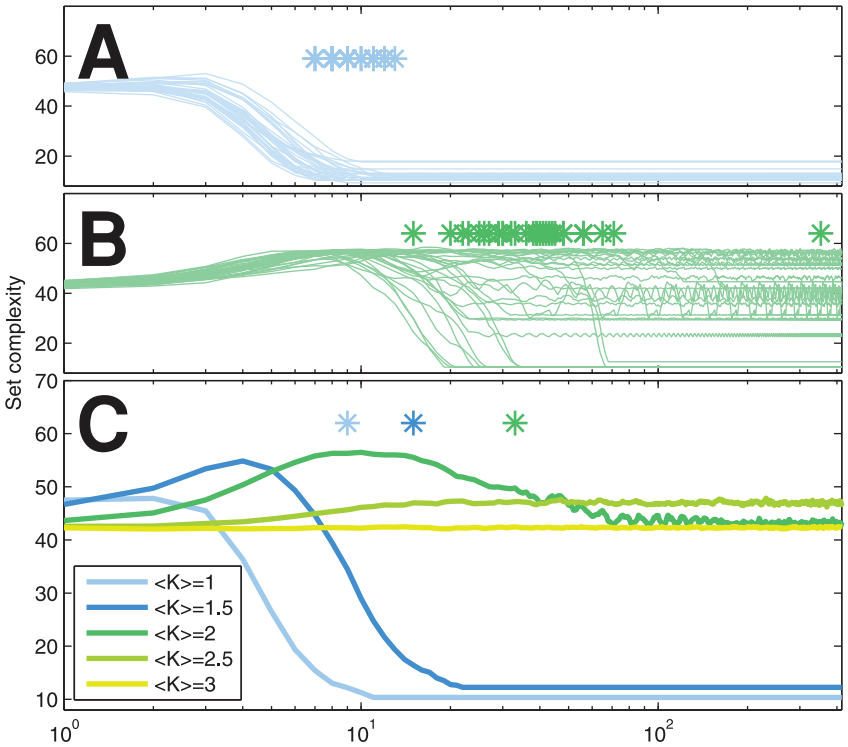

Figure 1. Set complexity time series for random Poisson Boolean networks shows temporal maximum prior to reaching the attractor in several networks with different mean number of inputs $\langle K \rangle$. (A–B): Set complexity trajectories of single simulations of $\langle K \rangle = 1$ (A) and $\langle K \rangle = 2$ (B) networks. The first arrivals to the attractor are marked with stars. (C) The median set complexity of 100 simulation results for five different $\langle K \rangle$s. The stars above the curves show the median of the time instant of first arrival to the attractor.
doi:10.1371/journal.pone.0056523.g001

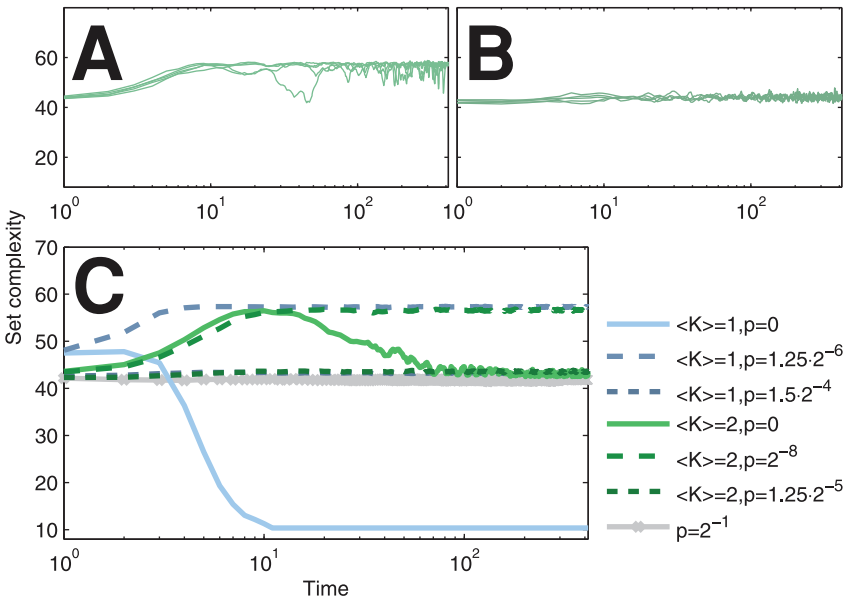

Figure 2. Noise can maintain the network in a high-complexity state. (A–B): Set complexity trajectories of single simulations of $\langle K \rangle = 2$ Poisson networks with moderate ($p = 2^{-8}$, A) and high ($p = 1.25 \cdot 2^{-5}$, B) levels of noise. (C): Medians of set complexity trajectories for noisy Poisson networks with different degrees $\langle K \rangle$ and flip probabilities p. The complexity trajectory of the maximally noisy network that is identical for all $\langle K \rangle$ is plotted in grey. 100 independent samples were used.
doi:10.1371/journal.pone.0056523.g002

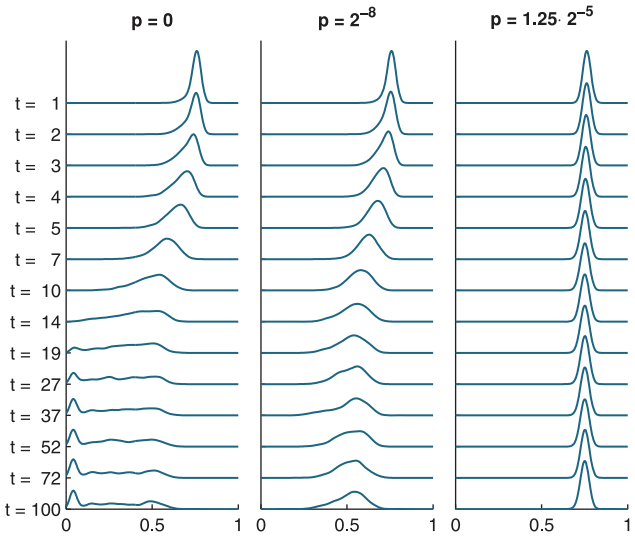

Figure 3. The propagation of NCD distributions explains the time course of the set complexity. The panels show the distributions of NCD values on interval [0,1] in noiseless (left), moderately noisy (middle) and highly noisy (right) Poisson networks with $\langle K\rangle=2$. The time instant of observation grows downwards with the figures plotted: The curve plotted for $t=1$ corresponds to the distribution of off-diagonal elements of NCD matrix $(d_{jk})_{j,k=1}^{6}$, while the curve for $t=2$ corresponds to $(d_{jk})_{j,k=2}^{7}$, and so forth. The distributions are pooled across 100 network realizations and smoothened with a Gaussian filter with standard deviation 0.02. The mean of the NCD distribution in noiseless critical networks (left) passes 0.5 around time instant $t=10$, as expected from the complexity peak at $t=10$ in Fig. 1. The small peaks of noiseless networks in the regime of low NCD correspond to point-attractors. In these attractors the state x_k remains constant, and since the Kolmogorov complexity of a dublicated string is not much higher than that of the original ($C(xx)\approx C(x)$), the resulting NCD values are very small. The mean of the NCD distribution in Poisson networks with moderate noise (middle) approaches 0.5 as time passes, accounting for the high set complexity values in the regime of large t in Fig. 2. In highly noisy networks (right) the NCD distributions have only values that are notably higher than 0.5 due to the excess of randomness, and hence the low set complexity value for these networks in Fig. 2.
doi:10.1371/journal.pone.0056523.g003

most ordered dynamics (low sensitivity s, low flip probability p). Another stable set complexity value is found in the other extreme, where the dynamics is either chaotic (large s) or random (p near to $\frac{1}{2}$), or both. Between these two extremes lies a region where the set complexity is actually higher than either of these extremes. The existence of this region is consistent for different system sizes (validated with $N=750$ and $N=2000$, data not shown). A corresponding plot of statistical complexity in fixed-K_{in}-K_{out} networks can be found in supplementary data (Fig. S1).

We can observe that among fixed-K ($K=3$) networks the ones near the critical network, which by Eqn. 1 is obtained by choosing the bias as $q=\frac{1}{2}-\sqrt{\frac{1}{12}}\approx 0.2113$, produce the maximal steady-state complexity. One can also observe that among Poisson networks one always finds a suitable noise level to obtain a near-to-maximal steady-state complexity (>55) as long as the sensitivity is restricted ($s\lesssim 1.1$). Qualitatively the same result can be obtained with *asynchronous* random Boolean networks, as Fig. 6 shows.

What is rather non-intuitive about Figs. 5 and 6 is the high complexity of noisy low-$\langle K\rangle$ Poisson networks, where a large proportion of the nodes receive zero inputs. The dynamics of these nodes are purely an effect of the noise that occasionally pushes the nodes from their constant output. The effect they have on the set complexity values of the dynamics is twofold. Firstly, from the temporal aspect these nodes lie somewhere between chaos and order, as they most of the time have constant value but may change their value temporarily. Secondly, although the surrounding nodes do not affect the dynamics of these nodes, these nodes might still output to other nodes, and hence the noisy nature of these nodes may contribute to the rest of the system. Clearly, we would like to diminish the first-mentioned effect without removing the latter aspect. Therefore, we repeat the set complexity calculation of Fig. 5, but neglect the nodes that we know to receive no input from the system. In other words, the dynamics of the system remains untouched, but the complexity is calculated only over those nodes that receive one or more inputs. Fig. 7 shows the steady state set complexity values of such networks. One can observe that the set complexity value for networks approaches zero as $\langle K\rangle\to 0$, which is due to the ever shortening strings x_j — and ever diminishing Kolmogorov complexity $C(x_j)$. What remains unchanged from Fig. 5 is the high complexity of networks near to criticality, where the critical and subcritical networks have to be tuned with moderate level of noise in order to obtain the maximal complexity and the slightly supercritical networks attain it with no or little noise. One should note that in order to perform the complexity analysis in this way we need external information on the network structure, in the minimum the notion on which nodes do not have any inputs. By contrast, when we assess the set complexity of the dynamics using all available nodes, no information on the structure of the network is required.

How great are these mentioned "moderate" levels of noise? In critical $\langle K\rangle=2$ Poisson networks the maximal steady-state set complexity was attained with flip probability $p=2^{-8}$, while in subcritical $\langle K\rangle=1$ and $\langle K\rangle=0$ networks it is attained with $p=1.5\cdot 2^{-6}$ and $p=1.25\cdot 2^{-5}$, respectively (Fig. 5). In the system size $N=1000$ these levels of noise mean that in the subcritical networks on average 39 ($\langle K\rangle=0$) or 23 ($\langle K\rangle=1$) nodes are flipped every time step, and in the critical network on average 3.9 nodes. In the critical network also much smaller noise levels suffice to attain 95% of the overall maximal steady-state complexity (the least noise level for this is $p=1.5\cdot 2^{-10}$, i.e., the states of 1.5 nodes on average flipped every time step). The same cannot be said of $\langle K\rangle=1$ and $\langle K\rangle=0$ networks, which attain the 95% of the overall maximum set complexity at the noise levels of $p=2^{-6}$ and $p=1.75\cdot 2^{-6}$, respectively.

The contribution of different levels of noise to the Boolean network dynamics can also be characterized by their Derrida curves (Eqn. 4). These are plotted for Poisson networks with $\langle K\rangle\in\{0,1,2,3\}$ in Fig. 8. For each network both noiseless and noisy case are plotted, where the noise level is chosen as the one that produces the maximal set complexity in Fig. 5. The critical and chaotic ($\langle K\rangle=2,3$) networks with noise are very similar to the corresponding noiseless ($\langle K\rangle=2,3$) networks in Derrida sense, whereas the noisy subcritical networks ($\langle K\rangle=0,1$) show greater difference from the corresponding noiseless networks. The inset in Fig. 8 shows the L^1 difference between the noisy and noiseless curve for each $\langle K\rangle$. This value represents the average amount of perturbation that is due to the noise, and can be considered the *perturbation-averaged disruption in information flow* of the system. For instance, the $\langle K\rangle=1$ network with the noise level that produces maximal complexity adds on average 3 percentage points to the perturbation of the noiseless network, while the corresponding values for $\langle K\rangle=2$ and $\langle K\rangle=3$ network are 0.3 and 0.05

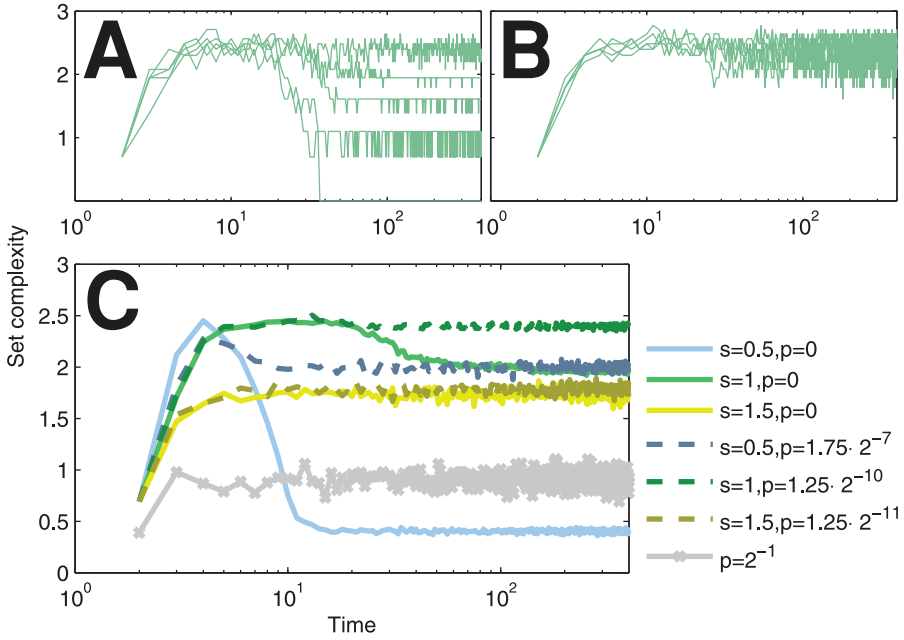

Figure 4. Statistical complexity produces qualitatively similar temporal complexity as the set complexity. (A–B): Statistical complexity trajectories of single simulations of noiseless (A) and noisy (B) critical networks. Both in- and out-degree of the nodes are fixed as $K=3$. (C): Mean statistical complexity time series of subcritical ($s=0.5$), critical ($s=1$) and supercritical ($s=1.5$) networks over 50 repetitions. The noisy networks are marked with dashed and the noiseless networks with solid line. The statistical complexity of the fully noisy ($p=2^{-1}$) network is plotted with grey for reference.
doi:10.1371/journal.pone.0056523.g004

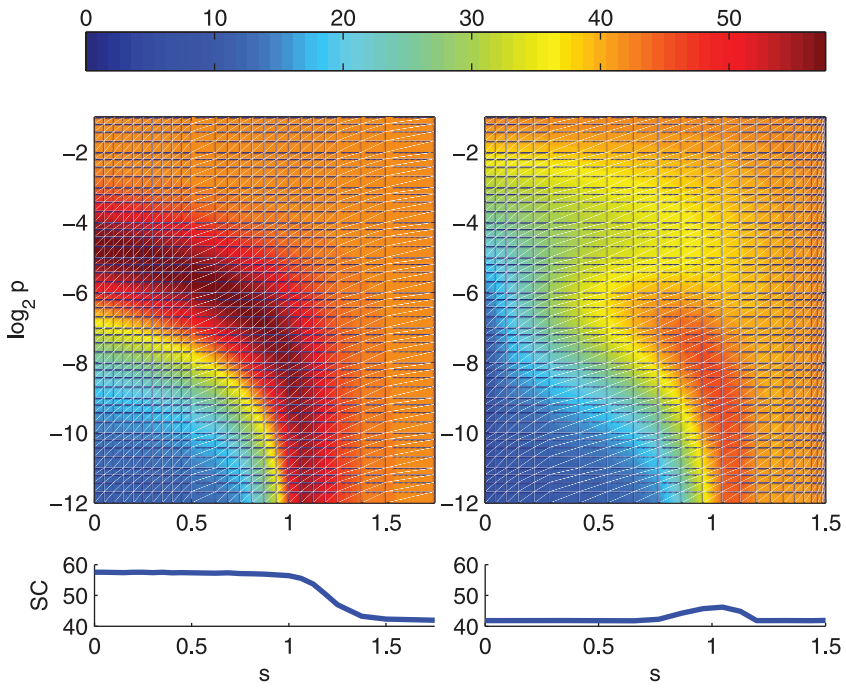

Figure 5. Poisson networks can be set a noise level that maximizes the steady-state set complexity. The color of the plot shows the steady-state set complexity of Boolean network dynamics for both Poisson networks (left) and fixed-K networks with $K=3$ (right) as functions of sensitivity s and flip probability p. For each simulation, a median of set complexities is taken over time steps $t=101,\ldots,400$. Further averaged, the color shows the median of 100 simulations, smoothened with bilinear interpolation. The lower panels show the maximum of the plane, taken over the flip probability.
doi:10.1371/journal.pone.0056523.g005

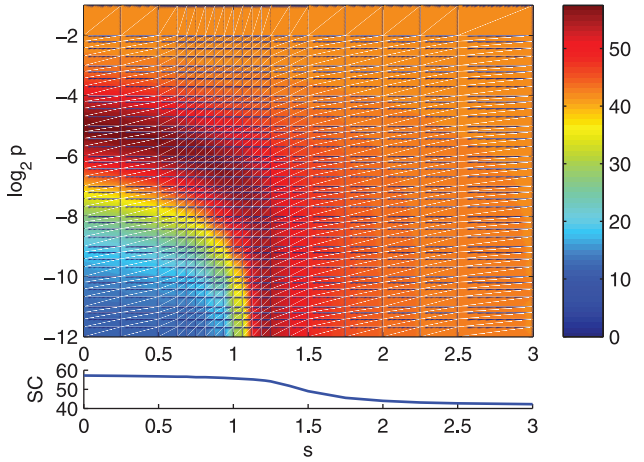

Figure 6. Asynchronous Poisson RBNs show qualitatively the same set complexity statistics as the synchronous ones. The color of the plot shows steady-state set complexities of asynchronous Boolean network dynamics for Poisson networks as functions of sensitivity s and flip probability p. The synchronous state update described in the Methods section is replaced by N successive single-node state updates. The node to update is picked by random every time instant, and thereby after the N state updates some nodes have most probably been updated several times and some nodes none. The set complexities are calculated for states at the modulus-N time steps $\{Nt, N(t+1), \ldots, N(t+T-1)\}$. Similarly to the Fig. 5, a median of set complexities is taken over time steps $t=101,\ldots,400$, and the color of the plot shows the median of 40 simulations, smoothened with bilinear interpolation. The lower panels show the maximum of the plane, taken over the flip probability. A slight difference to Fig. 5 is that in asynchronous networks the high-complexity regime extends more to the chaotic ($s>1$) regime. This is in agreement with [46], where networks with random asynchronous updating schemes were observed to reside more often in an attractor than their synchronous counterparts, suggesting that their dynamics be on average more redundant.
doi:10.1371/journal.pone.0056523.g006

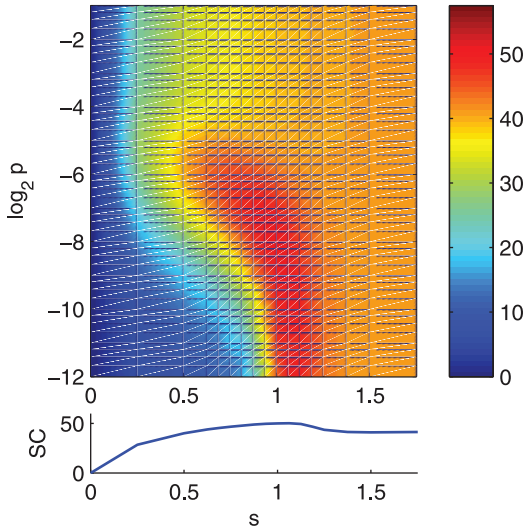

Figure 7. The subcritical Poisson networks lose their high steady-state complexity when nodes with zero inputs are neglected. In this figure, the set complexity is calculated similarly to the Poisson network steady-state complexity in 5, but only states of those nodes that receive at least one input from the system are included in the strings x_j.
doi:10.1371/journal.pone.0056523.g007

percentage points, respectively. This suggests that the chosen level of noise for subcritical networks is too great for the network to maintain the meaningful information in their dynamics.

Discussion

In this work we have shown that the steady-state complexity in Boolean network models can be maximized by choosing the noise level appropriately. In fixed-K networks with $K=3$ this is plausible only for near-to-critical networks (Fig. 5, S1). For Poisson networks this is possible for both sub-critical and near-to-critical networks (Fig. 2, 5). However, the levels of noise that maximize the set complexity in subcritical Poisson networks imply large decrease in information flow compared to those near criticality (Fig. 8). In addition, neglecting the nodes to which the system does not contribute fades the high complexity of these subcritical networks (Fig. 7). The results shown are qualitatively robust to changes in system size N, and the main result is confirmed with asynchronous Boolean networks (Fig. 6).

The complexity of dynamics is in this work primarily assessed through a measure of context-dependent information, i.e., set complexity [22], of successive states of the network. While a measure of context-independent information (such as Kolmogorov complexity) would increase with the unpredictability of the states, that is with the flip probability, the context-dependent information starts to decrease after reaching a certain level of noise (Fig. 5). We have oserved a similar result for the saturation and descent of set complexity in the context of a lattice gas system [27]. The shown results suggest that maximization of the complexity at the edge of chaos and order is robust to the choice of paradigm: One finds it either by adding order into chaotical dynamics, as is the case when a random Boolean network state approaches a short-cycle attractor (Fig. 1), or by increasing randomness into a system with ordered dynamics, as shown with the steady-state complexities of noisy Boolean networks (Fig. 5).

The fact that the complexity measure is maximized at the edge of chaos and order (and not in the totally unpredictable regime as is the case with Kolmogorov complexity) is not characteristic of the set-based complexity measure only, but is a design principle for many other measures of complexity [34], [28], [35], [36]. The common trend for complexity measures — stated even as a requirement for complexity measure in [34] — is that they are based on entropy or Shannon information, and are consequently dependent on the underlying prior distribution of the strings whose complexity is to be assessed. This prior knowledge is rarely at hand in, for instance, applications of biology, as discussed in [22]. For reference, we confirmed the main result with one such measure applicable to time series data, namely, the statistical complexity [30], where the state distributions are estimated from the data (Fig. 4, S1). The presented method of estimating the statistical complexity requires a fixed number of inputs and outputs for each node, and hence it could not be applied to Poisson networks, nor to fixed-K networks without modifications. In addition, the structure of the network must be known in order to estimate the statistical complexity. By contrast, the measure of set complexity is very flexible and does not require any knowledge on the state distributions nor the network structure. On the other hand, the set complexity is based on the Kolmogorov complexity, which has shown to be uncomputable in general. To this end, the use of general data compression algorithms for aprroximation of Kolmogorov complexity has proven to be a powerful tool. As an example, phylogenetic trees and language family trees have been successfully reconstructed in [37] and [20] using methods that

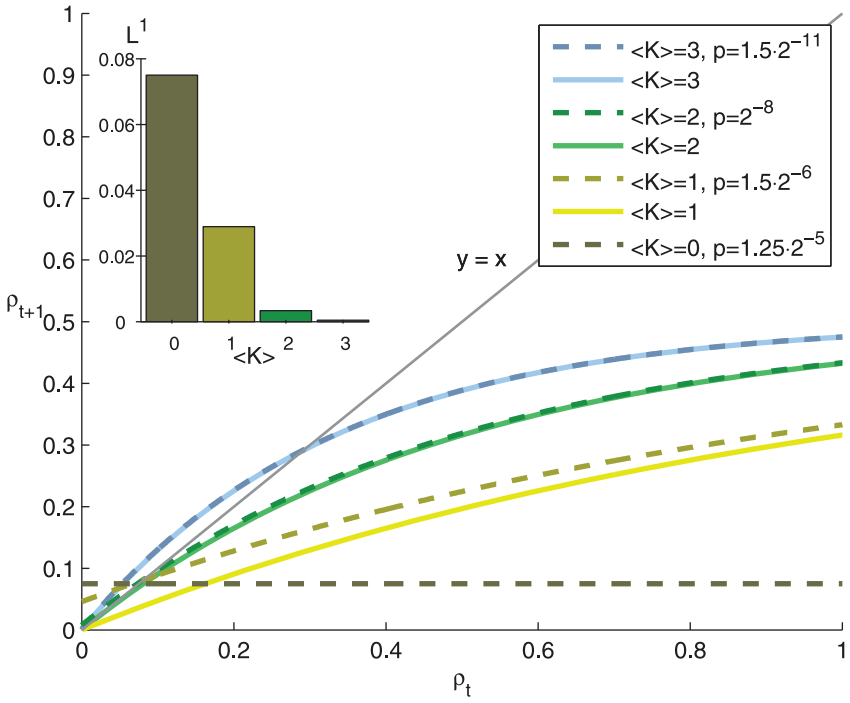

Figure 8. Subcritical networks with maximal steady-state set complexity suffer from disruption in information flow. The figure shows the Derrida curves of different networks according to Eq. 4. The networks are Poisson networks with $\langle K \rangle = 0,1,2,3$, where for each network the noise level is chosen such that the steady-state set complexity is maximized (dashed lines), and the corresponding noiseless networks (solid lines). The noiseless $\langle K \rangle = 0$ network is not plotted, as it has the property that $\forall \rho_t : \rho_{t+1} = 0$. The thin grey line shows the diagonal $\rho_{t+1} = \rho_t$, which would correspond to the state-preserving network $\mathbf{x}_{t+1} = \mathbf{x}_t$. **Inset**: The L^1 norm between the noisy and the corresponding noiseless networks.
doi:10.1371/journal.pone.0056523.g008

approximate Kolmogorov complexity with data compressors. In [20], the reconstruction is based on NCD estimated using several different data compressors, as the authors of [37] utilize only Lempel-Ziv algorithm for estimating the Kolmogorov complexity but several similarity metrics closely related to NCD. Built upon NCD, there is a great promise also in the set complexity measure. Although it was originally proposed as a heuristic measure, the set complexity has since then been shown to possess optimal properties in, e.g., assessing the structure of complete bipartite graphs [38].

The states with maximal complexity are of interest for several reasons. As discussed in [22] with aspect to biological systems, a high value of set complexity reflects large amount of meaningful information. In our earlier work [27] and in Fig. 1 we have shown that the temporal context-dependent information content in noiseless systems is maximized prior to reaching the attractor. This could mean that the system, if interpreted as a "decision maker" of on which attractor to fall, performs the crucial decision during this stage and not earlier when the dynamics are of low information content due to the lack of context, nor later when the dynamics are redundant. The interesting result reported in the present paper is the effect of moderate level of noise on the elevated steady-state complexity of the system. This suggests that a moderate level of noise be helpful in retaining the system in an agile state, i.e., ready to act in a meaningful way to different cues.

Our finding that asynchronous and synchronous random Boolean networks have very similar steady-state complexity behavior (Fig. 5 and Fig. 6) is a rather surprising result. Earlier theoretical and computational analyses show grave differences between these two model classes in, e.g., number of attractors [39] and Derrida curves [40]. However, both of these aspects may suffer from comparing the uncomparable. For instance, in synchronous RBNs attractors can be either point or cyclic attractors, as in asynchronous RBNs they are either point or loose attractors. As for the Derrida-based analysis, the ways to define the Derrida curve for asynchronous Boolean networks are many. The authors of [40] choose to compare the two runs after one synchronous update of a number m of nodes (m picked from a uniform distribution from 1 to N), while it might be more relevant to make the comparison after N updates of single node. By contrast, our analysis, which is based on the amount of redundancy in the steady-state dynamics, does not require a definition of any intermediate parameter of the dynamics, but is straightforwardly applicable to any discrete-time discrete-state system. Ultimately, assessing the set complexity of the steady-state dynamics could form a novel, intricate way of characterizing complex networks.

In addition to models of Boolean networks, above analysis is highly relevant also for understanding more complex dynamical systems. Living cells for example, need to maintain their homeostatic state under noisy environment. Early studies with Boolean networks have addressed the question of homeostasis by studying the effect of small perturbations [41]. We have shown how the Boolean network model parameters together with noise control information flow in the system. Our analysis in Fig. 8 shows that if too much noise is added to gain higher complexity, the system can no longer maintain its dynamical function. This is a hallmark event of the loss of homeostasis. The presented framework could serve as a general basis for estimating the noise levels that a given system can tolerate and still maintain its dynamical function, or a homeostatic state.

We have studied information flow in systems without external stimuli, but an important and much more challenging question is the homeostasis in systems that receive and transfer information. This could correspond to the case where a system is not only retaining current state information under noise but is also trying to adapt and respond to systematic changes in the surroundings. In doing this, the task is to filter useful information from the external signals, which also include noise. A key question for future studies is to analyze the connection between external and internal information and noise in the system. The real signicance of maximal complexity states could be in having suitable versatility to perform the filtering task efficiently, and tuning the system by noise may help in such filtering tasks as well.

Materials and Methods

Boolean networks

A *synchronous Boolean network* is defined as a collection of nodes $\{V_1,\ldots,V_N\}$ where at each time step t each node is assigned a Boolean value $x_i(t)$, i.e.

$$\forall t\in\mathbb{N}\ \forall i\in\{1,\ldots,N\} : x_i(t)\in\{0,1\}.$$

Here, $x_i(t)$ is the state of the node V_i at time instant t. Each node receives input from $K_i\in\{0,\ldots,N\}$ nodes and the state of the node at time instant $t+1$ is a Boolean function of the states of its input nodes at time instant t:

$$x_i(t+1)=f_i(x_{I_{i1}}(t),\ldots,x_{I_{iK_i}}(t)),$$

where I_{ij} ($j\in\{1,\ldots,K_i\}$) are the indices of the input nodes of node i.

In this work we use two types of synchronous random Boolean networks. The first class of networks is such that the number of inputs to a node is picked from a Poisson distribution and the input nodes are picked by random, creating a Poisson distribution for the outputs of the nodes as well. The update functions f_i are also picked by random, i.e., each combination of inputs is assigned an output value 0 or 1 with equal probabilities $q=\frac{1}{2}$. We refer to these networks as *Poisson networks*. In the other class of networks the number of input nodes is fixed. In this class functionally different networks are obtained by changing the probability q (also called the bias of the network) of Boolean function output being 0. We call this class of networks *fixed-K networks*. The dynamics in both Poisson and fixed-K networks can be characterized by *sensitivity s*, which is calculated [42] as

$$s=2\langle K\rangle q(1-q). \quad (1)$$

Networks with $s=1$ are considered critical, as lower and higher sensitivity values correspond to subcritical and supercritical dynamics, respectively [13]. Both types of networks can be assigned a level of noise through a nonzero flip probability p: At each time step for each node, there is a probability of p of getting the opposite state than the one dictated by the deterministic dynamics.

We consider networks of size $N=1000$ with variable levels of noise. The complexity of network dynamics at time t is estimated using the set complexity over T successive states: $X(t)$, $X(t+1)$, …, $X(t+T-1)$. The value of T used in the calculation determines the time resolution obtained, and has to be selected to correspond with the transient lengths observed. The results are consistent for T ranging from 2 to 10 — in this work, we present results for $T=6$. The complexity of dynamics is assigned for time instants $t=1,\ldots,400$. The initial state of the network is picked by random from a uniform distribution over the state space.

NCD and set complexity

We study the complexity of Boolean network dynamics following the framework we presented in [27]. The dynamics of a Boolean network is represented by a set of its successive states that are read into strings. To the obtained set of strings one applies the *set complexity* measure [22], defined as:

$$S(\{x_1,\ldots,x_N\})=\sum_j C(x_j)\frac{1}{N(N-1)}\sum_{j\neq k} d_{jk}(1-d_{jk}). \quad (2)$$

The function $C(x_j)$ denotes the approximation of Kolmogorov complexity of string x_j. The variable d_{jk} represents the *normalized compression distance* (NCD), a computable approximation of the normalized information distance [20] of strings x_j and x_k, defined as

$$d_{jk}=\mathrm{NCD}(x_j,x_k)=\frac{C(x_jx_k)-\min(C(x_j),C(x_k))}{\max(C(x_j),C(x_k))},$$

where x_jx_k is the concatenation of strings x_j and x_k. $C(\cdot)$ is calculated using LZMA compression.

For the basic properties of the set complexity measure we refer to [22], which shows, e.g., the effect of increasing level of noise on the resulting set complexity value of identical strings. In this work, we use the set complexity exclusively for time series data. We therefore illustrate the behavior of the set complexity in the case of random, periodic and quasiperiodic dynamics in the supplementary data of this paper (Fig. S2). These three types of dynamics are relevant in our study, as the Boolean network dynamics is *periodic* in the noiseless case ($p=0$) and *random* in the case of maximal noise ($p=\frac{1}{2}$). The dynamics in the case of moderate noise levels could be viewed as *quasiperiodic*. In the example of Fig. S2, the periodic dynamics produces the least set complexity values, while the complexity of the quasiperiodic dynamics is on average higher than either the periodic or random dynamics.

Generally, the framework of NCD allows the use of any lossless data compression method for the estimation of Kolmogorov complexity. However, in order to obtain reliable results the most efficient — in terms of compression ratio — should be used when possible. We have reviewed the use of different compressors for estimating Kolmogorov complexity in our earlier work [16,43]. In [43] the LZMA algorithm was found most efficient in compressing long repeated strings. In [43] an adaptive packing algorithm called prediction by partial matching (PPM) [44] was found in some aspects superior to LZMA. However, PPM produced in many cases NCD values larger than 1, which is not allowed when computing the set complexity. We have not encountered such problems with the use of LZMA algorithm. The LZMA software used in this study is LZMA SDK 4.65.

Statistical complexity

The statistical complexity [29,30] is defined as the amount of information in the statistic that is minimal and sufficient for predicting the future of the process. This is done locally through parametrization of the past states of the nodes that could affect the state at hand, and similarly, the future states that the node at hand could affect. These past states are referred to as the *past light cone* and the future states as the *future light cone* — the past light cone

includes the state of the considered node at the present time step [29]. The objects of interest are the conditional distributions $p(L^+|L^-)$, where L^+ and L^- are the future and past light cones, respectively. Whenever two past light cones produce the same distribution of future light cones, these past light cones are considered to belong to the same *causal state*. The statistical complexity of the process at time t is calculated as the logarithm of the number of causal states at that moment.

We follow the example given in [30]: We consider only one step into the past and into the future and estimate the number of causal states. To do this, we repeat each network simulation 50 times from random initial state in order to estimate the conditional distributions $p(L^+|L^-)$ at each time step and apply Pearson's χ^2-test with p-value 0.05 to obtain the causal states from them. Both in- and out-degree of the nodes are fixed to K in order to make the comparison of distributions possible. Our method is, however, different in one aspect. We quantify the states *relative* to the past state. That is, we consider the state of node V_i as $\tilde{x}_i(t)=x_i(t)\oplus x_i(t-1)$ instead of the absolute state $x_i(t)$, where $\oplus$ represents the exclusive or (XOR). This choice is due to the random choice of the Boolean functions: As we consider only one step ahead, we can only expect the absolute future states to be distributed as repeated Bernoulli distribution $p(x_1,\ldots,x_K)=q^{\sum x}(1-q)^{K-\sum x}$, while the distribution of the relative states successfully captures the dynamics of the system.

Derrida curves for Poisson networks

Derrida analysis [42] is a widely-used method for studying the dynamical behavior of discrete systems. The Derrida curve shows the average difference between the states of two identical networks at time instant $t+1$ given their difference at time instant t. To compute this curve we consider a noisy Poisson Boolean network, initially at state $\mathbf{x}(0)$, and a perturbed run of the same network, initially at state $\mathbf{x}'(0)$. The state update can be decomposed to two discrete stages. The first stage (1°) is the deterministic update $\hat{\mathbf{x}}(t+1)=\mathbf{f}(\mathbf{x}(t))$, and the second stage ($2^\circ$) is the possible bit flip, defined as

$$\mathrm{P}(\mathbf{x}_i(t+1)=\hat{\mathbf{x}}_i(t+1))=1-p.$$

The possible bit flips in the two runs occur independently of each other. Let us denote the fraction of nodes whose states are different in the two runs by $\hat{\rho}_{t+1}$ (after 1°) and ρ_{t+1} (after 2°).

For simplicity, we consider networks in the limit of the system size $N\to\infty$. The number of inputs to a node in the network is distributed as Poisson: $p(k)=\frac{L^k}{k!}e^{-L}$, $k=0,1,\ldots$, where $\langle K\rangle$ is represented by L for the sake of clarity. By the randomness in the choice of function $\mathbf{f}$, the probability of a node in the perturbed run having a different value from the one in the reference run after 1° is

$$\hat{\rho}_{t+1}=\frac{1}{2}\sum_{k=0}^{\infty}\frac{L^k}{k!}e^{-L}\left(1-(1-\rho_t)^k\right). \quad (3)$$

In the stage 2° there is a probability of $(1-p)^2+p^2$ that the states of the two runs stay the same with respect to one another, and a probability of $2p(1-p)$ that exactly one of the two bits is inverted. Hence we have

$$\rho_{t+1}=\hat{\rho}_{t+1}\times\left((1-p)^2+p^2\right)+(1-\hat{\rho}_{t+1})\times 2p(1-p),$$

which with Eq. (3) and a bit of algebra gives

$$\rho_{t+1}=\frac{1}{2}-\frac{1}{2}(2p-1)^2e^{-L\rho_t}. \quad (4)$$

Note that we applied the assumption of independence of the state $\mathbf{x}$ and the random function $\mathbf{f}$ in the derivation of Eq. (3). This assumption is fully valid only during the first state update $\mathbf{x}(0)\mapsto\hat{\mathbf{x}}(1)\mapsto\mathbf{x}(1)$. However, Derrida and Weisbuch [45] among others have shown that this *annealed approximation* predicts many aspects of network dynamical behavior to a fine degree.

Supporting Information

Figure S1 Networks near to critical can be tuned to maximal statistical complexity. The color of the plot shows the steady-state statistical complexity of fixed-K_{in}-K_{out} networks as function of sensitivity s and flip probability p. See Fig. 4 for reference. The result shown is the median of 65 network repetitions, smoothened with bilinear interpolation. The lower panel shows the maximum of the steady-state statistical complexity over the flip probability p.
(EPS)

Figure S2 Set complexity time series for random, periodic and quasiperiodπic dynamics. The upper panels show the control signals, which are functions $\mathbb{N}\to[0,1]$ that have either random (left), periodic (middle) or quasiperiodic (right) behavior. The periodic signal is chosen as $\frac{1}{2}+\frac{1}{2}\sin\left(t\cdot\sqrt[10]{\pi}\cdot 2\pi/10\right)$, where $t\in\mathbb{N}$. The factor $\sqrt[10]{\pi}$ is added to ensure that the control signal does not receive an exactly same value at distinct time points in finite time. The quasiperiodic signal is chosen as an interpolation of two periodic signals as $\frac{1}{2}+\frac{1}{4}\left(\sin(t\cdot 2\pi/10)+\sin(t\cdot\sqrt{\pi}\cdot 2\pi/10\right)$. In each of the three cases a set of $N=1000$ nodes are created, and each node is given a random threshold between 0 and 1. When the control signal is above the threshold, the node output is 1, and 0 otherwise. The middle row panels show the dynamics of the nodes, black representing 1 s and white 0 s. In the lower panels the curves show the average values (100 repetitions) of the set complexity trajectories of these systems. The set complexity is calculated using 20 successive time steps. The values of set complexity are lowest for the periodic system, and second lowest for the random data, while the quasiperiodic system produces the highest average set complexity.
(EPS)

Acknowledgments

We thank the reviewers for suggestions that helped to improve the paper at hand.

Author Contributions

Conceived and designed the experiments: TMM JK MN. Performed the experiments: TMM. Analyzed the data: TMM JK MN. Wrote the paper: TMM JK MN.

References

1. Luscombe N, Babu M, Yu H, Snyder M, Teichmann S, et al. (2004) Genomic analysis of regulatory network dynamics reveals large topological changes. Nature 431: 308–312.
2. Van Vreeswijk C, Sompolinsky H (1996) Chaos in neuronal networks with balanced excitatory and inhibitory activity. Science 274: 1724–1726.
3. Bastolla U, Fortuna M, Pascual-García A, Ferrera A, Luque B, et al. (2009) The architecture of mutualistic networks minimizes competition and increases biodiversity. Nature 458: 1018–1020.
4. Watts D, Strogatz S (1998) Collective dynamics of small-world networks. Nature 393: 440–442.
5. Barabási A, Albert R (1999) Emergence of scaling in random networks. Science 286: 509–512.
6. Strogatz S (2001) Exploring complex networks. Nature 410: 268–276.
7. Boccaletti S, Latora V, Moreno Y, Chavez M, Hwang D (2006) Complex networks: Structure and dynamics. Physics Reports 424: 175–308.
8. Aldana M, Coppersmith S, Kadanoff L (2003) Boolean dynamics with random couplings. pp. 23–89.
9. Krawitz P, Shmulevich I (2007) Basin entropy in Boolean network ensembles. Physical Review Letters 98: 158701.
10. Nykter M, Price N, Aldana M, Ramsey S, Kauffman S, et al. (2008) Gene expression dynamics in the macrophage exhibit criticality. Proceedings of the National Academy of Sciences 105: 1897.
11. Ribeiro A, Kauffman S, Lloyd-Price J, Samuelsson B, Socolar J (2008) Mutual information in random Boolean models of regulatory networks. Physical Review E 77: 011901.
12. Shmulevich I, Kauffman S, Aldana M (2005) Eukaryotic cells are dynamically ordered or critical but not chaotic. Proceedings of the National Academy of Sciences 102: 13439.
13. Nykter M, Price N, Larjo A, Aho T, Kauffman S, et al. (2008) Critical networks exhibit maximal information diversity in structure-dynamics relationships. Physical Review Letters 100: 58702.
14. Rämö P, Kauffman S, Kesseli J, Yli-Harja O (2007) Measures for information propagation in Boolean networks. Physica D: Nonlinear Phenomena 227: 100–104.
15. Lizier J, Pritam S, Prokopenko M (2011) Information dynamics in small-world Boolean networks. Artificial Life 17: 293–314.
16. Mäki-Marttunen T, Aáimović J, Nykter M, Kesseli J, Ruohonen K, et al. (2011) Information diversity in structure and dynamics of simulated neuronal networks. Frontiers in Computational Neuroscience 5.
17. Bornholdt S (2005) Systems biology: Less is more in modeling large genetic networks. Science 310: 449–451.
18. Kauffman S (1969) Metabolic stability and epigenesis in randomly constructed genetic nets. Journal of Theoretical Biology 22: 437–467.
19. Albert R, Othmer H (2003) The topology of the regulatory interactions predicts the expression pattern of the segment polarity genes in Drosophila melanogaster. Journal of Theoretical Biology 223: 1–18.
20. Li M, Chen X, Li X, Ma B, Vitanyi P (2004) The similarity metric. IEEE Transactions on Information Theory 50: 3250–3264.
21. Kolmogorov A (1965) Three approaches to the quantitative definition of information. Problems of Information Transmission 1: 1–7.
22. Galas D, Nykter M, Carter G, Price N, Shmulevich I (2010) Biological information as set-based complexity. IEEE Transactions on Information Theory 56: 667–677.
23. Sakhanenko N, Galas D (2011) Complexity of networks I: The set-complexity of binary graphs. Complexity 17: 51–64.
24. Galbiati G, Fischer M (1981) On the complexity of 2-output Boolean networks. Theoretical Computer Science 16: 177–185.
25. Alon N, Boppana R (1987) The monotone circuit complexity of Boolean functions. Combinatorica 7: 1–22.
26. Gong X, Socolar J (2012) Quantifying the complexity of random Boolean networks. Physical Review E 85: 066107.
27. Mäki-Marttunen T, Kesseli J, Kauffman S, Yli-Harja O, Nykter M (2011) Of the complexity of Boolean network state trajectories. In: Proceedings of the Eighth International Workshop on Computational Systems Biology, WCSB 2011, June 6–8, Zurich, Switzerland. TICSP series.
28. Crutchfield J, Young K (1989) Inferring statistical complexity. Physical Review Letters 63: 105–108.
29. Shalizi C (2003) Optimal nonlinear prediction of random fields on networks. Discrete Mathematics and Theoretical Computer Science : 11–30.
30. Shalizi C, Shalizi K, Haslinger R (2004) Quantifying self-organization with optimal predictors. Physical Review Letters 93: 118701.
31. Peixoto TP, Drossel B (2009) Noise in random Boolean networks. Physical Review E 79: 036108.
32. Klemm K, Bornholdt S (2005) Stable and unstable attractors in Boolean networks. Physical Review E 72: 055101.
33. Serra R, Villani M, Barbieri A, Kauffman S, Colacci A (2010) On the dynamics of random Boolean networks subject to noise: Attractors, ergodic sets and cell types. Journal of Theoretical Biology 265: 185–193.
34. Grassberger P (1986) Toward a quantitative theory of self-generated complexity. International Journal of Theoretical Physics 25: 907–938.
35. López-Ruiz R, Mancini HL, Calbet X (1995) A statistical measure of complexity. Physics Letters A 209: 321–326.
36. Shiner J, Davison M, Landsberg P (1999) Simple measure for complexity. Physical review E 59: 1459.
37. Otu H, Sayood K (2003) A new sequence distance measure for phylogenetic tree construction. Bioinformatics 19: 2122–2130.
38. Ignac T, Sakhanenko N, Galas D (2012) Complexity of networks II: The set complexity of edgecolored graphs. Complexity 17: 23–26.
39. Harvey I, Bossomaier T (1997) Time out of joint: Attractors in asynchronous random Boolean networks. In: Proceedings of the Fourth European Conference on Artificial Life. MIT Press, Cambridge, pp. 67–75.
40. Mesot B, Teuscher C (2003) Critical values in asynchronous random Boolean networks. Advances in Artificial Life : 367–376.
41. Kauffman S (1993) The origins of order: Self-organization and selection in evolution. Oxford University Press, USA.
42. Derrida B, Stauffer D (1986) Phase transitions in two-dimensional Kauffman cellular automata. Europhysics Letters 2: 739.
43. Hahne L, Kesseli J, Nykter M (2011) Evaluation of compressors for estimating normalized compression distance. In: Proceedings of the Eighth International Workshop on Computational Systems Biology, WCSB 2011, June 6–8, Zurich, Switzerland. TICSP series.
44. Cleary J, Witten I (1984) Data compression using adaptive coding and partial string matching. IEEE Transactions on Communications 32: 396–402.
45. Derrida B, Weisbuch G (1986) Evolution of overlaps between configurations in random Boolean networks. Journal de physique 47: 1297–1303.
46. Gershenson C (2004) Updating schemes in random Boolean networks: Do they really matter. In: Artificial Life IX: Proceedings of the Ninth International Conference on the Simulation and Synthesis of Living Systems. MIT Press, pp. 238–243.

Balance between Noise and Information Flow Maximizes Set Complexity of Network Dynamics — Supporting information

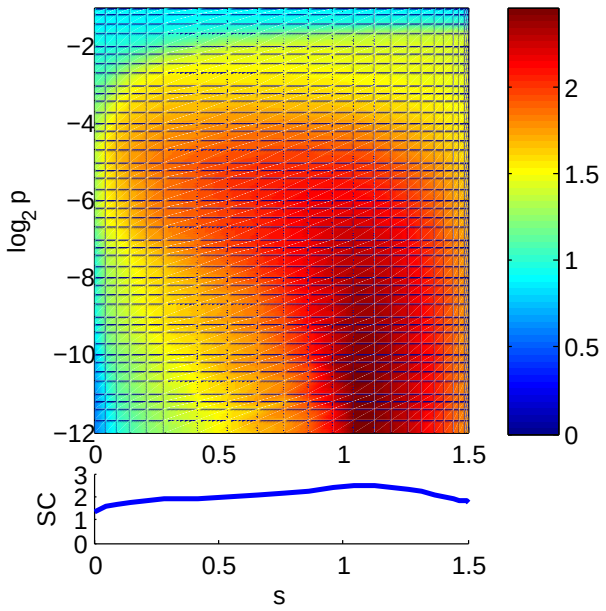

Figure S1. Networks near to critical can be tuned to maximal statistical complexity. The color of the plot shows the steady-state statistical complexity of fixed-K_{in}-K_{out} networks as function of sensitivity s and flip probability p. See Fig. 4 for reference. The result shown is the median of 65 network repetitions, smoothened with bilinear interpolation. The lower panel shows the maximum of the steady-state statistical complexity over the flip probability p.

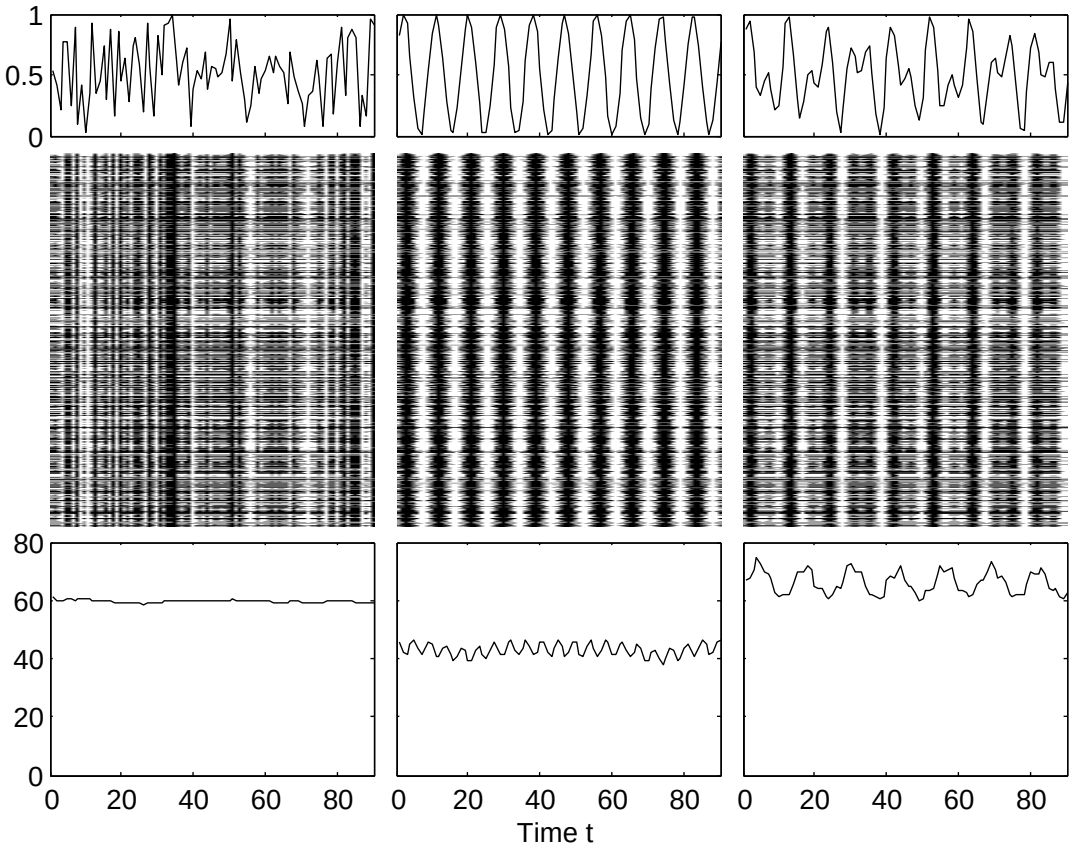

Figure S2. Set complexity time series for random, periodic and quasiperiodic dynamics. The upper panels show the control signals, which are functions $\mathbb{N} \to [0,1]$ that have either random (left), periodic (middle) or quasiperiodic (right) behavior. The periodic signal is chosen as $\frac{1}{2} + \frac{1}{2}\sin(t \cdot \sqrt[10]{\pi} \cdot 2\pi/10)$, where $t \in \mathbb{N}$. The factor $\sqrt[10]{\pi}$ is added to ensure that the control signal does not receive an exactly same value at distinct time points in finite time. The quasiperiodic signal is chosen as an interpolation of two periodic signals as $\frac{1}{2} + \frac{1}{4}(\sin(t \cdot 2\pi/10) + \sin(t \cdot \sqrt{\pi} \cdot 2\pi/10))$. In each of the three cases a set of $N = 1000$ nodes are created, and each node is given a random threshold between 0 and 1. When the control signal is above the threshold, the node output is 1, and 0 otherwise. The middle row panels show the dynamics of the nodes, black representing 1s and white 0s. In the lower panels the curves show the average values (100 repetitions) of the set complexity trajectories of these systems. The set complexity is calculated using 20 successive time steps. The values of set complexity are lowest for the periodic system, and second lowest for the random data, while the quasiperiodic system produces the highest average set complexity.

Publication VI

T. Mäki-Marttunen, J. Aćimović, K. Ruohonen, and M.-L. Linne. Structure-dynamics relationships in bursting neuronal networks revealed using a prediction framework. *PLoS ONE*, 8(7): e69373, 2013.

OPEN ACCESS Freely available online

PLOS ONE

Structure-Dynamics Relationships in Bursting Neuronal Networks Revealed Using a Prediction Framework

Tuomo Mäki-Marttunen[1,2]*, Jugoslava Aćimović[1], Keijo Ruohonen[2], Marja-Leena Linne[1]

1 Department of Signal Processing, Tampere University of Technology, Tampere, Finland, **2** Department of Mathematics, Tampere University of Technology, Tampere, Finland

Abstract

The question of how the structure of a neuronal network affects its functionality has gained a lot of attention in neuroscience. However, the vast majority of the studies on structure-dynamics relationships consider few types of network structures and assess limited numbers of structural measures. In this *in silico* study, we employ a wide diversity of network topologies and search among many possibilities the aspects of structure that have the greatest effect on the network excitability. The network activity is simulated using two point-neuron models, where the neurons are activated by noisy fluctuation of the membrane potential and their connections are described by chemical synapse models, and statistics on the number and quality of the emergent network bursts are collected for each network type. We apply a prediction framework to the obtained data in order to find out the most relevant aspects of network structure. In this framework, predictors that use different sets of graph-theoretic measures are trained to estimate the activity properties, such as burst count or burst length, of the networks. The performances of these predictors are compared with each other. We show that the best performance in prediction of activity properties for networks with sharp in-degree distribution is obtained when the prediction is based on clustering coefficient. By contrast, for networks with broad in-degree distribution, the maximum eigenvalue of the connectivity graph gives the most accurate prediction. The results shown for small ($N = 100$) networks hold with few exceptions when different neuron models, different choices of neuron population and different average degrees are applied. We confirm our conclusions using larger ($N = 900$) networks as well. Our findings reveal the relevance of different aspects of network structure from the viewpoint of network excitability, and our integrative method could serve as a general framework for structure-dynamics studies in biosciences.

Citation: Mäki-Marttunen T, Aćimović J, Ruohonen K, Linne M-L (2013) Structure-Dynamics Relationships in Bursting Neuronal Networks Revealed Using a Prediction Framework. PLoS ONE 8(7): e69373. doi:10.1371/journal.pone.0069373

Editor: Gennady Cymbalyuk, Georgia State University, United States of America

Received February 1, 2013; **Accepted** June 7, 2013; **Published** July 25, 2013

Funding: This work was supported by TISE graduate school, Academy of Finland project 132877, Foundation of Tampere University of Technology, and KAUTE foundation. The funders had no role in study design, data collection and analysis, decision to publish, or preparation of the manuscript.

Competing Interests: The authors have declared that no competing interests exist.

* E-mail: tuomo.maki-marttunen@tut.fi

Introduction

There is a great interest towards understanding the structure of neuronal networks, and ultimately, the full connectome [1,2]. The network structure lays a foundation to all collective activity observed in the system, and understanding this relationship is relevant both *in vivo* and *in vitro*. Promising experimental attempts have been made in controlling the growth of neurons to produce a pre-designed network structure [3,4]. If successful, such experiments would inform us on how the collective dynamics of the neurons is influenced by their patterns of synaptic connectivity. However, such information is extremely challenging to obtain using the state-of-the-art equipment due to the complexity of processes involved in neuronal growth. Furthermore, the connectivity patterns obtained using experimental setups are always subject to physical constraints posed by the growing platform of the neurons. For all this, most of the nowadays studies on structure-function relationship in neuronal networks are likely to be conducted *in silico*, where the connectivity can easily be modified and the effect on the network dynamics instantaneously screened.

In the past few decades a lot of theoretical and computational studies on the function of neuronal networks have been carried out in order to examine the behavior of the network under various circumstances and various stimuli. However, in most studies the structure of the network is at least in part based on purely *random networks*, i.e., the far and widely studied Erdös-Rényi networks. These networks are statistically described by a single parameter, namely, the connection probability p, and by far lack any spatial organization. Several studies have revealed the contribution of connection probability to various aspects of neuronal network dynamics, e.g., emergence of large-scale network synchronization [5,6] the amplitude of fast network oscillations [7], and emergence of spontaneous network-wide bursts [8].

Despite their vast usage, the random networks have been found an insufficient model for the synaptic connectivity in the brain [9–12]. Recently, steps toward deeper understanding of the details of the structure and their effects on the dynamics have been made, which is shown by the devotion of a recent special issue in Frontiers in Computational Neuroscience particularly to this topic [13]. The framework of small-world networks [14] which allows varying the proportion q of long-range connections in addition to the connection probability p has hitherto been the most studied alternative to Erdös-Rényi networks in models of neuronal networks. Analyses on the effects of the long-range connections on, e.g., oscillation coherency [15], modes of synchrony in models

of epilepsy [16,17], and self-sustained activity [18] have been carried out. However, a range of other extensions to random networks exists as well. The scale-free [19] networks possess a structure that is hierarchical over different scales, and are characterized by power-law distributed degrees. These networks have been applied in a range of neuronal modeling studies due to their resemblance to the hierarchical connectivity of the brain [20]. Nevertheless, the preferential attachment algorithm in [19] (and in most generalizations for directed graphs, e.g. [21]) for generating scale-free topology only uses the first order connectivity statistics, i.e., the number of contacts of the nodes, as the criteria for creating a link. In [22] the effect of second-order connectivity statistics, which can roughly be captured by the widths and correlation of the degree distributions, were studied. Similarly, [23] studied the effect of degree distribution widths through a framework where both degree distributions can be arbitrarily predefined, and the networks are created through random couplings. Both [22] and [23] agree on the significance of the in-degree over the out-degree in influencing the mode of synchrony in the network.

A frequent trend in structure-dynamics studies is to overlook the coeffect of structural measures. The changes in activity are monitored with respect to one graph measure, ignoring the possible mutual changes in other structural measures [24]. In this work we approach this problem by measuring a set of graph properties simultaneously. In addition, we apply multiple network generation algorithms in order to avoid too great correlation between some particular graph measures. As an example, studying only such networks that are described in [14] would bring about a large correlation between geodesic path length and clustering coefficient, which would make it difficult to tell which properties of dynamics are due to the high path length and which are due to the clustering.

The focus of this work is on excitability of spontaneously bursting networks, i.e., on how frequently network bursts occur and of what magnitude they are. Note that we adopt the term *burst* from literature on neuronal networks cultured on a micro-electrode array, where the term is widely used for a short period of high spiking activity (alternative names are many, e.g., *network spike*, *population spike*, and *synchronized spike*) [25,26]. By contrast, when we refer to a burst of a single neuron, we use the term *intrinsic burst* or *single-cell burst* to make a clear distinction. We apply two point-neuron models, one of which is based on the integrate-and-fire formalism and the other on the Hodgkin-Huxley formalism. In both models, the neurons are connected by chemical synapses expressing short-term plasticity. The synaptic currents (or conductances in the Hodgkin-Huxley type of model) are instantaneous and decay exponentially after a presynaptic action potential. In the case of strong enough recurrent excitation, both models produce network bursts. Our focus is on the regime of spontaneous bursting activity, where the bursting frequency lies between 0 and 60 bursts/min. This is a typical range of bursting in, e.g., cortical cultures [25].

In the present study, we apply a prediction framework to determine the importance of different graph-theoretic measures. Simulations of network activity are run on a large set of different network structures, and measures of both structure and activity are calculated. For each measure of structure we estimate its capability to predict the outcome of the activity properties, and to an extent, its capability to copredict the activity when used together with the other graph measures. We show that the prediction of activity properties in networks with sharp in-degree distribution (binomial) is best when clustering coefficient is used, whereas in networks with broad in-degree distribution (power-law) the predictions based on maximum eigenvalue of the connectivity matrix are the most accurate. Our results could serve as a general guideline for designing experiments in which several but not all aspects of structure are measured. With novel experimental techniques and tools for data analysis [12,27], graph-theoretic measures of the local connectivity could be estimated without unraveling the whole connectivity matrix, and our results may help to choose those measured aspects.

Materials and Methods

We restrict our study on networks in which the structure can be fully represented by a directed unweighted graph. We use the notation $G=(V,E)$, where G is the graph, $V=\{v_1,\ldots,v_N\}$ is the set of nodes, and $E=\{(x,y)|x\in V,y\in V\}$ is the set of egdes between the nodes. The connectivity matrix $M\in\{0,1\}^{N\times N}$ of a graph V is a binary matrix, where each element M_{ij} denotes the existence (1) or nonexistence (0) of an edge *from* node v_i *to* node v_j. Self-connections are excluded in this work. We call *neighbors* such pair of nodes, that have at least a unidirected edge between them. When no risk of confusion, we use the terms "node v_i" and "node i" interchangeably.

Network structure

We assess network structure using the following graph-theoretic measures.

- *Clustering coefficient* (CC). The local clustering coefficient CC_i of a node v_i describes the density of local connections in the neighborhood of node v_i. We say that the nodes v_i, v_j and v_k form a triangle if there is at least a unidirected edge between v_i and v_j, between v_i and v_k, and between v_j and v_k. The local clustering coefficient of node v_i is the number of triangles that include the node divided by the maximum number of such triangles if all neighbors of the node were connected [14,28]. The directions of the edges are respected, hence changing a unidirected edge to a bidirectional edge doubles the counted triangles that include the considered edge. In mathematical terms, we can write

$$\mathrm{CC}_i=\frac{1}{8\binom{n_i}{2}}\sum_{\substack{j=1\\ j\neq i}}^{N}\sum_{\substack{k=1\\ k\neq i}}^{j-1}(M_{ij}+M_{ji})(M_{ik}+M_{ki})(M_{jk}+M_{kj}),$$

where n_i is the number of neighbors of node v_i. The clustering coefficient CC of the whole network is calculated as the average over the local clustering coefficients of the nodes – only those nodes are taken into account that have more than one neighbor.

- *Harmonic path length* (PL). A geodesic path from a node to another means the shortest traversable path between the two nodes. To calculate the harmonic path length, the geodesic path length PL_{ij} between each pair of nodes (v_i,v_j), $i\neq j$ is first calculated, where $\mathrm{PL}_{ij}=\infty$ represents the case where no path exists from v_i to v_j. The harmonic path length of the network represents the average distance between two nodes of the network, and is computed as the harmonic mean of the geodesic path lengths [28,29]:

$$\mathrm{PL}=\left(\frac{1}{N(N-1)}\sum_{i}^{N}\sum_{\substack{j=1\\ j\neq i}}^{N}\frac{1}{\mathrm{PL}_{ij}}\right)^{-1}.$$

- *Node-betweenness* (NB). The local node-betweenness NB_i is a measure of centrality of the node v_i. It is calculated as the number of shortest paths that the considered node lies on [28]. If the node lies on a number $s_{jk}^{(i)}$ out of $s_{jk}^{(\mathrm{tot})}$ equally long geodesic paths between nodes v_j and v_k, then the increment of this pair of nodes is the fraction of the two quantities. Thus, we can write $\mathrm{NB}_i=\sum_{\substack{j=1\\ j\neq i}}^{N}\sum_{\substack{k=1\\ i\neq k\neq j\\ \mathrm{PL}_{jk}<\infty}}^{N}\frac{s_{jk}^{(i)}}{s_{jk}^{(\mathrm{tot})}}$. The node-betweenness NB of the network is the average of the local betweennesses NB_i.
- *Out-degree deviation* (OD). The sample standard deviation of the realized out-degrees of the nodes.
- *Degree correlation* (DC). The sample correlation coefficient between the realized in- and out-degrees of the nodes.
- *Length-to-self* (LtS). The mean geodesic length to self $\frac{1}{N}\sum_{i=1}^{N}\mathrm{PL}_{ii}$.
- *Maximum eigenvalue* (MEig). The largest eigenvalue of the connectivity matrix M. This is always real-valued as the connectivity matrix is non-negative [30].
- *Motif* count (Mot$N$, $N=1,\ldots,13$). The (absolute) number of different connectivity patterns of triples of nodes [31] (see Fig. 1).

Ideally, to study how measures of structure are linked to measures of dynamics, one would have a direct (possibly stochastic) function from the measures of structure to measures of dynamics. However, to obtain the measures of dynamics or their distributions, a network activity model has to be applied using a certain connectivity graph. Hence, this sort of mapping is not possible unless the measures of structure uniquely determine the underlying graph. To go around this problem, we generate networks with very different structural properties and simulate the neuronal activity in them. We concentrate on a few carefully selected random graph classes that we consider to span wide enough diversity of network types relevant in neuroscience: Watts-Strogatz-type networks (WS), networks with high local feed-forward structure (FF), and networks with high number of loops of certain length (L2,L3,L4,L6).

Let us motivate the choice of these classes. WS networks were first introduced in [14] as a class of networks expressing the small-world phenomenon, and have been extensively used ever since. In neuroscientific studies the WS networks between ordered and random topologies have been proposed as a model for, e.g., optimal signal propagation [15], maximal dynamical complexity [32], and optimal pattern restoration [33]. As for the FF networks, the feed-forward loop is a triple of nodes, v_i, v_j and v_k, where there is a direct connection from v_i to v_k, and a "secured" disynaptic connection from v_i through v_j to v_k. The feed-forward loops have been found more abundant in *C. Elegans* neuronal network than in random networks [31], and their contribution to neural processing has been much studied [34,35]. We include these networks in the present study as an alternative to WS networks that should show a great number of feed-forward loops and yet lack the spatial structure typical to WS networks. Finally, the loopy networks (L2, L3, L4 and L6) represent a network structure, where the connections are organized such that the feed-back loops of certain length and direction are promoted. The synaptic feed-back projections in general have been suggested as a mechanism for working memory [36,37]. Several papers discuss the existence of directed loops in the brain: [38] and [39] show that such loops could be produced by rules of spike-timing-dependent plasticity (STDP) in order to promote stability in the network, contradicting with the no-strong-loops hypothesis [40]. The reason to include loopy networks in this study is to address the question whether and to what extent such loops contribute to the dynamics in recurrent neuronal networks.

One of the statistically most dominant properties of recurrent neuronal networks is the connection probability of the neurons. Increasing or decreasing the connection probability has usually major effects on the neuronal activity, which has been discussed in several computational studies, including [7], [41] and [8]. In addition to this, not only the average number but also the variance in number of inputs to the neurons plays a significant role in the synchronization properties of the network [22,23]. Regarding these facts, we keep the in-degree distributions strictly constrained while studying the other aspects in the network structure. To do this we propose to use the following random graph algorithms in which the in-degree distribution $f_{\mathbf{ID}}$ can be explicitly set.

Watts-Strogatz [14] algorithm for bidirectional graphs. Initially, the nodes are placed in a metric space of choice. The number of inputs is drawn from $f_{\mathbf{ID}}$ for each node, and that number of spatially nearest nodes are chosen as inputs. Finally, all existing edges are rewired with probability q such that the postsynaptic node is held fixed but the presynaptic node is picked by random. We call these networks WS1 and WS2 networks, where the number 1 or 2 tells the dimensionality of the manifold where the nodes lie. In WS1 networks the nodes are placed on the perimeter of a ring, while in WS2 networks the nodes are placed on the surface of a torus. To be more specific, in the ring topology the nodes are placed into a ring in 2D plane as $(x,y)=(\sin\gamma,\cos\gamma)$, where $\gamma\in\{\frac{2\pi}{N},\frac{4\pi}{N},\ldots,2\pi\}$. Similarly, in the torus topology the 2D grid is nested into 4D space as $(x,y,z,w)=(\sin\gamma_1,\cos\gamma_1,\sin\gamma_2,\cos\gamma_2)$, where $\gamma_1,\gamma_2\in\{\frac{2\pi}{\sqrt{N}},\frac{4\pi}{\sqrt{N}},\ldots,2\pi\}$, given that $\sqrt{N}$ is an integer. In both

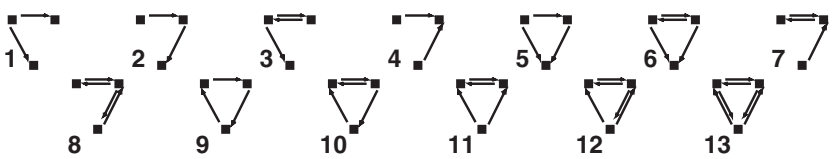

Figure 1. The 13 network motifs of three connected nodes. See [31] for reference.
doi:10.1371/journal.pone.0069373.g001

topologies the Euclidean distance is used as the metric. We refer to the limit topologies of Watts-Strogatz networks with zero rewiring ($q=0$) as *locally connected networks* (LCN1 and LCN2).

Scheme for generating graphs with high local feed-forward occurrence. For each node the number of inputs is drawn from $f_{\mathbf{ID}}$. The inputs are selected sequentially for each node. For the first node, the inputs are selected by random. For the next ones, the inputs are selected in such a way, that the emergence of feed-forward motifs is pronounced. This is done by giving higher weights to the nodes that project disynaptically to the considered node than to the others. A detailed scheme for generating these networks is given in Algorithm S1 in File S1. We refer to these networks by acronym FF. Note that this is not to be mistaken for the general term *feed-forward networks* in the meaning of opposite for recurrent networks. In this work all considered networks are recurrent.

Scheme for generating graphs with high occurrence of loops of length L. For each node the number of inputs is drawn from $f_{\mathbf{ID}}$. The edges are set one by one until each node has all its inputs selected. In the selection of presynaptic nodes, the emergence of loops of length L is promoted, while the addition of edges that shorten these loops is discredited. This is done by giving different weights to the nodes depending on the shortest path from the considered node to the candidate nodes. See Algorithm S2 in File S1 for the detailed algorithm. The resulting networks are rich in recurrent synfire chains of length L. This is however conditional to the choice of the in-degree distribution: If the number of connections is too great, the excessive edges have to create "shortcuts" into the loops. In this work we refer to these networks with acronym L2, L3, L4 or L6, depending on the promoted length of loops.

MATLAB functions to generate these networks are given in ModelDB entry 147117. Each of these algorithms can be used to generate both networks where the definitive property of the respective network is very pronounced, networks where the strength of that property is zero (random networks), and networks that lie in between these extremes on a continuous scale. We denote this *strength parameter* by $W\in[0,\infty]$. In Watts-Strogatz networks, we draw the relation between the rewiring probability q and the strength parameter as $q=\exp(-W/2)$. Hence, in all network classes $W=0$ produces strictly random networks (RN) and $W=\infty$ produces the other extreme of networks.

In addition to these networks, we consider biologically realistic 2-dimensional neuronal networks. To generate these, we use the NETMORPH simulator [42] with the model parameters taken from [43]. NETMORPH simulates the growth of dendrites and axons in a population of neurons and outputs the sites of potential synapses. The potential synapses are formed when an axon and a dendrite of distinct neurons come close enough to each other. To remove the effect of boundaries, we place the somas randomly inside a square-shaped box, and the neurites that grow outside the box are considered to appear on the opposite side of the box. For each simulation, we form the connectivity graph from the simulation result once the required amount of connections has been reached. We omit the question of to which degree the potential synapses become functional synapses and consider every potential synapse as an edge. Multiple synapses with the same pre- and postsynaptic neurons are considered as one edge. The in-degree distribution of these NETMORPH networks cannot be explicitly set, but it is fairly well approximated by binomial distributions (see Fig. S1 in supporting information). In the forthcoming sections, we abbreviate the networks obtained with the NETMORPH simulators as NM.

The different network classes are illustrated in Fig. 2. In addition, iterations for the generation of extreme FF and L4 networks are shown. Furthermore, a set of graph measures in extreme FF, L2, L3, L4 and L6 networks are shown. These statistics, compared to the corresponding statistics in random and locally connected networks, reveal that the algorithms indeed produce networks with the desired properties. Further properties of the networks are shown in Figs. S2, S3 and S4, and discussed in Section S2 in File S1.

Neuronal dynamics

We apply two neuron models with rather different intrinsic dynamics. The first one is a leaky integrate-and-fire model with short-term plasticity [44], and the second one is a Hodgkin-Huxley type of model with four ionic and three synaptic currents [45]. In the latter we import a model of synaptic short-term plasticity from [46]. In both models we input a stochastic white noise term into the membrane potential of the neurons to make them spontaneously active. The models are described in detail in Section S1.3 in File S1.

We refer to the first model as *LIF* model and to the latter as *HH* model throughout this work, although they are extensions of the ordinary leaky integrate-and-fire and Hodgkin-Huxley models. These two models were chosen to represent both a simple model that can easily be extended to larger networks, and a more biophysically detailed model that can be extended to study the effect of, e.g., various neurotransmitters and modulators on network activity. The latter was introduced as a model for studying synchronization in low extracellular magnesium concentration, but it allows the use of higher concentrations as well. Here, we use a value $[\mathrm{Mg}^{2+}]_o=0.7\mathrm{mM}$, which is in the range of magnesium concentrations normally used in studies of neuronal cultures (see, e.g., [25]).

Network bursts could be produced with simpler models that do not consider short-term plasticity, e.g., by using widely applied models of balanced excitation/inhibition [47] or Markov binary neurons [48]. The ending of the bursts in these models is dependent on the activation of the inhibitory population, which returns the elevated firing activity to a baseline level. By contrast, applying short-term depression to the excitatory synaptic currents allows the emergence of network bursts in both excitatory-only (E) and excitatory-inhibitory (EI) networks [44]. This is favorable, as the experiments carried out on neuronal cultures show that network bursts cease even in the pathological case of blocked inhibition (see, e.g., [49] and [26] for spinal cord cultures and [50] and [51] for cortical cultures). In this work, we study the bursting dynamics of both E and EI networks, and hence, we employ the short-term depressing synapses in both cases. In the EI networks, the structure is first generated using one of the network generation schemes and then 20% of the neurons, randomly picked, are assigned as the inhibitory population. The network size is $N=100$ unless otherwise stated.

As a major simplification to reality, we consider the synaptic transmission to be instantaneous. The transmission delays and their effect on neuronal network dynamics have been under wide examination (see e.g. [52]) and have been shown to play an important role in various contexts. Their inclusion can be, however, carried out in multiple ways. For instance, in WS1, WS2, and NM networks the long-range connections should have longer delay parameters than the local connections (see e.g. [53]), whereas for other network types such distance-delay relationship cannot be straightforwardly defined, and hence, different approaches should be tested. In this work we restrict our study to non-delayed networks in order to avoid excessive simulations.

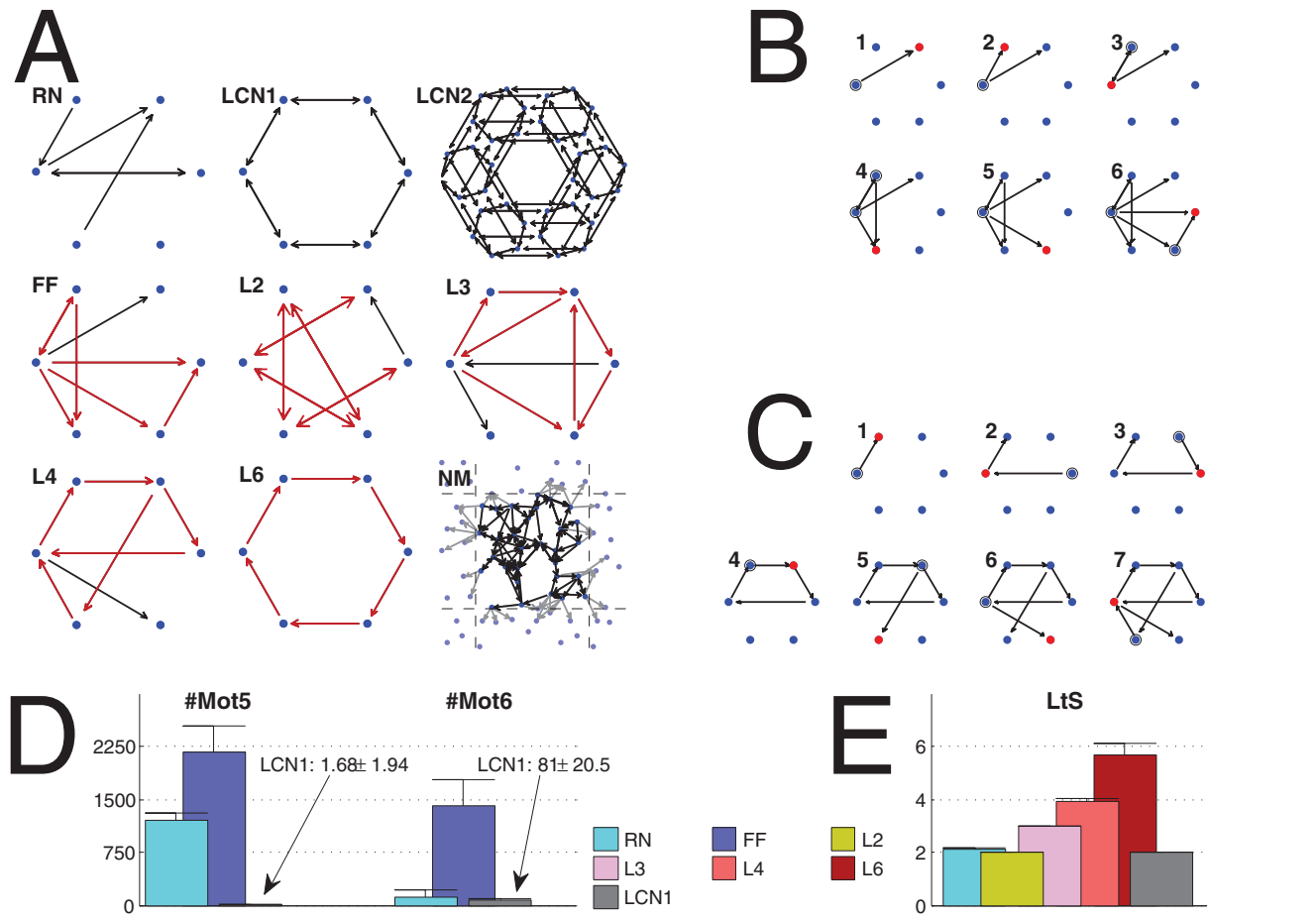

Figure 2. Illustration of network classes. A: Examples of the extreme network types used in the present work. Network size $N=6$, except in LCN2 $N=36$, and in NM $N=30$. The red arrows highlight the definitive properties of the networks. In NM the connections whose post-synaptic node lies across the box boundaries are replaced by a link to a copy of the post-synaptic node (plotted with gray at a corresponding location outside the box). **B, C:** Illustration of the generation of FF (B) and L4 (C) networks. The red dots show the node that has recently been added the inputs, and these inputs are in turn highlighted by circles. The number at the upper-left corner of each graph shows the iteration number. **D**: Mean and standard deviation of the number of motifs 5 (left) and 6 (right) in different extreme network types (RN, FF, and LCN1). The FF networks possess the greatest number of both these two motifs. The low number of these motfis in LCN1 networks is explained by the fact that they contain much more highly connected motifs (motifs 12 and 13) due to their locally coupled design. **E**: Mean and standard deviation of the length-to-self measure in different extreme network types (RN, L2, L3, L4, L6, and LCN1). The loopy networks L2, L3, L4, and L6, express a value of LtS near to the corresponding length of the promoted loop. In both D and E, all networks are of size $N=100$ and their in-degree distribution is binomial with $p=0.16$. Statistics are computed from 150 independent samples.
doi:10.1371/journal.pone.0069373.g002

The networks are set into a regime of spontaneous network bursting. This is done by tuning the synaptic weight η (see Section S1.3 of File S1) so that the moderately connected networks (RN, $p=0.2$, binomial in-degree) show a bursting frequency of 10 bursts/min. These values are in the range of connectivity and bursting activity in a typical cortical culture [25]. For the applied proportions of excitatory and inhibitory neurons and model parameters, we found that the mean bursting frequency is a monotonically increasing function of the synaptic weight in the regime of interest (0–60 bursts/min), and hence we use the bisection method to find the proper synaptic weight.

For each network simulation the spiking activity is solved for a one minute period (in fact for 61 s, but the first second is neglected for a possible transition stage). The model parameters and initial conditions for both models are described in Section S1.3 of File S1. The code files to carry out the simulations in PyNEST [54] (LIF model) and MATLAB (HH model) are given in ModelDB entry 147117. Fig. 3 illustrates the typical dynamics for a single neuron and a network of neurons.

Activity in a bursting network can be characterized by the quantity and quality of the network bursts. We employ the burst detection scheme applied in, e.g., [55] and [56]. The spikes are first divided into separate network bursts using a maximal inter-spike interval of 25 ms. This means that two consecutive spikes belong to the same network burst if and only if their distance is 25 ms or less. Those bursts which consist of less than $1.5N_E$ (with HH model) or $0.4N_E$ (with LIF model) spikes, where N_E denotes the size of the excitatory population, or in which less than $0.3N_E$ individual neurons contributed to the burst, are disregarded. Further, a *burst profile* is created by convoluting the population spike train in the range from the first to the last spike of the burst with a Gaussian with deviation 2.5 ms. The length of the *rising slope* and the *falling slope*, i.e., the halfwidths of the burst profile, are calculated with a resolution of 0.25 ms. These

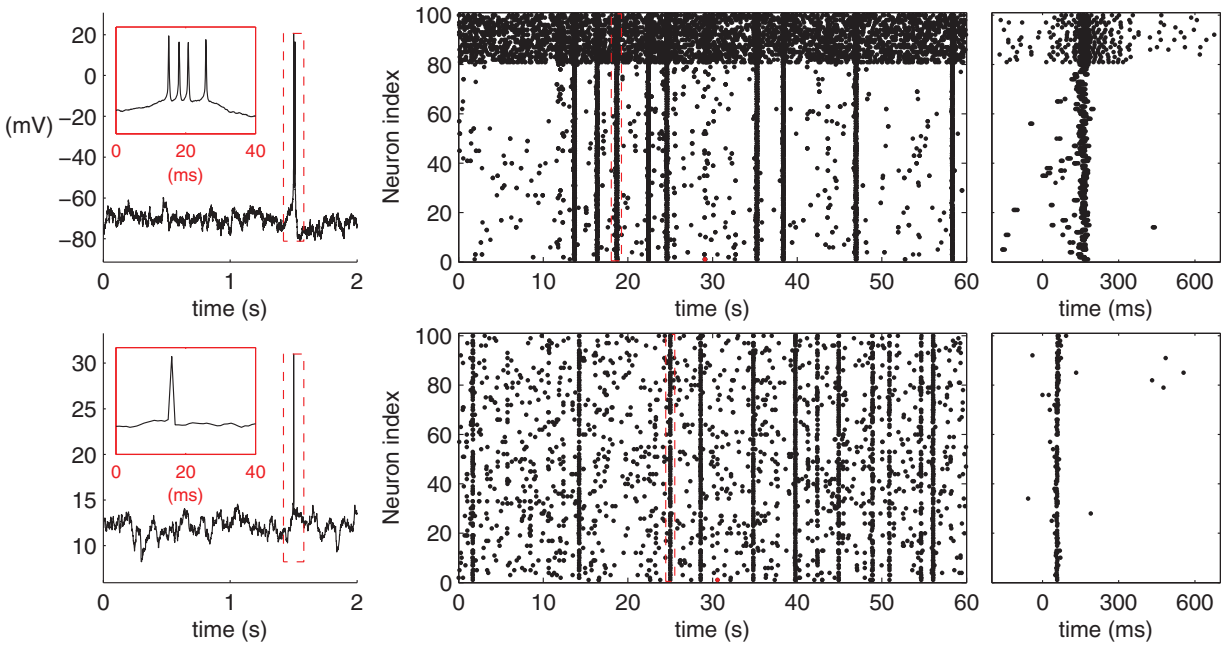

Figure 3. Illustration of the HH (upper panels) and the LIF (lower panels) model dynamics. Left: Single cell membrane potential with the spike magnified in the inset. The membrane potential at the time of spike in the LIF model explicitly set 30 mV for the sake of illustration. **Middle:** Network spike train in an excitatory-inhibitory RN with $p=0.2$ connectivity and binomial in-degree distribution. The upmost 20 neurons represent the inhibitory population. The red spike corresponds to the (first) spike shown in the left panel, and the burst with the red borders corresponds to the burst shown in the right panel. **Right:** The selected burst highlighted.
doi:10.1371/journal.pone.0069373.g003

measures are illustrated in Fig. 4. We consider the summed value of these two measures the *length of the burst*. This measure is more robust to addition of a single spike to the burst than the absolute duration of the burst, which is calculated as the time from the first spike to the last spike of the burst. To further characterize the burst, we consider the number of spikes in a burst, which we refer to as the *burst size*. To average the network activity over a one minute simulation, we use the median burst length and median burst size. An important characteristic of the network activity is also the *burst count*, i.e. the number of bursts during the time of simulation, which has been shown to vary substantially in spontaneously active networks with different structures [57]. In addition, we consider the total *spike count* of the network during the one minute simulation as an indicator of the overall amount of activity.

All above activity measures are calculated from the population spike train of the network. In the LIF model the spike trains are given explicitly by the model, but in the HH model they have to be extracted from the time series of the membrane potential. In this work, we consider any *local maximum* of the membrane potential above the threshold of -30 mV a spike. It should be noted that due to the Brownian noise injected to the membrane potential, we only consider local maxima at the resolution of $10dt$, where dt is the simulation time step. This means that the time instant t is considered a local maximum if and only if $V(t-10dt)<V(t)$ and $V(t)\geq V(t+10dt)$. Given the simulation time step $dt=0.0025$ms, this resolution was found scarce enough to prevent the noisy fluctuation of the membrane potential from being registered as spikes but on the other hand fine enough to correctly detect spikes in an intrinsic (single-cell) burst. The chosen threshold potential, -30 mV, is robust. In a RN with binomial in-degree distribution ($p=0.3$), the change of ± 2.5mV in the threshold potential had no effect on the detected spikes, and a change of ± 10.0mV changed the total number of detected spikes by less than 5%.

Structure-dynamics analysis

Using the above methods, a realization of activity properties can be obtained for any given connectivity graph by simulating one of the two neuron models and performing the burst detection. In purely excitatory networks the graph properties are extracted using the entire network, while in EI networks only the excitatory-excitatory part is considered. The activity properties are likewise calculated from the excitatory population merely.

Throughout this work, we divide the data into 24 *simulation settings*, as listed in Table 1. The networks in each simulation

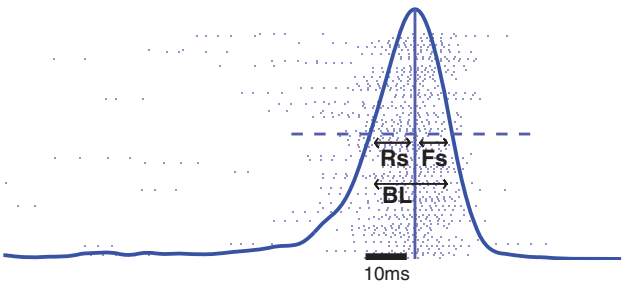

Figure 4. Illustration of the burst profile attributes. The shaded dots represent the spikes of the excitatory neurons. The thick blue curve represents burst profile, i.e., the smoothened firing rate curve. The time instants when the burst profile for the first and the last time crosses the value of half of the maximal value (shown with horizontal dashed line) are identified. The distances of these time instants from the time instant of the maximal firing rate (vertical line) are the lengths of the rising (Rs) and falling (Fs) slope. The burst length (BL) is the sum of these two attributes. The network activity in this figure is simulated with the HH model, and the structure of the underlying network is a RN with binomial in-degree distribution, $p=0.2$. Scale bar (black) 10 ms.
doi:10.1371/journal.pone.0069373.g004

Table 1. The list of the 24 simulation settings.

HH													LIF											
E						EI							E						EI					
BIN			POW			BIN			POW				BIN			POW			BIN			POW		
0.16	0.2	0.3	0.16	0.2	0.3	0.16	0.2	0.3	0.16	0.2	0.3		0.16	0.2	0.3	0.16	0.2	0.3	0.16	0.2	0.3	0.16	0.2	0.3

The first row denotes the model of dynamics, and the second row shows the choices of population. For each combination of these one may freely choose the shape (third row) and connection probability (fourth row) of the in-degree distribution.

doi:10.1371/journal.pone.0069373.t001

setting have a fixed average connection probability p (0.16, 0.2, or 0.3), a fixed shape of in-degree distribution (BIN as binomial or POW as power-law), a fixed choice of population (E or EI) and a fixed choice of model of dynamics (HH or LIF). Hence, all variation in activity properties between networks that belong to the same simulation setting is an effect of the network structure only. For each setting we generate a series of network structure realizations and for each of these we simulate a one minute sample of activity. The chosen network types are FF, WS1 and WS2 networks with $W=1,3,6,\infty$, and L2, L3, L4 and L6 networks with $W=3,6,12,\infty$. In addition, RNs are included, and NM networks are considered in settings with binomial in-degree distribution, which makes the total number of essentially different types of network structure $N_{\mathrm{nt}}=29$ (power-law) or 30 (binomial).

We use two methods for the data analysis, namely, a correlation analysis and a prediction framework. We use the first to restrict the number of analyses to be done with the latter. The correlation coefficient between activity property and graph property is calculated for each simulation setting separately as

$$\frac{\sum_{G\in\mathcal{G}}(x(G)-\mu_x)(y(G)-\mu_y)}{\sqrt{\sum_{G\in\mathcal{G}}(x(G)-\mu_x)^2}\sqrt{\sum_{G\in\mathcal{G}}(y(G)-\mu_y)^2}}. \quad (1)$$

In this notation, $\mathcal{G}$ is the set of networks (we use terms network and network realization interchangeably here) belonging to a said simulation setting. The term $x(G)$ is a graph property of network G, while the term $y(G)$ is an activity property obtained from a neuronal simulation done on network G, and μ_x and μ_y are the corresponding average values.

The correlation analysis is useful as a first approximation of the relationship between the graph measures and activity measures, but it only sheds light on the linear pair-wise dependence between the measures. We apply a prediction framework to answer the question: Which graph measures are the most important when aiming to predict the activity in the network? To do this, we divide the data into a teaching data set and a target data set. The teaching data set consists of $N_{\mathrm{te}}=35$ networks for each of the $N_{\mathrm{nt}}=30$ (29) network types, while the target data set contains only $N_{\mathrm{ta}}=5$ repetitions. An affine predictor

$$y=a_0+\sum_{i=1}^{K}a_i x_i \quad (2)$$

is built using the considered activity properties $\mathbf{Y}\in\mathbb{R}^{N_{\mathrm{te}}N_{\mathrm{nt}}}$ and the K chosen structural properties $\mathbf{X}\in\mathbb{R}^{N_{\mathrm{te}}N_{\mathrm{nt}}\times K}$ that are extracted from the teaching data. We include the realized average degree in the structural measures in order to compensate for the variety caused by in-degree variance, and hence, we always have $K\geq 1$. Least mean squares is used to solve the predictor coefficients, i.e.,

$$[a_0\ \ a_1\ \ \cdots\ \ a_K]=\left([1\ \mathbf{X}]^T[1\ \mathbf{X}]\right)^{-1}[1\ \mathbf{X}]^T\mathbf{Y},$$

where $1\in\mathbb{R}^{N_{\mathrm{te}}N_{\mathrm{nt}}}$ is a vector consisting of 1's.

The activity properties of the target data set can be predicted using Eqn. 2 for each of the $N_{\mathrm{nt}}N_{\mathrm{ta}}$ networks, and the prediction error can be calculated as the average absolute difference between the predicted and actual value of the activity property. The prediction is repeated for 10 times in total. During the repetition the target data are regenerated, but the teaching data are resampled from a total pool of 100 samples of each network type. The error distribution for a given predictor, i.e., a predictor that uses a chosen set of structural measures, is compared to the error distribution of other predictors. This is done using Mann-Whitney's U-test, which tests the null hypothesis that the medians of the distributions are equal.

It should be noted that we do not use the term "predict" in the meaning of forecasting the future based on the past. Instead, the task of the predictor is to estimate the outcome of an activity property in a separate, unknown network when only some aspects of the network structure are known to the predictor. This is closely related to *classification tasks*, but as the outcome of the predictor is a continuous value instead of discrete, it is best described by the term *prediction task* [58].

Results

As a first step for understanding the structure-dynamics relationships in bursting neuronal networks, we estimated the correlations of graph-theoretic measures and activity properties. Fig. 5 shows the correlation coefficients between the considered graph measures and measures of activity. We first calculated the correlation coefficient between all pairs of measures in each simulation setting by Eqn. 1. We then computed the mean and standard deviation of the obtained correlations, taken over the twelve simulation settings with the same shape (binomial or power-law) of in-degree distribution. We focus our analysis on those graph measures that at least *for some activity property* gave an absolute mean correlation *greater than 0.25 in both binomial and power-law settings*. Namely, they were CC, PL, NB, OD, MEig, Mot5, Mot12, and Mot13. However, CC and Mot13 were very strongly correlated with each other (correlation coefficient between these measures ranges from 0.85 to 0.99 in the 24 simulation settings, mean 0.94). This was the case also between PL and NB (0.91 to 0.99, mean 0.95), which is backed by the analytical derivations shown in section S2.4 in File S1. Hence we disregarded PL and Mot13 whenever NB and CC were considered. Other pairs of

measures were considerably less correlated: The strongest correlation among the remaining measures was between CC and Mot12, where the correlation coefficient ranged from 0.59 to 0.87, mean 0.77. It should be noted that MEig was to some extent correlated with the average degree of the network (correlation coefficient on range from 0.63 to 0.89, mean 0.79) as predicted by mean-field approximations in [59]. In our framework the mean degrees $E[\bar{d}]=(N-1)p$, where $\bar{d}$ represents the average degree of the nodes, were held fixed between compared networks. However, drawing from the in-degree distribution resulted in some variance in the network structure. In the case of binomial in-degree this variance was negligible ($\mathrm{Var}\,\bar{d}=\mathrm{Var}\left[\frac{1}{N}\sum_{i=1}^{N}d_i\right]=\frac{N-1}{N}p(1-p)\approx 0.158$ for $p=0.2$), where d_i represents the in-degree of a single node, but in networks with power-law distributed in-degree (with $p=0.2$) it was empirically found as large as $\mathrm{Var}\,\bar{d}\approx 2.96$. This variance had to be taken into account explicitly in the analyses of the following sections.

Similarly to structural measures, there was redundancy in the activity measures. Naturally, the total spike count was largely dictated by the product of burst count and median burst size: Correlation coefficient between these measures ranged from 0.866 to 0.999 with mean 0.978. In most of the following analyses we disregarded one of these measures, namely the burst size, due to its small coefficient of variation (mean CV 0.16, whereas those of spike count and burst count were 0.46 and 0.62, respectively). The low variance in burst size was also reflected in a high correlation between the spike count and the burst count (correlation coefficient ranged from 0.532 to 0.998, mean 0.918). Between other pairs of activity measures, the correlation coefficient ranged from negative to positive values. Hence, we also neglected the spike count in most of the forthcoming results and considered it to behave to a great degree similarly to the burst count.

Clustering coefficient regulates the bursting properties in networks with binomial in-degree distribution

To further analyze the dependency between activity and graph properties, we applied the prediction framework for different activity properties in different simulation settings. Fig. 6 shows the prediction errors of the burst count in simulation settings with excitatory-only networks, binomial in-degree distribution, and HH model. The error distribution (mean, std) is plotted for different predictors. One finds that predictors using CC are significantly better than the "null" predictors (the predictors where $K=1$, i.e., only the realized degree is used in the prediction). In the dense connectivity simulations ($p=0.3$) the OD performs approximately equally well, but in other connectivities the effect of OD is insignificant. The distribution of the values of burst count with respect to the values of CC are illustrated for the $p=0.2$ case.

The dominance of CC in prediction of activity properties can be observed for all simulation settings with binomial in-degree distribution. This is confirmed in Fig. 7, where the best predictor was named for the prediction of each activity property in each of the twelve simulation settings. Furthermore, Fig. 8 shows the averaged improvements that were obtained by using the said graph measures in the prediction of burst count and burst length. One can observe that the predictions were best improved from both the null predictor and from a predictor using an arbitrary other graph measure by including CC in the predicting graph measures. The next best predictors were Mot12 and NB. The improvements obtained by adding OD, MEig and Mot5 were small. The improvement in the prediction was most substantial in the case of burst count: By using only one predicting graph measure (CC) the error was reduced by up to 35% on average, while the corresponding prediction error reduction for burst length was on average 26%. The predictor using all available structural measures reached corresponding percentages of 49% for burst count and 45% for burst length (data not shown).

Maximum eigenvalue is the best predictor of activity when in-degree is power-law distributed

We repeated the analyses carried out in the previous section, now using networks with power-law distributed in-degree. The results were substantially different: Changing between excitatory-only and excitatory-inhibitory networks, between different activity models, or even between different connection probabilities did not affect the overall significance of the graph measures in the prediction of activity measures as much as the choice of in-degree distribution did. Fig. 9 shows the statistics corresponding to those shown in Figs. 6, 7 and 8.

One observes a great improvement in prediction by the inclusion of MEig in Fig. 9. This effect was most evident in the networks with the lowest connection probability ($p=0.16$, Fig. 9A) where the bursts were most rare (see Fig. S5). Fig. 9C shows the dominance of MEig across activity properties and all simulation settings with power-law distributed in-degree. The prediction errors of burst count and burst length were decreased from null predictions on average by 28% and 13% by the inclusion of MEig (Fig. 9D), respectively. The corresponding percentages for the predictor using all structural data were 41% and 34% (data not shown), which suggests that it be useful to employ more than one structural measure especially in the prediction of burst length.

In these analyses, the realized degree was included in all the predictions in order to cancel the effect of correlation between MEig and the average degree. If the degree was neglected, the effect of MEig was even more pronounced. By contrast, the exclusion of degree from the predictions of activity measures in networks with binomial in-degree had no notable effect due to the low intrinsic variance in the degree. Furthermore, the results stayed the same when a neural network predictor (default feed-forward backpropagation network in MATLAB) was used instead of linear predictor. If a diagonally quadratic predictor ($[1\ \mathbf{X}]$ replaced by $[1\ \mathbf{X}\ \mathbf{X}^{(2)}]$ where $\mathbf{X}^{(2)}$ is the element-wise second power) was used, the improvements by the addition of NB and OD were slightly increased, however retaining the statistical dominance of CC and MEig in the prediction of all activity properties (data not shown).

We carried out corresponding simulations with larger networks, $N=900$. We used the LIF model and excitatory-only networks, and varied the in-degree distribution. Fig. S6 shows the representative data about large network activity and the predictor performances. Our conclusions hold with large networks as well: The activity properties in networks with binomially distributed in-degree can be best predicted with CC, whereas the activity in networks with power-law distributed in-degree can be best predicted using MEig. In addition, we ran longer, 5 minute simulations using the LIF model networks with the normal network size $N=100$ (data not shown). Our results remained qualitatively the same and confirmed that the shorter (1 minute) simulations give statistically significant results in spite of the large variability in the activity properties.

Discussion

In this work we studied the graph-theoretic properties of several types of networks, and searched for the most relevant aspects of network structure from the viewpoint of bursting properties of the

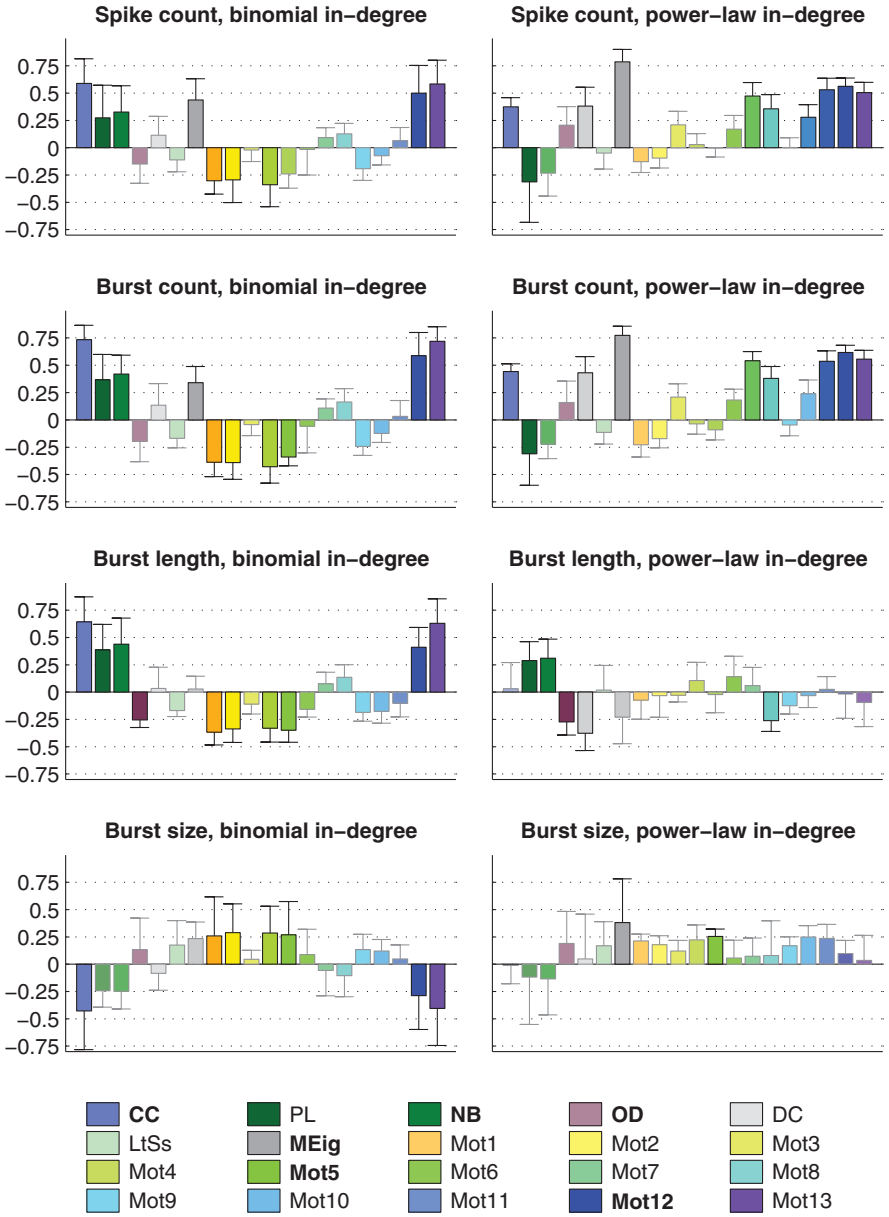

Figure 5. The mean and standard deviation of the correlations between graph measures (see legend) and the activity measures (spike count, burst count, burst length, and burst size). The Eqn. 1 is used for calculating the correlation coefficients for each simulation setting separately. The set of networks $\mathcal{G}$ consists of 150 repetitions of each of the $N_{\mathrm{nt}} = 30$ (29) network types. In the panels on the left the mean correlation is taken over correlation coefficients in the twelve simulation settings that use binomial in-degree distribution, while in the panels on the right the twelve simulation settings with power-law distribution are used. The faded bars represent pairs of measures with absolute mean correlations smaller than 0.25. The graph measures that were finally chosen for structure-dynamics study are bolded in the legend.
doi:10.1371/journal.pone.0069373.g005

network. Our framework for network generation allows the use of arbitrary in-degree distribution. This allows a fair comparison between the dynamics of different network types, given that the distribution of in-degree plays a crucial role in determining the network dynamics [22]. The relevance of the graph-theoretic properties of the network are assessed in a prediction framework. We calculated how much the prediction of an activity property, such as burst count or average length of a burst, is improved when the prediction is based on a given graph property. We found that in the networks with sharp (binomial) in-degree distribution CC plays the most crucial role (Figs. 7 and 8), whereas in networks with wide (power-law) in-degree distribution MEig is the most relevant graph property (Fig. 9C–D). These results are consistent with few exceptions in the twelve combinations of the two neuron models (HH and LIF), two choices of neuron population (excitatory-only and excitatory-inhibitory), and three connection probabilities ($p = 0.16$, 0.2, and 0.3). The simulations were run using small ($N = 100$) networks due to the high computational load needed for generation and analysis of a large enough data set, but we confirmed our main findings using a small subset of simulations with larger ($N = 900$) networks (Fig. S6).

Our framework that combines the use of multiple different types of networks allows the concurrent study of importance of different graph measures, namely CC, PL, NB, OD, DC, LtS, MEig, and

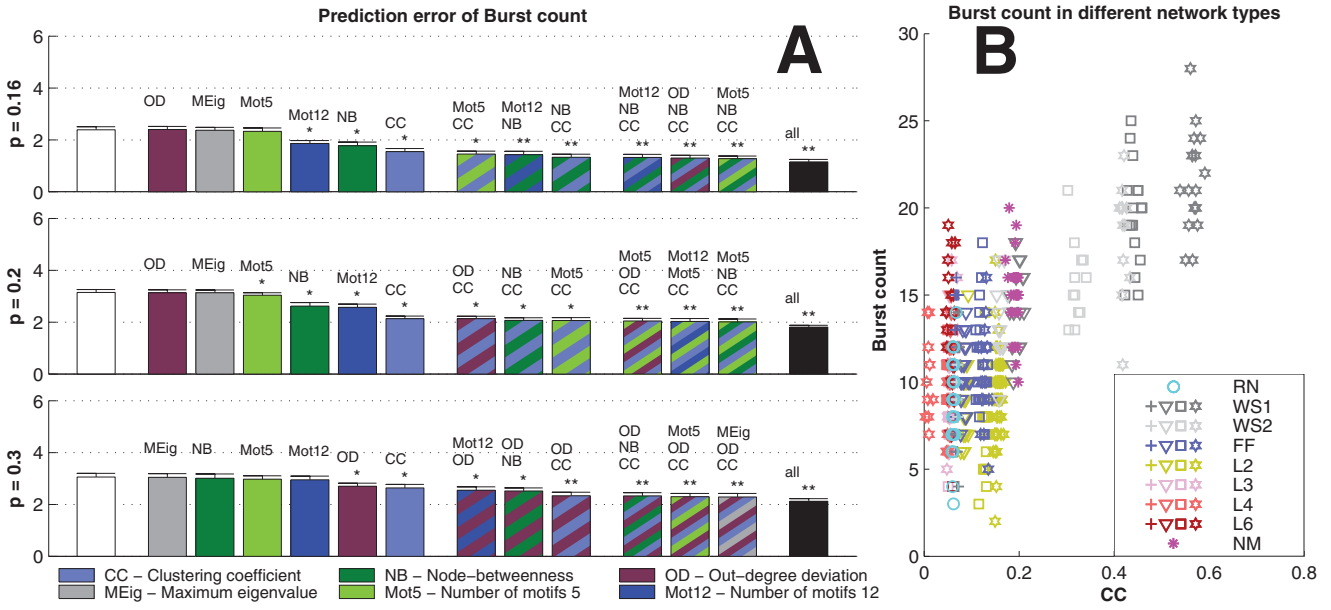

Figure 6. Burst count is best predicted using CC when in-degree is binomial. A: The bars in the three panels show the prediction errors (mean + std, $N_{\text{samp}} = 10$) when different graph properties are used as predictors. The errors are calculated as the difference between the predicted and realized number of bursts. The HH model is used in purely excitatory networks with binomial in-degree distribution and average connectivities $p = 0.16$ (upper), $p = 0.2$ (middle) and $p = 0.3$ (lower). The leftmost bar (white) shows the mean prediction error of the null predictor. The next group of six bars shows the prediction errors of predictors with an additional graph property, in the order of descending prediction error. The next three bars correspond to the best three predictors that use two graph measures, and the next three bars correspond the ones with three measures. The final bar (black) shows the prediction error of the predictor that uses all available structural data (20 measures in addition to the realized degree). If the error is significantly (U-test, $p < 0.05$) smaller than that of the null predictor, an asterisk (*) is plotted, whereas (**) announces that the error is also significantly smaller than that of the best predictor using one graph property (here always CC). The more graph measures are included in the prediction, the more accurate the prediction is. The error values shown are absolute: For reference, the mean burst counts (averaged over all network types) in the three connection probabilities are 3.4 ($p = 0.16$), 11.7 ($p = 0.2$) and 31.5 ($p = 0.3$). **B:** Values of burst count plotted w.r.t. CC in networks with connection probability $p = 0.2$. Different network classes are plotted with different colors, and the different markers of WS1, WS2, FF, L2, L3, L4 and L6 networks represent different values of parameter W ('+' for the lowest value, and stars for the highest value). One finds that the burst count ascends with increasing CC, as suggested by the positive correlation of burst count and CC in Fig. 5.
doi:10.1371/journal.pone.0069373.g006

Mot$N$, $N \in \{1,...,13\}$. The structural measures were chosen according to the mainstream trends in the theory of complex networks. MEig, which is closely related to DC [59], has been previously shown to play a crucial role in the synchronization of the network [60], [22] using the measure of complete synchrony or its derivatives. We found similar results for networks with power-law distributed in-degree. We considered the measures of activity that we find the most describing of spontaneously bursting networks, namely, the spike count, burst count, burst length, and burst size. The computational framework allows the study of many other aspects of dynamics, e.g., Lyapunov exponents during the onset of the bursts, but in this work we restrict to those measures of activity that can be obtained experimentally as well. The effect of variable average degree of the network that is due to the high variance of the power-law distribution was compensated for by including the realized degree into all predictions. Excluding the degree from the prediction would further stress the importance of MEig in prediction (data not shown). Moreover, the results in Fig. 8 stay qualitatively the same if MEig is replaced by DC (data not shown). Furthermore, the domination of MEig and DC remains even if all 20 graph measures are included in the study or if quadratic or mathematical neural net based prediction is used instead of the affine predictor.

However, MEig (or DC) is not the only structural measure that is determinant of the network activity. The sharp in-degree distribution in networks with binomially distributed in-degree results in little variation of MEig and DC compared to networks with power-law distributed in-degrees. At the same time, the measures of network dynamics, such as spike count and burst count, show comparable – although somewhat smaller – ranges of values for both networks. We found out that in networks with sharp in-degree distribution the most determinant property is the CC (or Mot13). The role of CC has been previously highlighted in other types of systems. To name a few, in [61] the degree of local synchrony is suggested to be dictated by CC while the global synchrony is more influenced by PL, and in [62] CC is found superior to PL in affecting the onset of synchronization. The result of [61] was obtained using a pulse-coupled leaky integrate-and-fire model, whereas in [62] the Kuramoto [63] model of oscillating particles was used. High clustering coefficient has also been linked with poorer performance of artificial neural (Hopfield) networks [64], yet experimental studies show that *in vivo* [65] as well as *in vitro* [66] networks possess much greater clustering coefficient than random networks. Similarly to the study at hand, in our earlier work we have found that the amount of network bursts increases with the locality of the network (where also CC is correlated with the locality) [57] in a network of spontaneously active neurons. Our results are backed by [67], where the number of 3-node triangles (comparable to motif 13, see Fig. 1) in the graphs were positively correlated with the mean level of activity in a discrete-state model of neuronal networks. Our results are also in line with [68], where multiple network structures (many of which were similar to ours) consisting of heterogeneous excitatory neuron populations were considered. The authors of [68] found that the

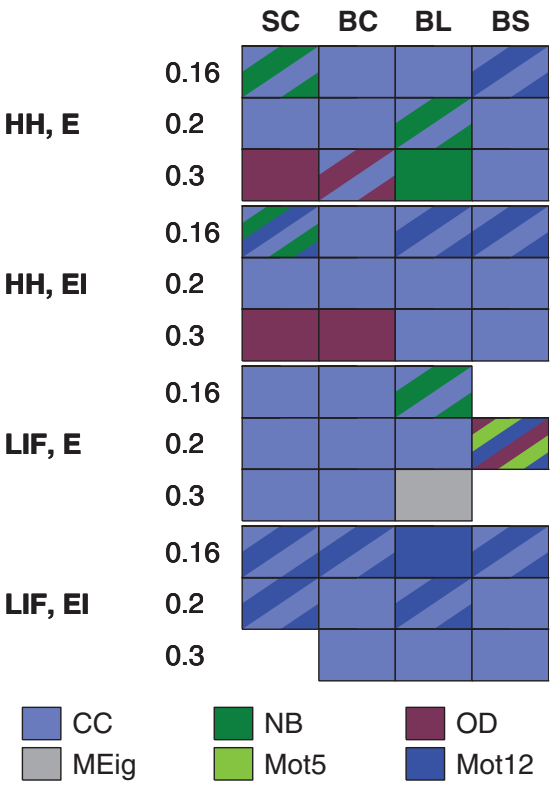

Figure 7. CC gives the best prediction in most simulation settings with binomial in-degree distribution. The best predictor is named for each simulation setting (the 12 rows) and each activity property (the 4 columns: spike count, burst count, burst length, and burst size). The color of the box indicates the graph measure that gives the smallest prediction error when used together with the realized degree of the network. Boxes with stripes mean that another or several other graph measures have statistically indistinguishable error compared to the best predictor. The missing boxes indicate that no predictor is statistically better than the null predictor (U-test, $p<0.05$). CC wins 38 unique or shared best performances, as the respective numbers for Mot12, OD, NB, Mot5 and MEig are 11, 5, 5, 4, 1 and 1.
doi:10.1371/journal.pone.0069373.g007

local connections encourage (single-cell) bursting in the network, and they propose that the high number of local feed-back loops (which corresponds to a high CC in our terminology) could facilitate the spreading of the bursting activity across the network. Opposite or bilateral results were observed in [53], where the network bursting frequency was either decreasing or increasing with the rewiring probability q of WS networks (which is anti-correlated with CC), depending on the fraction of the inhibitory population. The differences between their and our results could emerge from the differences in the burst detection procedures. In [53] the burst detection is based on finding the peaks in the smoothened global firing rate, as we applied the burst detection based on maximum inter-spike interval and minimum burst size [56]. We found the latter method more reliable in detecting bursts of variable shape. In addition, it allows the further observation of the burst length and burst size in a straightforward way.

We did not find consistent trends in the importance of other structural measures. The good performance of predictors based on Mot12 (as seen in some simulation settings with binomial in-degree distribution in Fig. 7) is most likely an effect of the high correlation between CC and Mot12. The importance of NB (and hence PL as well) is mostly expressed in the prediction of burst length, but even considering solely burst length it gives the smallest prediction error in fewer cases than CC (in binomial in-degree, Fig. 7) or MEig (in power-law distributed in-degree, Fig. 9C) do. The importance of OD is highlighted in the prediction of spike count and burst count in dense ($p=0.3$) networks with binomial in-degree distribution, but only in HH model, and hence, no conclusions without deeper investigations can be made. Similar observations on the subsidiary effects of the width of the out-degree distribution were reported in [22] and [23].

Another full dimensionality to the aspects of structure-dynamics relationship would be brought about if *modular networks* [69] were studied. In such networks, not only the local connectivity but also the connectivity pattern between the clusters would greatly affect the collective dynamics. This aspect is highly relevant when unraveling the function of a vertebrate brain, and ground-laying studies have already been carried out in the context of, e.g., emergence of sustained activity [67,70]. Promising attempts were also done in [68], where a biologically inspired modular network model of the mammalian pre-Bötzinger complex was studied by computational means. In their framework, not only the network structure was varied, but also the effect of placing neurons with different intrinsic dynamics (three in total) in different ways was screened. However, we consider that the use of modularly designed networks requires intricate analysis on both intra- and inter-modular connectivities as well as the interplay between them, and leave them to our future studies.

In the generation of the network structure, we fixed the in-degree distribution and allowed the other aspects of the structure to vary. In the framework of [22], all the second-order statistics, which roughly correspond to in-degree deviation, degree correlation, and out-degree deviation, can be controlled in the generation of the graphs. In our framework, the degree correlation and out-degree deviation are affected by the other structural aspects of the network that cannot be ranked by the order of connectivity, such as the proportion of long-range connections in the generation of WS networks. By contrast, networks comparable to FF networks and loopy networks could in principle be generated in a framework similar to [22], but this would require the use of motifs of order higher than 2. In fact, to promote loops of length 6, motifs up to 6th order should be considered, and this might not be computationally feasible. The choice of letting the second order statistics vary could lead to misinterpretations of results if their effect was not screened by other means. Our correlation and prediction framework, by contrast, ensures that the major effect of CC on activity properties in networks with binomial in-degree is not mediated by the other second-order connectivity statistics (or their correlates DC and OD).

It should be noted that we cannot exclude the possibility that there exist measures of structure that perform better than CC and MEig in the prediction of the activity properties. In fact, there may exist a measure that by itself performs better in the prediction task than CC does in networks with sharp in-degree and MEig in networks with wide in-degree distribution. However, the results shown here restrict the properties of such measure – it should be highly correlated with the measures of clustering (CC, Mot13) in networks with binomial in-degree and with measures of degree-degree correlation (MEig, DC) in networks with power-law distributed in-degree. The correlations between graph measures across several network types have been studied in [71], and high correlation coefficient is found between, e.g., the mean of local clustering coefficients (denoted by CC in the present study) and their variance. The high correlation between these measures can also be observed in our network types (correlation coefficient ranges from 0.80 to 0.94, mean 0.90). Indeed, if we replace CC

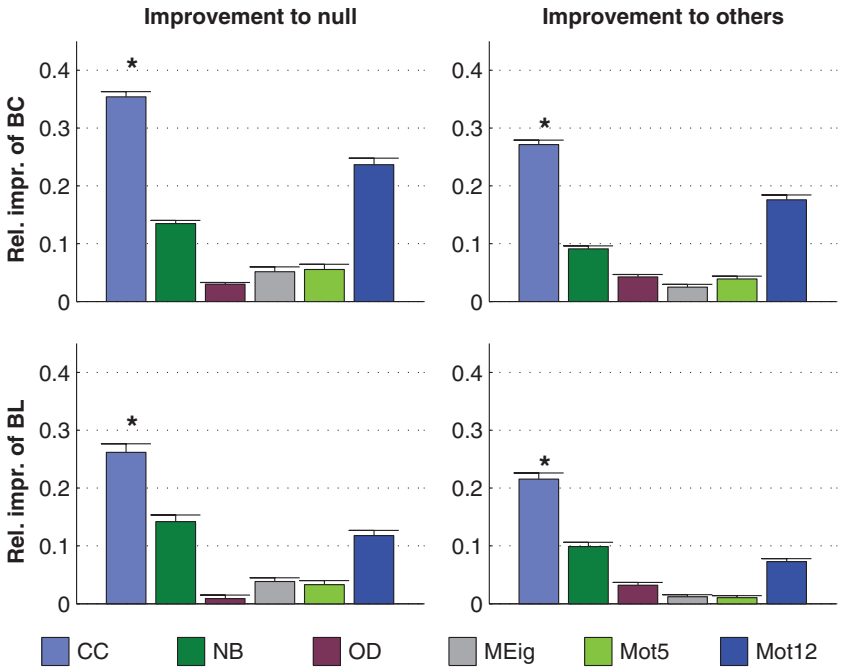

Figure 8. CC brings greatest improvements to the predictions of burst count (BC) and burst length (BL) in networks with binomial in-degree distribution. Left: The y-axis shows the relative improvements with respect to null prediction. For each simulation setting, the prediction error for null predictor and the predictor with a considered graph property x are calculated, using $N_{\mathrm{ta}}=5$ and $N_{\mathrm{te}}=35$. The relative improvements $\frac{\mathrm{ME}_{\mathrm{null}}-\mathrm{ME}_x}{\mathrm{ME}_{\mathrm{null}}}$ are averaged over all 12 simulation settings with binomial in-degree distribution. Plotted is the improvement (mean and std) for $N_{\mathrm{samp}}=10$ repetitions. The improvement obtained by using CC (*) in the prediction is significantly greater than that obtained by any other single graph measure. **Right:** The y-axis shows relative improvements with respect to prediction by other graph properties. As an example, the first bar shows the relative improvement $\frac{\mathrm{ME}_x-\mathrm{ME}_{\mathrm{CC},x}}{\mathrm{ME}_x}$, averaged over graph properties $x\in\{\mathrm{NB,OD,MEig,Mot5,Mot12}\}$. The improvements are further averaged over all 12 simulation settings, and the mean + std of $N_{\mathrm{samp}}=10$ repetitions are shown. The procedure is similar for the other bars. The improvement obtained by using CC (*) in the coprediction is significantly greater than that obtained by any other graph measure (U-test, $p<0.05$).
doi:10.1371/journal.pone.0069373.g008

with the standard deviation of the local clustering coefficients, the results in Fig. 7 stay the same. However, if both are included, the mean of local clustering coefficient remains dominating (data not shown).

The activity properties we measured lie in a noisy regime: Multiple runs on an identical connectivity graph results in a great variance in the dynamics (data not explicitly shown, but the trend visible in Fig. 6B). The noisiness of the data is explained by the spontaneous nature of the bursts. As discussed in [53], the dynamical regime that produces the amount of spontaneous activity that is typically seen in neuronal cultures may reside near to the transient from regular to chaotic activity. This transient can be observed in our results in the sparse ($p=0.16$) networks with binomial in-degree distribution: These networks lie near the shift from tonic spontaneous spiking to spontaneous bursting activity (the mean burst count is very low in RN, L2, and L4 networks, as seen in Fig. S5). Our results show that both in the regime of numerous and few network bursts the prediction of activity properties using measures of structures *is* feasible. Yet, in some cases the improvements made are not that major, see e.g. the modest difference in prediction errors of the best (black) and the worst (white) predictors of burst count in the densest ($p=0.3$) networks in Figs. 6A and 9A. In these networks, the variance of burst count among the networks of same type is considerable, compared to the variability of burst count across the network types (Fig. S5). However, the statistical significance between the prediction errors of different predictors indicates that the fine details of structure still have an effect on the dynamics despite the noisy nature of the bursts.

In the simulations of the excitatory-inhibitory networks, the inhibitory subpopulation was randomly picked once the network structure had been generated. In many brain areas, the connections to and from the inhibitory population obey different connectivity rules than the connections of the excitatory population do. Many *in silico* studies take this diversity into account by applying a specific structure only to the excitatory-excitatory subnetwork, and connecting the excitatory population randomly to the inhibitory population. We conducted our simulations on such networks as well for comparison. The structures of the excitatory subnetworks were first generated by the graph generation algorithms described in the methods section and then randomly coupled to the inhibitory populations. The NETMORPH networks were dismissed from these simulations. The results on the importance of different graph-theoretic measures in predicting activity properties in such networks were qualitatively similar to those reported for EI networks in Figures 7 and 9C (data not shown). Together these results confirm the importance of CC and MEig (of the excitatory subnetwork) also in the presence of inhibition. Due to the different choices of the synaptic weights in excitatory-only and excitatory-inhibitory networks (see Section S1.3 of File S1), which were chosen to restrict the number of bursts on the same range, the difference in the overall network dynamics

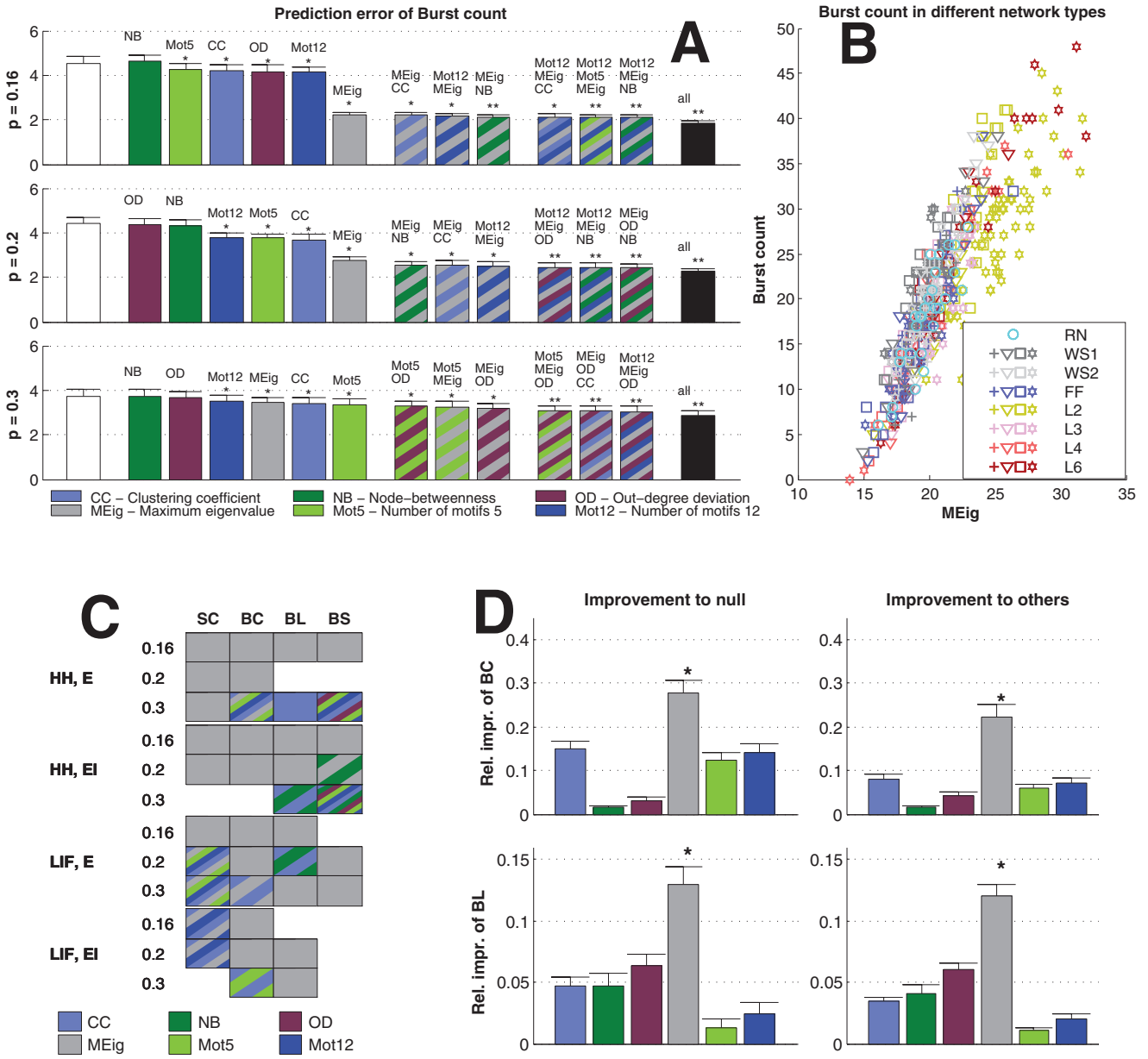

Figure 9. Maximum eigenvalue gives the best prediction of the activity properties across the 12 simulaton settings with power-law distributed in-degree. A: Prediction errors of burst counts in simulation settings with the HH model, purely excitatory networks and power-law distributed in-degree. The average burst counts in the three simulation settings are 8.7 ($p = 0.16$), 20.0 ($p = 0.2$) and 40.3 ($p = 0.3$). See Fig. 6 for details. **B:** The distribution of the values of burst count in different networks with $p = 0.2$, plotted against the MEig of the underlying graph. See Fig. 6 for details. **C:** MEig is the best predictor of activity in most cases (32 unique or shared best performances, in comparison to 12 for CC, 6 for Mot5, 7 for Mot12, 3 for NB, and 2 for OD). See Fig. 7 for details. **D:** In the prediction of burst count and burst length, MEig brings the greatest improvement both to the null predictor and to the predictors based on other graph measures. See Fig. 8 for the details.
doi:10.1371/journal.pone.0069373.g009

was not that significant between the two regimes. Nevertheless, several differences exist. In the repetitive simulations of a chosen network type, the spike count varied considerably more in the excitatory-only networks than in excitatory-inhibitory networks (data not shown). Hence, in this sense the inhibitory population brought stability to the total spiking activity of the network. By contrast, the variance in burst length was larger in excitatory-inhibitory networks (data not shown). This could be explained by the many alternatives when and how the inhibitory population can become active during the network burst. Detailed analyses on how the different ways of coupling the inhibitory population to the excitatory population (and the different intrinsic dynamics that the inhibitory neurons may have) affects the network excitability should be carried out in order to draw further conclusions. Moreover, the graph measures should be tuned to consider both the excitatory and inhibitory populations if detailed structure-dynamics relationships were to be uncovered.

Our simulations were conducted in different simulation settings to argue for the generality of our results. The two neuron models applied in this work differ from each other in many aspects: Spiking at the crossing of a threshold membrane potential vs. spiking through the ionic gating variable dynamics; tonic spiking vs.

intrinsic bursting; current vs. conductance based synapses; one vs. two excitatory synaptic current components. Although only these two models were used, we believe that similar results would be obtained with any neuron model that represents another combination of these four properties. In both models, the synaptic currents decay exponentially, although in HH model the exact form of the decay is also shaped by the effects of the presynaptic and postsynaptic membrane potentials. A key restriction of our results is that they apply to network bursting that emerges from spontaneous spiking activity in the excitatory neurons. A distinction should be made to synchronization of *rhythmically* active neurons, e.g., the Kuramoto model neurons and the phase response curve model neurons as described in [22]. In such systems, the neurons possess a constant drive toward the "forward" phase, whereas in the models used in this work such a drive is replaced by a white noise current. The effect of CC that is observed in our work could emerge from the deeper need of local integration to attain the network burst. In rhythmically active systems this need may be diminished due to the constant "forward" drive, and hence, only the effect of MEig (or DC) is highlighted in such systems, as discussed in [60] and [22]. Another restriction of our conclusions is that only such models are considered where the network bursts are ceased by the depletion of the excitatory synaptic resources – although in the excitatory-inhibitory networks also the activation of the inhibitory population can contribute to the burst cessation. The first restriction could be relaxed by considering both networks of rhythmically active neurons and networks with spontaneously active neurons, and possibly a continuum between them, while the second restriction cannot be relaxed without applying another mechanism for the cessation of the network bursts. We leave both of these questions to be answered by the future studies.

The focus of this paper is on the bursting properties of networks. No unified theory on the relevance of network bursts has been established, but they have been hypothesized as, e.g., a mechanism of secured information transfer [72], a means for synaptic modification [73,74], and in the case of power-law distributed burst size, an optimal information transfer and a sign of the network acting in a critical regime [75]. In addition to the nervous system of a maturing (e.g. [76]) and behaving (e.g. [77]) animal, bursts of large populations of neurons are observed in the most primitive neuronal systems such as dissociated neuronal cultures (see for instance [49] or [51]), which emphasizes the fundamentality of the phenomenon. Earlier computational studies enlighten the cellular mechanisms needed for bursting in neuronal networks (see for example [45]), but few pieces of work monitor the effect of network structure on bursting.

Network bursts represent an extreme type of synchronized spiking activity, and understanding which aspects of structure contribute to the emergence of this synchronization is a crucial milestone in structure-dynamics research in neuroscience. The implications of such knowledge are manifold. The future techniques may allow indirect measurements of certain structural properties of the network [12,27] although the full connectome is unavailable. Knowing which properties are crucial for the network dynamics could help make predictions on the statistics of the activity basing on the measured aspects of the structure. On the other hand, knowledge on structure-dynamics relationship in neuronal networks could be useful in the design of artificial intelligence in the future. The increasing computational power will allow the use of artificial neural networks that are biologically more realistic than the currently existing ones. Given an *in silico* implementation, the designing of the structure in such networks need not be restricted by the physical limitations, such as wiring cost, that exist in their biological counterparts.

Supporting Information

Figure S1 In-degree distributions for NM networks with connection probabilities $p=0.16$ (orange), 0.2 (purple), and 0.3 (blue). The dashed lines show the binomial PDFs with these connection probabilities, and the legend shows the KL-divergence of the NM in-degree distributions from these binomial distributions. The obtained values of D_{KL} are considerably small – the corresponding values between NM in-degree distributions and the best-fit triangular distribution are 0.22 ($p=0.16$), 0.24 ($p=0.2$), and 0.24 ($p=0.3$), and further, the corresponding D_{KL} values are 1.8, 1.7 and 1.6 between NM distributions and uniform distribution. The NM in-degree distributions are constructed from a pool of 400 network realizations.
(EPS)

Figure S2 CC in FF networks as a function of parameter W, and, for comparison, the respective values of RN, LCN1, LCN2 and NETM networks. By the increase of W the CC of FF networks approaches that of the extreme FF networks, yet remains lower than that in LCN1, LCN2 or even NM. Different colors represent networks with different (binomial) in-degree distributions. The solid line shows the average over $N_{\mathrm{samp}}=400$ trials, and the shaded area the standard deviation.
(EPS)

Figure S3 Number (mean and std, $N_{\mathrm{samp}}=400$) of FF-motifs in FF networks as a function of parameter W, and, for comparison, the respective values of RN, LCN1 and NETM networks. The in-degree distribution of FF, RN and LCN1 networks is chosen as binomial with the shown average connectivities.
(EPS)

Figure S4 Distribution of eigenvalues λ of L2, L3, L4 and L6 networks with parameter $W=3,6,12$ and ∞. Different colors represent networks with different binomial in-degree distributions, average connectivities chosen as $p=0.16$ (orange), 0.2 (purple), and 0.3 (blue). Each plot shows the combined spectra of $N_{\mathrm{samp}}=400$ networks. The corresponding spectra for RN, LCN1, LCN2 and NETMORPH networks are plotted for comparison. In the extreme ($W=\infty$) L2, L3, L4 and L6 networks one can observe the division of the eigenvalues to 2, 3, 4 and 6 distinct horns, respectively. The number of horns reflects the frequent occurrence of paths of the corresponding length in the graphs.
(EPS)

Figure S5 Statistics (mean and std) on the activity properties of different network classes. For the network classes that allow the use of the strength parameter W (WS1, WS2, FF, L2, L3, L4 and L6), only the statistics for the extreme networks ($W=\infty$) shown.
(EPS)

Figure S6 CC is most the determinant graph property in large networks with binomial in-degree, while MEig is the most relevant in large networks with power-law distributed in-degree. The upmost panel shows the burst count statistics for the extreme networks, see Fig. S5 for reference. The second and third panels show the prediction errors of burst count in large networks with binomial or power-law distributed in-degree, respectively, and the 2D-plots show the burst count w.r.t. dominant graph measure in mid-dense ($p=0.2$) networks. The corresponding data for small networks are shown in Figs. 6 and 9A–B. The lowest panel shows the prediction improvements in large networks, see Figs. 8 and 9D for comparison with small networks. In the repetition of the

predictions both the target and teaching data are resampled from the total number of 40 networks.
(EPS)

File S1 Supporting Information.
(PDF)

Author Contributions

Conceived and designed the experiments: TMM JA KR MLL. Performed the experiments: TMM. Analyzed the data: TMM JA KR MLL. Wrote the paper: TMM JA MLL.

References

1. Helmstaedter M, Briggman K, Denk W (2011) High-accuracy neurite reconstruction for highthroughput neuroanatomy. Nature Neuroscience 14: 1081–1088.
2. Kaiser M (2011) A tutorial in connectome analysis: Topological and spatial features of brain networks. Neuroimage 57: 892–907.
3. Wheeler B, Brewer G (2010) Designing neural networks in culture. Proceedings of the IEEE 98: 398–406.
4. Marconi E, Nieus T, Maccione A, Valente P, Simi A, et al. (2012) Emergent functional properties of neuronal networks with controlled topology. PLoS ONE 7: e34648.
5. Wang X, Buzsáki G (1996) Gamma oscillation by synaptic inhibition in a hippocampal interneuronal network model. Journal of Neuroscience 16: 6402–6413.
6. Golomb D, Hansel D (2000) The number of synaptic inputs and the synchrony of large, sparse neuronal networks. Neural Computation 12: 1095–1139.
7. Brunel N, Hakim V (1999) Fast global oscillations in networks of integrate-and-fire neurons with low firing rates. Neural Computation 11: 1621–1671.
8. Baltz T, Herzog A, Voigt T (2011) Slow oscillating population activity in developing cortical networks: Models and experimental results. Journal of Neurophysiology 106: 1500–1514.
9. Yoshimura Y, Dantzker J, Callaway E (2005) Excitatory cortical neurons form fine-scale functional networks. Nature 433: 868–873.
10. Song S, Sjöström P, Reigl M, Nelson S, Chklovskii D (2005) Highly nonrandom features of synaptic connectivity in local cortical circuits. PLoS Biology 3: e68.
11. Sporns O (2011) The non-random brain: Effciency, economy, and complex dynamics. Frontiers in Computational Neuroscience 5: 5.
12. Stetter O, Battaglia D, Soriano J, Geisel T (2012) Model-free reconstruction of excitatory neuronal connectivity from calcium imaging signals. PLoS Computational Biology 8: e1002653.
13. Aertsen A, Rotter S, Kumar A, Cardanobile S (2011). Structure, dynamics and function of brains: Exploring relations and constraints. Special issue in Frontiers in Computational Neuroscience, 2011.
14. Watts D, Strogatz S (1998) Collective dynamics of small-world networks. Nature 393: 440–442.
15. Lago-Fernández L, Huerta R, Corbacho F, Siguenza J (2000) Fast response and temporal coherent oscillations in small-world networks. Physical Review Letters 84: 2758–2761.
16. Netoff T, Clewley R, Arno S, Keck T, White J (2004) Epilepsy in small-world networks. Journal of Neuroscience 24: 8075–8083.
17. Percha B, Dzakpasu R, Żochowski M, Parent J (2005) Transition from local to global phase synchrony in small world neural network and its possible implications for epilepsy. Physical Review E 72: 031909.
18. Roxin A, Riecke H, Solla S (2004) Self-sustained activity in a small-world network of excitable neurons. Physical Review Letters 92: 198101.
19. Barabási A, Albert R (1999) Emergence of scaling in random networks. Science 286: 509–512.
20. Eguiluz V, Chialvo D, Cecchi G, Baliki M, Apkarian A (2005) Scale-free brain functional networks. Physical Review Letters 94: 18102.
21. Bollobás B, Borgs C, Chayes J, Riordan O (2003) Directed scale-free graphs. In: Proceedings of the Fourteenth Annual ACM-SIAM Symposium on Discrete Algorithms. Society for Industrial and Applied Mathematics, 132–139.
22. Zhao L, Bryce Beverlin I, Netoff T, Nykamp D (2011) Synchronization from second order network connectivity statistics. Frontiers in Computational Neuroscience 5: 28.
23. Roxin A (2011) The role of degree distribution in shaping the dynamics in networks of sparsely connected spiking neurons. Frontiers in Computational Neuroscience 5: 8.
24. Arenas A, Díaz-Guilera A, Kurths J, Moreno Y, Zhou C (2008) Synchronization in complex networks. Physics Reports 469: 93–153.
25. Wagenaar D, Pine J, Potter S (2006) An extremely rich repertoire of bursting patterns during the development of cortical cultures. BMC Neuroscience 7: 11–29.
26. Legrand J, Darbon P, Streit J (2004) Contributions of NMDA receptors to network recruitment and rhythm generation in spinal cord cultures. European Journal of Neuroscience 19: 521–532.
27. Vlachos I, Aertsen A, Kumar A (2012) Beyond statistical significance: Implications of network structure on neuronal activity. PLoS Computational Biology 8: e1002311.
28. Boccaletti S, Latora V, Moreno Y, Chavez M, Hwang DU (2006) Complex networks: Structure and dynamics. Physics Reports 424: 175–308.
29. Newman M (2003) The structure and function of complex networks. SIAM Review 45: 167–256.
30. MacCluer C (2000) The many proofs and applications of Perron's theorem. SIAM Review 42: 487–498.
31. Milo R, Shen-Orr S, Itzkovitz S, Kashtan N, Chklovskii D, et al. (2002) Network motifs: Simple building blocks of complex networks. Science 298: 824–827.
32. Shanahan M (2008) Dynamical complexity in small-world networks of spiking neurons. Physical Review E 78: 041924.
33. Morelli L, Abramson G, Kuperman M (2004) Associative memory on a small-world neural network. The European Physical Journal B - Condensed Matter and Complex Systems 38: 495–500.
34. Takahashi Y, Kori H, Masuda N (2009) Self-organization of feed-forward structure and entrainment in excitatory neural networks with spike-timing-dependent plasticity. Physical Review E 79: 051904.
35. Guo D, Li C (2009) Stochastic and coherence resonance in feed-forward-loop neuronal network motifs. Physical Review E 79: 051921.
36. Lorente de Nó R (1933) Vestibulo-ocular reex arc. Archives of Neurology & Psychiatry (Chicago) 30: 245–291.
37. Wang X (2001) Synaptic reverberation underlying mnemonic persistent activity. Trends in Neurosciences 24: 455–463.
38. Levy N, Horn D, Meilijson I, Ruppin E (2001) Distributed synchrony in a cell assembly of spiking neurons. Neural Networks 14: 815–824.
39. Kitano K, Câteau H, Fukai T (2002) Sustained activity with low firing rate in a recurrent network regulated by spike-timing-dependent plasticity. Neurocomputing 44: 473–478.
40. Crick F, Koch C (1998) Constraints on cortical and thalamic projections: The no-strong-loops hypothesis. Nature 391: 245–50.
41. Jia L, Sano M, Lai P, Chan C (2004) Connectivities and synchronous firing in cortical neuronal networks. Physical Review Letters 93: 88101.
42. Koene R, Tijms B, van Hees P, Postma F, de Ridder A, et al. (2009) NETMORPH: A framework for the stochastic generation of large scale neuronal networks with realistic neuron morphologies. Neuroinformatics 7: 195–210.
43. Aćimović J, Mäki-Marttunen T, Havela R, Teppola H, Linne ML (2011) Modeling of neuronal growth in vitro: Comparison of simulation tools NETMORPH and CX3D. EURASIP Journal on Bioinformatics and Systems Biology 2011: 616382.
44. Tsodyks M, Uziel A, Markram H (2000) Synchrony generation in recurrent networks with frequency-dependent synapses. Journal of Neuroscience 20: 1–5.
45. Golomb D, Shedmi A, Curtu R, Ermentrout G (2006) Persistent synchronized bursting activity in cortical tissues with low magnesium concentration: A modeling study. Journal of Neurophysiology 95: 1049–1067.
46. Golomb D, Amitai Y (1997) Propagating neuronal discharges in neocortical slices: Computational and experimental study. Journal of Neurophysiology 78: 1199–1211.
47. Van Vreeswijk C, Sompolinsky H (1996) Chaos in neuronal networks with balanced excitatory and inhibitory activity. Science 274: 1724–1726.
48. Benayoun M, Cowan J, Van Drongelen W, Wallace E (2010) Avalanches in a stochastic model of spiking neurons. PLoS Computational Biology 6: e1000846.
49. Keefer E, Gramowski A, Gross G (2001) NMDA receptor-dependent periodic oscillations in cultured spinal cord networks. Journal of Neurophysiology 86: 3030–3042.
50. Robinson H, Kawahara M, Jimbo Y, Torimitsu K, Kuroda Y, et al. (1993) Periodic synchronized bursting and intracellular calcium transients elicited by low magnesium in cultured cortical neurons. Journal of Neurophysiology 70: 1606–1616.
51. Watanabe S, Jimbo Y, Kamioka H, Kirino Y, Kawana A (1996) Development of low magnesiuminduced spontaneous synchronized bursting and gabaergic modulation in cultured rat neocortical neurons. Neuroscience Letters 210: 41–44.
52. Pérez T, Garcia G, Eguíuz V, Vicente R, Pipa G, et al. (2011) Effect of the topology and delayed interactions in neuronal networks synchronization. PLoS ONE 6: e19900.
53. Maheswaranathan N, Ferrari S, VanDongen A, Henriquez C (2012) Emergent bursting and synchrony in computer simulations of neuronal cultures. Frontiers in Computational Neuroscience 6: 15.
54. Gewaltig MO, Diesmann M (2007) NEST (neural simulation tool). Scholarpedia 2: 1430.
55. Chiappalone M, Bove M, Vato A, Tedesco M, Martinoia S (2006) Dissociated cortical networks show spontaneously correlated activity patterns during in vitro development. Brain research 1093: 41–53.
56. Gritsun T, Le Feber J, Stegenga J, Rutten W (2010) Network bursts in cortical cultures are best simulated using pacemaker neurons and adaptive synapses. Biological Cybernetics 102: 293–310.

57. Mäki-Marttunen T, Aćimović J, Nykter M, Kesseli J, Ruohonen K, et al. (2011) Information diversity in structure and dynamics of simulated neuronal networks. Frontiers in Computational Neuroscience 5: 26.
58. Han J, Kamber M (2006) Data mining: Concepts and techniques. Morgan Kaufmann.
59. Restrepo J, Ott E, Hunt B (2007) Approximating the largest eigenvalue of network adjacency matrices. Physical Review E 76: 056119.
60. Restrepo J, Ott E, Hunt B (2006) Emergence of synchronization in complex networks of interacting dynamical systems. Physica D: Nonlinear Phenomena 224: 114–122.
61. Masuda N, Aihara K (2004) Global and local synchrony of coupled neurons in small-world networks. Biological Cybernetics 90: 302–309.
62. Gómez-Gardeñes J, Moreno Y (2007) Synchronization of networks with variable local properties. International Journal of Bifurcation and Chaos 17: 2501–2507.
63. Kuramoto Y (1984) Chemical oscillations, waves, and turbulence. Springer-Verlag.
64. Kim B (2004) Performance of networks of artificial neurons: The role of clustering. Physical Review E 69: 045101.
65. Hilgetag C, Burns G, O'Neill M, Scannell J, Young M (2000) Anatomical connectivity defines the organization of clusters of cortical areas in the macaque and the cat. Philosophical Transactions of the Royal Society of London Series B: Biological Sciences 355: 91–110.
66. Shefi O, Golding I, Segev R, Ben-Jacob E, Ayali A (2002) Morphological characterization of in vitro neuronal networks. Physical Review E 66: 021905.
67. Garcia G, Lesne A, Hütt M, Hilgetag C (2012) Building blocks of self-sustained activity in a simple deterministic model of excitable neural networks. Frontiers in Computational Neuroscience 6: 50.
68. Gaiteri C, Rubin J (2011) The interaction of intrinsic dynamics and network topology in determining network burst synchrony. Frontiers in Computational Neuroscience 5: 10.
69. Meunier D, Lambiotte R, Bullmore E (2010) Modular and hierarchically modular organization of brain networks. Frontiers in Neuroscience 4: 200.
70. Kaiser M, Hilgetag C (2010) Optimal hierarchical modular topologies for producing limited sustained activation of neural networks. Frontiers in Neuroinformatics 4: 8.
71. Cardanobile S, Pernice V, Deger M, Rotter S (2012) Inferring general relations between network characteristics from specific network ensembles. PLoS ONE 7: e37911.
72. Lisman J (1997) Bursts as a unit of neural information: Making unreliable synapses reliable. Trends in Neurosciences 20: 38–43.
73. Chrobak J, Buzsáki G (1996) High-frequency oscillations in the output networks of the hippocampal–entorhinal axis of the freely behaving rat. Journal of Neuroscience 16: 3056–3066.
74. Marom S, Shahaf G (2002) Development, learning and memory in large random networks of cortical neurons: Lessons beyond anatomy. Quarterly Reviews of Biophysics 35: 63–87.
75. Beggs J, Plenz D (2003) Neuronal avalanches in neocortical circuits. Journal of Neuroscience 23: 11167–11177.
76. Chiu C, Weliky M (2001) Spontaneous activity in developing ferret visual cortex in vivo. Journal of Neuroscience 21: 8906–8914.
77. Buzsáki G, Lai-Wo SL, Vanderwolf C (1983) Cellular bases of hippocampal EEG in the behaving rat. Brain Research Reviews 6: 139–171.

Structure-Dynamics Relationships in Bursting Neuronal Networks Revealed using a Prediction Framework — Supporting information

S1 Supporting information on the methods

S1.1 Network generation algorithms

In this section we show the pseudo-codes for generating the networks with higher occurrence of feed-ferward loops (Algorithm S1) and the networks with higher occurrence of directed loops of length L (Algorithm S2). The MATLAB implementations for the algorithms are given in ModelDB entry 147117. Both algorithms are given the number of nodes N, the in-degree distribution $f_{\mathbf{ID}}$, and the strength parameter W as attributes. The algorithms start with an empty connectivity matrix $M \in \{0,1\}^{N\times N}$ that is updated every time a connection is made, and finally they output M.

Algorithm S1 Scheme for FF networks.

for node index $i \in \{1,\ldots,N\}$ **do**
  · Draw number of inputs $n_i \sim f_{ID}$.
  for input index $j \in \{1,\ldots,n_i\}$ **do**
    · Give weights a_k to all nodes $k \neq i$ that do not yet project to i s.t. $a_k = 1 + |\{l|M_{kl} \wedge M_{li}\}|$.
    · Compute the probability to draw node k as $P(k) = \frac{a_k^W}{\sum_k a_k^W}$.
    · Randomly pick k according to the probability mass distribution P and create a connection from k to i.
  end for
end for

In Algorithm S1 all inputs of a node i are set successively before setting the inputs of other nodes. The connectivity graph is updated every time a connection is made, and hence also the probability distribution $P(k)$ of possible inputs changes with every step. These probabilities are given on the basis of the number of disynaptic paths they have to the considered node i. That is, higher priority is given to nodes that project to the input nodes of node i. Conversely, in Algorithm S2 the edges are set in such a way that the node i for which the input is selected is changed in every iteration. By default, the node i is selected as the node that was last chosen as an input to another node. This promotes the creation of chains in the early stage of the iteration, which is crucial for the succesful creation of loops in the later stage. In case the node that was last chosen as input already has all its inputs set, the node to be updated is picked by random on the basis of the number of unset inputs of each node. This is also done in the first iteration of the algorithm.

In addition, the weighting scheme in the picking of inputs in Algorithm S2 is more diverse than that in Algorithm S1. The highest priority ($4+\epsilon_k$ points) is given to such nodes k that, if chosen as an input to i, would create a loop of length L from i to itself without shortcuts. The second highest priority (3) is given to such nodes that would not create a loop of length L, but would not either create a shorter loop from i to itself. The third highest priority ($2+\epsilon'_k$) is given to nodes that would create a loop of length L, but would simultaneously create shorter loops. The lowest priority (1) is given to the rest, i.e., the nodes that, if chosen as input to i, would create a loop shorter than L but would not add loops of length L. Further difference between nodes on the first or third priority level is given by $\epsilon_k = \frac{(M^{L-1})_{ik}}{\left(\frac{N-2}{L-2}\right)^{L-2}}$ and $\epsilon'_k = \frac{(M^{L-1})_{ik}}{(N-1)^{L-2}}$, both of which are proportional to the number of paths of length L that would be formed if the node k was chosen as input. To ensure that these extra terms are subsidiary to the named four

Algorithm S2 Scheme for loopy networks of length L.

for node index $i \in \{1, \ldots, N\}$ **do**
· Draw number of inputs $n_i \sim f_{\mathbf{ID}}$.
end for
while not all edges set **do**
if this is the very first edge or if the node that was last selected has already been set all its inputs **then**
· Give weights b_i to all nodes i such that b_i is the number of inputs of i that have not yet been set.
· Compute the probability to draw node i as $P(i) = \frac{a_k^W}{\sum_i a_i^W}$.
· Randomly pick i according to the probability mass distribution P
else
· Set i to be the node that was selected as the input node in the last round.
end if
For each $l < L$ and each possible input k, calculate $(M^l)_{ik}$, i.e., the number of existing paths of length l from node i to node k. Give weights a_k to all nodes that do not project to i as follows.
for node index $k \in \{1, \ldots, N\} \setminus \{i\} \setminus \{l | M_{li} = 1\}$ **do**
if $\forall l = 1, \ldots, L-2 : (M^l)_{ik} = 0$ **then**
if $(M^{L-1})_{ik} > 0$ **then**
· Set $a_k = 4 + \frac{(M^{L-1})_{ik}}{\left(\frac{N-2}{L-2}\right)^{L-2}}$
else
· Set $a_k = 3$
end if
else
if $(M^{L-1})_{ik} > 0$ **then**
· Set $a_k = 2 + \frac{(M^{L-1})_{ik}}{(N-1)^{L-2}}$
else
· Set $a_k = 1$
end if
end if
· Compute the probability to draw node k as $P(k) = \frac{a_k^W}{\sum_k a_k^W}$.
· Randomly pick k according to the probability mass distribution P and create a connection from k to i.
end for
end while

priority levels, we show that $\epsilon_k, \epsilon'_k \leq 1$ as follows.

Proof for ϵ_k:

It can be shown that $(M^{L-1})_{ik} \leq \left(\frac{N-2}{L-2}\right)^{L-2}$. As the choice of k as an input would not create loops shorter than L, the minimum path length from i to k has to be $L-1$. The maximum number of such paths is attained by (if possible) ordering the remaining $N-2$ nodes into $L-2$ layers, each of which contains a maximum of $\lceil (N-2)/(L-2) \rceil$ nodes. In this construction i projects to all nodes in the first layer, the nodes of the first layer nodes project to all nodes in the second layer, and continuing until the last layer, where all nodes project to k. The maximum number of paths of length $L-1$ from i to k is then $(\frac{N-2}{L-2})^{L-2}$.

Proof for ϵ'_k:

We can show by induction that $\forall k : (M^t)_{ik} \leq (N-1)^{t-1}$ in any graph of interest. Since no graph can have more paths than the fully connected graph, that is, a graph M where $M_{ij} = 1 \; \forall j \neq i$ and $M_{ii} = 0 \; \forall i$, it suffices to show the result for that particular graph.

1. The statement is true for $t = 1$, as the number of paths of length 1 from i to any node are either 0 or 1.

2. Suppose the statement is true for $t = t_0 - 1$. Then, the number of paths of length t_0 from i to any k is $\sum_{j=1}^{N} (M^{t_0-1})_{ij} M_{jk} = \sum_{j=1,\ j\neq k}^{N} (M^{t_0-1})_{ij} \leq (N-1)(N-1)^{t_0-1} = (N-1)^{t_0}$. Hence, the statement is true for $t = t_0$.

Thus, $\forall k : \epsilon'_k \leq 1$ in any graph M.

In both algorithms the limit case $W = \infty$ is allowed. In this case, after calculating the weights a_k, the probability mass is divided equally between the nodes that have the exact maximum weight $\max a_k$, and other nodes are given zero probability mass. This can be shown in a simple limit value analysis as follows. Consider the weight for node $k \neq i$.

1. Suppose $\exists j$ such that $a_k < a_j$. Then $\frac{a_k^W}{\sum_{l\neq i} a_l^W} \leq \frac{a_k^W}{a_j^W} = \left(\frac{a_k}{a_j}\right)^W \to 0$. Hence, $\frac{a_k^W}{\sum_{l\neq i} a_l^W} \to 0$.

2. Suppose $a_k = \max_{l\neq i} a_l$. Denote $I = \{l \neq i | a_l = a_k\}$, and denote the size of the set by $n = |I| < N$. If all nodes have the maximum weight a_k, i.e., $n = N-1$, we have $\frac{a_k^W}{\sum_{l\neq i} a_l^W} = \frac{1}{N-1}$, and hence the statement is true. Otherwise, let us consider the remaining nonempty set $J = \{1, \ldots, N\} \setminus \{i\} \setminus I$. Let us choose $j = \arg\max_{l\in J} a_l$. Thus, we have $\frac{a_k^W}{\sum_{l\neq i} a_l^W} = \frac{a_k^W}{\sum_{l\in I} a_l^W + \sum_{l\in J} a_l^W} \geq \frac{a_k^W}{n a_k^W + (N-1-n) a_j^W} = \frac{1}{n + (N-1-n)\left(\frac{a_j}{a_k}\right)^W} \to \frac{1}{n}$. On the other hand we have $\frac{a_k^W}{\sum_{l\neq i} a_l^W} \leq \frac{a_k^W}{n a_k^W} = \frac{1}{n}$. Hence, we have $\frac{a_k^W}{\sum_{l\neq i} a_l^W} \to \frac{1}{n}$.

S1.2 Truncated power-law distribution

In this work, both binomial and power-law distributions are used for the in-degree of the networks. The power-law distribution is truncated as follows:

$$f_{\mathbf{ID}}^{\mathrm{POW}}(n|N,\alpha,p) = \begin{cases} 1 - \sum_{k=n_{\min}}^{N-1} a k^{\alpha}, & n = n_{\min} \\ a n^{\alpha}, & n_{\min} < n < N \\ 0, & \text{otherwise} \end{cases}, \tag{S1}$$

where $n_{\min} \in \mathbb{N}$ and $a \in [0, \infty)$ are chosen such that $p = \frac{1}{N-1} \mathrm{E}_{f_{\mathbf{ID}}^{\mathrm{POW}}}[\mathbf{n}]$, and $n_{\min}$ is minimized with the restriction that $1 - \sum_{k=n_{\min}}^{N-1} a k^{\alpha}$ be non-negative. The slope of the power-law distribution is chosen

$\alpha = -2$ throughout this work, based on the data from functional connectivity graphs [S1]. In the following we show that such a and $n_{\min}$ exist for every $N \in \mathbb{N}$, $\alpha \in \mathbb{R}$, and $p \in [0, 1]$.

Let $N \in \mathbb{N}$ be the number of nodes in the network, $p \in [0, 1]$ the desired connection probability, and $\alpha \in \mathbb{R}$ the slope of the power-law distribution. Let $N > 1$ — otherwise, the connection probability is undefined. Let us show that there exist $a \in [0, \infty)$ and $n_{\min} \in \mathbb{N}$ such that the function

$$g(n|N, \alpha, a, n_{\min}) = \begin{cases} 1 - \sum_{k=n_{\min}+1}^{N-1} ak^{\alpha}, & n = n_{\min} \\ an^{\alpha}, & n_{\min} < n \leq N-1 \\ 0, & \text{otherwise} \end{cases}, \tag{S2}$$

is a probability density function on $\Omega = \{0, 1, \ldots, N-1\}$ and satisfies

$$\mathrm{E}_g[\mathbf{n}] = p(N-1). \tag{S3}$$

First, we find that $g(\cdot|\alpha, a, n_{\min})$ is a well-defined probability density function if and only if $n_{\min} = N-1$, or $n_{\min} < N-1$ and $a \in [0, 1/\sum_{k=n_{\min}+1}^{N-1} k^{\alpha}]$. Let us now study the Equation S3.

- If $p = 1$, we find that $n_{\min} = N-1$ satisfies Equation S3 for any a.
- If $p < 1$, we find that $n_{\min} = N-1$ cannot satisfy the Equation S3 for any a. Consider now an arbitrary $n_{\min} \in \{0, 1, \ldots, N-2\}$. The expectation value

  $$\mathrm{E}_g[\mathbf{n}] = (1 - \sum_{k=n_{\min}+1}^{N-1} ak^{\alpha})n_{\min} + \sum_{k=n_{\min}+1}^{N-1} ak^{\alpha+1} = a\left(\sum_{k=n_{\min}+1}^{N-1} k^{\alpha+1} - n_{\min}\sum_{k=n_{\min}+1}^{N-1} k^{\alpha}\right) + n_{\min}$$

  is a monotonically increasing function w.r.t. a. For $a = 0$ we have $\mathrm{E}_g[\mathbf{n}] = n_{\min}$, as for other extreme $a = 1/\sum_{k=n_{\min}+1}^{N-1} k^{\alpha}$ we have

  $$\mathrm{E}_g[\mathbf{n}] = \frac{\sum_{k=n_{\min}+1}^{N-1} k^{\alpha+1}}{\sum_{k=n_{\min}+1}^{N-1} k^{\alpha}}. \tag{S4}$$

  As in the summation terms the index $k \geq n_{\min} + 1$ and k^{α} is non-negative, we have

  $$\sum_{k=n_{\min}+1}^{N-1} k^{\alpha} = \sum_{k=n_{\min}+1}^{N-1} k^{\alpha} \cdot 1 \leq \sum_{k=n_{\min}+1}^{N-1} k^{\alpha}(k - n_{\min}) = \sum_{k=n_{\min}+1}^{N-1} k^{\alpha+1} - n_{\min}\sum_{k=n_{\min}+1}^{N-1} k^{\alpha},$$

  which gives us

  $$\sum_{k=n_{\min}+1}^{N-1} k^{\alpha+1} \geq (n_{\min}+1)\sum_{k=n_{\min}+1}^{N-1} k^{\alpha}$$

  and further

  $$\frac{\sum_{k=n_{\min}+1}^{N-1} k^{\alpha+1}}{\sum_{k=n_{\min}+1}^{N-1} k^{\alpha}} \geq n_{\min} + 1.$$

  Hence, the range of expectation values $\mathrm{E}_g[\mathbf{n}]$ covers at least the range $[n_{\min}, n_{\min}+1]$. Hence, there is at least one $n_{\min}$ for which a can be chosen (the choice is unique because of the strict monotonicity) such that Equation S3 is satisfied and $g(\cdot|N, \alpha, a, n_{\min})$ is a probability density function. Since there are a finite number of viable values of $n_{\min}$, we may choose the smallest one and the corresponding a. □

Table S1. Synaptic weights η for different simulation settings, optimized to make BC in moderately connected networks (RN, $p = 0.2$, binomial in-degree) 10bursts/min. The same synaptic weights are used in simulation settings with different choices of in-degree distribution.

	HH, $N = 100$	LIF, $N = 100$	LIF, $N = 900$
E	0.144	14.52	2.81
EI	0.177	17.21	

S1.3 The LIF and HH models

The parameters for LIF model are taken from [S2] with the following exceptions. In [S2] the background current I_b has differing values for every neuron, making some neurons in the network intrinsically active pacemakers and others excitable only with positive input. In this work we set all the neurons of a given type (excitatory, inhibitory) to the same mean level by their spontaneous activity. The noise level was chosen such that the neurons express spontaneous spikes with a rate of ≈ 10 spikes/min when no inputs are given. The lack of pacemakers prevents the network from having a prominent heterogeneousity that is not due to the structure of the network. The synaptic weights η are tuned such that a RN with a connection probability $p = 0.2$ produces approximately 10 bursts/min, see Table S1 for exact values. The values of the other synaptic parameters (U, τ_{rec}, τ_{facil}, τ_{I}) are set as the mean value given in [S2] without perturbation. The simulations are carried out in PyNEST with time step $dt = 0.2$ms.

The HH model is taken from the Appendix in [S3] with some retuning for our purposes. Here too we apply random current $\mathbf{I}_b(t)$ to the membrane potential such that the neurons fire spontaneously with a moderate rate (8.1 spikes/min for excitatory neurons and 137 spikes/min for inhibitory neurons; these values fit fairly well to experimental data [S4]). Euler-Maruyama method with time step $dt = 0.0025$ms is used for the integration. The Kdr conductance for excitatory neurons is set $g_{\text{Kdr}} = 6\text{mS/cm}^2$ instead of the 3mS/cm^2 stated in [S3] — the value 6mS/cm^2 (given in a ModelDB entry corresponding to their article) was found to give the correct shape of action potentials.

The proportions of the synaptic currents are similar to [S3] with the exception that also the inhibitory–inhibitory currents are considered. The dynamics for AMPA currents are modeled according to the Appendix of [S5]. The model for NMDA currents is a combination with both the synaptic depression from [S5] and the dynamics of slow rise-time from [S3]. The values of the parameters, when different, are taken from the Appendix of [S3]. The synaptic depression affects both AMPA and NMDA currents through the amount of glutamate resources $T_{\text{Glu}} \in [0, 1]$. In the following, all the model equations and parameters are listed.

The membrane potential of a LIF neuron obeys

$$C_m \frac{dV_m}{dt} = -\frac{V_m}{R_m} + I_{\text{syn}} + \mathbf{I}_b,$$

with C_m=30pF and R_m=1GΩ. The threshold potential is 15mV, the reset potential is 13.5mV, and the refractory period is 3ms for excitatory neurons and 2ms for inhibitory neurons. The synaptic current I_{syn} to the neuron j is the sum of the currents from the presynaptic cells:

$$I^j_{\text{syn}} = \begin{cases} \eta(1.0\text{pA} \cdot \sum_{i=1}^{N_E} M_{ij} y_{ij} - 3.0\text{pA} \cdot \sum_{i=N_E+1}^{N} M_{ij} y_{ij}), \text{if } j \text{ excitatory} \\ \eta(4.0\text{pA} \cdot \sum_{i=1}^{N_E} M_{ij} y_{ij} - 4.0\text{pA} \cdot \sum_{i=N_E+1}^{N} M_{ij} y_{ij}), \text{if } j \text{ inhibitory} \end{cases},$$

where the neurons are assumed to be ordered such that the excitatory population consists of neurons with indices $1, \ldots, N_E$ and the inhibitory population of neurons $N_E+1, \ldots, N_E+N_I$. Thus, the synaptic

currents are functions of the dynamic synaptic variables y_{ij}, each of which is determined by the following set of equations:

$$\begin{aligned}
\frac{du}{dt} &= -\frac{u}{\tau_{\text{facil}}} + U(1-u)\delta_{t_{\text{sp}}}(t) \\
\frac{dx}{dt} &= \frac{z}{\tau_{\text{rec}}} - ux\delta_{t_{\text{sp}}}(t) \\
\frac{dy}{dt} &= -\frac{y}{\tau_I} + ux\delta_{t_{\text{sp}}}(t) \\
\frac{dz}{dt} &= \frac{y}{\tau_I} - \frac{z}{\tau_{\text{rec}}},
\end{aligned} \tag{S5}$$

where t_{sp} is the time instant of a presynaptic spike. The parameters are as follows: $U(E \to E) = U(I \to E) = 0.5$, $U(E \to I) = U(I \to I) = 0.04$, $\tau_{\text{rec}}(E \to E) = \tau_{\text{rec}}(I \to E) = 800\text{ms}$, $\tau_{\text{rec}}(E \to I) = \tau_{\text{rec}}(I \to I) = 100\text{ms}$, $\tau_I(E \to E) = \tau_I(I \to E) = \tau_I(E \to I) = \tau_I(I \to I) = 3\text{ms}$, $\tau_{\text{facil}}(E \to E) = \tau_{\text{facil}}(I \to E) = 0\text{ms}$, $\tau_{\text{facil}}(E \to I) = \tau_{\text{facil}}(I \to I) = 1000\text{ms}$. The background current $\mathbf{I}_b$, chosen independently for each neuron, is a stepwise constant random (Gaussian) current with mean 12pA and standard deviation 7.3pA. The value of the background current is re-initialized every 1ms.

The time course of an excitatory HH neuron is determined by

$$C_m \frac{dV_m}{dt} = -I_{\text{Na}} - I_{\text{NaP}} - I_{\text{Kdr}} - I_{\text{K-slow}} - I_{\text{L}} - I_{\text{AMPA}}^{\text{E}\to\text{E}} - I_{\text{NMDA}}^{\text{E}\to\text{E}} - I_{\text{GABA}} + \mathbf{I}_b,$$

where $C_m = 1\mu\text{F/cm}^2$. The sodium currents I_{Na} obey the following equations:

$$\begin{aligned}
I_{\text{Na}}(V_m, h) &= g_{\text{Na}} m_\infty^3(V_m) h (V_m - V_{\text{Na}}) \\
\frac{dh}{dt} &= (h_\infty(V_m) - h)/\tau_h(V_m) \\
m_\infty(V) &= (1 + \exp(-(V - \theta_m)/\sigma_m))^{-1} \\
h_\infty(V) &= (1 + \exp(-(V - \theta_h)/\sigma_h))^{-1} \\
\tau_h(V) &= 0.1 + 0.75 \cdot (1 + \exp(-(V - \theta_{th})/\sigma_{th}))^{-1} \\
I_{\text{NaP}}(V_m) &= g_{\text{NaP}} p_\infty(V_m)(V_m - V_{\text{Na}}) \\
p_\infty(V) &= (1 + \exp(-(V - \theta_p)/\sigma_p))^{-1},
\end{aligned}$$

where $g_{\text{Na}} = 35\text{mS/cm}^2$, $V_{\text{Na}} = 55\text{mV}$, $\theta_m = -30\text{mV}$, $\sigma_m = 9.5\text{mV}$, $\theta_h = -45\text{mV}$, $\sigma_h = -7\text{mV}$, $\theta_{th} = -40.5\text{mV}$, $\sigma_{th} = -6\text{mV}$, $g_{\text{NaP}} = 0.2\text{mS/cm}^2$, $\theta_p = -47\text{mV}$, and $\sigma_p = 3\text{mV}$. The potassium currents are described by the following equations:

$$\begin{aligned}
I_{\text{Kdr}}(V_m, n) &= g_{\text{Kdr}} n^4 (V_m - V_{\text{K}}) \\
\frac{dn}{dt} &= (n_\infty(V_m) - n)/\tau_n(V_m) \\
n_\infty(V) &= (1 + \exp(-(V - \theta_n)/\sigma_n))^{-1} \\
\tau_n(V) &= 0.1 + 0.5 \cdot (1 + \exp(-(V - \theta_{tn})/\sigma_{tn}))^{-1} \\
I_{\text{K-slow}}(V_m, z) &= g_{\text{K-slow}} z (V_m - V_{\text{K}}) \\
\frac{dz}{dt} &= (z_\infty(V_m) - z)/\tau_z \\
z_\infty(V) &= (1 + \exp(-(V - \theta_z)/\sigma_z))^{-1},
\end{aligned}$$

where $g_{\rm Kdr} = 6{\rm mS/cm}^2$, $V_{\rm K} = -90{\rm mV}$, $\theta_n = -33{\rm mV}$, $\sigma_n = 10{\rm mV}$, $\theta_{tn} = -27{\rm mV}$, $\sigma_{tn} = -15{\rm mV}$, $g_{\rm K-slow} = 1.8{\rm mS/cm}^2$, $\theta_z = -39{\rm mV}$, $\sigma_z = 5{\rm mV}$, and $\tau_z = 75{\rm ms}$. The leak current obeys

$$I_{\rm L}(V_m) = g_{\rm L}(V_m - V_{\rm L}),$$

where $g_{\rm L} = 0.05{\rm mS/cm}^2$ and $V_{\rm L} = -70{\rm mV}$.

Inhibitory neurons in networks of HH neurons are described by the Wang-Buzsaki model as follows:

$$C_m \frac{dV_m}{dt} = -I_{\rm Na}^{\rm I} - I_{\rm Kdr}^{\rm I} - I_{\rm L}^{\rm I} - I_{\rm AMPA}^{\rm E\to I} - I_{\rm NMDA}^{\rm E\to I} - I_{\rm GABA} + \mathbf{I}_b.$$

The currents are described as follows:

$$\begin{aligned}
I_{\rm Na}^{\rm I}(V_m, h) &= g_{\rm Na}^{\rm I}(m_\infty^{\rm I}(V_m))^3 h(V_m - V_{\rm Na}^{\rm I}) \\
\frac{dh}{dt} &= \alpha_h(V_m)(1-h) - \beta_h(V_m)h \\
m_\infty^{\rm I}(V) &= \alpha_m(V)/(\alpha_m(V) + \beta_m(V)) \\
\alpha_h(V) &= 0.35\exp(-(V+58)/20) \\
\beta_h(V) &= 5/(1+\exp(-(V+28)/10)) \\
\alpha_m(V) &= 0.5(V+35)/(1-\exp(-(V+35)/10)) \\
\beta_m(V) &= 20\exp(-(V+60)/18) \\
I_{\rm Kdr}^{\rm I}(V_m, n) &= g_{\rm Kdr}^{\rm I} n^4 (V_m - V_{\rm K}^{\rm I}) \\
\frac{dn}{dt} &= \alpha_n(V_m)(1-n) - \beta_n(V_m)n \\
\alpha_n(V) &= 0.05(V+34)/(1-\exp(-(V+34)/10)) \\
\beta_n(V) &= 0.625\exp(-(V+44)/80) \\
I_{\rm L}^{\rm I}(V_m) &= g_{\rm L}^{\rm I}(V_m - V_{\rm L}^{\rm I}),
\end{aligned}$$

with $g_{\rm Na}^{\rm I} = 35{\rm mS/cm}^2$, $V_{\rm Na}^{\rm I} = 55{\rm mV}$, $g_{\rm Kdr}^{\rm I} = 9{\rm mS/cm}^2$, $V_{\rm K}^{\rm I} = -90{\rm mV}$, $g_{\rm L}^{\rm I} = 0.1{\rm mS/cm}^2$, and $V_{\rm L}^{\rm I} = -65{\rm mV}$.

The synaptic currents in the HH model are the AMPA and NMDA currents elicited by excitatory neurons and the GABA currents elicited by the inhibitory neurons. The AMPA and NMDA currents express synaptic depression [S5]. For an excitatory neuron ($j \le N_e$), they can be described as follows:

$$\begin{aligned}
I_{{\rm AMPA},j}^{\rm E\to E}(V_m, \{s_{\rm AMPA}\}) &= g_{\rm AMPA}^{\rm E\to E}(V_m - V_{\rm Glu})\eta \sum_{i=1}^{N_E} M_{ij} s_{{\rm AMPA},i} \\
\frac{ds_{{\rm AMPA},i}}{dt} &= k_{fP} T_{{\rm Glu},i} s_\infty(V_i)(1 - s_{{\rm AMPA},i}) - s_{{\rm AMPA},i}/\tau_{\rm AMPA} \\
\frac{dT_{{\rm Glu},i}}{dt} &= -k_t s_\infty(V_i) T_{{\rm Glu},i} + k_v(1 - T_{{\rm Glu},i}) \\
s_\infty(V) &= (1+\exp(-(V-\theta_s)/\sigma_s))^{-1}, \\
I_{{\rm NMDA},j}^{\rm E\to E}(V_m, \{s_{\rm NMDA}\}) &= g_{\rm NMDA}^{\rm E\to E} f_{\rm NMDA}(V_m)(V_m - V_{\rm Glu})\eta \sum_{i=1}^{N_E} M_{ij} s_{{\rm NMDA},i} \\
\frac{{\rm d}x_{{\rm NMDA},i}}{{\rm d}t} &= k_{xN} s_\infty(V_i)(1 - x_{{\rm NMDA},i}) - (1 - s_\infty(V_i)) x_{{\rm NMDA},i}/\tilde{\tau}_{\rm NMDA} \\
\frac{{\rm d}s_{{\rm NMDA},i}}{{\rm d}t} &= k_{fN} T_{{\rm Glu},i} x_{{\rm NMDA},i}(1 - s_{{\rm NMDA},i}) - s_{{\rm NMDA},i}/\tau_{\rm NMDA} \\
f_{\rm NMDA}(V) &= (1+\exp(-(V-\theta_{\rm NMDA})/\sigma_{\rm NMDA}))^{-1},
\end{aligned}$$

where $\theta_s = -20\text{mV}$, $\sigma_s = 2\text{mV}$, $k_{fP} = 1\text{ms}^{-1}$, $\tau_{\text{AMPA}} = 5\text{ms}$, $g^{\text{E}\to\text{E}}_{\text{AMPA}} = 0.08\text{mS/cm}^2$, $V_{\text{Glu}} = 0\text{mV}$, $k_t = 1\text{ms}^{-1}$, $k_v = 0.001\text{ms}^{-1}$, $k_{xN} = 1\text{ms}^{-1}$, $\tilde{\tau}_{\text{NMDA}} = 14.3\text{ms}$, $k_{fN} = 1\text{ms}^{-1}$, $\tau_{\text{NMDA}} = 100\text{ms}$, $g^{\text{E}\to\text{E}}_{\text{NMDA}} = 0.07\text{mS/cm}^2$, and $\sigma_{\text{NMDA}} = 10\text{mV}$. The value of θ_{NMDA} is dependent on the magnesium concentration as follows: $\theta_{\text{NMDA}} = 10.5\text{mV} \cdot \ln([\text{Mg}^{2+}]_o/38.3\text{mM})$. Here, the magnesium concentration of $[\text{Mg}^{2+}]_o = 0.7\text{mM}$ is used, which is a typical value in cortical cultures. The values of synaptic weights η are given in Table S1.

The AMPA and NMDA currents to inhibitory neurons ($j > N_E$) differ from the corresponding currents to excitatory neurons only through the synaptic conductances:

$$\begin{aligned} I^{\text{E}\to\text{I}}_{\text{AMPA},j}(V_m, \{s_{\text{AMPA}}\}) &= g^{\text{E}\to\text{I}}_{\text{AMPA}}(V_m - V_{\text{Glu}})\eta \sum_{i=1}^{N_E} M_{ij} s_{\text{AMPA},i} \\ I^{\text{E}\to\text{I}}_{\text{NMDA},j}(V_m, \{s_{\text{NMDA}}\}) &= g^{\text{E}\to\text{I}}_{\text{NMDA}} f_{\text{NMDA}}(V_m)(V_m - V_{\text{Glu}})\eta \sum_{i=1}^{N_E} M_{ij} s_{\text{NMDA},i} \end{aligned} \tag{S6}$$

where $g^{\text{E}\to\text{I}}_{\text{AMPA}} = 0.2\text{mS/cm}^2$ and $g^{\text{E}\to\text{I}}_{\text{NMDA}} = 0.05\text{mS/cm}^2$. The GABA currents to both excitatory and inhibitory neurons are described as follows:

$$\begin{aligned} I_{\text{GABA},j}(V_m, \{s_{\text{GABA}}\}) &= g_{\text{GABA}}(V_m - V_{\text{GABA}})\eta \sum_{i=N_E+1}^{N} M_{ij} s_{\text{GABA},i} \\ \frac{ds_{\text{GABA},i}}{dt} &= k_{fA} s_\infty(V_i)(1 - s_{\text{GABA},i}) - s_{\text{GABA},i}/\tau_{\text{GABA}}, \end{aligned}$$

where $k_{fA} = 1\text{ms}^{-1}$, $\tau_{\text{GABA}} = 10\text{ms}$, $g_{\text{GABA}} = 0.05\text{mS/cm}^2$, and $V_{\text{GABA}} = -70\text{mV}$. The background current is a zero-mean Brownian white noise term, described as $\mathbf{I}_b(t) = 0.9\mu\text{A/cm}^2 \cdot \mathbf{W}_t$, where $\mathbf{W}_t$ is the independent Wiener process (the "time derivative" of dimensionless Brownian motion).

The initial state of the system is chosen such that all neurons are at or near rest. In LIF model this is done by setting all membrane potentials to the reset value, and in HH model the membrane potential and gating variable values are given by steady states of unconnected, noiseless neurons. In the beginning all synaptic resources are set to the maximum value ($x = 1$ and $y = z = 0$ in LIF model, and $T_{\text{Glu}} = 1$ in HH model).

S2 Supporting results on network structure

S2.1 NETMORPH networks have roughly binomial in-degree distribution

Fig. S1 shows that the in-degree distribution in 2-dimensional NETMORPH networks with continuous boundaries is fairly well approximated by binomial distribution. This is opposite to 2-dimensional NETMORPH networks without the boundary continuity that are characterised by broader in-degree distribution, as we have shown in [S6]. Hence, we consider NM networks comparable to networks with binomial in-degree.

S2.2 FF networks have high number of feed-forward loops but relatively low clustering coefficient

Fig. S2 shows the clustering coefficient of FF networks as a function of parameter W, together with the RN, LCN1, LCN2, and NM networks. One can observe the rising of the CC in FF networks with the parameter W, which yet remains lower than the CC in locally connected networks LCN1 and LCN2. Fig.

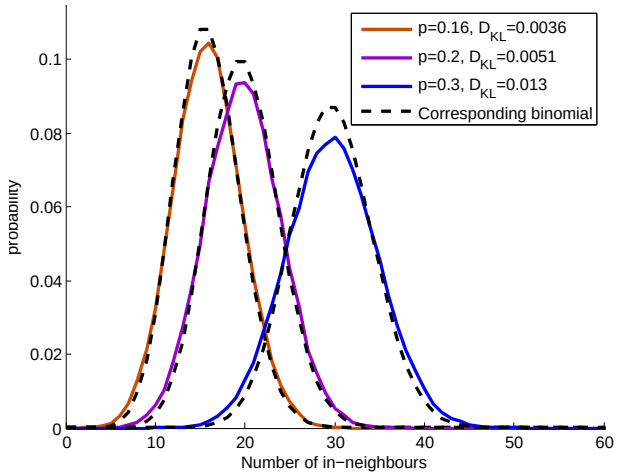

Figure S1. In-degree distributions for NM networks with connection probabilities $p = 0.16$ (orange), 0.2 (purple), and 0.3 (blue). The dashed lines show the binomial PDFs with these connection probabilities, and the legend shows the KL-divergence of the NM in-degree distributions from these binomial distributions. The obtained values of D_{KL} are considerably small — the corresponding values between NM in-degree distributions and the best-fit triangular distribution are 0.22 ($p = 0.16$), 0.24 ($p = 0.2$), and 0.24 ($p = 0.3$), and further, the corresponding D_{KL} values are 1.8, 1.7 and 1.6 between NM distributions and uniform distribution. The NM in-degree distributions are constructed from a pool of 400 network realizations.

S3 in turn shows the number of FF-motifs in FF networks with varying parameter W, and for comparison the corresponding number in RN, LCN1, and NM networks. The number of FF-motifs is calculated as the number of such ordered triples, whose edges form the functional form of motif 5 (see Fig. 1), i.e. $|\{(i,j,k) \in \{1,...,N\}^3 | M_{ij} \wedge M_{jk} \wedge M_{ik}\}|$. The amount of FF-motifs in FF networks is increased with the increase of parameter W. The abundance of FF-motifs in LCN1 networks is explained by the frequent occurrence of motif 13, each of which in itself contains six permutations of the FF-motif. The extreme FF networks acquire a comparable number of FF-motifs, yet they preserve the relatively low degree of clustering, as seen in Fig. S2.

S2.3 Loopy networks express loops in their eigenvalue spectra

One way to illustrate the occurrences of loops in a graph is to plot the eigenvalue spectrum of the connectivity matrix into the complex plane. Consider as an example a perfect ring graph M, consisting of N nodes, where each node has exactly one input and one output, and where the nodes form a traversable ring. The Nth power of the underlying connectivity matrix is an identity matrix, in which all eigenvalues are 1. By basic linear algebra, these eigenvalues must be the Nth powers of the eigenvalues of M, and hence the eigenvalues of M are evenly distributed on the unit circle in $\mathbb{C}$. Fig. S4 shows the eigenvalue spectra of L2, L3, L4 and L6 networks with different parameters W, and for comparison the eigenvalue spectra of RN, LCN and NM networks. In the extreme cases $W = \infty$ the division of the eigenvalues to 2, 3, 4 or 6 horns is evident. This is fairly non-trivial in the case of denser L6 networks: Since the connection probability is as high as 0.2 or 0.3, it would be reasonable that the abundance of connections break the loopy structure of the network. This abundance does bring up malformations in the star-shaped spectra in the case of $p = 0.3$, but not notably in the case of $p = 0.2$.

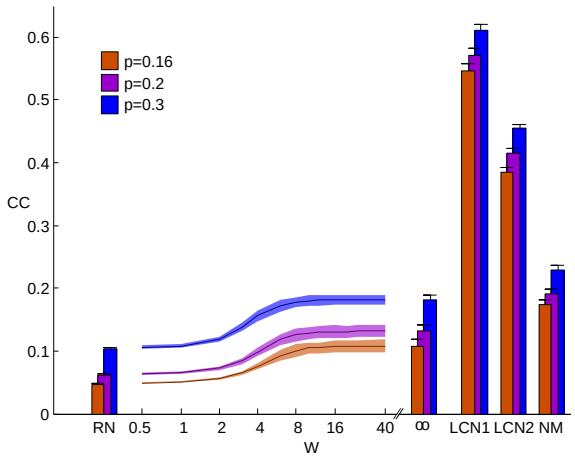

Figure S2. CC in FF networks as a function of parameter W, and, for comparison, the respective values of RN, LCN1, LCN2 and NETM networks. By the increase of W the CC of FF networks approaches that of the extreme FF networks, yet remains lower than that in LCN1, LCN2 or even NM. Different colors represent networks with different (binomial) in-degree distributions. The solid line shows the average over $N_{\text{samp}} = 400$ trials, and the shaded area the standard deviation.

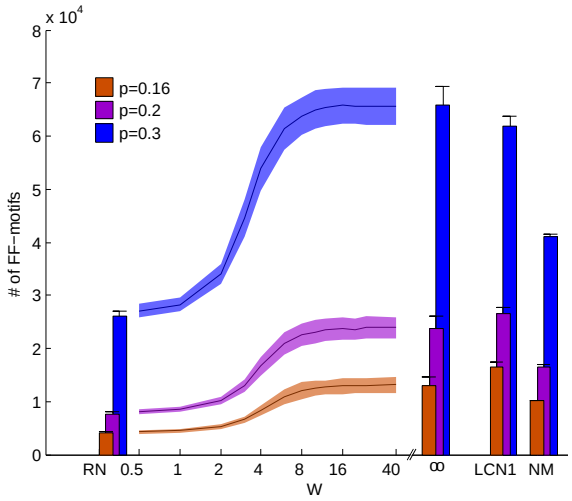

Figure S3. Number (mean and std, $N_{\text{samp}} = 400$) of FF-motifs in FF networks as a function of parameter W, and, for comparison, the respective values of RN, LCN1 and NETM networks. The in-degree distribution of FF, RN and LCN1 networks is chosen as binomial with the shown average connectivities.

S2.4 The relation of mean node-betweenness and mean shortest path length

The mean value of node-betweenness correlates highly with the mean path length. In this section we will analytically derive the connection of these two quantities. The mean betweenness value is calculated as

$$\mathrm{NB} = \frac{1}{N}\sum_{i=1}^{N} \mathrm{NB}_i = \frac{1}{N}\sum_{i=1}^{N} \sum_{\substack{j=1 \\ j\neq i}}^{N} \sum_{\substack{k=1 \\ i\neq k\neq j \\ \mathrm{PL}_{jk}<\infty}}^{N} \frac{s_{jk}^{(i)}}{s_{jk}^{(\mathrm{tot})}}. \tag{S7}$$

The term $s_{jk}^{(i)}$ is the number of such shortest paths from j to k where the node i lies on, and $s_{jk}^{(\mathrm{tot})}$ represents the total number of shortest paths from j to k. The nodes k where no path from j to k exists are excluded from the summation, and hence the quantity is well-defined for any graph.

Let us denote the length of shortest path from j to k by L_{jk}. A necessary and sufficient condition for i lying on the shortest path from j to k is that there be a path of length $l \in \{1, \ldots, L_{jk}-1\}$ from j to i and a path of length $L_{jk}-l$ from i to k. The total number of such paths can be counted as the product of the number of paths of length l from j to i and the number of paths of length $L_{jk}-l$ from i to k. This can be expressed using the elements of the lth and $(L_{jk}-l)$th exponent of the connectivity matrix as $(M^l)_{ji} \cdot (M^{L_{jk}-l})_{ik}$. Hence, the total number of shortest paths from j through i to k is calculated by

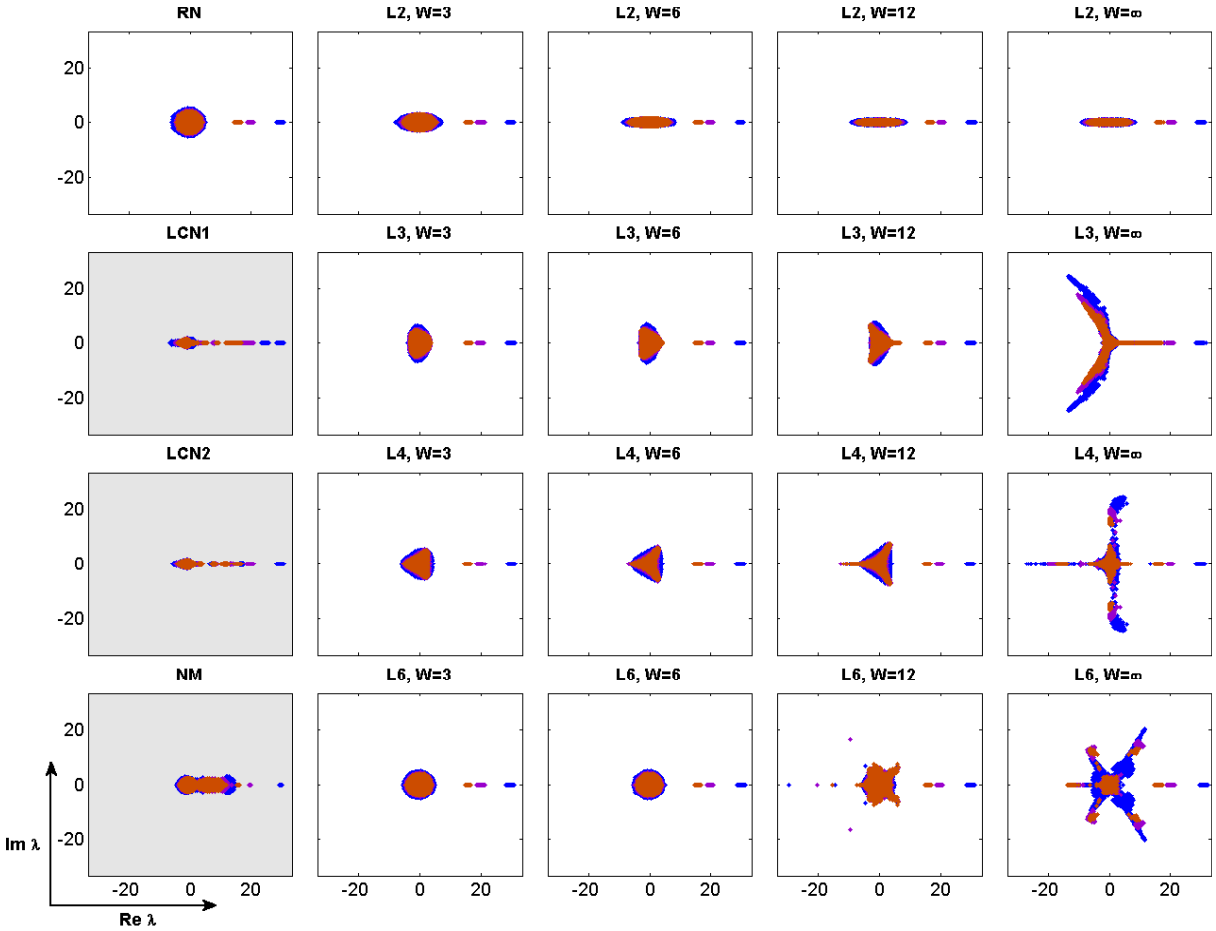

Figure S4. Distribution of eigenvalues λ of L2, L3, L4 and L6 networks with parameter $W = 3, 6, 12$ and ∞. Different colors represent networks with different binomial in-degree distributions, average connectivities chosen as $p = 0.16$ (orange), 0.2 (purple), and 0.3 (blue). Each plot shows the combined spectra of $N_{\text{samp}} = 400$ networks. The corresponding spectra for RN, LCN1, LCN2 and NETMORPH networks are plotted for comparison. In the extreme ($W = \infty$) L2, L3, L4 and L6 networks one can observe the division of the eigenvalues to 2, 3, 4 and 6 distinct horns, respectively. The number of horns reflects the frequent occurrence of paths of the corresponding length in the graphs.

summing this over all possible lengths l as

$$s_{jk}^{(i)} = \sum_{l=1}^{L_{jk}-1} (M^l)_{ji} \cdot (M^{L_{jk}-l})_{ik},$$

while the total number of shortest paths is simply

$$s_{jk}^{(\text{tot})} = (M^{L_{jk}})_{jk}.$$

These can be substitued into Eq. S7, and changing the order of summation gives us

$$\mathrm{NB} = \frac{1}{N}\sum_{j=1}^{N} \sum_{\substack{k=1 \\ k\neq j \\ \mathrm{PL}_{jk}<\infty}}^{N} \sum_{l=1}^{L_{jk}-1} \sum_{\substack{i=1 \\ j\neq i\neq k}}^{N} \frac{(M^l)_{ji}\cdot(M^{L_{jk}-l})_{ik}}{(M^{L_{jk}})_{jk}}.$$

Ordered this way, we notice that the summation over running variable i is actually nothing more than the matrix multiplication of M^l and $M^{L_{jk}-l}$. The elements corresponding to $i = j$ and $i = k$ can be excluded, as they cannot contribute to the summed value. If they did, i.e., if $(M^l)_{jj}\cdot(M^{L_{jk}-l})_{jk}$ or $(M^l)_{jk}\cdot(M^{L_{jk}-l})_{kk}$ were greater than zero, then there would exist a path of length $l < L_{jk}$ or $L_{jk}-l < L_{jk}$ from j to k, contradicting with our definition of L_{jk}. Thereby, we are left with the formula for average node-betweenness

$$\mathrm{NB} = \frac{1}{N}\sum_{j=1}^{N} \sum_{\substack{k=1 \\ k\neq j \\ \mathrm{PL}_{jk}<\infty}}^{N} \sum_{l=1}^{L_{jk}-1} \frac{(M^{L_{jk}})_{jk}}{(M^{L_{jk}})_{jk}} = \frac{1}{N}\sum_{j=1}^{N} \sum_{\substack{k=1 \\ k\neq j \\ \mathrm{PL}_{jk}<\infty}}^{N} (L_{jk}-1).$$

Hence, the mean node-betweenness is proportional to the mean (non-harmonic, infinite path lengths excluded) path length substracted by the overall proportion of pairs connected by a path of edges. The non-harmonic mean path length in turn correlates with the harmonic mean path length: They are both generalized power means of the same data with exponents 1 and -1, respectively.

S3 Supporting data on network simulations

Fig. S5 shows an overview of the activity properties (SC, BC, BL, and BS) obtained for different extreme ($W = \infty$) networks. Each bar shows the mean and standard deviation of the named activity property in 150 network simulations. The results of purely excitatory (E) networks with medium connectivity ($p = 0.2$), modeled by HH, is shown for all activity properties and both in-degree distributions. The statistics of BC in the excitatory-inhibitory (EI) networks, networks with different connection probabilities, and LIF networks are shown for reference.

The difference in network activity between the network classes (RN, LCN1, LCN2, FF, L2, L3, L4, L6 and NM) is evident. The main trend in networks with binomially distributed in-degree is that the LCN1, LCN2 and NM networks produce the most networks bursts and also the longest bursts. However, in networks with power-law distributed in-degree some of the loopy networks express higher BC than LCN1s. In addition, the variance of BC is less negligible than in their counterparts with binomial in-degree, suggesting that considering a network class as a unity may not be feasible. This serves as an extra motivation for exploring graph theoretic properties of the networks and their contribution to the dynamics.

Fig. S6 shows the results of the prediction framework for larger (N=900) networks. The different panels correspond to the results shown in Figs. S5, 6, 8, and 9. The figure justifies that our conclusions hold for the bigger networks as well.

References

S1. Eguiluz V, Chialvo D, Cecchi G, Baliki M, Apkarian A (2005) Scale-free brain functional networks. Physical Review Letters 94: 18102.

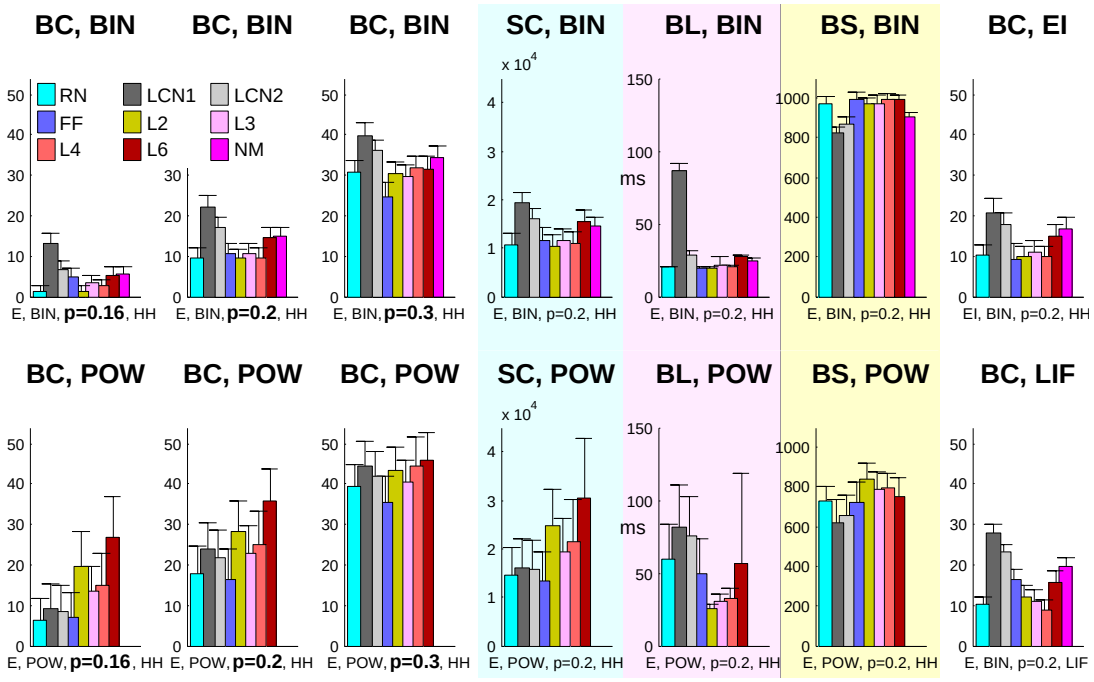

Figure S5. Statistics (mean and std) on the activity properties of different network classes. For the network classes that allow the use of the strength parameter W (WS1, WS2, FF, L2, L3, L4 and L6), only the statistics for the extreme networks ($W = \infty$) shown.

S2. Tsodyks M, Uziel A, Markram H (2000) Synchrony generation in recurrent networks with frequency-dependent synapses. Journal of Neuroscience 20: 1–5.

S3. Golomb D, Shedmi A, Curtu R, Ermentrout G (2006) Persistent synchronized bursting activity in cortical tissues with low magnesium concentration: A modeling study. Journal of Neurophysiology 95: 1049–1067.

S4. Klostermann O, Wahle P (1999) Patterns of spontaneous activity and morphology of interneuron types in organotypic cortex and thalamus-cortex cultures. Journal of Neuroscience 92: 1243–1259.

S5. Golomb D, Amitai Y (1997) Propagating neuronal discharges in neocortical slices: Computational and experimental study. Journal of Neurophysiology 78: 1199–1211.

S6. Mäki-Marttunen T, Havela R, Aćimović J, Teppola H, Ruohonen K, et al. (2010) Modeling growth in neuronal cell cultures: Network properties in different phases of growth studied using two growth simulators. In: Proceedings of the 7th International Workshop on Computational Systems Biology (WCSB 2010).

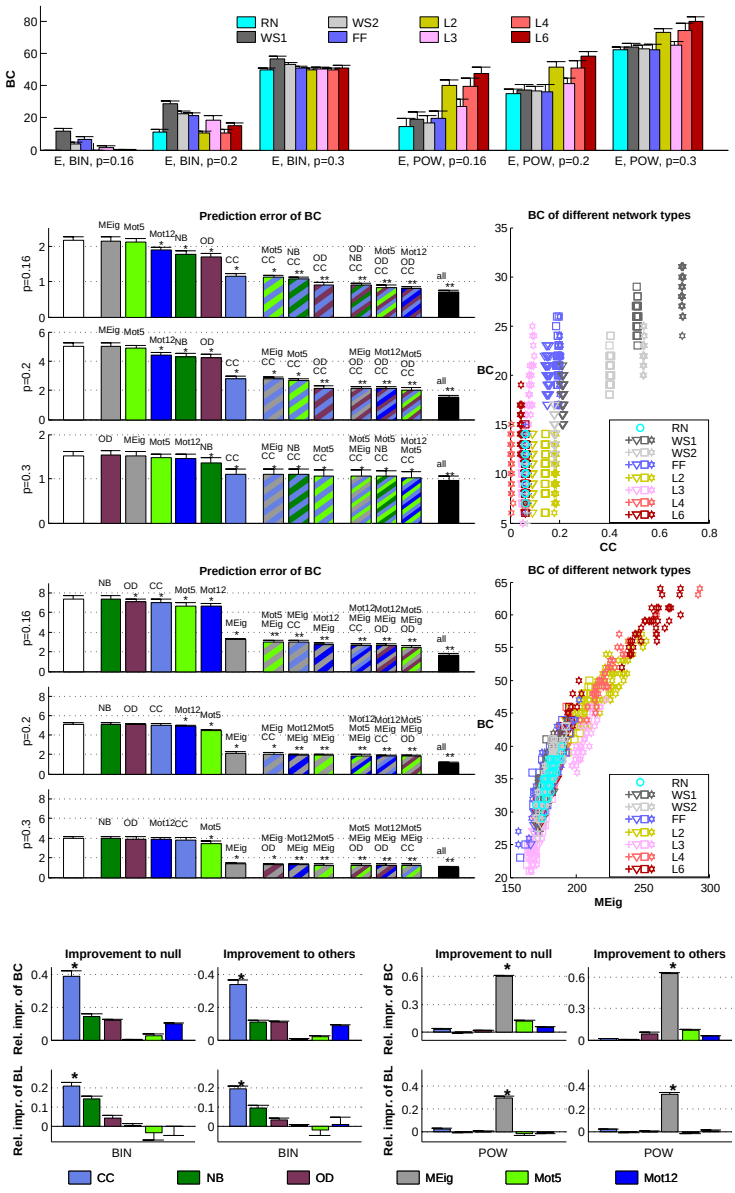

Figure S6. CC is most the determinant graph property in large networks with binomial in-degree, while MEig is the most relevant in large networks with power-law distributed in-degree. The upmost panel shows the burst count statistics for the extreme networks, see Fig. S5 for reference. The second and third panels show the prediction errors of burst count in large networks with binomial or power-law distributed in-degree, respectively, and the 2D-plots show the burst count w.r.t. dominant graph measure in mid-dense ($p = 0.2$) networks. The corresponding data for small networks are shown in Figs. 6 and 9A–B. The lowest panel shows the prediction improvements in large networks, see Figs. 8 and 9D for comparison with small networks. In the repetition of the predictions both the target and teaching data are resampled from the total number of 40 networks.

Tampereen teknillinen yliopisto
PL 527
33101 Tampere

Tampere University of Technology
P.O.B. 527
FI-33101 Tampere, Finland

ISBN 978-952-15-3195-8
ISSN 1459-2045